The Hong Kong Polytechnic University

Department of Applied Biology and Chemical Technology

Protoberberine Derivatives as Potent Inhibitors of the Bacterial Cell Division Protein FtsZ

SUN Ning

A Thesis Submitted in Partial Fulfillment of the

Requirements for the Degree of Doctor of Philosophy

October, 2012

Certificate of Originality

I hereby declare that this thesis is my own work and that, to the best of my knowledge and belief, it reproduces no material previously published or written, nor material that has been accepted for the award of any other degree or diploma, except where due acknowledgement has been made in the text.

— ———————————————

SUN Ning

October, 2012

Abstract

Antibiotic-resistant bacterial infection has become epidemic all over the world. To overcome the drug resistance problem, existing antibiotics have been modified extensively to preserve activity against their targets. Due to the low efficiency and great difficulties of chemical modification, antibacterial agents targeting at new sites become critical to solve this problem. FtsZ (filamenting temperature sensitive strain Z), a bacterial cell division protein, has become attractive as a new target for antibacterial agents discovery because it is the most important and conserved protein in bacterial cytokinesis. Nowadays, several compounds that inhibit the biological activity of the FtsZ protein and block the bacterial cell division have been reported, and most of them bind either to the GTP binding pocket or the H7 helix. However, none of these compounds have entered clinical trials yet.

Natural products are important sources for drug discovery and development and many of them show tolerable toxicity on humans. Berberine and

palmatine, which are alkaloids in the protoberberine group from herbs, are known to exhibit various pharmacological effects, such as antibacterial, anti-arrhythmia and anti-cancer. A recent report revealed that berberine binds to FtsZ in the hydrophobic region of the GTP binding pocket, destabilizes FtsZ protofilaments, inhibits the FtsZ GTPase activity and shows antibacterial activities though the effects are relatively weak. In this study, berberine and palmatine were chosen as lead compounds for further modification. Two series of compounds, 9-phenoxyalkyl berberines and 9-phenoxyalkyl palmatines, were synthesized, and their antibacterial activity and interactions with FtsZ protein were investigated. The results showed that these protoberberine derivatives exhibited greatly improved antibacterial activities against a broad spectrum of bacteria with enhanced inhibitory effect on the GTP hydrolysis and polymerization of FtsZ. These derivatives have IC_{50} values of GTPase activity in the range of 30 – 80 μM, which are 4 – 9 folds stronger than their parent compounds. In addition, all of them possess a potent antimicrobial activity with MIC values in the range of 2 – 64 μg/mL against Gram-positive bacterial strains and show a moderate inhibition against Gram-negative strains. Among them, compound **B2** was identified as the most potent derivatives against bacterial strains. **B2** not only inhibits the growth of *E. coli* with an MIC value of 32 μg/mL, but

also exhibits an impressive activity against *S. aureus*, including methicillin and ampicillin resistant *S. aureus*, with an MIC value of 2 μg/mL.

Molecular docking of these derivatives to the FtsZ protein suggested that the berberine or palmatine core bound to the GTP binding site while the phenoxy moiety interacted with the residues at the C-terminal domain of another FtsZ monomer. This bivalent binding at different locations on two adjacent FtsZ monomers might explain the improved activities of these synthetic compounds compared to their parent compounds which only bind to the GTP binding pocket.

To assess the potential of **B2** and **P2** in treating bacterial infections, the synergistic effects in combination with some conventional antibiotics and the cytotoxicity effects on some mammalian cell lines were investigated. **B2** and **P2** exhibited a synergistic or partial synergistic effect with conventional antibiotics against drug-resistant bacterial strains. The results of cytotoxicity test showed that these two compounds are toxic to mammalian cells, but the toxicity of **B2** can be reduced to an acceptable range when it is used together with ampicillin to treat drug-resistant *S. aureus*.

Acknowledgements

From the bottom of my heart, I hereby express my deep gratitude to my supervisor Professor K. Y. Wong for his enthusiastic supervision, unwavering support and valuable comments during my postgraduate study. In addition, I am grateful to him for providing me a meaningful project and teaching me to think critically about problems.

Moreover, I would like to express my appreciation to Prof. Y. C. Leung and Prof. T. H. Chan for their valuable comments and suggestions. I would also like to thank Dr. F. Y. Chan for teaching me the basic techniques and assistance in molecular modeling, Dr. L. K. Wong for her assistance and expertise with the cytotoxicity experiment, Dr. S. C. Yan for his assistance in NMR spectroscopy, and Dr. P. K. So for his assistance in mass spectrometry.

In addition, I am deeply indebted to my groupmates, Dr. P. H. Chan, Dr. K. C. Cheung, Dr. W. L. Wong, Dr. K. P. Ho, Dr. L. Zou, Dr. Y. J. Lu, Dr. W.

H. Chung, Dr. K. M. Lam, Dr. K. F. Chan, Dr. Lawrence. Y. S. Lee, Dr. B. Qiu, Dr. C. Y. Li, Dr. W. H. Chan, Dr. F. H. Li, Mr. Y. Wong, Mr. M. H. So, Mr. S. M. Ng, Mr. H. K. Liu, Mr. H. M. Leung, Mr. W. L. Cheong, Mr. Hugo. Fung, Miss K. Y. Chow, Miss Enna. Ha and Miss Cherry. Wong for their encouragement and assistance throughout my study period.

I give my utmost thanks to my family and best friends for their persistent love, unceasing support and encouragement to never give up.

Furthermore, I would like to thank Prof. Laurence Hurley of the University of Arizona for giving me the opportunity to attach to his laboratory in 2010. I would also like to express my gratitude to Prof. L. Q. Gu and Prof. Z. S. Huang of Sun Yat-sen University for their encouragement during my research study.

Last, but not the least, I would like to thank the Research Committee of the Hong Kong Polytechnic University for offering me a studentship in 2008-2012

Table of Contents

List of Abbreviations

ATCC	American Type Culture Collection
BLAST	Basic Local Alignment Search Tool
BPMC	Biased probability Monte Carlo
B. subtilis	*Bacillus subtilis*
BSA	Bovine serum albumin
CH_3CN	Acentonitrile
CLSI	Clinical and Laboratory Standards Institute
DMF	Dimethylformamide
DMSO	Dimethyl sulfoxide
E. cloacae	*Enterobacter cloacae*
E. coli	*Escherichia coli*
EDTA	Ethylene Diamine Tetraacetic Acid
E. faecium	*Enterococcus faecium*
E. faecalis	*Enterococcus faecalis*
FICI	Fractional inhibitory concentration index
FtsZ/ *ftsZ*	Filamenting temperature sensitive strain Z
GDP	Guanosine diphosphate

GFP	Green fluorescence protein
GTP	Guanosine triphosphate
ICM	Internal Coordinate Mechanics
IPTG	Isopropyl β-D-1-thiogalactopyranoside
KCl	Potassium chloride
K_2CO_3	Potassium carbonate
K. pneumoniae	*Klebsiella pneumoniae*
kDa	Kilodaltons
LB medium	Luria–Bertani medium
$MgCl_2$	Magnesium chloride
MOPS	4-morpholinepropanesulfonic acid
MIC	Minimum inhibitory concentration
MRSA	Methicillin resistant *Staphylococcus aureus*
MTS	3-(4,5-dimethylthiazol-2-yl)-5-(3-carboxy-methoxyphenyl)-2-(4-sulfophenyl)-2H-tetrazolium
min	Minute(s)
MMFF	Merck Molecular Force Field
NCBI	National Center for Biotechnology Information
OD_x	Optical density at wavelength of x nm
PBS	Phosphate-buffered saline

PDB	Protein Data Bank
PMSF	Phenazine methosulfate
PTA	Phosphotungstic acid
Res.	Resolution
RMSD	Root mean standard derivation
rpm	Revolution per min
SCARE	SCan Alanines and REfine
S. auerus	*Staphylococcus aureus*
S. epidermidis	*Staphylococcus epidermidis*
SDS	Sodium dodecyl sulphate
SDS-PAGE	Sodium dodecyl sulphate- polyacrylamide gel electrophoresis
STD	Saturation transfer difference
TEM	Transmission electron microscopy
VLS	Virtual library screening
3-MBA	3- Methoxybenzamide

Chapter 1

Introduction

1.1 Bacterial infection and antibiotic resistance

Bacterial infection has become an alarming health problem all over the world, mainly caused by antibiotic-resistant bacteria. This problem has become more serious because of the abuse of antibiotics [1, 2]. In the United States, bacterial infections are among the top ten leading causes of death. The Center for Disease Control and Prevention estimated that more than 90,000 people died from hospital-acquired bacterial infections each year [3, 4]. The deaths caused by bacterial infections were even more than those caused by AIDS and cancers [5]. Since many infectious diseases were not classified as reportable diseases, the number of deaths caused by infectious disease has been highly under-estimated.

Antibiotic resistance has emerged as a global health threat [6]. Nowadays, many clinically used antibiotics have become ineffective against

drug-resistant bacteria. For example, the methicillin-resistant *S. aureus* (MRSA) has developed resistance to many beta-lactam antibiotics [5]. In the United States, MRSA have become epidemic in hospitals and communities. From 1999 to 2005, the estimated MRSA-related hospitalizations increased more than two folds [7]. It has been estimated that the numbers of people died from MRSA-related infections were even more than the people died from HIV [3]. MRSA is not only associated with high mortality, it also leads to high hospital expenditures and increased costs for therapy [8, 9]. In China, tuberculosis is still prevalent in some regions [10]. Recently, a study conducted by a team of microbiologists for the Hong Kong Hospital Authority showed that antibiotics in Hong Kong have become less effective on some bacterial strains, such as the increasing resistance of *Streptococcus pneumoniae* to fluoroquinolones [11].

There are four major resistant mechanisms against clinically used antibiotics (Figure 1.1). One mechanism is to hinder the passage of antibiotics through the membrane of bacteria by mutation of the outer membrane proteins. Besides, some organisms have evolved an active efflux mechanism which pumps antibiotics out from the cytoplasm before they reach the targets so as to prevent the access of antibiotics to the target [12]. Efflux pumps can be

found in both Gram-positive and Gram-negative bacteria. Some efflux pumps may be responsible for the resistance of one class of antibiotics but others may be responsible for multiple classes of antibiotics [13, 14]. Apart from the hindrance of binding of antibiotics to their targets, bacteria may produce inactivating enzymes to modify or destroy the chemical structure of an antibiotic [12, 14]. Beta-lactamase is one of the inactivating enzymes secreted by many bacteria. It can hydrolyze the beta-lactam ring of beta-lactam antibiotics resulting in the inactivation of these antibiotics against bacteria [15]. The last resistant mechanism is to alter the binding sites of antibiotic targets, such as the penicillin-binding protein, through mutagenesis, so that the antibiotics could not effectively bind to them [12-14, 16]. As a result, there is a desperate need for solutions of the antibiotic resistance problem through development of new antibiotics with novel mechanisms of action.

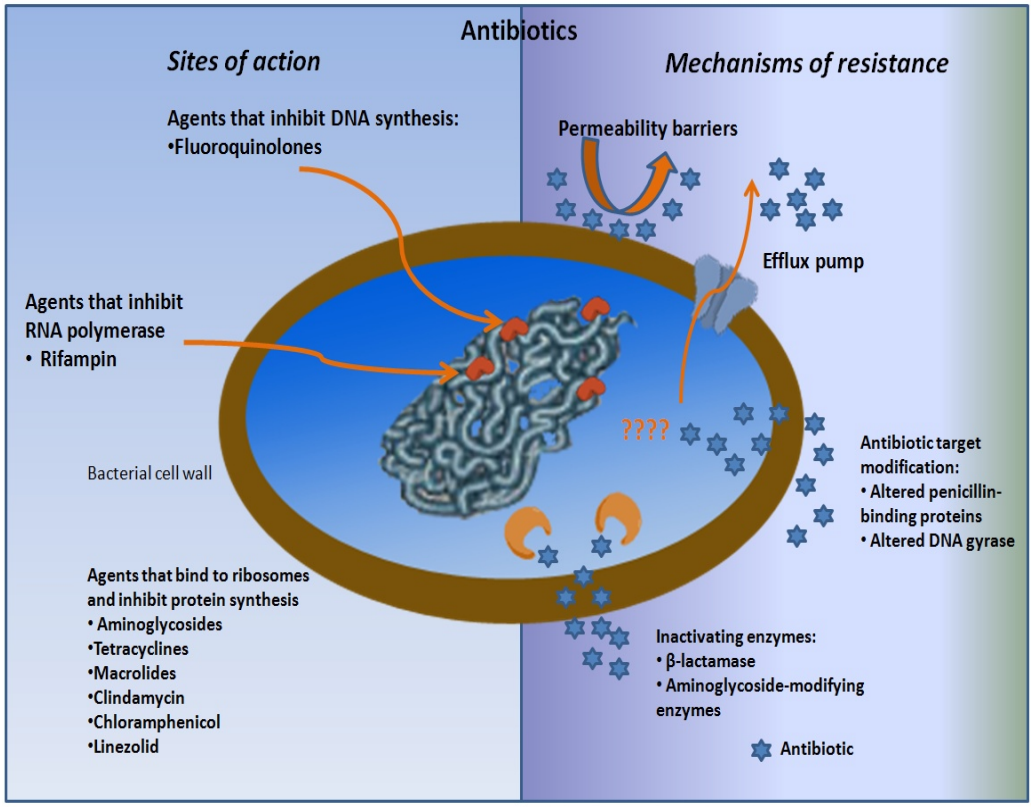

Figure 1.1 Sites of antibiotics action and mechanisms of antibiotic resistance (Adapted from [12]).

1.2 Bacterial cell division and the FtsZ protein

Cell division is an essential process in bacterial life cycle which must be coordinated with other cellular events such as chromosome replication and nucleoid segregation. The cell division of two rod-shaped bacteria, *B. subtilis* and *E. coli*, have been extensively studied over the past two decades [17-20]. Many essential cell division proteins were identified in these model organisms by screening temperature-sensitive mutants that normally grow and divide at the permissive temperature. So far, the crystal structures of some bacterial cell division proteins are available, their catalytic activity has been studied and their interactions with other proteins have been identified and characterized.

FtsZ, named after "Filamenting temperature-sensitive mutant Z", was the first protein of the prokaryotic cytoskeleton to be identified [21]. FtsZ plays a variety of roles in cell division. It has the ability to bind to GTP and also exhibits a GTPase domain that allows it to hydrolyze GTP to GDP and a phosphate group. The nucleotide-binding domain of FtsZ is shown in Figure 1.2. *In vivo*, FtsZ forms filaments with a repeating arrangement of subunits, all arranged head-to-tail. These filaments form a ring around the

longitudinal midpoint, or septum, of the cell. This ring is called the Z-ring [22]. During cell division, FtsZ is the first protein to move to the division site, and is essential for recruiting other proteins that produce a new cell wall between the dividing cells. At the division site, the GTP-bound FtsZ monomers firstly assemble into protofilament by hydrolyzing GTP into GDP during the association [6, 23-25]. FtsZ protofilaments then assemble laterally into bundles. Subsequently, a dynamic Z-ring is formed. The dynamicity of Z-ring can be recognized by the exchange of FtsZ between the Z-ring and the FtsZ in cytoplasm [6, 26-28]. In bacteria, Z-ring is formed at the mid-cell, which is the place of the septum formation [29]. The Z-ring acts as a scaffold to recruit other cell division proteins to the Z-ring. An unknown signal triggers the constriction of the cell wall and cell membrane. The septum formation is accompanied by the constriction of the cell membrane. Finally, two identical daughter cells are formed (Figure 1.3) [27, 29-31].

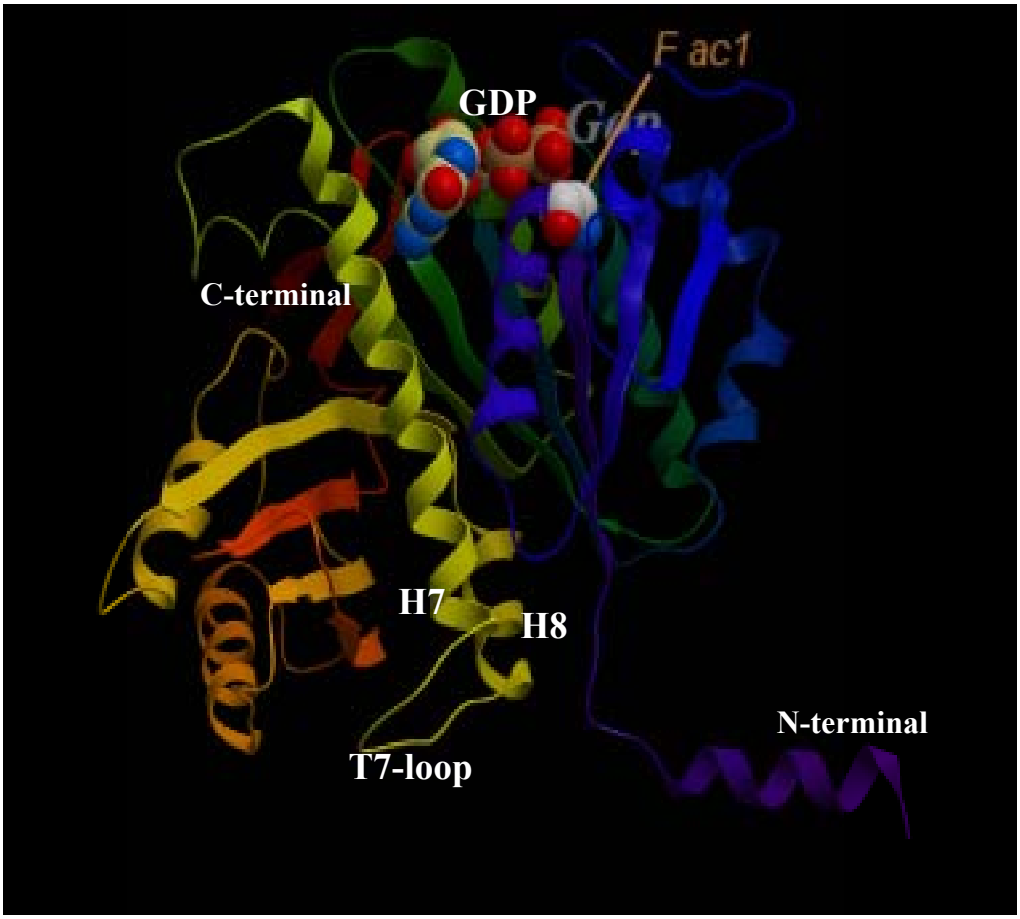

Figure 1.2 The nucleotide-binding domain of FtsZ:GDP (PDB code 1FSZ) (prepared by ICM Molsoft LCC).

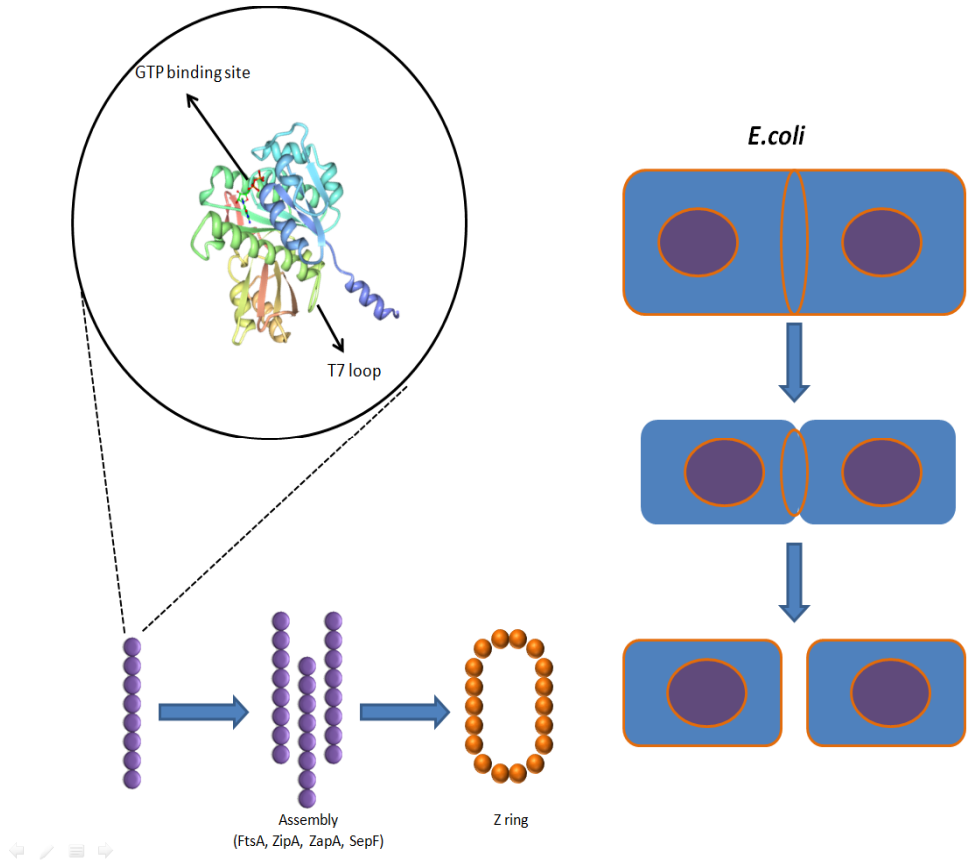

Figure 1.3 The formation of dynamic Z-ring and the cell division of *E. coli* cells (Adapted from [30, 31]).

1.3 FtsZ as a novel antibacterial target

The existing clinically used antibiotics are mainly directed at a small number of targets, such as cell wall, DNA, and protein synthesis. In fact, fewer than 30 proteins have been exploited as targets for antimicrobials in the past 50 years [32, 33]. The small number of targets limits the possibility of discovering new antibiotics for treatment of drug resistant bacteria. Thus, there is a need for new antibiotics with novel mechanisms of action to overcome the emerging resistance problem.

Cell division is a crucial process for the growth and reproduction of bacteria. Hence, cell division proteins have been regarded as attractive antibacterial targets, especially FtsZ. FtsZ is an essential cytoskeleton protein in bacteria. Previous studies have shown that bacterial proliferation can be inhibited by perturbation of FtsZ function [34-36]. In addition, FtsZ is a highly conserved protein in bacteria, which is found in most of the Gram-positive and Gram-negative bacteria with a few exceptions [30, 31, 37, 38]. FtsZ is a GTPase protein [25, 39, 40]. During bacterial cell division, FtsZ monomers assemble into protofilaments by hydrolysis of GTP to GDP [24, 41, 42].

Besides, the biochemical activities of FtsZ have been well studied. The availability of high-resolution crystal structures of FtsZ also allows us to discover novel FtsZ inhibitors using a structure-based virtual screening method. It can improve the successful rate and reduce the cost of drug discovery processes because only compounds which fit best with the protein are purchased and tested experimentally [43].

Considering the short period since the discovery of bacterial cytoskeletal elements, it is not surprising that bacterial cell division is not yet targeted by clinically approved antibiotics. Nonetheless, the search for inhibitors of FtsZ has begun. Previous findings showed that some inhibitory compounds not only killed wild type bacteria, but also inhibited the growth of drug resistant strains effectively [3, 33, 44]. Therefore, discovery of FtsZ inhibitors is an attractive approach in the search for new antibacterial agents with board-spectrum activity.

1.4 FtsZ inhibitors

1.4.1 Synthetic and semi-synthetic compounds as FtsZ inhibitors

So far several synthetic and semi-synthetic compounds have been reported targeting at FtsZ (Table. 1.1). The compound named PC190723 is the most potent one against FtsZ so far. It is derived from 3-methoxybenzamide (3-MBA), and has been identified to possess potent activity against *S. aureus* strains, including multiple drug resistant *S. aureus*, with an MIC value of 1 μg/mL [44]. According to crystallography study, PC190723 binds to the H7 helix of FtsZ [45], and its binding pose in FtsZ protein is shown in Figure 1.4. SRI-3072 was identified to inhibit *M. Tuberculosis* (*Mtb*) FtsZ assembly and GTPase activity after screening more than 200 synthetic alkoxycarbonylpyridines, and was found to effectively inhibit the growth of *B. subtilis* strain. Some GTP derivatives were identified to be competitive inhibitors for FtsZ polymerization and GTPase activity. For example, 8-morpholino-GTP was found to inhibit FtsZ assembly in the 100 – 500 μM range but did not show any antibacterial activity [46]. After screening 95,000 synthetic compounds, A189, a

4-aminofurazan derivative, was found to possess potent antibacterial activity. It can inhibit FtsZ assembly *in vitro* and Z ring formation *in vivo* without influencing chromosome segregation [47]. A cell-based assay with *B. subtilis* was used to screen for cell division inhibitors. Several compounds were identified, among which were specific inhibitors of FtsZ like compounds PC58538 and PC170942, the later was found to be active against a broad spectrum of antibiotic-sensitive and antibiotic-resistant Gram-positive species [48]. Five small molecules named Zantrins were found to inhibit GTPase activity and polymerization of FtsZ through a high-throughput protein-based chemical screening approach. Z1, Z2 and Z4 were found to destabilize FtsZ assembly while Z3 and Z5 stabilized FtsZ bundles [49]. After screening of 120 taxane derivatives, a group of taxanes (the C-seco-TRAs) was identified to stabilize *Mtb* FtsZ against depolymerization *in vitro* and found to be active against drug-sensitive and drug-resistant strains of *M. Tuberculosis* without cytotoxicity *in vivo*, with MIC values in the micromolar range. These compounds might be applied as antituberculosis agents in the future [50]. Amikacin, a potent semi-synthetic aminoglycoside derived from kanamycin and a commonly used antibiotic in the treatment of bacterial infections, was found to cause cell elongation and perturb FtsZ ring assembly *in vivo* [51]. Recently, a compound called

OBTA that exhibited a different antibacterial mechanism from other known FtsZ inhibitors was found after screening 81 compounds with different structural scaffolds. This compound was shown to increase the bundling of FtsZ protofilaments by promoting FtsZ assembly *in vitro*, cause filamentation and inhibit the formation of cytokinetic Z-rings in bacteria, but did not influence the proliferation of mammalian cells [34].

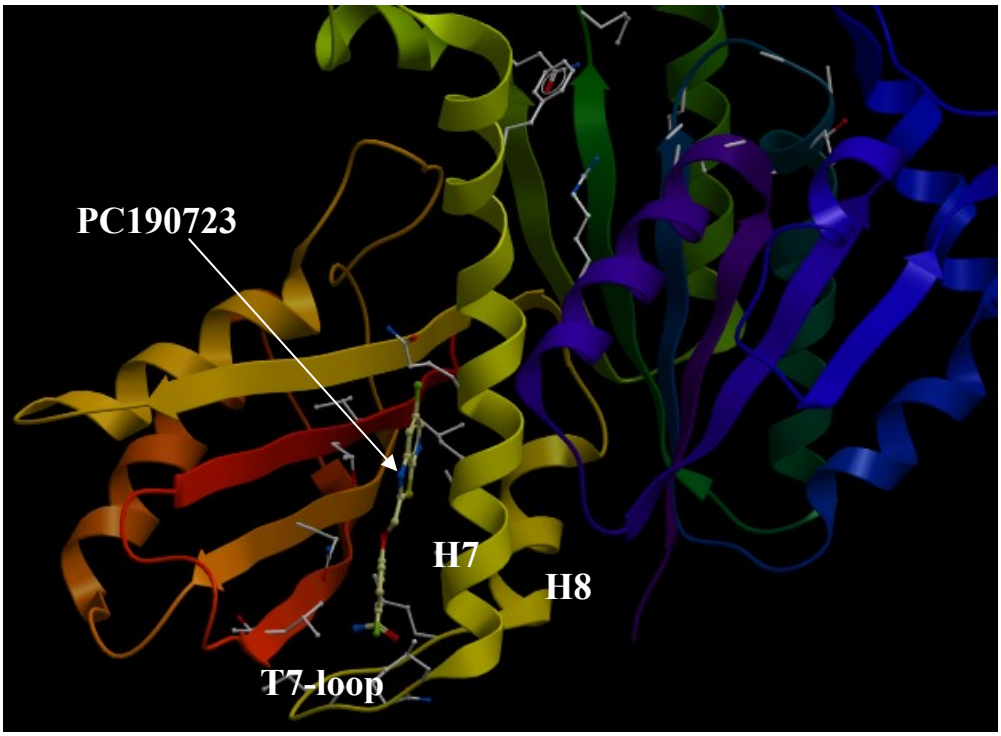

Figure 1.4 The binding pose of PC190723 in *S.aureus* FtsZ (PDB code 3OVB) (prepared by ICM Molsoft LCC).

Table 1.1 Synthetic and semi-synthetic FtsZ inhibitors

Compound (source/class)	Structure	Binding site and inhibitory activity	Antibacterial activity
A-189 (4-aminofurazan derivative)	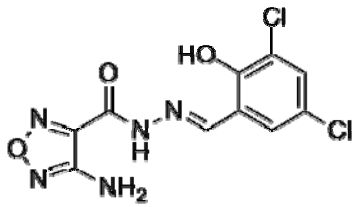	Binding site unknown; Inhibits GTPase activity (IC_{50} = 80 μg/ml) and Z-ring assembly	*E. coli* (MIC = 128 μg/ml) and *S. auerus* (MIC = 16 μg/ml)
Amikacin(Semi-synthetic aminoglycoside derived from kanamycin)	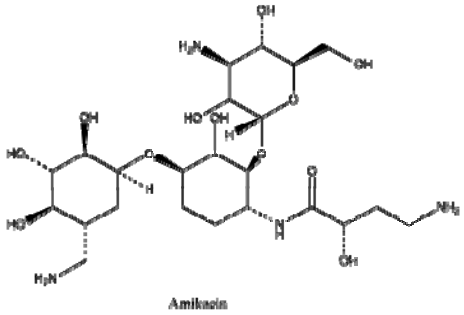	Binding site unknown; Perturbs Z-ring formation	*E. coli*
8-morpholino-GTP (GTP analogues)	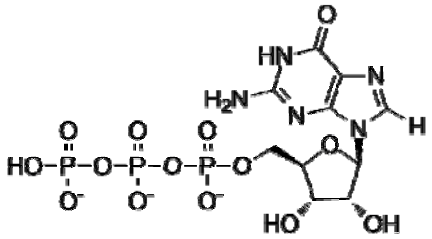	Binds to GTP binding site; Inhibits assembly and GTPase in the 100 – 500 μM.	Ineffective

Compound (source/class)	Structure	Binding site and inhibitory activity	Antibacterial activity
OTBA	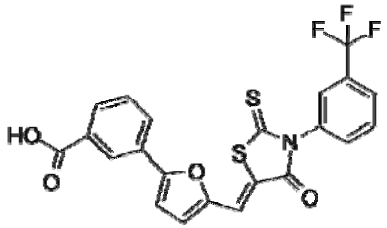	Binding site unknown; Inhibits *Bs*FtsZ and *Ec*FtsZ GTPase activity, but promotes assembly of FtsZ	*B. subtilis* (MIC = 2 μM)
PC 170942	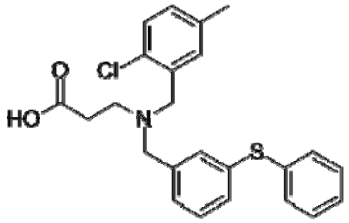	Binds to GTP binding site; Inhibits GTPase activity (IC_{50} = 24 μg/ml)	*B. subtilis* (MIC = 16 μg/ml), *S. auerus* (MIC = 64 μg/ml) and *E. coli* (MIC > 256 μg/ml)
PC 190723	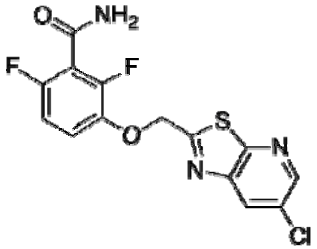	Binds to H7 helix; Inhibits *Sa*FtsZ GTPase activity (IC_{50} =55 ng/mL) and perturbs Z ring formation	*B. subtilis and S. auerus* (MICs = 1 μg/mL), *E. coli* (MIC = > 64 μg/mL)

Compound (source/class)	Structure	Binding site and inhibitory activity	Antibacterial activity
SRI-3072 (2-alkoxycarbonylaminopyridine)	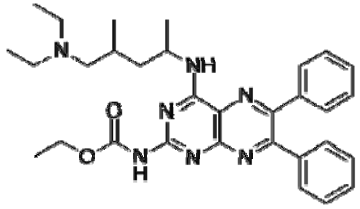	Binding site unknown; Inhibits *Mtb*GTPase activity and polymerization	*B. subtilis* (MIC = ~ 0.28 μM)
Taxane derivatives	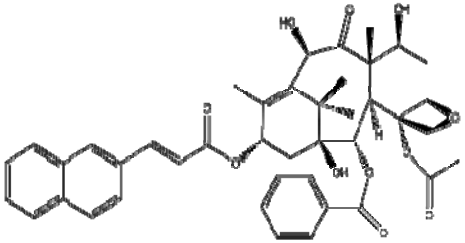	Binding site unknown; Stabilizes *Mtb*FtsZ against depolymerization	*B. subtilis* (MIC = 2.5 μM)
Z1-Z5 (Zantrins (polyphenols))	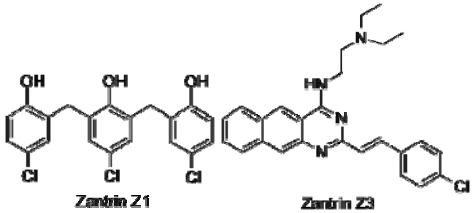	Binding site unknown; Z1, Z2 and Z4 destabilize FtsZ assembly, Z3 and Z5 hyperstabilize FtsZ assembly, inhibit *Ec*FtsZ and *Mt*FtsZ GTPase activity (IC_{50} = 2-15 μg/ml)	Broad range (MICs of Z1 on *S. aureus* and *E. coli* = 1 μg/ml and 8 μg/ml)

1.4.2 Natural products as FtsZ inhibitors

Natural products represent a rich source of drug leads in pharmaceutical research. In the history of antibiotic discovery, many effective compounds are natural products or their derivatives. Examples include penicillin and vancomycin. Other examples include daptomycin, a natural compound found in the soil saprotroph *Streptomyces roseosporus* and a novel lipopeptide antibiotic used in the treatment of bacterial infections caused by Gram-positive bacteria [52], is now is marketed in the United States. Telavancin is a bactericidal lipoglycopeptide for use in MRSA or other Gram-positive infections [52]. It is a semi-synthetic derivative of vancomycin and has been approved as a drug in 2009 for complicated skin and infections. Natural products not only provide hints on structural scaffold for drug discovey, but also exhibit additional advantages such as low toxicity against mammalian cells [53]. In the past few years, a number of natural products were reported to inhibit FtsZ (Table 1.2). Berberine, a common natural alkaloid extracted from various species of *Berberis*, was found to target at FtsZ [35, 54]. It was shown to destabilize FtsZ protofilaments and inhibit the FtsZ GTPase activity *in vitro*, and has a weak

activity against Gram-positive strains, including methicillin-resistant *S. aureus*. Viriditoxin, a natural compound isolated from *Aspergillus viridinutans* in 1971, was identified to inhibit FtsZ polymerization and GTPase actibity with IC_{50} values of 8.2 μg/mL and 7.0 μg/mL respectively [33]. Viriditoxin has a potent activity against drug sensitive and resistant Gram-positive strains with MIC values between 2 and 16 μg/mL, but it cannot inhibit the Gram-negative bacteria. Cinnamaldehyde, a phenylpropanoid compound, is a natural product found in spices. It has been demonstrated that cinnamaldehyde binds to the T7 loop of FtsZ leading to inhibition of GTPase activity and perturbation of the Z-ring morphology *in vivo* [38]. Curcumin, a dietary polyphenolic compound, was demonstrated to perturb FtsZ assembly and induce filamentation in *B. subtilis* 168 by binding to the T7 loop of FtsZ. Interestingly, curcumin showed a totally different mechanism from the other known FtsZ inhibitors. It was found to perturb the assembly dynamic of FtsZ by increasing the GTPase activity of FtsZ. An increase of 35 % GTPase activity was found in the presence of 30 μM curcumin. This compound reduced the formation of Z-ring, but did not affect the nucleoid segregation. However, the main limitation of curcumin is poor bioavailability [55]. Sanguinarine, a benzophenanthridine alkaloid from the rhizomes of *Sanguinaria canadensis* known to exhibit a wide range

of antimicrobial activity, was recently shown to block cell division in gram-positive and gram-negative bacteria by perturbation of Z-ring formation through binding to FtsZ. However, sanguinarine is toxic to mammalian cells because it inhibits tubulin assembly into microtubules [36]. Totarol, a diterpenoid phenol, was reported to inhibit the assembly dynamic of *M. tuberculosis* (*Mtb*) FtsZ *in vitro* without affecting the mammalian cells. In addition, totarol also induced the filamentation of *B. subtilis* cells and caused bacterial cytokinesis *in vivo* [56]. Recently, Chrysohaentins A-H, a series of antimicrobial natural products, were found to inhibit the GTPase activity of FtsZ and showed potent antimicrobial activity against Gram-positive strains, including some drug resistant bacteria, in the micromolar range. Among these compounds, Chrysohaentin A, the most potent inhibitor, was found to bind to the GTP binding site of FtsZ by saturation transfer difference NMR and *in silico* docking [3].

Table 1.2 FtsZ inhibitors from natural products.

Compound (source/class)	Structure	Binding site and inhibitory activity	Antibacterial activity
Berberine (*Berberis aquifolium*, *Berberis aristata*)	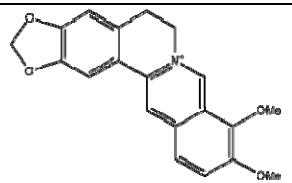	Binds to the hydrophobic core of GTP binding site; Inhibits *Ec*FtsZ GTPase activity	*B. subtilis* (MIC = 100 μg/mL) and *E. coli* (MIC = > 400 μg/mL)
Chrysohaentins A-H (Yellow aglae *Chrysophaeum taylori*)	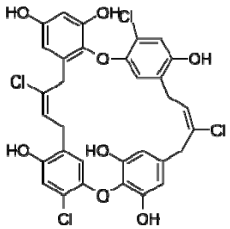	Binds to GTP binding site; Inhibits *Ec*FtsZ GTPase activity (IC_{50} = 6.7 ± 1.7 μg/mL) and assembly	Inhibit both of sensitive and drug-resistant Gram-positives; (MIC_{50} = 1.3 ± 0.4 μg/mL)
Cinnamaldehyde (*Cinnamomum cassia*)	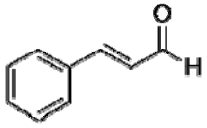	Binds to T7 loop; Inhibits *Ec*FtsZ GTPase activity and FtsZ polymerization	*B. subtilis* (MIC = 4 μg/mL) and *E. coli* (MIC = 1000 μg/mL)
Curcumin (*Curcuma longa*)	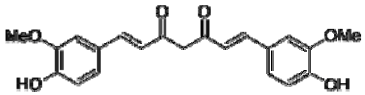	Binding site unknown; Increases GTPase activity	*B. subtilis* (MIC = 37 μg/mL)

Compound (source/class)	Structure	Binding site and inhibitory activity	Antibacterial activity
Sanguinarine (Rhizomes of *Sanguinaria canadensis*)	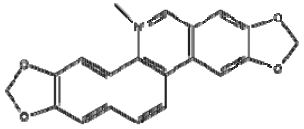	Binding site unknown; Inhibits *Ec*FtsZ FtsZ assembly and protofilament bundling	*B. subtilis* (MIC = 10 μM) and *E. coli* (MIC = 70 μM)
Totarol (*Podocarpus totara*)	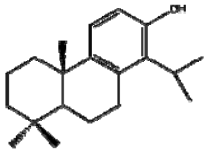	Binding site unknown; Inhibits *Mt*FtsZ GTPase activity and assembly	*B. subtilis* (MIC = 2 μM)
Viriditoxin (*Aspergillus viridinutans*)	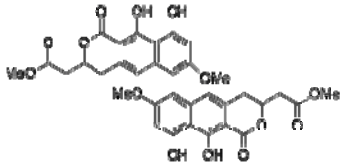	Binding site unknown; Inhibits GTPase activity (IC_{50} = 7 μg/mL) and polymerization	Inhibit sensitive and drug-resistant Gram-positive strains

1.5 Drug discovery and computer-aided drug design

Identification of a hit compound and development of lead compounds into new drugs for pathognostic diseases is an extremely time-consuming process. The major difficulties in drug discovery are the long process and the high development cost. It is very common that drug companies take more than 10 years and millions of dollar to develop a new prescription drug into the market.

Over the last several decades, drug discovery and development have evolved into a new stage. The use of computer becomes an alternative method in addition to the traditional drug design strategies to improve the successful rate of drug discovery processes and curtail the long discovery period.

Computer-aided drug design (CADD) uses computational chemistry to discover, enhance, or study drugs and related biologically active molecules. The most fundamental goal is to predict whether and how strongly a given molecule will bind to a target [57, 58]. Molecular mechanics or molecular

dynamics are often used to predict the conformation of the small molecule and to model conformational changes in the biological target that may occur when the small molecule binds to it. Quantum chemistry methods and density functional theory are often used to provide optimized parameters for the molecular mechanics calculations and an estimate of the electronic properties (electrostatic potential, polarizability, etc.) of the drug candidate that will influence binding affinity. In addition, molecular mechanics may also be used to provide semi-quantitative prediction of the binding affinity [59-61].

Ideally the computational method should be able to predict affinity before a compound is synthesized, hence only one compound which shows the best affiny with its target needs to be synthesized in principle. However, the reality is that computational methods are imperfect and provide at best only qualitatively accurate estimates of affinity so far [58]. Therefore in practice it still takes several iterations of design, synthesis, and testing before an optimal molecule is discovered. Nevertheless, computational methods have accelerated the drug discovery process by reducing the number of iterations required and have provided substantial novel small molecule structures which have pharmacological activity. The drug discovery and development

processes are shown in Figure 1.4. Drug discovery with the help of computers may be used at all stages of drug screening, design and development, such as hit identification via visual screening, hit-to-lead optimization of affinity and selectivity, and lead optimization of pharmaceutical properties while maintaining activity [62, 63]. There are many successful examples of rational computer-aided drug design, including zanamivir (Relenza® from GlaxoSmithKline, a neuraminidase inhibitor for influenza virus treatment) [64], dorzolamide (Trusopt® from Merck, a carbonic anhydrase inhibitor for glaucoma treatment) [65], imatinib (Gleevec® from Novartis, a tyrosine kinase inhibitor for the treatment of chronic myeloid leukemia) [66] and lopinavir (Kaletra® from Abbott, a protease inhibitor for HIV treatment) [67].

With the technology of computer-aided drug design and the availability of high resolution crystal structures of FtsZ [21, 44, 68-71], structure-based virtual screening method can facilitate the identification of new scaffolds of FtsZ inhibitors. Recently, our research group has identified some new chemotype of FtsZ inhibitors after a docking-based virtual ligand screening (ICM, Molsoft) [72] of over 20,000 natural product compounds. The hit compounds containing a quinuclidine ring shows good ICM binding scores

(high affinity to bind the GTP binding site *in silico*) and were further validated by both *in vitro* and *in vivo* biological assays [73].

Figure 1.5 Drug discovery and development processes.

1.6 Drug combination and synergistic effect

Combination of drugs is a promising strategy to overcome multiple drug resistant problems. For several decades, many studies on the effectiveness of drug combinations have been reported which include analgesics, fungicides, insecticides and antibiotics. There are three possibilities of drug combination: synergism, zero-interaction and antagonism [74, 75]. Synergistic combinations of two or more drugs can overcome toxicity and other side effects caused by high doses of a single drug by reducing dosage of each compound or accessing context-specific multiple target mechanisms. In addition, synergism can minimize or slow down the development of drug resistance [76-78]. For these therapeutic benefits, drug combinations have been widely used and became the leading choice for treating the most dreadful diseases, such as cancer and infectious diseases, including methicillin-resistant *S. aureus* (MRSA) and AIDS [79]. There are two commonly used approaches for studying drug synergistic effect [80]. The first one is to use multiple drugs to target multiple targets at the same time. One example is the combination of clavulanic acid with amoxicillin overcome bacterial resistance to the antibiotic. The other one is to use

multiple drugs with different mechanisms or modes of action that may affect a single target or a disease so as to treat it more effectively. For instance, amdinocillin can enhance the bactericidal activity of the combined beta-lactam [81].

In the treatment of bacterial infection, resistance to antibiotics has led to the emergence of new and reemergence of old infectious diseases. This situation calls for the combined use of drugs. Therefore, use of paired and triple combinations of inhibitory agents such as beta-lactams together with beta-lactamase inhibitors is very common. There are many models to measure combination effects, and the best known and common one is the checkerboard method. In this assay, a two dimensional array of serial concentrations of test compounds is used for calculation of a fractional inhibitory concentration index (FICI) to demonstrate whether the paired compounds can exert antibacterial effects that are stronger than the sum of their effects alone (synergistic or partial synergistic effect with FICI less than 1), or weaker than the sum of their individual effects [82].

1.7 Aims and objectives

As described in the previous sections, many existing antibiotics have become less effective because of emergence of drug resistant bacteria strains. This critical problem calls for new antibacterial agents which target at new sites to overcome the drug resistance problem. FtsZ protein has become a hot target in the development of antibitics because it plays a key role in bacterial cell division, and is absent in the mammaliam cells. In addition, there is no clinically approved drug targeting bacterial cell division proteins so far.

Natural products are important sources in drug discovery and development and many of them are nontoxicit to humans. Protoberberines are an important group of isoquinoline natural alkaloids. Alkaloids in this group include berberine, palmatine and jatrorrhizine. All these natural alkaloids contain an isoquinoline core. The structures of protoberberines are shown in Figure 1.5. The most important member in the protoberberine family is berberine, which is a yellow compound extracted from plants such as *Berberis*, *Hydrastis canadensis* (goldenseal) and, *Pehllodendron amurense*

[83]. Berberine is known to exhibit various pharmacological effects, such as antibacterial, anti-arryhythmia and anti-cancer [84].

Berberine has been used as an antibacterial agent for a number of years [85]. In 1966, two berberine products have been accepted into Japanaese Pharmacopoeia for treatment of enteric infection. In 1996, Iwasa and his team have synthesized more than 40 protoberberine derivatives and tested their antibacterial activity [86]. They reported that these protoberberine derivatives have a better inhibition on the growth of Gram-positive bacterial strains than the negative strains. In addition, they found that change of the quaternary ammonium isoquinoline core and addition of substituted group at the C-13 position of protoberberines would affect the antibacterial activity. Recent study revealed that berberine inhibits the assembly of FtsZ protein and shows antibacterial activity without toxicity effect [35, 54]. Based on these studies, berberine and its analogue palmatine were chosen as lead compounds to develop potent derivatives as FtsZ inhibitors in this research project.

In this thesis, the antibacterial study of berberine and its 9-phenoxyalkyl derivatives will be described in chapter 2. Chapter 3 is mainly on the

biological study of palamtine and its derivetives. Building a homology model for molecular docking simulation of the above-mentioned compounds to FtsZ will be discussed in chapter 4. Lastly, the combination effects with conventional antibiotics and the cytotoxicity of these compounds will be reported in chapter 5.

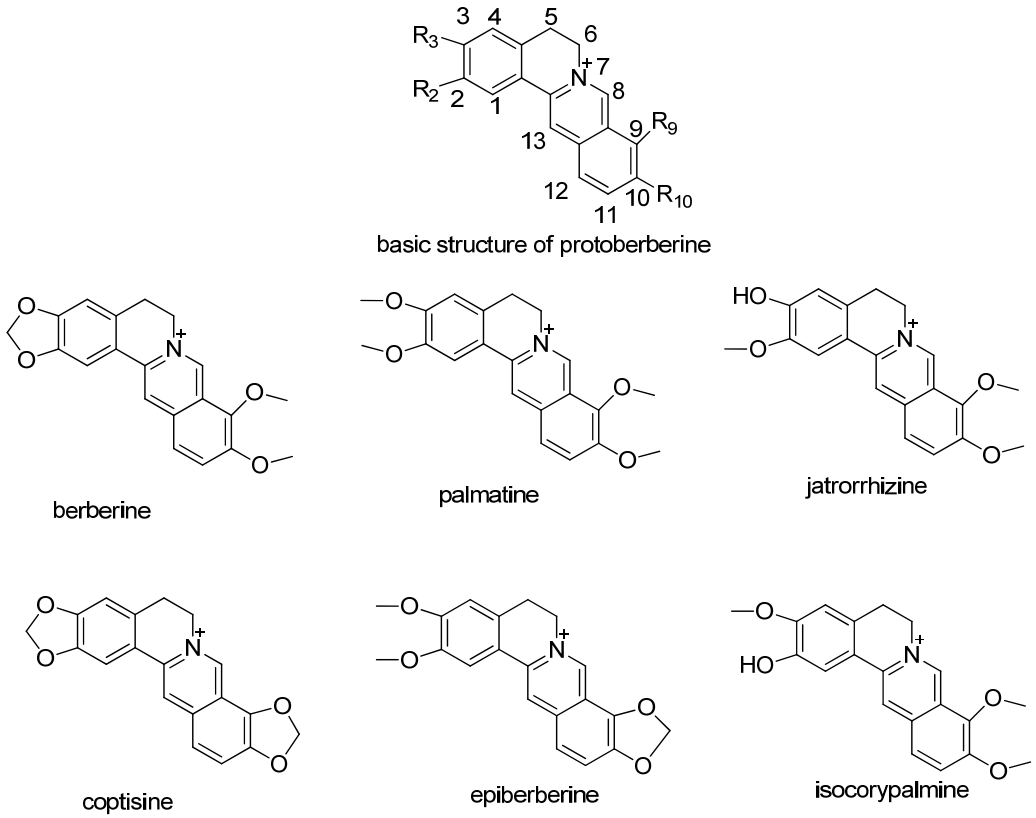

Figure 1.6 Chemical structures of some natural protoberberine alkaloids.

Chapter 2

Berberine and its 9-phenoxyalkyl substituted derivatives as FtsZ inhibitors and anti-bacterial agents

---

2.1 Introduction

The protoberberine alkaloid berberine has been used as an antibacterial agent in traditional medicine [85]. In a recent work, berberine was identified as an inhibitor on the assembly of the FtsZ protein. Biochemical studies suggested that berberine binds to the hydrophobic region in the nucleotide binding site of FtsZ [35]. A clinical research study also shows that, at clinically relevant concentrations, berberine functions more as a cytostatic agent than a cytotoxic agent [87]. Although many beneficial properties of berberine have been reported, the spectrum of antimicrobial activity and potency are limited. In the past decade, several structural modification studies on berberine have been reported to improve the antibacterial activity as well as the spectrum of activity [86, 88, 89]. It was found that the isoqunoline core containing the quaternary ammonium group in berberine is an important structure for its antibacterial activity [86]. In 1998, Iwasa *et al.*

reported the antimicrobial activity of several protoberberine derivatives with different alkoxy substituents on different locations of the isoqunoline core [88, 89]. Interestingly, it was found that linking a lipophilic group at C-8 or C-13 position of berberine can enhance its antimicrobial activity.

Two more recent reports indicated that berberine possessed moderate antibacterial activity against *S. aureus* and *B. subtilis* [35, 54]. However, although the quaternary ammonium in the isoquinoline core is an essential integrant for its pharmocological activity, its low lipophilicity makes berberine difficult to permeate the bacterial cell membrane and limits its bioavailability [86]. In this chapter, the synthesis of some 9-phenoxyalkyl substituted berberine derivatives are repoeted, and *in vitro* and *in vivo* assays were used to verify whether these derivatives possess stronger binding affinity against FtsZ protein and antibacterial activity against a broad spectrum of bacteria.

2.2 Experimental section

2.2.1 Chemical synthesis of berberine derivatives

2.2.1.1 Materials

Berberine chloride, 1,3-dibromopropane, 1,4-dibromobutane, phenol, 4-cholorophenol, 4-methoxyphenol, *o*-cresol, 4-nitrophenol, 4-fluorophenol and potassium carbonate were purchased from Sigma-Aldrich. All the analytical grade reagents and solvents were used as received without further purification.

2.2.1.2 Instrumentation

^{1}H NMR spectra were obtained with a Bruker 400 MHz DPX-400 NMR spectrometer. Mass spectra were recorded with a Finnigan MAT 95S mass spectrometer.

2.2.1.3 Synthesis and characterization

The synthetic pathway of compounds **2**, **3** and the berberine derivatives are shown in the Scheme 2.1. Firstly, the ω-bromoalkyl ether derivatives were synthesized from the commercially available phenol derivatives, which reacted with α,ω-dibromoalkanes in the presence of potassium carbonate in DMF to give a good yield. The reaction conditions followed those published by C. Sheng *et al.* [90]. Then, the selective demethylation of berberine at 190 ℃ under the vacuum gave a 68% yield of berberrubine (compound **1**) [84]. Finally, the target compounds (**4**, **B1** to **B6**) were obtained according to previous protocols [91], by reaction of berberrubine (compound **1**) with the ω-bromoalkyl ether derivatives in acetonitrile for 12 h.

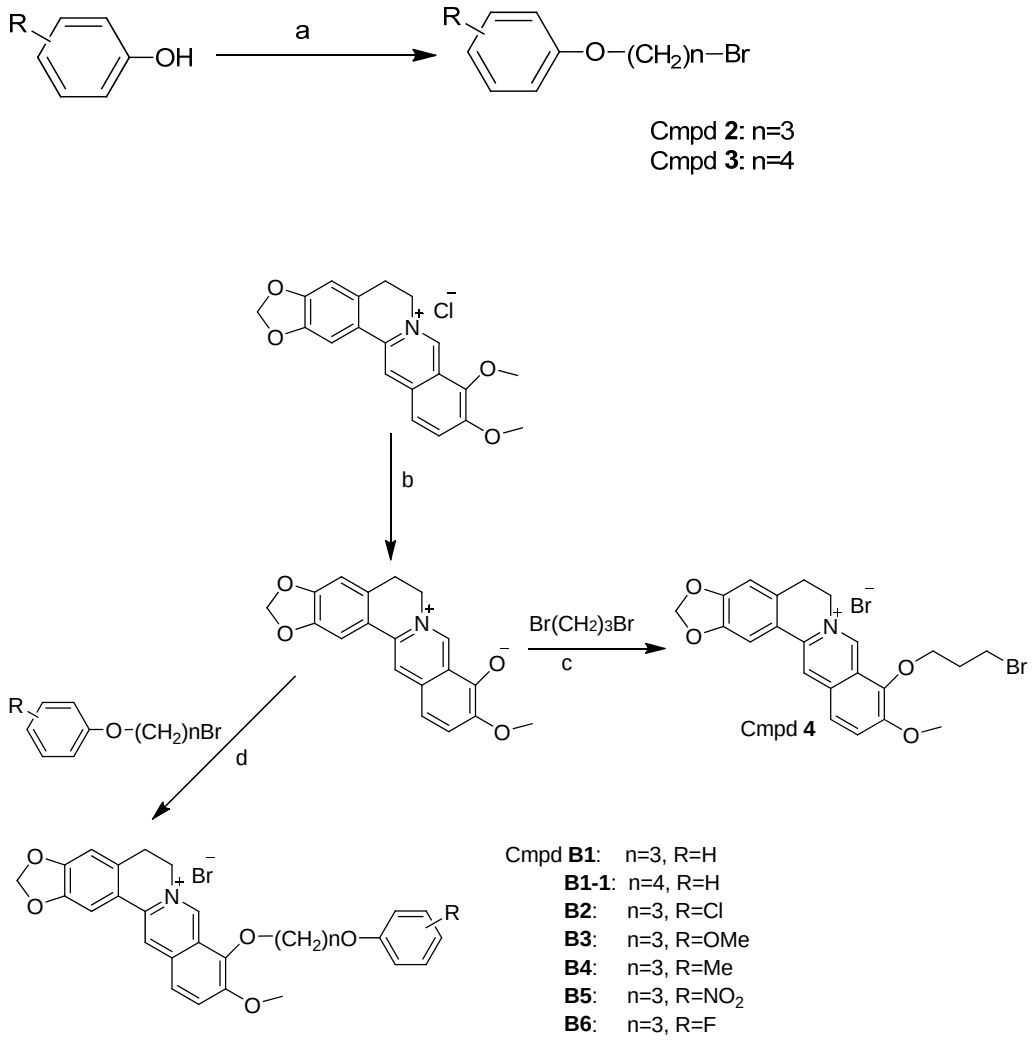

Scheme 2.1 Synthetic routes of compounds **2** and **3**, and berberine derivatives.

Reagents and conditions: (a) $Br(CH_2)nBr$ (n=3 or 4), K_2CO_3, DMF, 70 ℃, 2 h; (b) 190 ℃, under vacuum, 30 min; (c) DMF, 80 ℃; (d) CH_3CN, 80 ℃ [84, 90, 91].

2.2.1.3.1 Preparation of berberrubine (compound 1)

To remove the methyl group at C-9 position of berberine, 5 mmol berberine was heated at 190 ℃ under vacuum for 30 - 50 min until the color of powder turned into dark brown. The powder was then purified by flash chromatography (CH_2Cl_2 / MeOH = 10:1) to yield a carmine powder after solvent removal. The high resolution mass spectrum and ^{1}H NMR spectrum of berberrubin (compound **1**) are shown in Appendices I and II respectively. Yield: 68%. ^{1}H NMR (400 MHz, DMSO-*d*6): δ 3.04 (t, *J* = 6.0 Hz, 2H), 3.73 (s, 3H), 4.8 (t, *J* = 6.0 Hz, 2H), 6.1 (s, 2H), 6.36 (d, *J* = 8.0 Hz, 1H), 6.96 (s, 1H), 7.16 (d, *J* = 7.6 Hz, 1H), 7.61 (s, 1H), 7.98 (s, 1H), 9.07 (s, 1H). ESI-MS m/z: 322.1 $[M + H]^+$.

2.2.1.3.2 Preparation of compounds 2 and 3

A solution of phenol (2 mmol) in DMF (5 mL) was added dropwise to a stirred suspension of 1,3-dibromopropane or 1,4-dibromobutane (4 mmol) with K_2CO_3 (3 mmol) in DMF (5 mL). After stirred at room temperature for 2 h, the mixture was heated at 75 ℃ for another 2 h. The mixture was filtered, and the solution was diluted with ethyl acetate (50 mL) and washed with deionized water (3 × 50 mL). The crude product was obtained by removing organic solvent. The residue was purified by flash chromatography (petroleum ether / ethyl acetate = 50:1) to give compound **2** or **3** as a colorless oil. The high resolution mass spectra of **2** and **3** are shown in Appendixes I. ESI-MS m/z: **2**, 215.9 [M]; **3**, 230.0 [M].

2.2.1.3.3 Preparation of compounds 4, B1 to B6

Berberrubine [Compound **1** (0.15 mmol)] and 1,3-dibromopropane [(0.5 mmol), for synthesis of compound **4**] or one of the ω-bromoalkyl ether derivatives [(0.5 mmol), for synthesis of **B1** to **B6**] were mixed in 10 mL acetonitrile, and stirred for 12 h at 90 ℃. After reaction, the crude product was obtained by removal of organic solvent under vacuum and then purified by flash chromatography (CH_2Cl_2 / MeOH = 20:1) to yield a yellow powder. The high resolution mass spectra and ^{1}H NMR spectra of them are shown in Appendices I and II respectively. Yield: 40 – 55 %. ^{1}H NMR (400 MHz, DMSO-d_6): **4:** δ 2.40-2.46 (m, 2H), 3.22 (t, *J* = 6.0 Hz, 2H), 3.83 (t, *J* = 6.4 Hz, 2H), 4.08 (s, 3H), 4.21 (t, *J* = 6.4 Hz, 2H), 4.95 (t, *J* = 6.0 Hz, 2H), 6.19 (s, 2H), 7.10 (s, 1H), 7.81 (s, 1H), 8.10 (d, *J* = 9.2 Hz, 1H), 8.21 (d, *J* = 9.2 Hz, 1H), 8.95 (s, 1H), 9.81 (s, 1H); ESI-MS m/z: 442.1 $[M - Br]^+$; **B1:** δ 3.35 (t, *J* = 6.4 Hz, 2H), 3.22 (t, *J* = 6.0 Hz, 2H), 4.01(s, 3H), 4.27 (t, *J* = 6.4 Hz, 2H), 4.49 (t, *J* = 6.4 Hz, 2H), 4.87 (t, *J* = 6.0 Hz, 2H), 6.18 (s, 1H), 6.93-6.99 (m, 3H), 7.10 (s, 1H), 7.31 (t, *J* = 7.6 Hz, 2H), 7.80 (s, 1H), 8.05 (d, *J* = 8.8 Hz, 1H), 8.20 (d, *J* = 9.2 Hz, 1H), 8.94 (s, 1H), 9.78 (s, 1H);

ESI-MS m/z: 456.2 $[M - Br]^+$; **B1-1:** δ 2.01-2.09 (m, 4H), 3.20 (t, *J* = 6.4 Hz, 2H), 4.05 (s, 3H), 4.09 (t, *J* = 6.0 Hz, 2H), 3.37 (t, *J* = 6.0 Hz, 2H), 4.94 (t, *J* = 6.4 Hz, 2H), 6.18 (s, 2H), 6.91-6.95 (m, 3H), 7.10 (s, 1H), 7.29 (t, *J* = 7.2 Hz, 2H), 7.81 (s,1H), 7.99 (d, *J* = 9.2 Hz, 1H), 8.21 (d, *J* = 9.2 Hz, 1H), 8.94 (s, 1H), 9.78 (s, 1H); ESI-MS m/z: 470.2 $[M - Br]^+$; **B2:** δ 2.31-2.37 (m, 2H), 3.2 (t, *J* = 6.4 Hz, 2H). 4.01 (s, 3H), 4.26 (t, *J* = 6.4 Hz, 2H), 4.70 (t, *J* = 6.4 Hz, 2H), 4.90 (t, *J* = 6.4 Hz, 2H), 6.18 (s, 2H), 7.01 (d, *J* = 6.0 Hz, 1H), 7.10 (s, 1H), 7.35 (d, *J* = 6.0 Hz, 1H), 7.81 (s, 1H), 7.99 (d, *J* = 5.2 Hz, 1H), 8.19 (d, *J* = 5.2 Hz, 1H), 8.94 (s, 1H), 9.79 (s, 1H); ESI-MS m/z: 490.1 $[M - Br]^+$; **B3:** δ 2.29 (t, *J* = 6.4 Hz, 2H), 3.17 (t, *J* = 6.0 Hz, 2H), 3.67 (s, 3H), 4.00 (s, 3H), 4.17 (t, *J* = 6.4 Hz, 2H), 4.45 (t, *J* = 6.4 Hz, 2H), 4.85 (t, *J* = 6.0 Hz, 2H), 6.16 (s, 2H), 6.83-6.89 (m, 4H), 7.07 (s, 1H), 7,78 (s,1H), 7.97 (d, *J* = 8.8 Hz, 1H), 8.17 (t, *J* = 8.8 Hz, 1H), 8.91 (s, 1H), 9.75 (s, 1H); ESI-MS m/z: 486.2 $[M - Br]^+$; **B4:** δ 2.14 (s, 3H), 2.36 (m, 2H), 3.18 (t, *J* = 6.0 Hz, 2H), 3.99 (s, 3H), 4.27 (t, *J* = 6.0 Hz, 2H), 4.52 (t, *J* = 6.4 Hz, 2H), 4.86 (t, *J* = 6.4 Hz, 2H), 6.18 (s, 2H), 6.85 (t, *J* = 8.0 Hz, 1H), 7.00 (d, *J* = 8.0 Hz, 1H), 7.09 (s, 1H), 7.13-7.19 (m, 2H), 7.81 (s, 1H), 8.10 (d, *J* = 9.2 Hz, 1H), 8.19 (d, *J* = 9.2 Hz, 1H), 8.96 (s, 1H), 9.78 (s, 1H); ESI-MS m/z: 470.2 $[M - Br]^+$; **B5:** δ 2.36-2.42 (m, 2H), 3.20 (t, *J* = 6.0 Hz, 2H), 4.00 (s, 3H), 4.43 (t, *J* = 6.4 Hz, 2H), 4.48 (t, *J* = 6.4 Hz, 2H), 4.92 (t, *J* = 6.0 Hz,

2H), 6.18 (s, 2H), 7.10 (s, 1H), 7.20 (d, *J* = 2.0 Hz, 2H), 7.80 (s, 1H), 8.00 (d, *J* = 7.2 Hz, 1H), 8.10 (d, *J* = 7.2 Hz, 1H), 8.24 (d, *J* = 2.0 Hz, 2H), 8.93 (s,1H), 9.81 (s, 1H); ESI-MS m/z: 501.2 $[M - Br]^+$; **B6:** ^1H NMR (400 MHz, $CDCl_3$), δ 2.46-2.52 (m, 2H), 3.19 (t, *J* = 6.4 Hz, 2H), 3.87 (s, 3H), 4.29 (t, *J* = 6.0 Hz, 2H), 4.63 (t, *J* = 6.0 Hz, 2H), 5.26 (t, *J* = 6.4 Hz, 2H), 6.01 (s, 2H), 6.73 (s,1H), 6.86-6.93 (m, 4H), 7.23 (s, 1H), 7.68 (d, *J* = 7.2 Hz, 1H), 7.75 (d, *J* = 7.2 Hz, 1H), 8.17 (s, 1H), 10.38 (s, 1H); ESI-MS m/z: 474.2 $[M - Br]^+$.

2.2.2 Biological assays

2.2.2.1 Materials

(A) Media

Nutrient agar, tryptone and yeast extract were obtained from Oxoid Ltd. (Nepean, Ontario, Canada). Luria-Bertani (LB) medium was purchased from USB Corporation and used for preparation and transformation of *E. coli* competent cells and *in vivo* assays. 2 × TY medium for the over-expression of FtsZ protein was prepared by the addition of 3.2 g tryptone, 2 g yeast extract and 1 g sodium chloride into 200 mL deionized water and sterilized. Müller-Hinton broth (MHB), cation-adjusted Müller-Hinton broth (CA-MHB) and trypticase soy broth (TSB) for Minimum Inhibitory Concentration (MIC) determination were purchased from Becton, Dickinson and Company (New Jersey, USA).

(B) Chemicals

Ampicillin, kanamycin sulfate, chloramphenicol, 3-methoxylbenzamide, 4-morpholinepropane sulfonic acid (MOPS), magnesium chloride, potassium chloride, EDTA, guanosine 5'-triphosphate (GTP) and phosphotungstic acid (PTA) were purchased from Sigma-Aldrich. Sodium chloride, potassium hydroxide, potassium dihydrogenphosphate and isopropyl β-D-1-thiogalactopyranoside (IPTG) were obtained from USB Corporation. FM 4-64 was purchased from Invitrogen (Eugene, Oregon).

(C) Proteins

BSA and lysozyme were obtained from Sigma-Aldrich.

2.2.2.2 Bacterial strains

The *S. auerus* FtsZ was over-expressed in a host of *E. coli* BL21 (DE3). The bacterial strains used in minimum inhibitory concentration (MIC) determination are: *S. aureus* ATCC 29213, *S. aureus* ATCC 29247, *S. aureus* ATCC BAA-41, *S. epidermidis* ATCC 12228, *E. faecalis* ATCC 29212, *E. faecium* ATCC 49624, *E. faecium* ATCC 700221, *E. cloacae* ATCC BAA-1143 and *K. pneumoniae* ATCC BAA-1144 which were purchased from American Type Culture Collection (USA). *B. subtilis* 168 and *E. coli* ATCC 25922 are our laboratory collections. *E. coli* JM109 WM647 is a gift from Dr. W. Margolin.

2.2.2.3 Preparation of *S. aureus* FtsZ protein

2.2.2.3.1 Expression and purification of FtsZ protein

E. coli BL21 cells containing the *S. aureus ftsZ* gene was obtained from our laboratory stock. For the overexpression and purification of FtsZ protein, the *E. coli* strain was taken from the stock to a LB medium containing 100 µg/mL ampicillin. The cells were allowed to grow at 37 ^{o}C for 14-16 h. The bacterial culture (2 mL) was transferred to 200 mL of 2 X TY medium containing 100 µg/mL ampicillin and allowed to grow at 37 ^{o}C until the cells reached the early lag phase with OD_{600} around 0.8. Protein expression was induced by the addition of 0.4 mM isopropyl β-D-1-thiogalactopyranoside (IPTG) for another 4 h. Cells were then harvested by centrifugation at 9000 rpm at 4 ^{o}C for 20 min followed by resuspension in 20 mL solubilization buffer (50 mM Tris-HCl, 150 mM NaCl, 1 mM PMSF and 1 mM EDTA, pH 7.4). Lysozyme (20 µg/mL) was added to the cell suspension and incubated in 30 ^{o}C for 45-60 min. Subsequently, the cells were lyzed by sonication operated at 50% amplitude

with 30-s pulse at 30-s intervals between the pulses for five cycles. The insoluble debris was removed by centrifugation at 13000 rpm at 4 ^{o}C for 1 h. Most his-tagged FtsZ protein was collected in the supernatant.

The FtsZ protein was purified by Fast Protein Liquid Chromatography (FPLC). Purification of the protein was further carried out using 5-mL HiTrap chelating column (Amersham-Pharmacia) which was charged with nickel (II) sulphate solution. The soluble protein sample was passed through a 0.22 μm filter before loaded onto the column, which was equilibrated with starting buffer (20 mM sodium phosphate and 500 mM NaCl, pH 7.4). His-tagged FtsZ was eluted with elution buffer (20 mM sodium phosphate, 500 mM NaCl and 500 mM imidazole, pH 7.4). The chromatogram is shown in Figure 2. 1. The fractions containing the desired protein (Peak A in Figure 2.1) were collected and analyzed by SDS-PAGE (Section 2.2.2.3.2), then dialyzed extensively against 50 mM MOPS buffer and then stored at -80 ^{o}C.

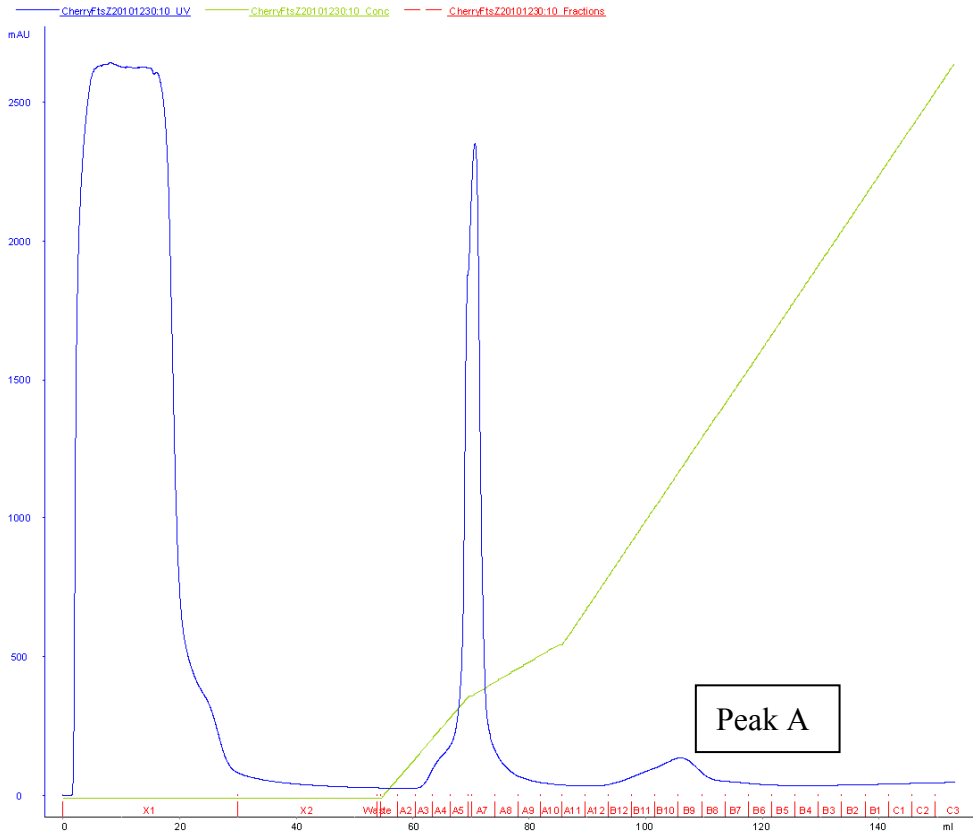

Figure 2.1 The FPLC chromatogram of *S. aureus* FtsZ.

2.2.2.3.2 Sodium dodecyl sulfate-polyacrylamide gel electrophoresis (SDS-PAGE) Analysis

The collected protein fractions were analyzed by 12 % SDS-PAGE in a Mini-PROTEAN III dual slab cell (Bio-Rad Laboratories). 10 μL of sample was mixed with same volume of the reducing agent β-mercaptoethanol and SDS, and boiled for 10 min. The SDS-PAGE gel was made by 5 % stacking gel (pH 6.8) and 12 % separating gel (pH8.8). After loading 10 μL of the boiled sample into the well, the gel was subjected to electrophoresis in 1 X running buffer (25 mM Tris-HCl, 192 mM glycine, 3 mM SDS, pH 7.4) at 100 V for the first 20 min, and then at 200 V for 50 min. Subsequently, the gel was stained with coomassie blue for 10 min and then destained with shaking until the backgroud of the gel became clear. The SDS-PAGE gel photograph is shown in Figure 2.2.

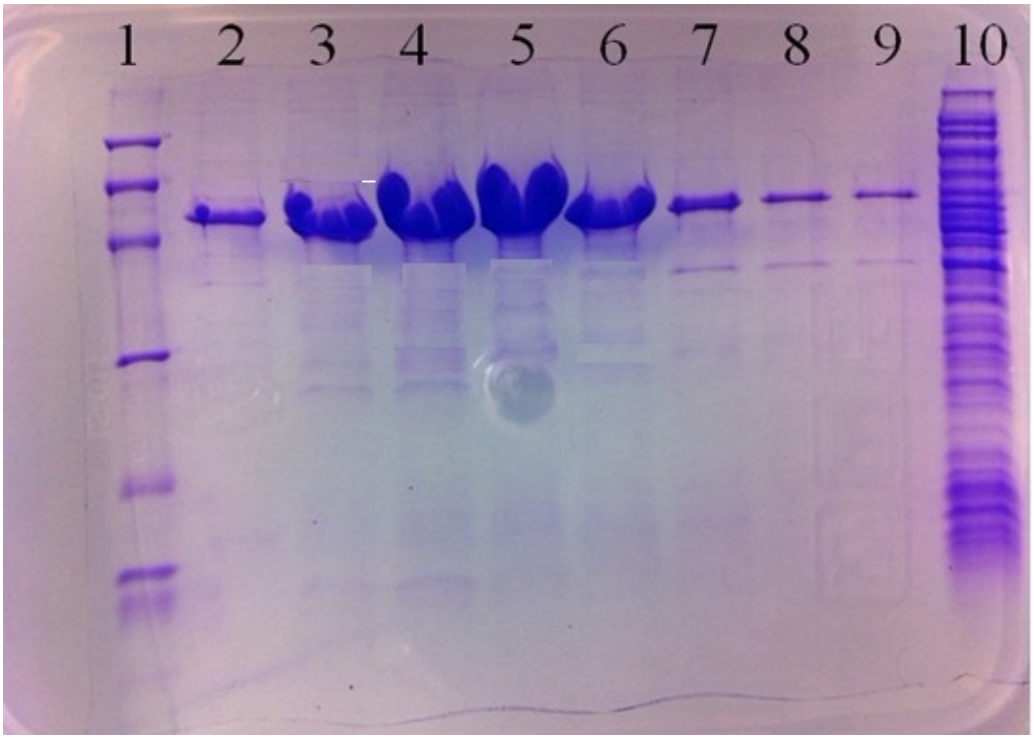

Figure 2.2 The SDS-Page gel photo of *S. aureus* FtsZ. Lane 1, low range molecular markers: rabbit muscle phosphorylase b (97400 Da), BSA (66200 Da), hen egg white ovalbumin (45000 Da), bovine carbonic anhydrolase (31000 Da), soybean trypsin inhibitor (21500 Da), hen egg white lysozyme (14400Da); lanes 2-9, elution of *S. auerus* His_6-FtsZ by elution buffer; lane 10, flow through.

2.2.2.3.3 Electrospray ionization-mass spectrometry (ESI-MS)

ESI-MS was used to confirm the molecular weight of the S. auresu FtsZ. To prepare the sample for ESI-MS, the protein was buffer-exchanged with 20 mM ammonium acetate before analyzing. ESI-mass spectrum was obtained using a VG Platform single quadrupole or quadrupole-time of flight (Q-TOF2) mass spectrometer (Micromass, Altrincham, Cheshire, UK) equipped with an electrospray interface. Protein samples dissolved in H_2O/CH_3CN (1:1 v/v) or H_2O/MeOH (1:1 v/v) containing 0.2% formic acid (v/v) were injected into the electrospray source through a 20 µL-loop injector (Rheodyne 5717) at a flow rate of 10 µL/min. The mass spectrometer was scanned over m/z 570 – 1600 range. Myoglobin (10 ρmol/µL, average molecular mass 16,951.5) was used to calibrate the instrument. The ESI-mass spectrum of the protein is shown in Figure 2.3.

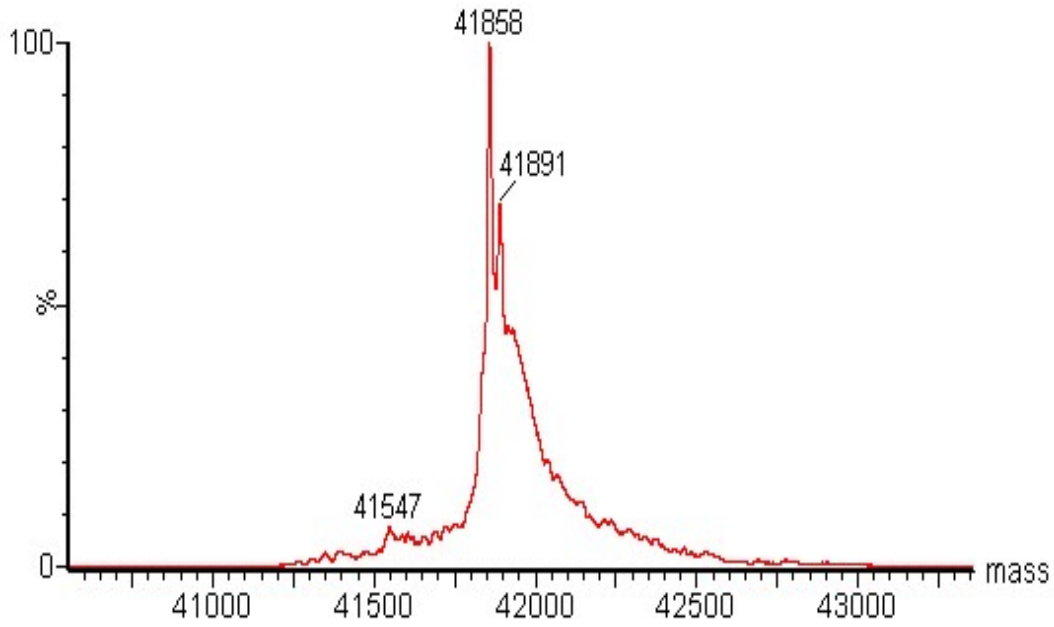

Figure 2.3 ESI-mass spectrum of *S. aureus* FtsZ.

2.2.2.3.4 Determination of protein concentration

The concentration of the purified protein sample can be determined by Bradford's method. 200 μL of the Bradford's Reagent Dye (Bio-Rad) was added to 800 μL of sample and incubated for 10 min at room temperature. The absorbance of the sample was measured using a UV-vis spectrophotometer at 595 nm. The concentration of the sample can be determined by comparing the absorbance with the protein standard curve using BSA as standard.

2.2.2.4 GTPase activity assay

The GTPase activitiy of of recombinant *S. aureus* FtsZ was measured in a 96-well microplate using a CytoPhos™ phosphate assay Biochem Kit™ (Cytoskeleton, USA) [73]. In this assay, *S. aureus* FtsZ (3.5 μM) was pre-incubated with serial dilutions of the test compounds in 50 mM MOPS buffer for 10 min at 25 ^{o}C. The control sample contained only 1% DMSO. Then, 5 mM of $MgCl_2$ and 200 mM of KCl were added. Reactions were started with the addition of 500 μM GTP and incubated at 37 ^{o}C. After 30 min, the reactions were quenched by adding 100 μL of Cytophos reagent. After 10 min incubation, inorganic phosphate was quantified by measuring the absorbance (A_{650}) in a 96-well microplate reader (BioRad 680). The IC_{50} values for the compounds in study were determined from the relative slopes of GTP hydrolysis at different concentrations compared to the control with DMSO only. Three independent assays were performed. The data represented the mean of ± S.D. and were analyzed by nonlinear regression using a sigmoidal concentration–response curve available in the Origin 6.0 software.

2.2.2.5 Light scattering assay

The kinetics of FtsZ assembly were measured using a 90^{o} light scattering method in a thermostatically (37 ^{o}C) controlled spectrofluorometer (LS-50B, Pekin Elmer) using a 0.5 ml quartz cuvette (10 mm, Hellma). Both excitation and emission wavelengths were set to 600 nm with a slit width of 2.5 nm. *S. aureus* FtsZ (6 μM) in 50 mM MOPS buffer (pH 6.5) was incubated with DMSO or different concentrations of the test compound for 10 min at 25 ^{o}C. Then, 50 mM KCl and 10 mM $MgCl_2$ were added to establish a baseline. After 8 min, the final concentration of 1 mM GTP was added at the last fraction and the increase in light scattering measured for an additional 2000 seconds. The rate and extent of polymerization were measured. Appropriate blanks were subtracted from all experimental data. Results shown are the average of three independent experiments.

2.2.2.6 Transmission electron microscopy

S. aureus FtsZ (12 μM) was incubated in the absence and presence of different concentrations of the test compounds in 50 mM MOPS buffer (pH 6.5) at 25 ^{o}C. After 10 min, 5 mM $MgCl_2$, 50 mM KCl, and 1 mM GTP were added to the reaction mixtures and incubated at 37 ^{o}C for 15 min. Then, 10 μL of sample mixtures were placed on a glow-discharged Formvar carbon-coated copper grid (400 mesh) for 10 min. The grids were subsequently subjected to negative staining using 10 μL of 0.5% PTA for 30 s, air-dried and digital images of the specimen were observed with a transmission electron microscope (JEOL model JEM 2010) operated at 200 kV and equipped with a Gatan MSC 794 CCD camera.

2.2. 2.7 Saturation transfer difference (STD) NMR spectroscopy

The exchangeable protons of FtsZ were subjected to H-D exchange in a 50 mM sodium phosphate buffer, which contained 10 % deuterium water, 50 mM NaCl and 5mM $MgCl_2$ (pH 6.5, uncorrected due to deuterium effects). The STD NMR experiment was performend on a Bruker AvanceIII 600 instrument equipped with a 5-mm QCI cryoprobe. Acquisitions were performed at 298 K using the standard STD pulse sequence with a train of 50 ms Gauss-shaped pulses, each separated by a 1 ms delay for selective protein irradiation, and an alternation between on and off resonances. A T1ρ spinlock filter (50 ms) was incorporated to suppress protein resonances. The NMR spectrum of 20 μM FtsZ and 1 mM **B2** or **B3** (molar ratio 1: 50) was recorded using the standard pulse sequence [92]. Presaturation of the protein resonances was performed with an on-resonance irradiation at 1.2 ppm to saturate mainly Ile, Leu and Val; off resonance irradiation was applied at -10 ppm where no NMR resonances of ligand or protein were present. The STD signals were obtained by performing experiments at 5s saturation and recorded with a recovery delay of 10 s to avoid incomplete relaxation to

thermal equilibrium. Experiments were recorded using a minimum of 128 scans and 32K points. On- and off-resonance spectra were processed independently, and subtracted to provide a difference spectrum. Data processing was performed using the TopSpin program suite (Bruker BioSpin Pte Ltd).

2.2.2.8 Antibacterial susceptibility test

The minimum inhibitory concentrations (MICs) of the test compounds were determined using a broth microdilution method according to the Clinical and Laboratory Standards Institute (CLSI) guidelines. Four to five single colonies of the testing bacterial strain on a TSB agar plate were inoculated in 5 mL of MH or CA-MH broths. The cells were incubated at 37 ^{o}C until the OD_{600} (absorbance of 600 nm) of the growing cells reached 1.0. The cells were then diluted to a final concentration of approximately 5 x 10^5 CFU/mL in MH or CA-MH broth containing two fold dilutions of the test compounds in a 96-well microtiter plate. After 18 h of incubation at 37 ^{o}C, the OD_{600} values were measured to calculate the percentage inhibition of bacterial growth with respect to control. The MIC value is defined as the lowest concentration of tested compounds that causes ≥ 90% inhibition of bacterial growth.

2.2.2.9 Visualization of bacterial morphology

The *B. subtilis* 168 cells were grown in LB medium. The cultures at an OD_{600} of 0.01 from an overnight culture were inoculated in the same medium containing different concentrations of the test compounds and grown at 37 ^{o}C. After 4 h, the bacterial cells were harvested and resuspended in 100 μL of PBS buffer containing 0.25% agarose. Then, a total of 10 μL suspension mixture was placed on the microscopic slide pretreated with 0.1% (w/v) poly-L-lysine and the morphology of the bacterial cells was observed under a light phase-contrast microscope at 40 × magnification. The images were captured using a Nikon camera. The length of the bacterial cell was measured using pre-installed Nikon software.

2.2.2.10 Membrane staining

The *B. subtilis* 168 cells were grown in LB medium. The overnight grown *B. subtilis* cells were diluted to OD_{600} of 0.01 and were grown in the absence and presence of different concentrations of the test compound for 4 h at 37 ^{o}C. FM 4-64, a fluorescent dye, was used to stain the membrane. 1.6 μM of FM 4-64 was added to the growing cultures and incubated for an additional 30 min at 37 ^{o}C without shaking. The cells were then harvested and resuspended in 100 μL PBS containing 0.25% agarose. Then, a total of 10 μL suspension mixture was placed on the microscopic slide pretreated with 0.1% (w/v) poly-L-lysine and the morphology of the bacterial cells was observed at 40 × magnification using an Olympus Bio Imaging Navigator FSX 100 microsope. The length of the bacterial cell was measured using pre-installed Olympus software.

2.2.2.11 Visualization of Z-ring in bacterial cells

A culture of *E. coli* JM109 WM647 containing an IPTG-inducible plasmid for the production of green fluorescence protein (GFP)-tagged FtsZ was grown in LB medium supplemented with 30 μg/mL of chloramphenicol. After overnight incubation, a sample of the culture was diluted to 1% in the LB medium containing different concentrations of the test compound and 40 μM of IPTG. After 4 h incubation at 37 ^{o}C, the *E. coli* cells were fixed, harvested and resuspended in PBS buffer containing 0.25% of agarose. 10 μL of sample mixture was added to the pretreated microscopy slide with 0.1% (w/v) poly-L-lysine and visualized using a fluorescence microscope at 60 × oil immersion magnification , with a standard FITC filter set. The images were captured using an Olympus Bio Imaging Navigator FSX 100 microscope.

2.3 Results and discussion

2.3.1 Biological study of berberine, Compounds B1, B1-1, 1 – 4

In this section, the effect of berberine**,** compounds **B1, B1-1,** and **1** to **4** on the GTPase activity of *S. aureus* FtsZ were measured. Combination tests of compound **1** plus compound **2** or compound **3** against *S. aureus* FtsZ were also measured. The susceptibility test was used to determine their antimicrobial activity. The chemical structures of these compounds are shown in Figure 2.4.

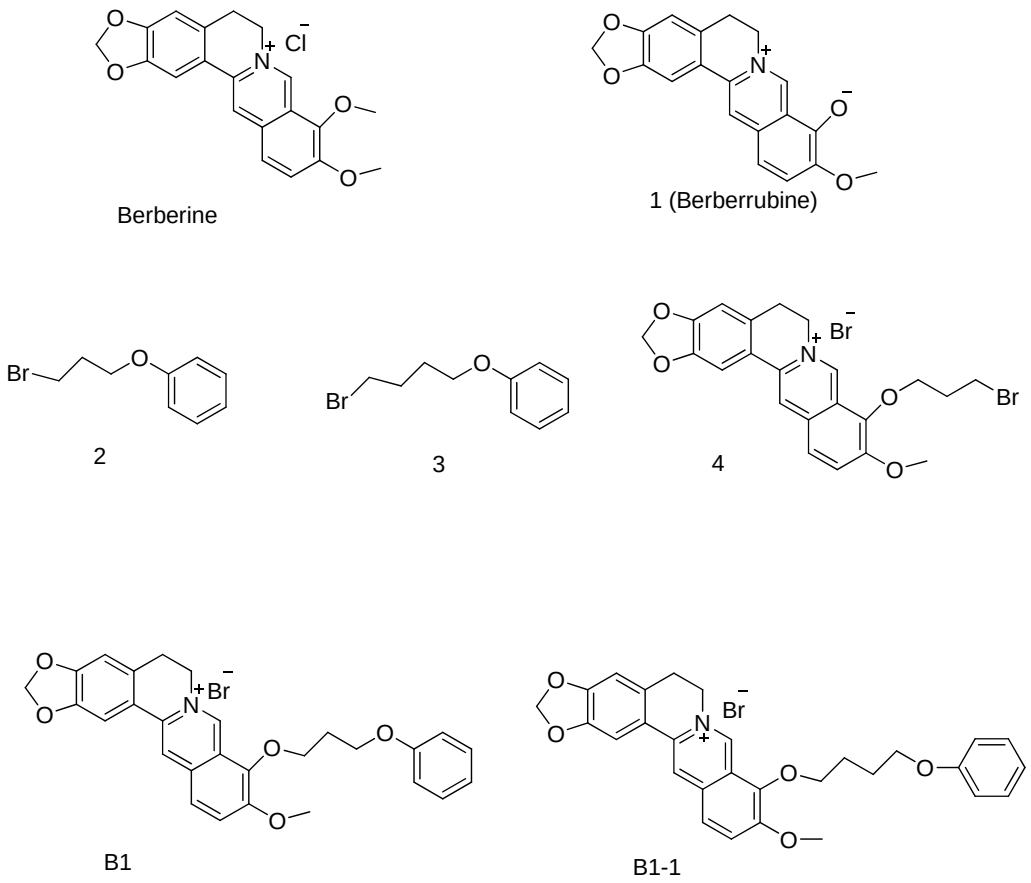

Figure 2.4 Chemical structures of berberine, compound **1** (berberrubine), **2**, **3**, **4**, **B1** and **B1-1**.

2.3.1.1 GTPase activity

The inhibition ability of the compounds synthesized were tested against the GTPase activity of *S. aureus* FtsZ *in vitro*. The dynamic assembly of FtsZ protein was regulated and controlled by the GTPase activity of FtsZ [23, 41]. The effect of these compounds on the GTPase activity of *S. aureus* FtsZ was measured from the half-maximal inhibitory concentration (IC_{50}). As shown in Table 2.1, berberine was found to moderately reduce the GTPase activity of *S. aureus* FtsZ in a concentration-dependent manner with an IC_{50} value of 272 $\pm$ 46.6 μM, which is similar to the inhibitory activity against *w*Bm-FtsZ [54]. Compound **1** (berberrubine) also inhibited the GTPase activity of *S. aureus* FtsZ although it is less potent than berberine This may be due to the lack of methyl group in the C-9 position compared to berberine, as the methyl protons were found to interact with FtsZ protein via STD-NMR [35]. Compound **2** and compound **3** displayed very weak inhibition of *S. aureus* FtsZ GTPase (15 $\pm$ 5% at 2 mM compound concentration). The results of combination test (compound **1** plus compound

2 or compound **3**, concentration 1:1) and the inhibition activity of compound **4** were very similar to that of compound **1**. The concentration-response curves for berberine, berberrubine and compound **4** against *S. aureus* FtsZ are shown in Figure 2.5. As shown in Figure 2.6, compounds **B1** and **B1-1** exhibited a linear decrease in the GTPase activity with increase in concentration similar to their parent compound; Compound **B1** showed an affinity 5-folds higher than berberine, and compound **B1-1** was slightly less potent than **B1**. The flat aromatic scaffold of 9-phenoxyalkyl group in **B1** and **B1-1** might interact with FtsZ through π-stacking, which makes **B1** and **B1-1** more potent than compound **4** which has only a bromoalkyl linker in the C-9 position.

Table 2.1 IC_{50} values of berberine and its derivatives on the inhibition of GTPase activity of *S. aureus* FtsZ

Compound	IC_{50} ± SEM[a] (μM)
berberine	272 ± 46.6
1	320.83 ± 64.2
2	NE[b]
3	NE[b]
4	240.43 ± 30.3
1 + 2	283 ± 45.4
1 + 3	292 ± 53.3
B1	56.8 ± 10.4
B1-1	63.5 ± 4.7

[a] SEM: standard error of the mean

[b]NE: no effect at a high concentration (2 mM)

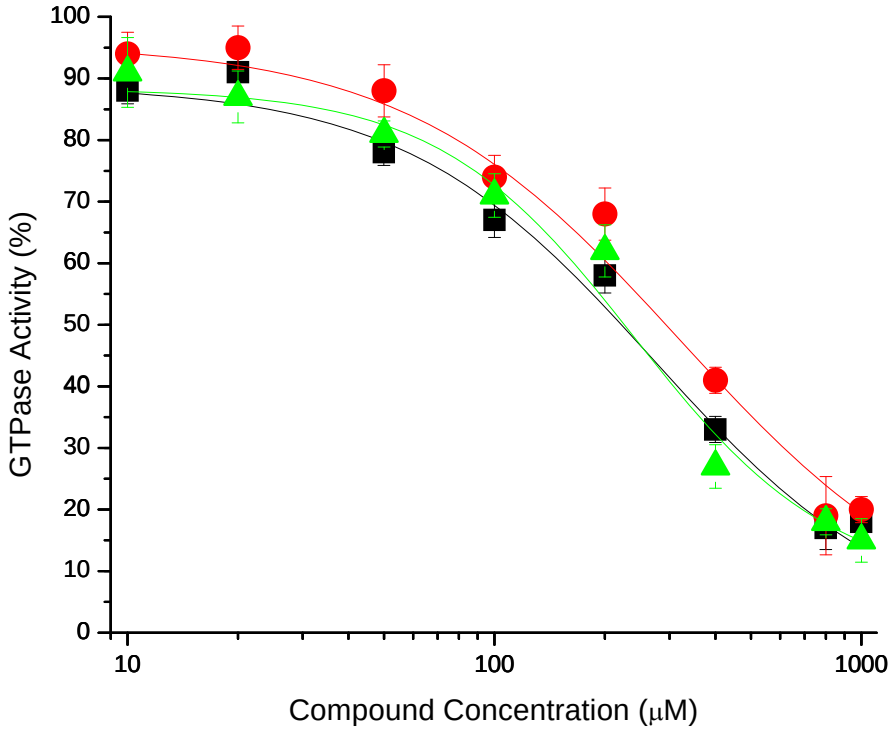

Figure 2.5 Concentration-response curve of berberine (■), berberrubine (●) and compound **4** (▲) on the inhibition of GTPase activity of *S. aureus* FtsZ. Each point represents the mean of three independent assays, and the vertical bars show the standard derivation of the mean. The IC_{50} was calculated by nonlinear regression using a sigmoidal concentration-response curve (Origin Software).

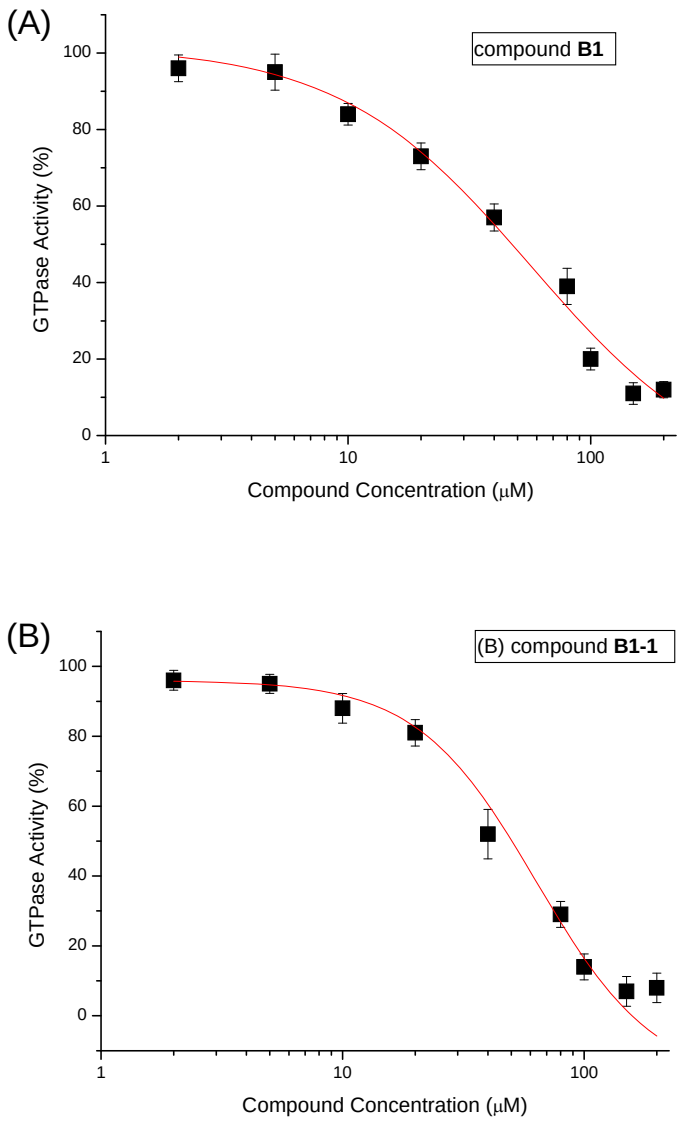

Figure 2.6 Concentration-response curve of **B1** (A) and **B1-1** (B) on the inhibition of GTPase activity of *S. aureus* FtsZ. Each point represents the mean of three independent assays, and the vertical bars show the standard derivation of the mean. The IC_{50} was calculated by nonlinear regression using a sigmoidal concentration-response curve (Origin Software).

2.3.1.2 Antimicrobial activity

Since FtsZ is an intracellular protein in bacteria, the small molecular inhibitors identified should be cell permeable and able to penetrate through the bacterial cell wall. The antimicrobial activities of **1** plus **2** or **3** (the concentrations of compound 2 and 3 were fixed at 2500 μg/mL) were determined by measuring the minimal inhibitory concentrations (MICs) against *S. aureus* ATCC 29213, *E. coli* ATCC 29522 and *B. subtilis* 168 for their potency and activity spectrum. In line with Clinical and Laboratory Standards Institute (CLSI) approved standards, the reproducibility of the MIC test is within one 2-fold dilution of the actual end point [93]. The MIC values are summarized in Table 2.2. The antibacterial activities of these compounds were compared with those of berberine, ampicillin, kanamycin sulfate and some literature reported FtsZ inhibitors (Table 2.3). The results indicated that **B1** and **B1-1** have broad spectrum antibacterial activity, whereas berberine, the parent compound, only inhibits the Gram-positive strains. **B1** and **B1-1** strikingly kill *S. aureus* ATCC 29213 at 4 μg/mL and *B. subtilis* 168 at around 8 μg/mL, which are similar to kanamycin sulfate

and much more potent than berberine, but weaker than ampicilllin and PC190723. Comparing the data of **1**, **1 + 2**, **1 + 3**, and **4** with **B1** and **B1-1**, it is clear that **B1** and **B1-1** which have phenoxyalkyl substituted group in the C-9 position possess stronger antibacterial activity. It is noted that compounds which exhibit higher GTPase inhibitory activity also show stronger antibacterial activity, as shown by a comparison of the results in Table 2.1 and Table 2.2.

As a whole, **B1** is much more active than the parent compound as well as **1** to **4** against both Gram-positive and Gram-negative bacteria. It has slightly stronger inhibitory effect on GTPase activity of *S.aureus* FtsZ than compound **B1-1**. Therefore, more derivatives based on **B1 (B2 to B6)** were prepared and their biological activities were tested. The results will be discussed in the next section.

Table 2.2 MICs of berberine, **B1**, **B1-1** and compounds **1** to **4** against

Gram-positive and Gram-negative bacteria

Organism	MIC (μg/mL)								
	Berberine	**1**	**2**	**3**	**4**	**Cpd 1 + 2**	**Cpd 1 + 3**	**B1**	**B1-1**
S. aureus ATCC 29213	128	>128	>2500	>2500	112	>128	>128	4	4
B. subtilis 168	128	>128	>2500	>2500	112	>128	>128	8	6
E. coli ATCC 25922	512	>512	>2500	>2500	384	>512	>512	96	96

Table 2.3 MICs of positive controls against Gram-positive and Gram-negative bacteria

Organism	MIC (μg/mL)					
	Ampicillin	Kanamycin	Totarol	Cinnamaldehdye	3-MBA	PC190723※
B. subtilis 168	0.1	2	1.5	250	2500	1
E. faecalis ATCC 29212	6	n.d.	n.d.	n.d.	n.d.	n.d.
E. faecium ATCC 49624	3	n.d.	n.d.	n.d.	n.d.	n.d.
E. coli ATCC 25922	6	64	400	500	>2500	n.d.
S. epidermidis ATCC 12228	3	n.d.	1.5	250	n.d.	1
S. aureus ATCC 29213	1.5	8	1.5	250	2500	1
S. aureus ATCC 29247	48	8	n.d.	n.d.	n.d.	n.d.

n.d. is not determined

※ is reported by David J. Haydon *et al* [44].

2.3.2 Biological study of berberine, compounds B1, B1-1, B2 to B6

In this section, five derivatives of compound **B1** (**B2 to B6**) were synthesized to investigate the effect of substituents on the 9-phenoxyalkyl group on FtsZ activity and bacterial growth. The chemical structures of these compounds are shown in Figure 2.7.

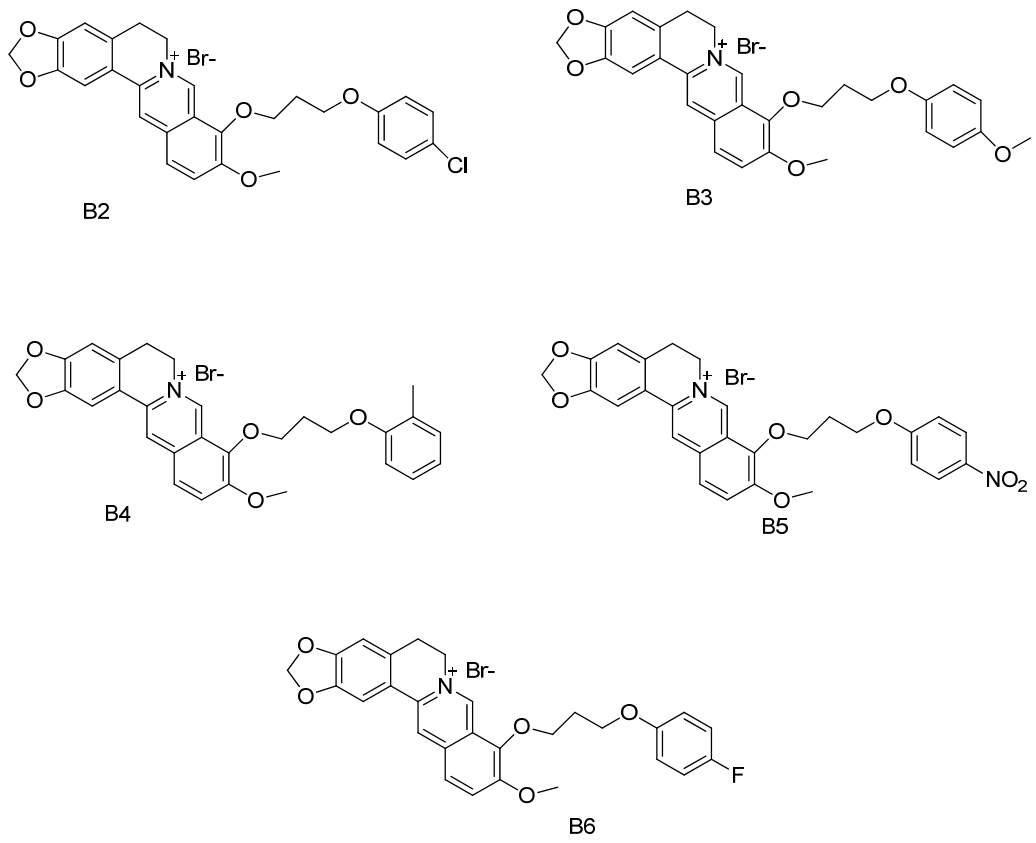

Figure 2.7 Chemical structures of **B2** to **B6**.

2.3.2.1 *In vitro* biological study

2.3.2.1.1 GTPase activity

Compounds **B2 to B6** were firstly tested against the GTPase activities of *S. aureus* FtsZ *in vitro*. The IC_{50} values of these compounds are summarized in Table 2.4. All compounds demonstrated a linear decrease in the GTPase activity with an increase in compound concentration. For instance, the concentration-response curves for compounds **B2** and **B4** against *S. aureus* FtsZ are shown in Figure 2.8. As shown in Table 2.4, compounds **B2** to **B6** inhibited the GTPase activity of *S. aureus* FtsZ with IC_{50} values between 37.8 to 63.7 μM, and these results are similar to that of compound **B1** (Table 2.1). Among these compounds, **B2**, **B3**, **B5** and **B6** were found to exert a slightly stronger effect than **B1** and **B4**. This may be due to the electron density change caused by the substituent groups in the para-position of phenyl group. As a whole, these compounds do not show significant difference in the inhibition of GTPase activity of FtsZ.

Table 2.4 IC_{50} values of compounds **B2** to **B6** on the inhibition of GTPase activity of *S. aureus* FtsZ

Compound	$IC_{50} \pm SEM^{a}$ (μM)
B2	37.8 ± 3.8
B3	47.3 ± 4.6
B4	63.7 ± 4.8
B5	43.4 ± 5.2
B6	40.2 ± 3.4

[a] SEM: standard error of the mean

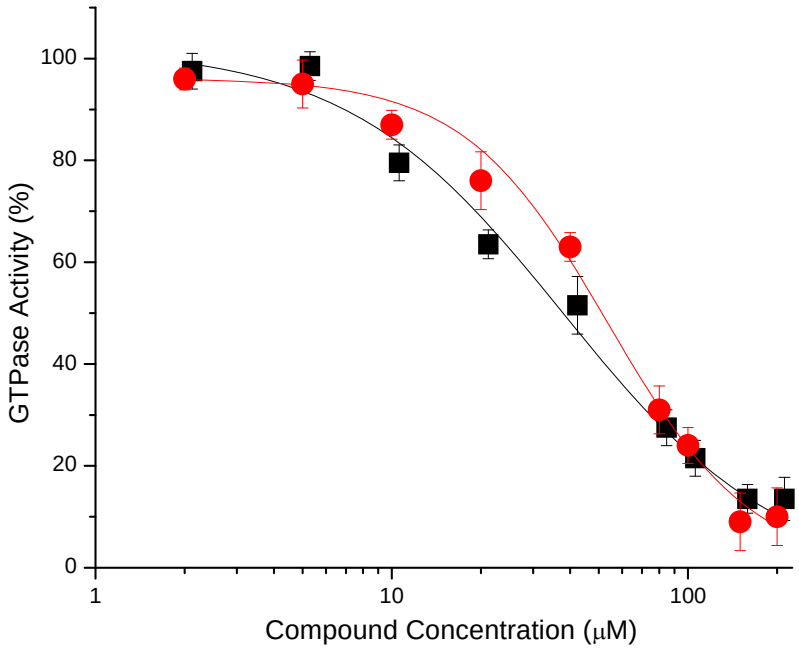

Figure 2.8 Concentration-response curve of **B2** (■) and **B4** (●) on the inhibition of GTPase activity of *S. aureus* FtsZ. Each point represents the mean of three independent assays, and the vertical bars show the standard derivation of the mean. The IC_{50} was calculated by nonlinear regression using a sigmoidal concentration-response curve (Origin Software).

2.3.2.1.2 Light scattering assay

The inhibitory activity of berberine and its derivatives for *S. aureus* FtsZ polymerization and depolymerization was investigated by light scattering assay. This assay can be used to trace the dynamics of FtsZ assembly into protofilaments *in vitro*, because light scattering signal at 600 nm is directly proportional to the polymer mass of FtsZ [94]. Berberine and compounds **B1** and **B2** were evaluated for their ability to inhibit the polymerization of the wild-type *S. aureus* FtsZ. Berberine can moderately inhibit the light scattering signal of FtsZ assembly. The decrease in light scattering intensity of the FtsZ assembly in the presence of berberine indicates the decrease in the polymer mass of FtsZ protofilaments. Figure 2.9 shows the effect of berberine on the kinectics of FtsZ assembly *in vitro*, and around 80 % inhibition was achieved at 500 μM. **B1** and **B2** can strongly inhibit FtsZ polymerization in a dose-dependent manner; around 60 % and 80 % inhibition were achieved at 35 μM of **B1** and **B2** respectively. The results are summarized in Figure 2.10 and Figure 2.11. The addition of compound **B1** or **B2** resulted in weaker light scattering

signals suggesting that they inhibited the assembly and bundling of FtsZ protofilaments *in vitro*. Comparing with berberine, **B1** and **B2** are much more potent in inhibiting the polymerization of *S. aureus* FtsZ. These results suggest that they have higher affinity to FtsZ than their parent compound.

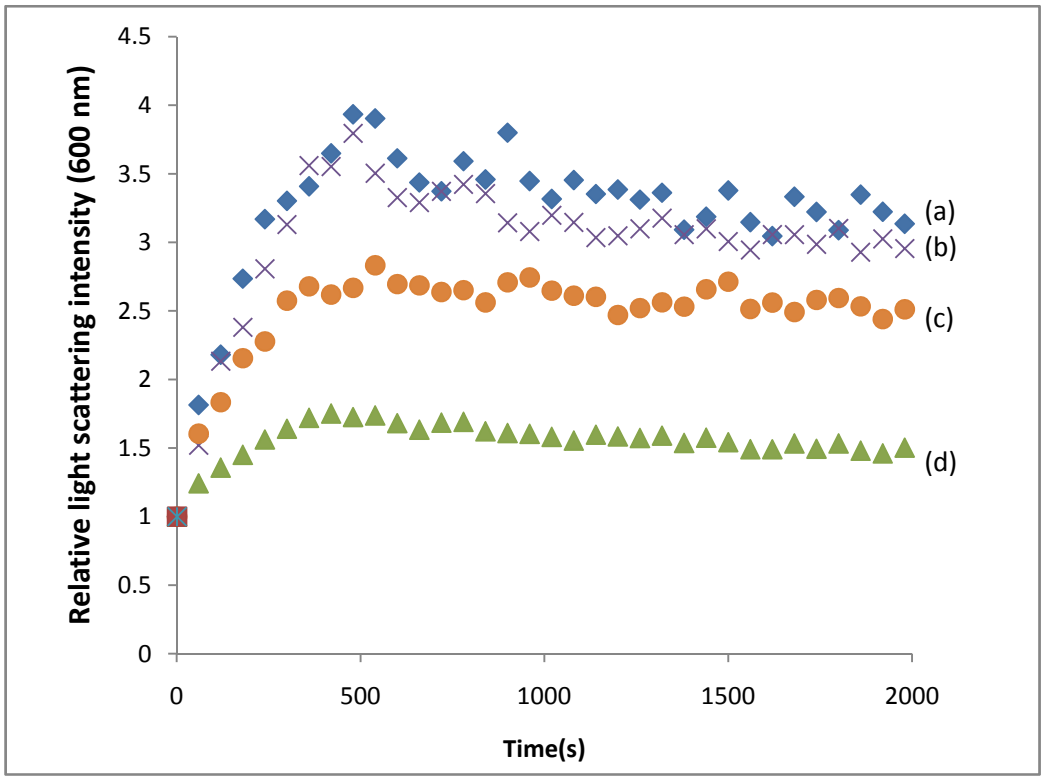

Figure 2.9 Effect of berberine on FtsZ assembly *in vitro*. *S. auerus* FtsZ (6 μM) was polymerized in 50 mM MOPS, pH 6.5, 50 mM KCl, 10 mM $MgCl_2$ and 1 mM GTP in the absence of berberine (a), in the presence of 100 μM (b), 200 μM (c) and 500 μM (d) of berberine. Appropriate blanks were subtracted from all the traces. Each experiment was repeated three times.

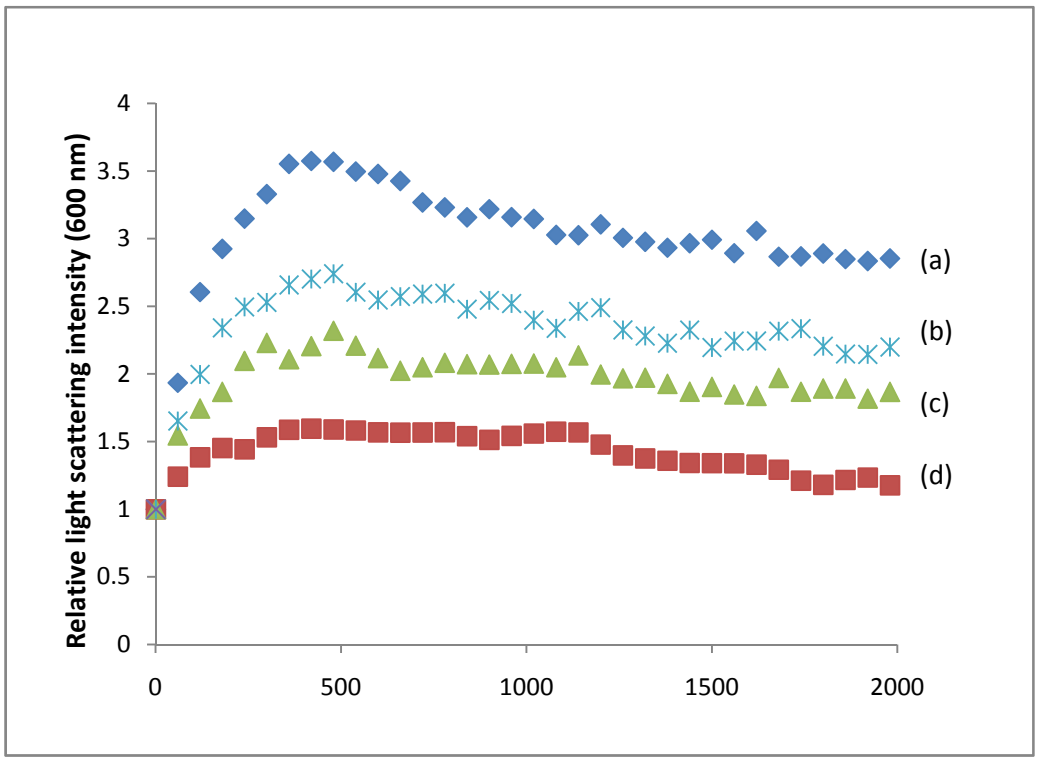

Figure 2.10 Effect of **B1** on FtsZ assembly *in vitro*. *S. auerus* FtsZ (6 μM) was polymerized in 50 mM MOPS, pH 6.5, 50 mM KCl, 10 mM $MgCl_2$ and 1 mM GTP in the absence of **B1** (a), in the presence of 15 μM (b), 35 μM (c) and 70 μM (d) of **B1**. Appropriate blanks were subtracted from all the traces. Each experiment was repeated three times.

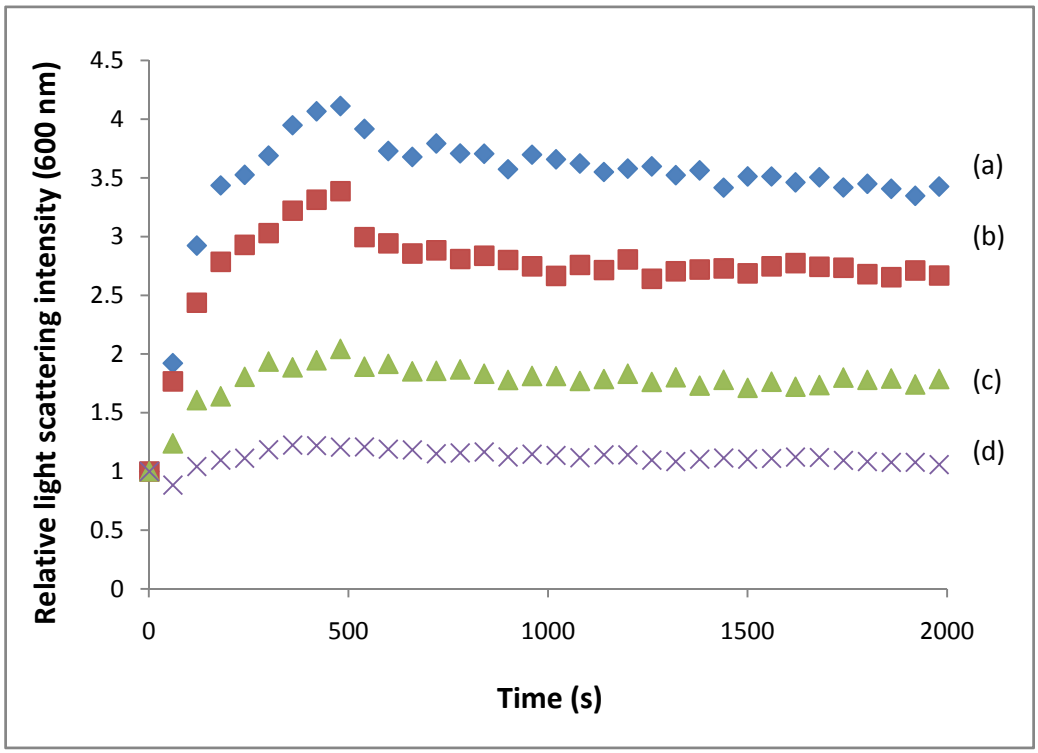

Figure 2.11 Effect of **B2** on FtsZ assembly *in vitro*. *S. auerus* FtsZ (6 μM) was polymerized in 50 mM MOPS, pH 6.5, 50 mM KCl, 10 mM $MgCl_2$ and 1 mM GTP in the absence of **B2** (a), in the presence of 15 μM (b), 35 μM (c) and 70 μM (d) of **B2**. Appropriate blanks were subtracted from all the traces. Each experiment was repeated three times.

2.3.2.1.3 Transmission electron microscopy (TEM) analysis

The effect of berberine, compounds **B1** and **B2** on the assembly of *S. aureus* FtsZ protofilament was also examined by transmission electron microscopy. The electron microscopic images for berberine, compounds **B1** and **B2** are shown in Figures 2.12 – 2.14 respectively. These three compounds inhibited FtsZ protofilaments in a dose-dependent manner. In the absence of compounds, a dense network of FtsZ protofilaments with an average width of 120 ± 24 nm was observed (Figures 2.12 A – 2.14 A). Berberine can reduce the size and thickness of FtsZ polymers at a high concentration (Figure 2.12 B and C). On the other hand, **B1** and **B2** were found to drastically reduce the size and thickness of FtsZ polymers and the bundling of FtsZ protofilaments at much lower concentrations than their parent compound. **B1** (8.8 μM) and **B2** (4.08 μM) reduced the thickness of the bundles of FtsZ protofilaments by 60% to 70% respectively (Figures 2.13 B and 2.14 B). For instance, **B2** (4.08 μM) reduced the thickness of FtsZ protofilaments from 120 ± 24 nm to 38 ± 7 nm. Only a few straight, short and thin FtsZ filaments were observed in the presence of 26.4 μM **B2**

(Figure 2.14 C). On the contrary, the parent compound was found to incompletely inhibit the polymerization and bundling of FtsZ protofilaments (Figure 2.12). The above observations suggested that **B1** and **B2** may disturb and weaken the lateral interaction between FtsZ protofilaments as well as the interaction between FtsZ monomers, resulting in a reduction in bundling and thickness of FtsZ protofilaments.

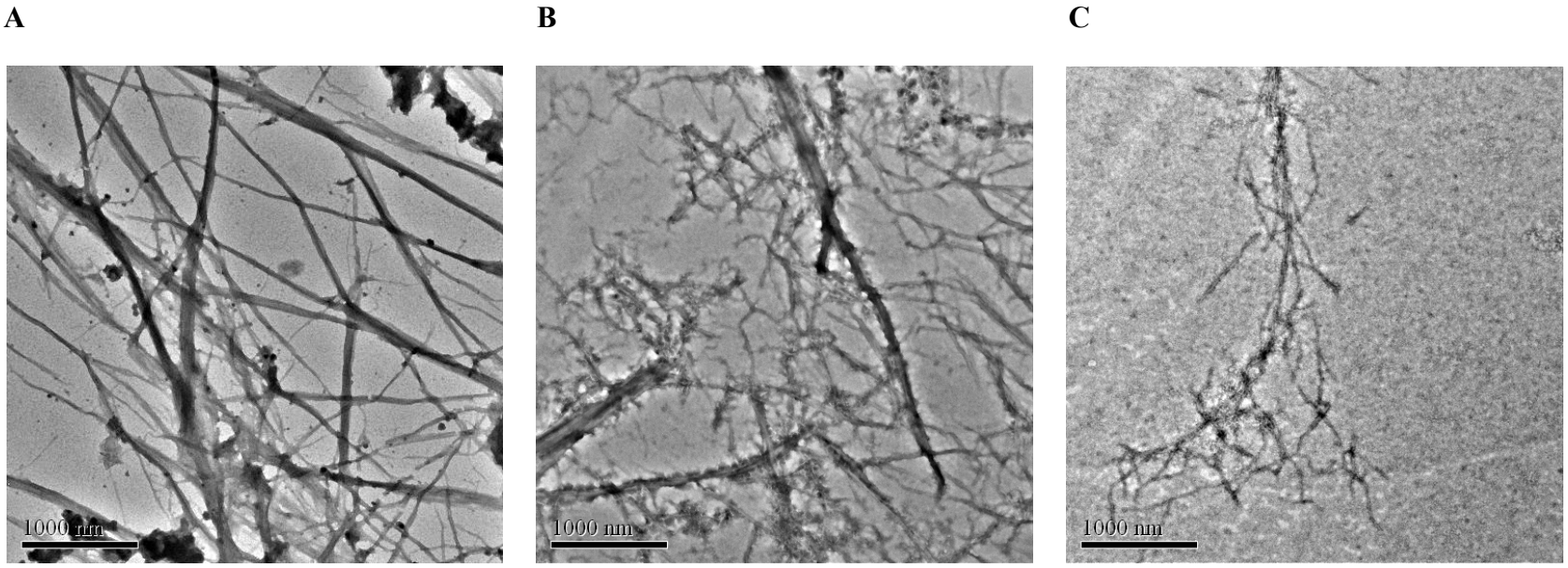

Figure 2.12 Electron micrographs of FtsZ polymers. *S. auerus* FtsZ (12 μM) was polymerized in 50 mM MOPS buffer, pH 6.5, containing 50 mM KCl, 5 mM $MgCl_2$, and 1 mM GTP in the absence and presence of berberine for 15 min at 37 ^{o}C. The pictures shown are the electron micrographs of FtsZ polymers formed in the absence (A) and presence of 200 μM (B) and 500 μM (C) of berberine. The scale bar is 1000 nm.

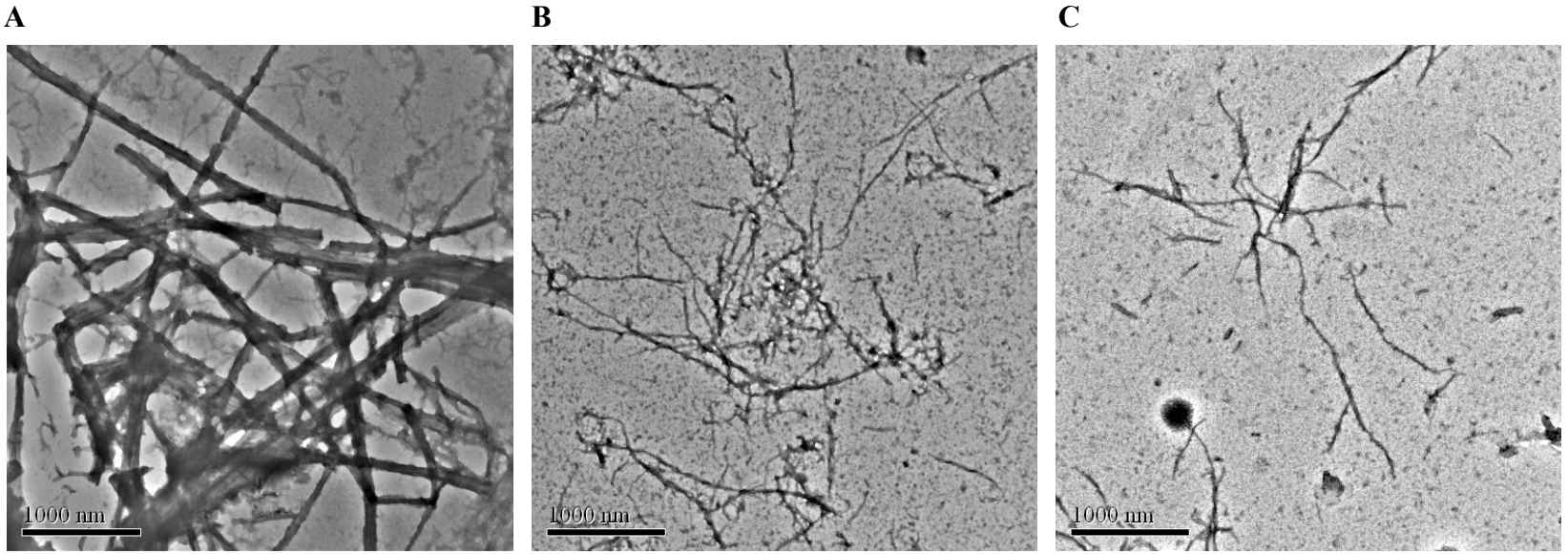

Figure 2.13 Electron micrographs of FtsZ polymers. *S. auerus* FtsZ (12 μM) was polymerized in 50 mM MOPS buffer, pH 6.5, containing 50 mM KCl, 5 mM $MgCl_2$, and 1 mM GTP in the absence and presence of **B1** for 15 min at 37 ^{o}C. The pictures shown are the electron micrographs of FtsZ polymers formed in the absence (A) and presence of 4 μg/mL (8.8 μM) (B) and 12 μg/mL (26.4 μM) (C) of **B1**. The scale bar is 1000 nm.

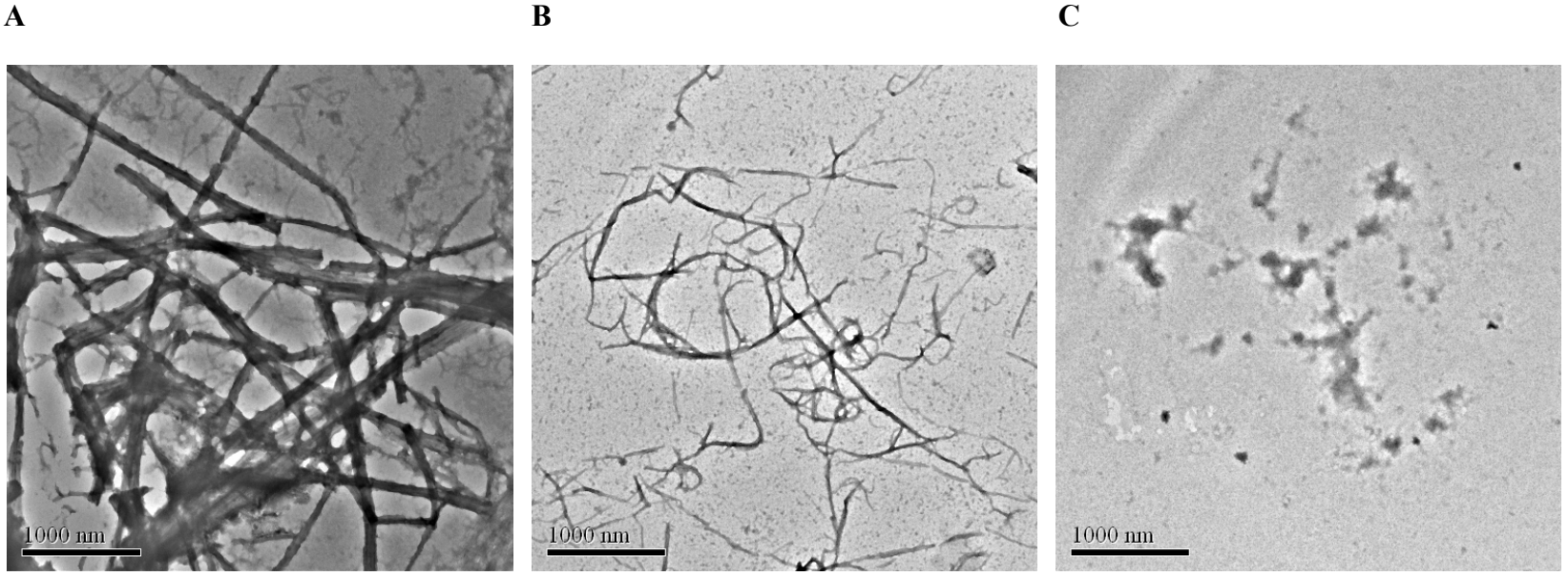

Figure 2.14 Electron micrographs of FtsZ polymers. *S. auerus* FtsZ (12 μM) was polymerized in 50 mM MOPS buffer, pH 6.5, containing 50 mM KCl, 5 mM $MgCl_2$, and 1 mM GTP in the absence and presence of **B2** for 15 min at 37 ^{o}C. The pictures shown are the electron micrographs of FtsZ polymers formed in the absence (A) and presence of 2 μg/mL (4.08 μM) (B) and 8 μg/mL (16.32 μM) (C) of **B2**. The scale bar is 1000 nm.

2.3.2.1.4 Saturation transfer difference (STD) NMR spectroscopy

STD NMR spectroscopy is commonly used to characterize binding and identify epitopes of the ligand that bind to a protein receptor [92, 95, 96]. To determine the pharmacophoric groups of the ligand bound to FtsZ, 1D STD NMR spectroscopy was performed [3, 35, 38]. The STD NMR spectroscopy detected the magnetization that was transferred from FtsZ to the bound ligand protons. To identify the regions of the 9-phenoxyalkyl substituted berberine derivatives involved in FtsZ binding, the STD NMR spectra of **B2** and **B3** in the presence of *S. aureus* FtsZ were recorded. Samples typically contained a 50-fold excess of **B2** or **B3** (1.0 mM) relative to FtsZ (20 μM). Selective irradiation of the signal from FtsZ (on resonance spectrum) that is not overlapping with the ligand signal exclusively transfers the effective magnetization via spin diffusion from FtsZ to the compound. Subtraction of the above spectrum from a reference proton NMR spectrum (Figures 2.15 A and 2.16 A) in which the FtsZ is not saturated resulted in the STD NMR spectrum (Figures 2.15 B and 2.16 B). Figures 2.15 B, C and Figures 2.16 B, C reflect the protons of **B2** and **B3** which interact with FtsZ respectively.

It was found that apart from the protons in the isoquinoline core of berberine, which have been reported to bind to FtsZ [35], protons H17 and H18 in the substituted phenoxy group also contribute to the STD NMR signal (the proton peaks from 0 – 5 ppm cannot be detected due to the solvent effect and the precipitation of compounds **B2** and **B3**). The finding, together with the results of light scattering and GTPase activity assays, suggest that the stronger inhibitory effect of **B2** and **B3** may be caused by the interaction between the substituted phenoxy group and FtsZ.

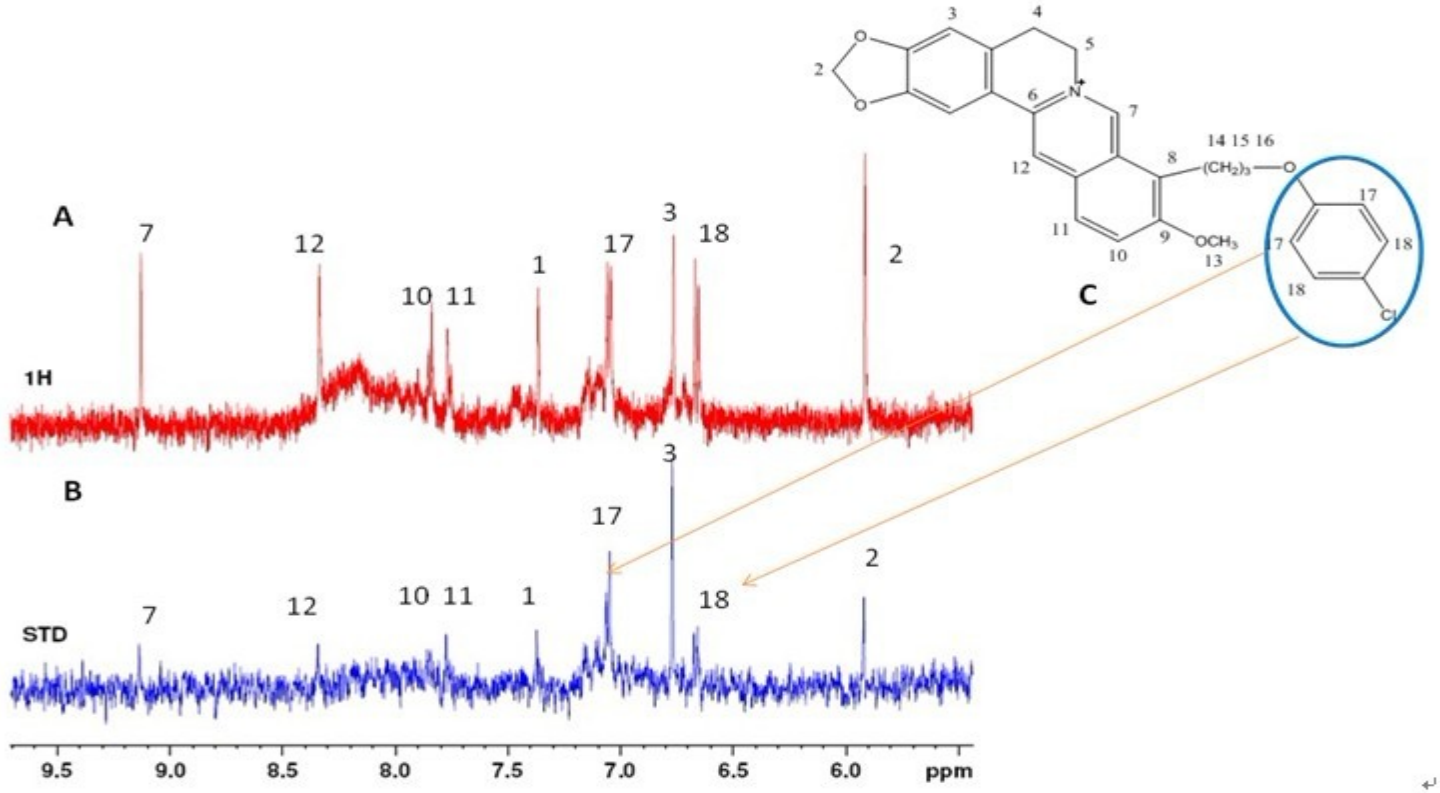

Figure 2.15 STD NMR spectra of the FtsZ – **B2** complex. (A) Reference 1D NMR spectrum. (B) Corresponding STD NMR spectrum showing that **B2** binds to FtsZ. (C) Structure and group epitope mapping of **B2**.

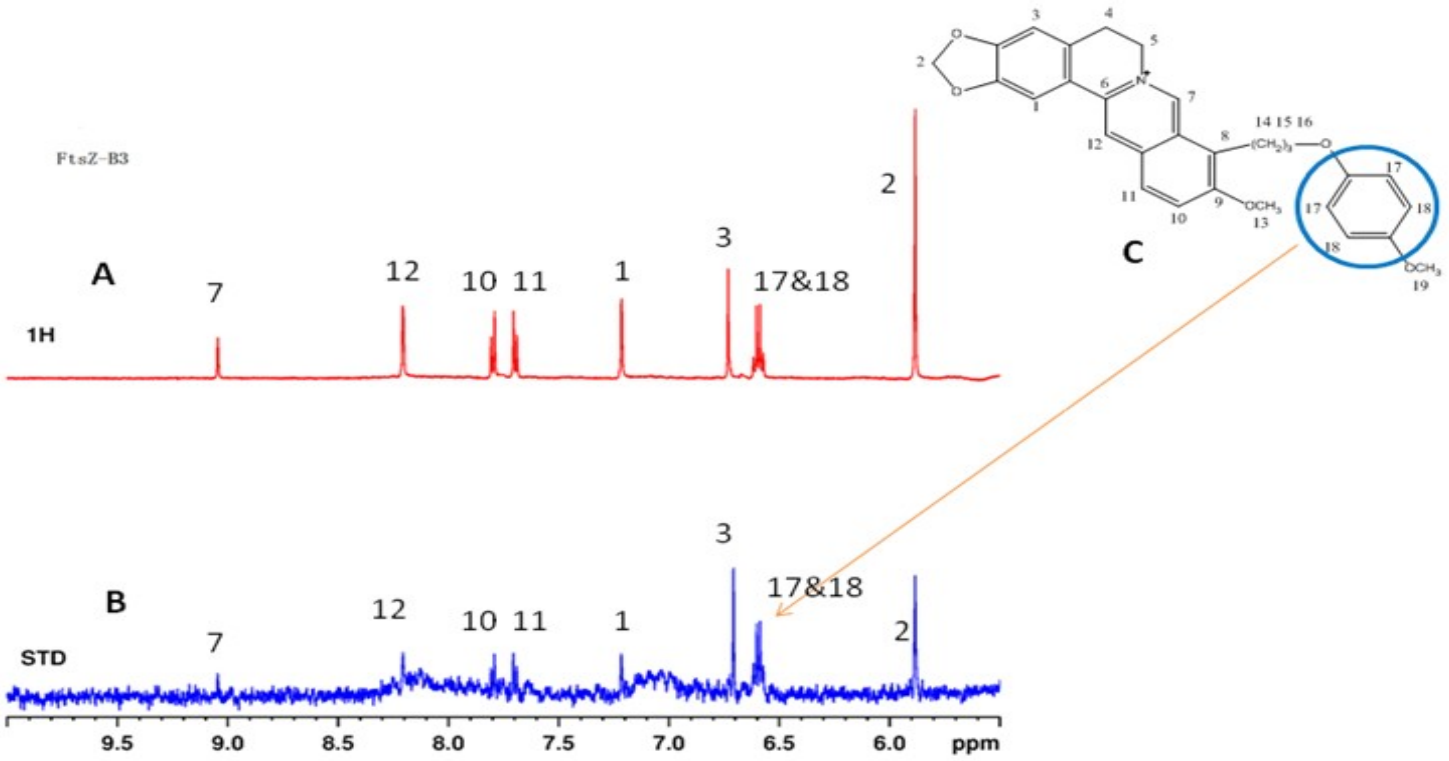

Figure 2.16 STD NMR spectra of the FtsZ – **B3** complex. (A) Reference 1D NMR spectrum. (B) Corresponding STD NMR spectrum showing that **B3** binds to FtsZ. (C) Structure and group epitope mapping of **B3**.

2.3.2.2 *In vivo* biological study

2.3.2.2.1 Antimicrobial activity of 9-phenoxyalkyl substituted berberine derivatives

To test the effect of 9-phenoxyalkyl substituted berberine derivatives *in vivo*, the MICs of the compounds against a range of Gram–positive and –negative bacterial strains were determined. The MIC values of these compounds are tabulated in Table 2.5. The results revealed that derivatives bearing phenoxyalkyl group in the C-9 position of berberine not only caused lethality on *S. aureus* and *E. coli* cells, but also possessed higher potency and exhibited a broader spectrum of antibacterial activity than their parent compound. These derivatives inhibited the growth of drug sensitive and drug resistant *S. aureus* with MIC values of 2—8 μg/mL. The growth of drug sensitive and vancomycin-resistant *E. faecium* were inhibited with MIC values of 4—16 μg/mL. In addition, it was found that compounds **B2**, **B5** and **B6** with halogen or nitro substituents demonstrated greater potency than the others against various bacterial strains, especially on the

Gram-negative strains. The halogens and the nitro group may enhance the permeability of these compounds to the bacterial strains. Similar observation has been reported for the alkoxybenzamide inhibitors of FtsZ [97]. As a whole, addition of the phenoxyalkyl group in the C-9 position of berberine resulted in a substantial improvement in antibacterial activity. Some derivatives, like **B2** and **B5**, even have a better antimicrobial activity than ampicillin against the Gram-positive strains (Table2.3).

Table 2.5 A MICs of berberine derivatives against Gram-positve bacteria

Organism	MIC (μg/mL)					
	B1	**B2**	**B3**	**B4**	**B5**	**B6**
B. subtilis 168	8	4	8	8	8	4
S. aureus ATCC 29213	4	2	8	4	2	2
S. aureus ATCC 29247	4	2	8	4	2	2
S. aureus ATCC BAA-41	4	2	8	4	2	2
E. faecium ATCC 49624	8	4	16	8	4	4
E. faecium ATCC 700221	8	4	16	8	8	4
E. faecalis ATCC 29212	16	4	32	8	8	4
S. epidermidis ATCC 12228	4	2	4	4	2	2

S. aureus ATCC 29247 is an ampicillin-resistant *S. aureus* strain.

S. aureus ATCC BAA-41 is a methicillin-resistant *S. aureus* (MRSA) strain.

E. faecium ATCC 700221 is a vancomycin-resistant *E. faecium* strain.

Table 2.5 B MICs of berberine derivatives against Gram-negative bacteria

Organism	MIC (μg/mL)					
	B1	**B2**	**B3**	**B4**	**B5**	**B6**
E. coli ATCC 25922	96	32	128	96	32	32
E.cloacae ATCC BAA-1143	>128	32	>128	>128	32	32
K. pneumoniae ATCC BAA-1144	128	64	128	64	64	64

2.3.2.2.2 Effects of berberine, compounds B1 and B2 on the morphology of *B. subtilis* cells

To determine whether these 9-phenoxyalkyl substituted berberine derivatives possess *in vivo* on-target activity, **B1** and **B2** were tested for their effect on bacterial cell morphology against *B. subtilis* 168 strain. Berberine and 3-MBA were also tested as positive controls. The log-phase culture of *B. subtilis* 168 was treated with 1% DMSO or the four compounds; the final concentrations of the compounds were half of the MICs values. Untreated *B. subtilis* cells have typical short rod morphology (Figure 2.17 A). After treatment with the above-mentioned compounds, the cell morphology of *B. subtilis* was found to become long rod shaped. The microscopic results indicated that **B1** and **B2** had the ability to inhibit bacterial cell division, causing filamentation of *B. subtilis* cells (Figure 2.17 D and E). The results obtained were similar to the positive controls (Figure 2.17 B and C). The average cell length of untreated *B. subtilis* was about 3.7 ± 1 μm (Figure 2.17 A). These four compounds were found to cause lengthening in cell size of *B. subtilis* from 12 folds to 18 folds (Figure 2.17

B-E). For example, **B2** extended the average cell length of *B. subtilis* from 3.7 ± 1 μm to 72 ± 10 μm. The effect of berberine, **B1** and **B2** on the length of *B. subtilis* 168 cells are compared in Figure 2.18. In the absence of compounds, the length of the *B. subtilis* 168 cells were found to be within 0—5 μm (89 %) and 5—10 μm (11 %) respectively. When the *B. subtilis* 168 cells were treated with **B2** (4 μM), only 7% and 18% cells were found to be within 0—5 and 5—10 μm respectively. 75% of the cells were longer than 10 μm length. **B1** produced a similar distribution of the *B. subtilis* cell length. Comparing with berberine, **B1** and **B2** showed a stronger inhibitory effect on the proliferation of *B. subtilis* cells, and the average cell length of *B. subtilis* was increased by 2—3 folds, which are in line with the antibacterial activity and *in vitro* tests of these compounds.

A **B** **C**

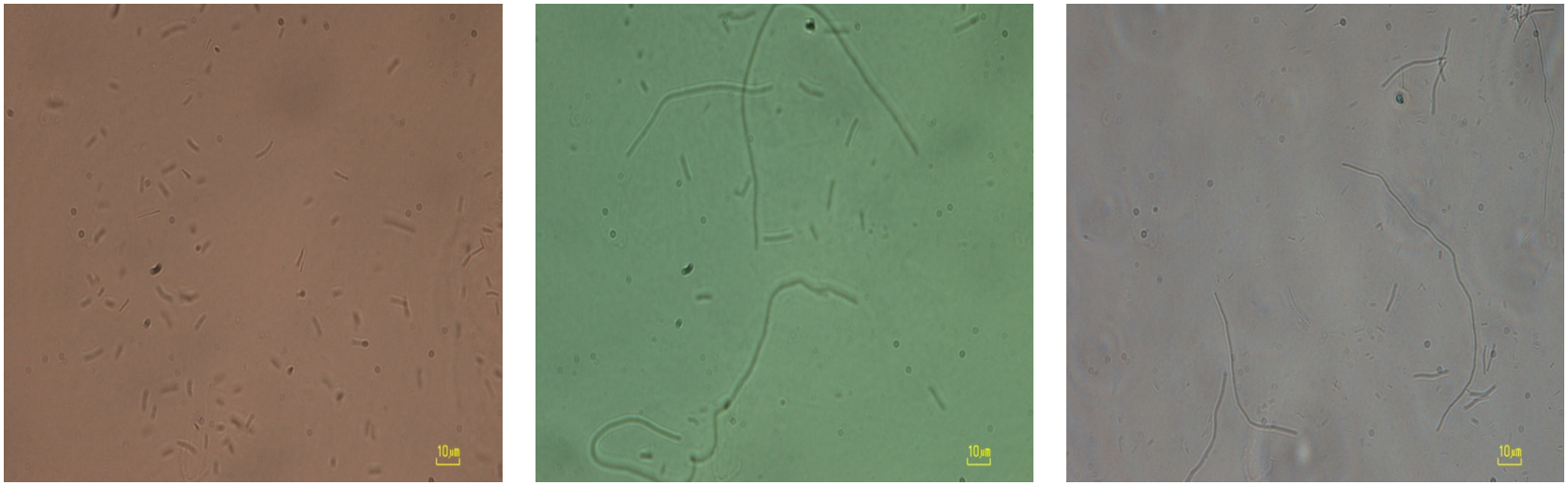

Figure 2.17 Effects of berberine, 3-MBA, **B1** and **B2** on cell division and cell morphology. *B. subtilis* 168 cells were grown for 4 h in the absence (A) or presence of 172 μM of berberine (B) or 8.3 mM of 3-MBA (C) or 8.8 μM of **B1** (D) or 4 μM of **B2** (E). The cells were observed under a phase contrast microscope. The scale bar is 10 μm. Each experiment was repeated 3 times. (Figures 2.17 D and E are shown in the next page.)

D

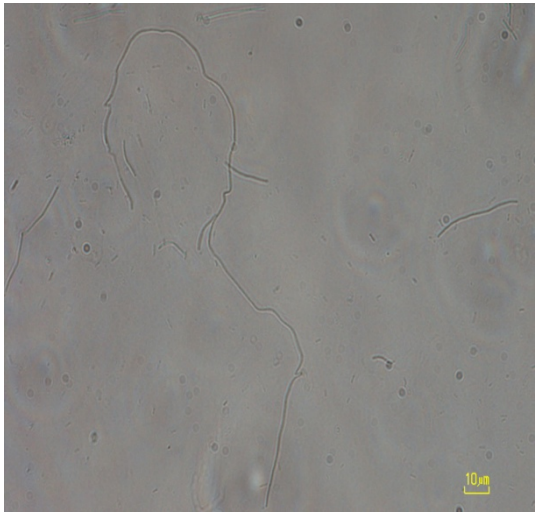

E

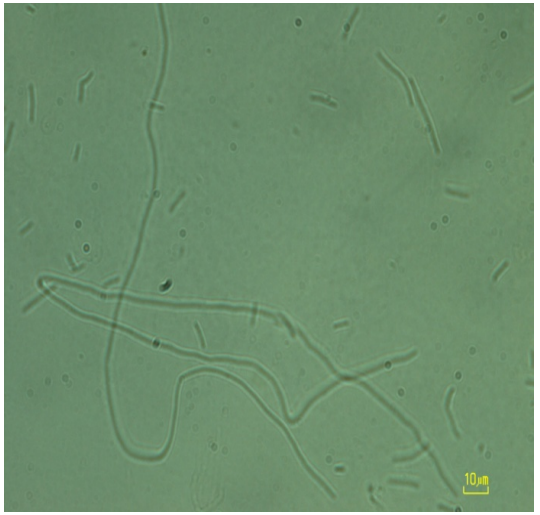

Figure 2.17 continued.....

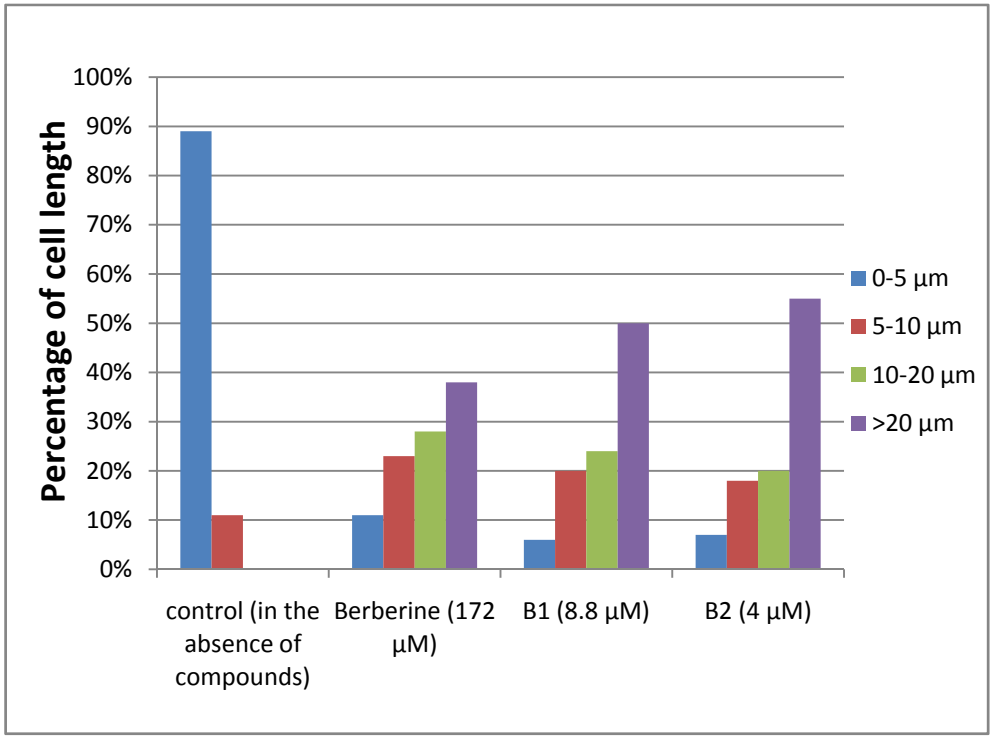

Figure 2.18 Berberine, **B1** and **B2** induced cell elongation in *B. subtilis* 168.

2.3.2.2.3 Effects of berberine and compound B2 on the cell membrane of *B. subtilis* cells

Because the perturbation of cell membrane may also lead to cell lysis [36], the effects of berberine and compound **B2** on the cell membrane of *B. subtilis* cells were also investigated (Figures 2.19 B and C). FM 4-64, a fluorescent staining dye, was used to stain the cell membrane of overnight grown *B. subtilis* cells. As shown in Figure 2.19, although cell elongation had been induced by the compounds, integrity of membrane of *B. subtilis* cells was still observed after treatment with berberine and **B2**.

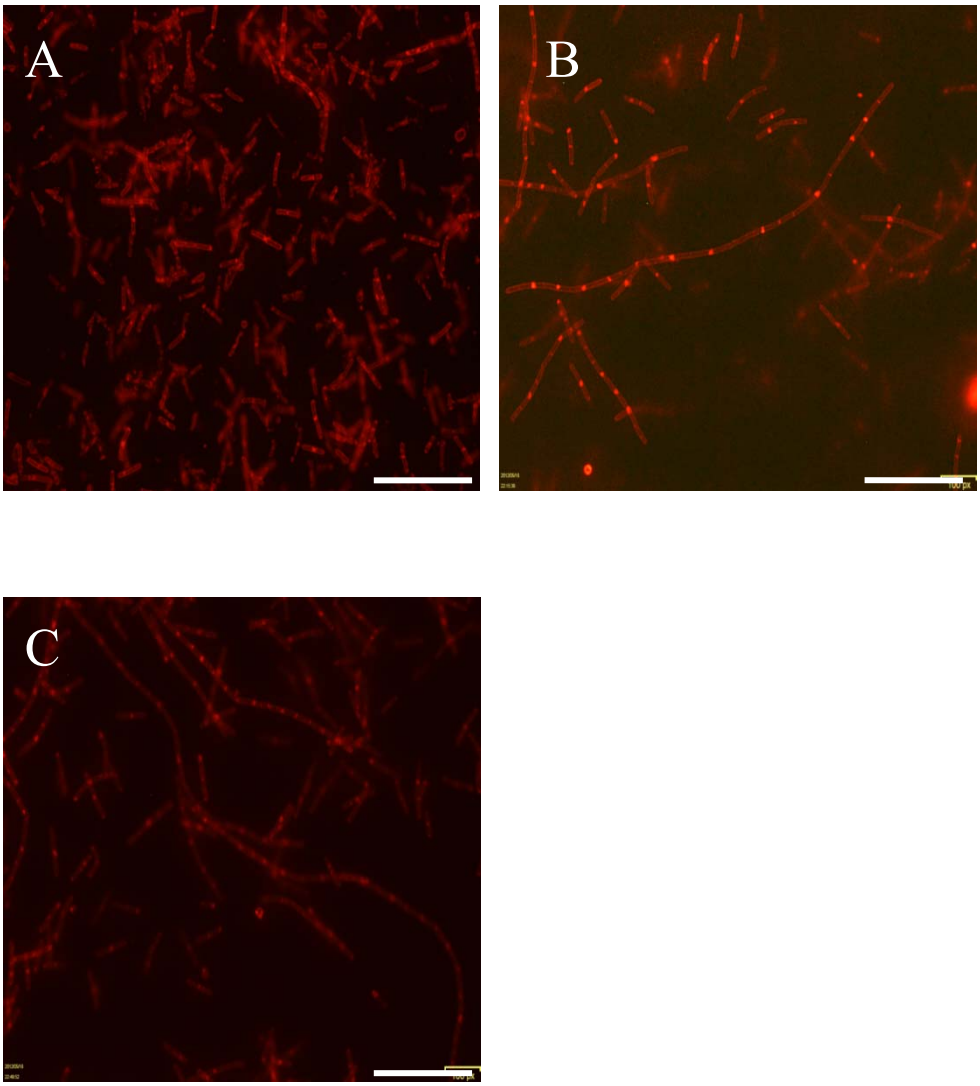

Figure 2.19 Effect of berberine and **B2** on the cell membrane of *B. Subtilis* 168. The bacterial cells were grown in the absence (A) and presence of 172 μM of berberine (B) or 4 μM of **B2** (C). The cells were then observed under a phase-contrast microscope. The scale bar is 10 μm.

2.3.2.2.4 Effects of compound B2 on the formation of cytokinetic Z-ring in *E. coli* cells

As another approach to confirm that the 9-phenoxyalkyl substituted berberine derivatives have target at the FtsZ protein, the effect of **B2** on the formation of the dynamic Z ring in *E.coli* JM109 (WM647) was studied. In rod-shaped *E. coli*, septum formation is initialized by the dynamic Z-ring during cell division. Previous studies have shown that perturbation of FtsZ function could lead to the inhibition of bacterial proliferation[34-36]. In the absence of **B2**, a fluorescent band at the cell midpoint was apparent in a high percentage of *E. coli* cells as visualized by the GFP-tagged FtsZ (Figure 2.20 A). These fluorescent bands represented the septation-competent localized Z-rings (cytoskeletal structures). In the presence of 48 μM (24 μg/mL) **B2**, GFP-FtsZ dispensed as discrete foci throughout the elongated cell (Figure 2.20 B), indicating that **B2** caused mislocalization of the FtsZ protein.

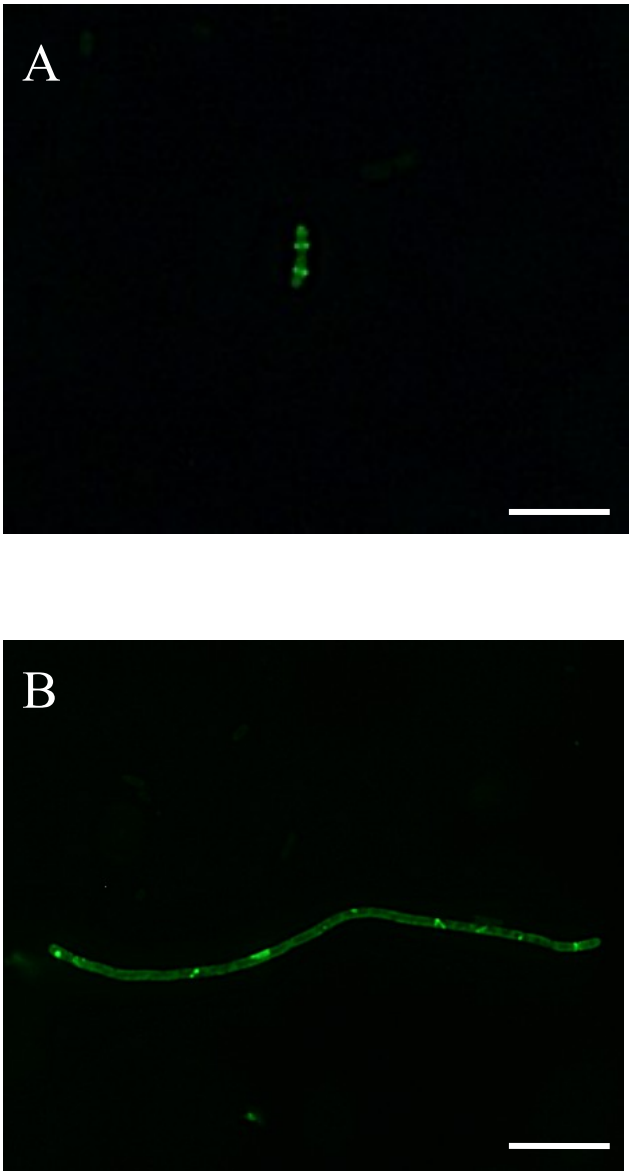

Figure 2.20 Perturbation of cytokinetic Z-ring in *E. coli* (JM109 WM647) as visualized by GFP-tagged FtsZ. The bacterial cells were grown in the absence (A) or presence of 48 μM of **B2** (B). The scale bar is 10 μm. Each experiment was repeated 3 times.

2.4 Concluding remarks

It can be concluded that all the 9-phenoxyalkyl substituted berberine derivatives exhibit stronger effect on the inhibition of FtsZ activity and against the growth of bacterial strains than berberine. The 3-carbon linker with a phenoxy group greatly improved the inhibitory activity on FtsZ. STD NMR data suggested that not only the berberine moiety binds to the GTP binding site, but also the phenoxy ring which interacts with the FtsZ protein.

Furthermore, different substituent groups were incorporated into the ortho or para position of the phenoxy group. These compounds (compounds) were proven to inhibit FtsZ effectively, although not much difference in inhibitory activity was observed among **B2** to **B6**. The study of the binding poses of these derivatives with *S.aureus* FtsZ dimer will be discussed in chapter 4.

Chapter 3

Palmatine and its 9-phenoxyalkyl substituted derivatives as FtsZ inhibitors and anti-bacterial agents

3.1 Introduction

Palmatine, like berberine, is also a protoberberine alkaloid found in some plants including *Phellodendron amurense*, *Rhizoma coptidis* and *Corydalis yanhusuo* [98]. It has been used in the treatment of dysentery, jaundice, inflammation, hypertension and liver-related diseases [99]. Recently, it was found that palmatine could potentially be used for the treatment of flavivirus infection [100]. It was also reported that palmatine has moderate antibacterial activity against some *S.aureus* strains [86, 88], but so far there is no report on its antibacterial mechanism and structure modification.

In this chapter, the effects of palmatine and its semi-synthetic 9-phenoxyalkyl derivatives on *S. aureus* FtsZ and their antimicrobial activities against various bacterial strains are reported. The chemical

structures of these compounds are shown in Figure 3.1, and the synthesis of 9-phenoxyalkyl palmatine derivatives will be described in section 3.2.

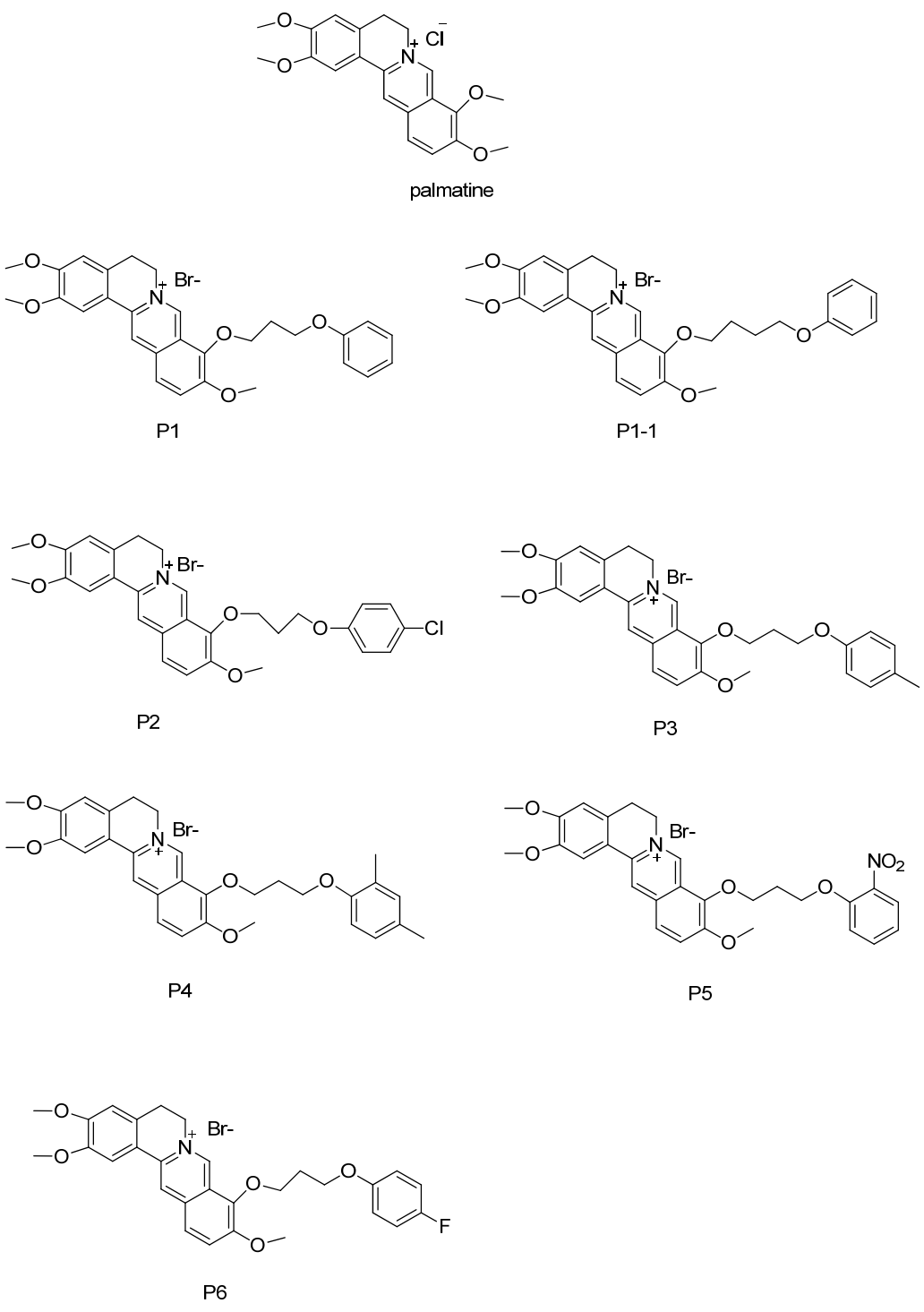

Figure 3.1 Chemical structures of palmatine and its 9-phenoxyalkyl derivatives.

3.2 Experimental section

3.2.1 Chemistry

3.2.1.1 Materials

Palmatine chloride was purchased from Shenzhen Winkey Bio-Tech Co., Ltd. 1,3-Dibromopropane, 1,4-dibromobutane, phenol, 4-chlorophenol, 2,4-dimethylphenol, *o*-cresol, 2-nitrophenol, 4-fluorophenol and potassium carbonate were purchased from Sigma-Aldrich. All the analytical grade reagents and solvent were used as received without further purification.

3.2.1.2 Instrumentation

^{1}H NMR spectra were obtained with a Bruker 400 MHz DPX-400 NMR spectrometer. Mass spectra were recorded with a Finnigan MAT 95S mass spectrometer.

3.2.1.3 Synthesis

The synthetic patheway of 9-phenoxyalkyl substituted palmatine derivatives are shown in the Scheme 3.1. Firstly, the ω-bromoalkyl ether derivatives were synthesized from the commercially available phenol derivatives following the procedures published by C. Sheng *et al.* [90]. Selective demethylation of palmatine at 180 ℃ under vacuum gave the demethyl-palmatine [101]. The target compounds (**P1** to **B6**) were obtained by reaction of demethyl-palmatine with the ω-bromoalkyl ether derivatives in acetonitrile for 12 h.

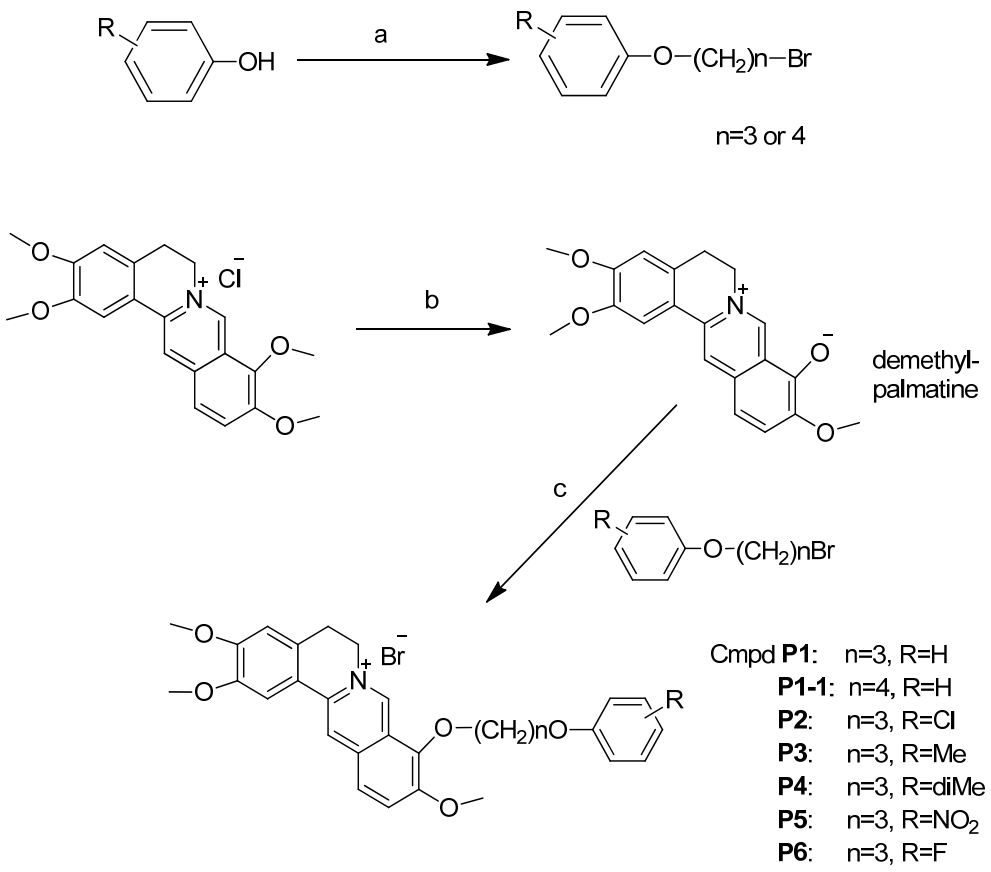

Scheme 3.1 Synthetic routes of palmatine derivatives.

Reagents and conditions: (a) $Br(CH_2)nBr$ (n=3 or 4), K_2CO_3, DMF, 70 ℃, 2 h [90]; (b) 180 ℃, under vacuum, 30 min [101]; (c) CH_3CN, 85 ℃.

3.2.1.3.1 Preparation of ω-bromoalkyl ether derivatives

A solution of a phenol derivative (2 mmol) in DMF (5 mL) was added dropwise to a stirred suspension of 1,3-dibromopropane or 1,4-dibromobutane (4 mmol) with K_2CO_3 (3 mmol) in DMF (5 mL). After stirring at room temperature for 2 h, the mixture was heated at 75 ℃ for another 2 h. The mixture was filtered, and the solution was diluted with ethyl acetate (50 mL) and washed with deionized water (3 × 50 mL). The crude product was obtained by removal of organic solvent under vacuum. The residue was purified by flash chromatography (petroleum ether / ethyl acetate = 50:1) to give the product as a colorless or light yellow oil.

3.2.1.3.2 Preparation of demethyl-palmatine

To remove the methyl group at C-9 position of palmatine, 5 mmol palmatine was heated at 180 ℃ under the vacuum for 30 - 50 min until the color of powder turned into dark brown. The powder was purified by flash chromatography (CH_2Cl_2 / MeOH = 10:1) to yield a carmine powder after solvent removal. The high resolution mass spectrum and ^{1}H NMR spectrum of demethyl-palmatine are shown in Appendices I and II respectively. Yield: 60%. ^{1}H NMR (400 MHz, DMSO-*d*6): δ 3.02 (t, *J* = 6.0 Hz, 2H), 3.69 (s, 3H), 3.78 (s, 3H), 3.85 (s, 3H), 4.46 (t, *J* = 6.0 Hz, 2H), 6.34 (d, *J* = 7.6 Hz, 1H), 6.93 (s, 1H), 7.18 (d, *J* = 8.0 Hz, 1H), 7.47 (s, 1H), 8.03 (s, 1H), 9.05 (s, 1H); ESI-MS m/z: 338.2 $[M + H]^+$.

3.2.1.3.3 Preparation of compounds P1 to P6

Demethyl-palmatine (0.15 mmol) and one of ω-bromoalkyl ether derivatives (0.5 mmol) were mixed in 10 mL acetonitrile, and stirred for 12 h at 85 ℃. After reaction, the crude product was obtained by removing the organic solvent under vacuum and then purified by flash chromatography (CH_2Cl_2 / MeOH = 25:1) to yield a yellow powder. The high resolution mass spectra and ^{1}H NMR spectra of **P1** to **P6** are shown in Appendices I and II respectively. Yield: 30 – 45 %. **P1**: ^{1}H NMR (400 MHz, $CDCl_3$): δ 2.48-2.54 (m, 2H), 3.15 (t, *J* = 6.0 Hz, 2H), 3.90 (s, 3H), 3.95 (s, 3H), 4.13 (s, 3H), 4.43 (t, *J* = 6.0 Hz, 2H), 4.61 (t, *J* = 6.0 Hz, 2H), 4.83 (t, *J* = 6.0 Hz, 2H), 6.65 (s, 1H), 6.97 (t, *J* = 7.2 Hz, 1H), 7.02 (d, *J* = 8.0 Hz, 2H), 7.32-7.35 (m, 2H), 7.51 (s, 1H), 7.59 (d, *J* = 9.2 Hz, 1H), 8.16 (d, *J* = 9.2 Hz, 1H), 8.93 (s, 1H), 9.88 (s, 1H); ESI-MS m/z: 472.2 $[M - Br]^+$; **P1-1**: ^{1}H NMR (400 MHz, DMSO-*d*6): δ 2.32-2.38 (m, 4H), 3.22 (t, *J* = 6.0 Hz, 2H), 3.88 (s, 3H), 3.95 (s, 3H), 4.02 (s, 3H), 4.27 (t, *J* = 6.0 Hz, 2H), 4.49 (t, *J* = 6.0 Hz, 2H), 4.88 (t, *J* = 6.0 Hz, 2H), 6.93-6.99 (m, 3H), 7.11 (s, 1H), 7.31 (t, *J* = 8.4 Hz, 2H), 7.72 (s, 1H), 8.03 (d, *J* = 9.2 Hz, 1H), 8.21 (d, *J* = 9.2 Hz,

1H), 9.03 (s, 1H), 9.77 (s, 1H); ESI-MS m/z: 486.2 $[M - Br]^+$; **P2**: ^1H NMR (400 MHz, DMSO-*d*6): δ 2.33 (t, *J* = 6.4 Hz, 2H), 3.21 (t, *J* = 6.0 Hz, 2H), 3.87 (s, 3H), 3.94 (s, 3H) 4.00 (s, 3H), 4.26 (t, *J* = 6.0 Hz, 2H), 4.47 (t, *J* = 6.0 Hz, 2H), 4.90 (t, *J* = 6.0 Hz, 2H), 7.00 (d, *J* = 8.8 Hz, 2H), 7.10 (s, 1H), 7.34 (d, *J* = 8.8 Hz, 2H), 7.71 (s, 1H), 8.02 (d, *J* = 8.8 Hz, 1H), 8.19 (d, *J* = 8.8 Hz, 1H), 9.03 (s, 1H), 9.77 (s, 1H); ESI-MS m/z: 506.2 $[M - Br]^+$; **P3**: ^1H NMR (400 MHz, DMSO-*d*6): δ 2.23 (s, 3H), 2.32 (t, *J* = 6.4 Hz, 2H), 3.20 (t, *J* = 6.4 Hz, 2H), 3.88 (s, 3H), 3.94 (s, 3H), 4.02 (s, 3H), 4.22 (t, *J* = 6.4 Hz, 2H), 4.48 (t, *J* = 6.4 Hz, 2H), 4.87 (t, *J* = 6.4 Hz, 2H), 6.86 (d, *J* = 8.4 Hz, 2H), 7.10 (d, *J* =8.4, 2H), 7.71 (s,1H), 8.02 (d, *J* = 9.2 Hz, 1H), 8.20 (d, *J* = 9.2 Hz, 1H), 9.02 (s, 1H), 9.75 (s, 1H); ESI-MS m/z: 486.2 $[M - Br]^+$; **P4**: ^1H NMR (400 MHz, DMSO-*d*6): δ 2.09 (s, 3H), 2.20 (s, 3H), 2.33-2.37 (m, 2H), 3.20 (t, *J* = 6.4 Hz, 2H), 3.88 (s, 3H), 3.94 (s, 3H), 4.00 (s, 3H), 4.23 (t, *J* = 6.0 Hz, 2H), 4.52 (t, *J* = 6.0 Hz, 2H), 4.85 (t, *J* = 6.4 Hz, 2H), 6.88 (d, *J* = 8.0 Hz, 1H), 6.95 (s, 1H), 6.96 (d, *J* = 8.0 Hz, 1H), 7.10 (s, 1H), 7.71 (s, 1H), 8.03 (d, *J* = 9.2 Hz, 1H), 8.20 (d, *J* = 9.2 Hz, 1H), 9.02 (s, 1H), 9.73 (s, 1H); ESI-MS m/z: 500.2 $[M - Br]^+$; **P5**: ^1H NMR (400 MHz, $CDCl_3$): δ 2.62 (t, *J* = 6.0 Hz, 2H), 3.22 (t, *J* = 5.6 Hz, 2H), 3.99 (s, 6H), 4.11 (s, 3H), 4.66-4.72 (m, 4H), 5.19 (t, *J* = 5.6 Hz, 2H), 6.75 (s, 1H), 7.03 (t, *J* = 8.0 Hz, 1H), 7.42-7.45 (m, 2H), 7.61 (t, *J* = 8.0 Hz, 1H), 7.00 (d, *J* =

9.2 Hz, 1H), 7.81 (d, *J* = 8.0 Hz, 1H), 7.96 (d, *J* = 8.8 Hz, 1H), 8.63 (s,1H), 10.32 (s, 1H); ESI-MS m/z: 517.2 $[M - Br]^+$; **P6**: ^1H NMR (400 MHz, $CDCl_3$): δ 2.37-2.43 (m, 2H), 3.09 (t, *J* = 6.4 Hz, 2H), 3.81 (s, 3H), 3.87 (s, 3H), 4.03 (s, 3H), 4.31 (t, *J* = 6.0 Hz, 2H), 4.51 (t, *J* = 6.0 Hz, 2H), 4.85 (t, *J* = 6.4 Hz, 2H), 6.57 (s, 1H), 6.87-6.95 (m, 4H), 7.37 (s,1H), 7.49 (d, *J* =9.2 Hz, 1H), 8.01 (d, *J* = 9.2 Hz, 1H), 8.72 (s, 1H), 9.87 (s, 1H); ESI-MS m/z: 490.2 $[M - Br]^+$.

3.2.2 Biological assays

Palmatine chloride used in biological assays was purchased from Sigma-Aldrich. The biological activities of palmatine and ite derivatives were tested according to the procedures of *in vitro* and *in vivo* assays described in section 2.2.2.

3.3 Results and discussion

3.3.1 Inhibition of *S. aureus* FtsZ assembly by palmatine

3.3.1.1 GTPase activity

Palmatine was firstly subjected to the GTPase activity assay to investigate whether this berberine analog can interfere with the GTPase activity of *S. aureus* FtsZ. The result shown in Figure 3.2 revealed that, although the inhibitory activity of palmatine against FtsZ protein is weaker than berberine, it can still moderately reduce the GTPase activity of *S. aureus* FtsZ in a concentration-dependent manner with an IC_{50} value of 327.71 ±50.0 μM. The result suggests that palmatine can also inhibit the GTPase activity of *S. aureus* FtsZ.

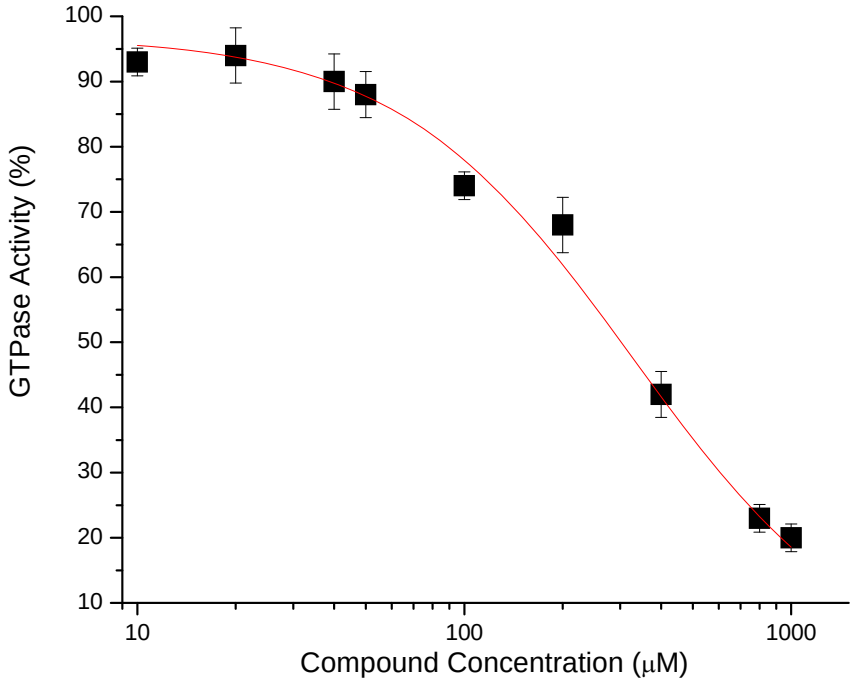

Figure 3.2 Concentration-response curve of palmatine (■) on the inhibition of GTPase activity of *S. aureus* FtsZ. Each point represents the mean of three independent assays, and the vertical bars show the standard derivation of the mean. The IC_{50} was calculated by nonlinear regression using a sigmoidal concentration-response curve (Origin Software).

3.3.1.2 Light scattering assay of palmatine on *S. aureus* FtsZ

Light scattering assay was used to further verify the inhibition of palmatine against FtsZ assembly. Figure 3.3 shows the effect of palmatine on the kinetics of FtsZ assembly *in vitro*. The decrease in light scattering intensity of the FtsZ assembly in the presence of palmatine indicated the decrease in the polymer mass of FtsZ protofilaments. In the presence of 1.3 mM palmatine, the light scattering data showed that almost 60 % inhibition of FtsZ polymerization was achieved.

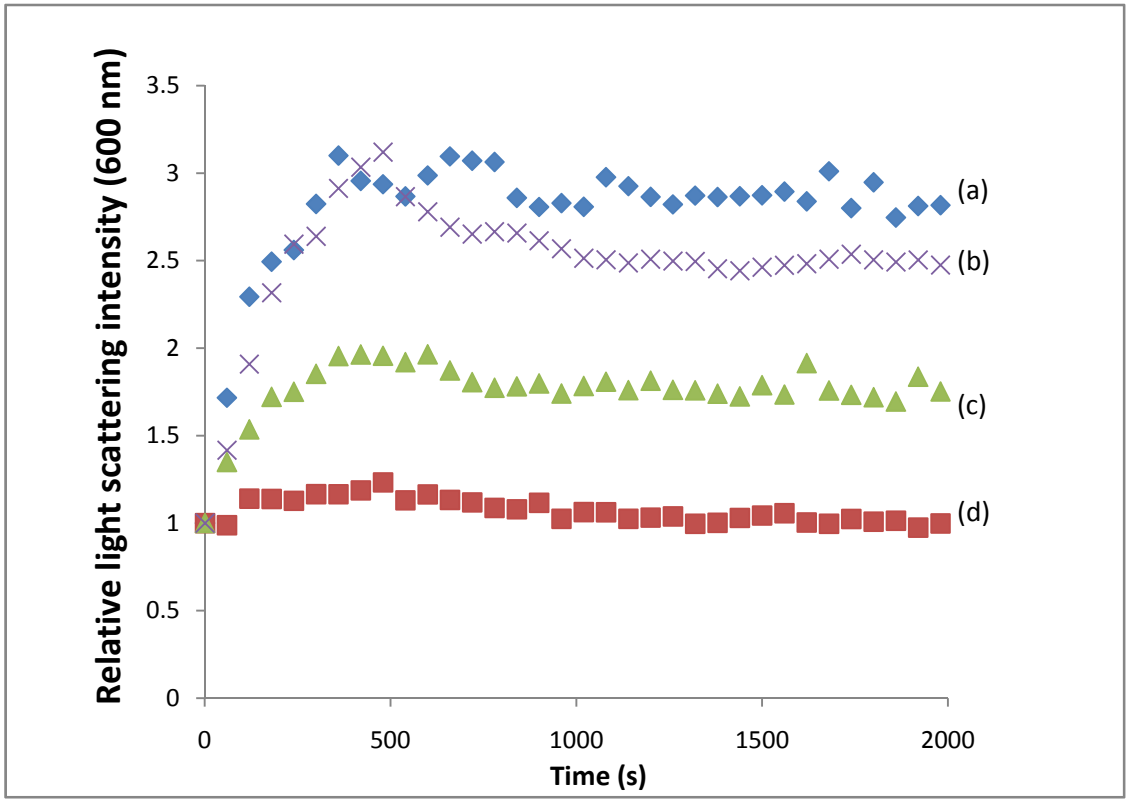

Figure 3.3 Effect of palmatine on FtsZ assembly *in vitro*. *S. aureus* FtsZ (6 μM) was polymerized in 50 mM MOPS, pH 6.5, 50 mM KCl, 10 mM $MgCl_2$ and 1 mM GTP in the absence of (a), and the presence of 0.65 mM (b), 1.3 mM (c) and 2.6 mM (d) of palmatine. Appropriate blanks were subtracted from all the traces. Each experiment was repeated three times.

3.3.1.3 Transmission electron microscopy (TEM) analysis

In addition to GTPase activity assay and light scattering assay, transmission electron microscopy was used to study the effect of palmatine on FtsZ protein. The electron microscopic images provided the visual evidence for the inhibition of wild type *S. aureus* FtsZ protofilaments in the presence of palmatine. In the absence of palmatine, a dense network of GTP induced FtsZ protofilaments was observed (Figure 3.4 A). Palmatine inhibited the *in vitro* bundling of FtsZ protofilaments in a dose-dependent manner. The size and thickness of FtsZ polymers were reduced in the presence of 0.66 mM palmatine (Figure 3.4 B). In the presence of 1.3 mM palmatine, except for a few straight, thin filaments, nearly complete inhibition of polymerization was observed (Figure 3.4 C).

As a whole, palmatine can moderately inhibit *S. aureus* FtsZ assembly, but its effect on the FtsZ protein is weaker than berberine. This may be due to the lack of methylenedioxyl group, which has a strong interaction with FtsZ protein, at C-2 and C-3 position of the isoquinoline core of berberine [35].

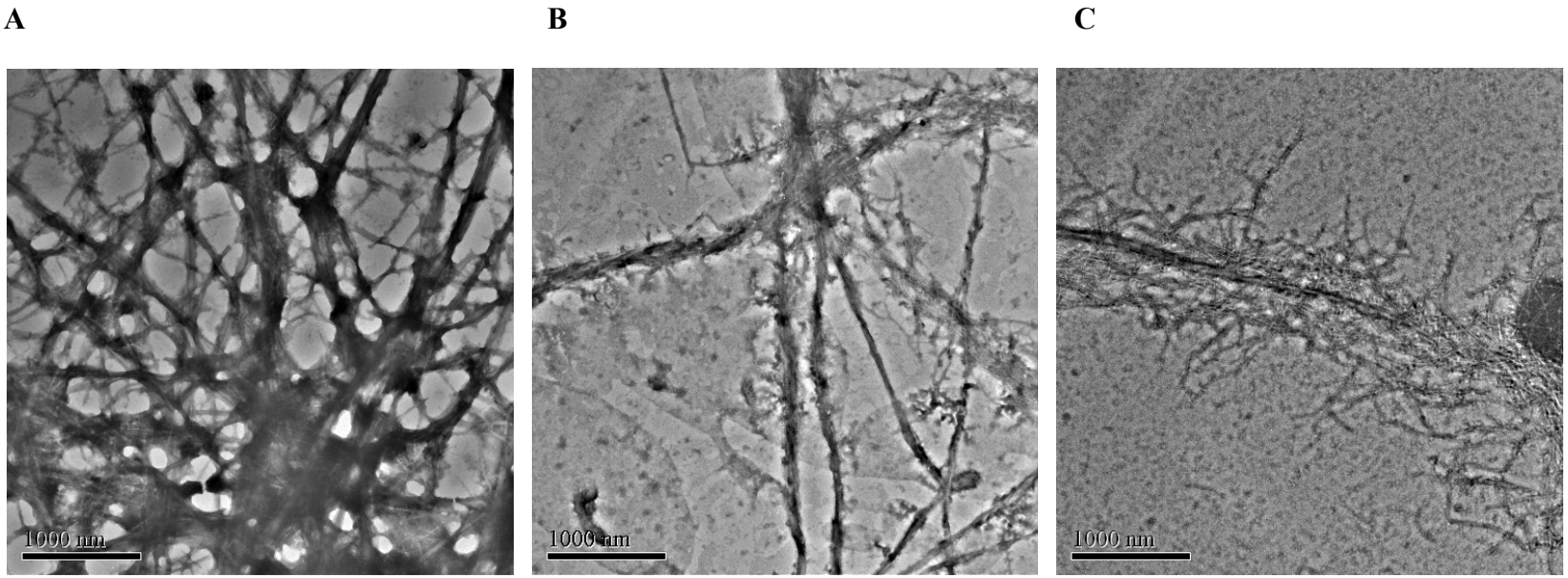

Figure 3.4 Electron micrographs of FtsZ polymers. *S. aureus* FtsZ (12 μM) was polymerized in 50 mM MOPS buffer, pH 6.5, containing 50 mM KCl, 5 mM $MgCl_2$, and 1 mM GTP in the absence and presence of palmatine for 15 min at 37 ^oC. The pictures shown are the electron micrographs of FtsZ polymers formed in the absence (A) and presence of 0.66 mM (B) and 1.3 mM (C) palmatine. The scale bar = 1000 nm.

3.3.2 Biological study of palmatine and its 9-phenoxyalkyl substituted derivatives.

In this section, some synthetic 9-phenoxyalkyl substituted palmatine derivatives (Figure 3.1), which resemble the structure of the berberine derivaties described in chapter 2, were studied on their inhibitory activities against *S. aureus* FtsZ *in vitro*. In addition, the spectrum and potency of antimicrobial activity of palmatine and its 9-phenoxyalkyl substituted derivatives were studied against various Gram-positive and –negative bacterial strains.

3.3.2.1 *In vitro* biological study

3.3.2.1.1 GTPase activity

To verify that the 9-phenoxyalkyl substituent can enhance the inhibitory activities of palmatine against *S. aureus* FtsZ, these compounds were firstly tested against the GTPase activities of FtsZ protein *in vitro*. The IC_{50} values of these compounds are tabulated in Table 3.1. All compounds exhibit a dose-dependent inhibition of GTPase activity. The concentration-response curves for compounds **P1** and **P2** against FtsZ protein are shown in Figure 3.5. As shown in Table 3.1, these derivatives showed 4 – 8 folds higher affinity than palmatine (Figure 3.2). Among these derivatives, compounds **P2**, **P3** and **P6** show a stronger effect on FtsZ protein than the others; this may be due to the effect of the small substituted group at the para-position of phenyl ring. Compound **P1-1**, which has 4 carbons in the ether linker, is slightly less potent than compound **P1**. This suggested that the length of a 3-carbon linker may be more suitable for the compound to bind to the protein.

Table 3.1 IC_{50} values of compounds **P1** to **P6** on the inhibition of GTPase activity of *S. aureus* FtsZ

Compound	IC_{50} ± SEM[a] (μM)
P1	70.1 ± 10.9
P1-1	79.2 ± 0.5
P2	45.1 ± 2.1
P3	57.4 ± 10.8
P4	75.3 ± 6.4
P5	78.6 ± 5.7
P6	46.8 ± 4.7

[a] SEM: standard error of the mean

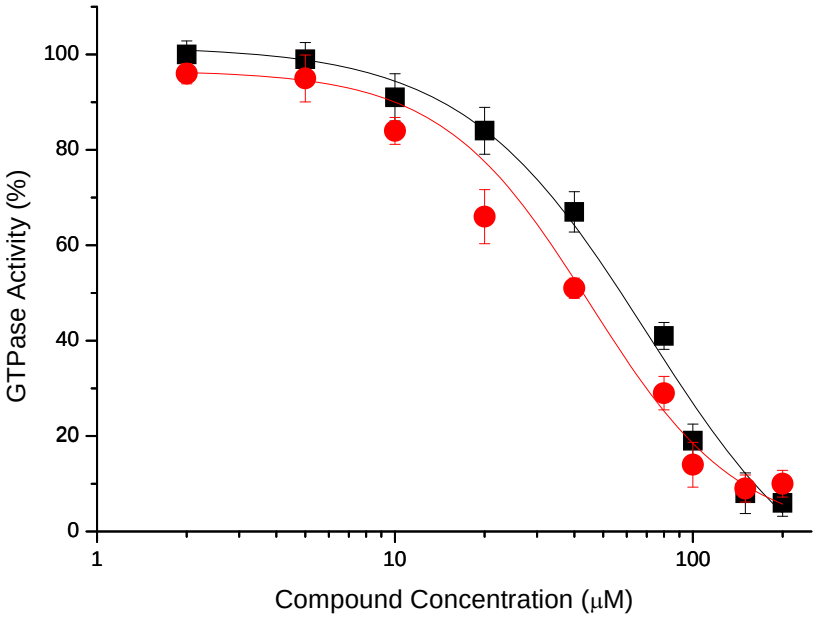

Figure 3.5 Concentration-response curve of **P1** (■) and **P2** (●) on the inhibition of GTPase activity of *S. aureus* FtsZ. Each point represents the mean of three independent assays, and the vertical bars show the standard derivation of the mean. IC_{50} was calculated by nonlinear regression using a sigmoidal concentration-response curve (Origin Software).

3.3.2.1.2 Light scattering assay

Subsequently, compounds **P1** and **P2** were chosen to test their inhibitory activities on the polymerization of the *S. aureus* FtsZ. Both of them can strongly weaken the light scattering signal of FtsZ assembly compared to the parent compound palmatine. Figures 3.6 and 3.7 show the effect of **P1** and **P2** on the kinetics of FtsZ assembly *in vitro*. The light scattering intensity was decreased by approximate 50 % and 70 % in the presence of 35 μM **P1** and **P2** respectively, suggesting that both of them inhibited the assembly and/or the bundling of *S. aureus* FtsZ protofilaments.

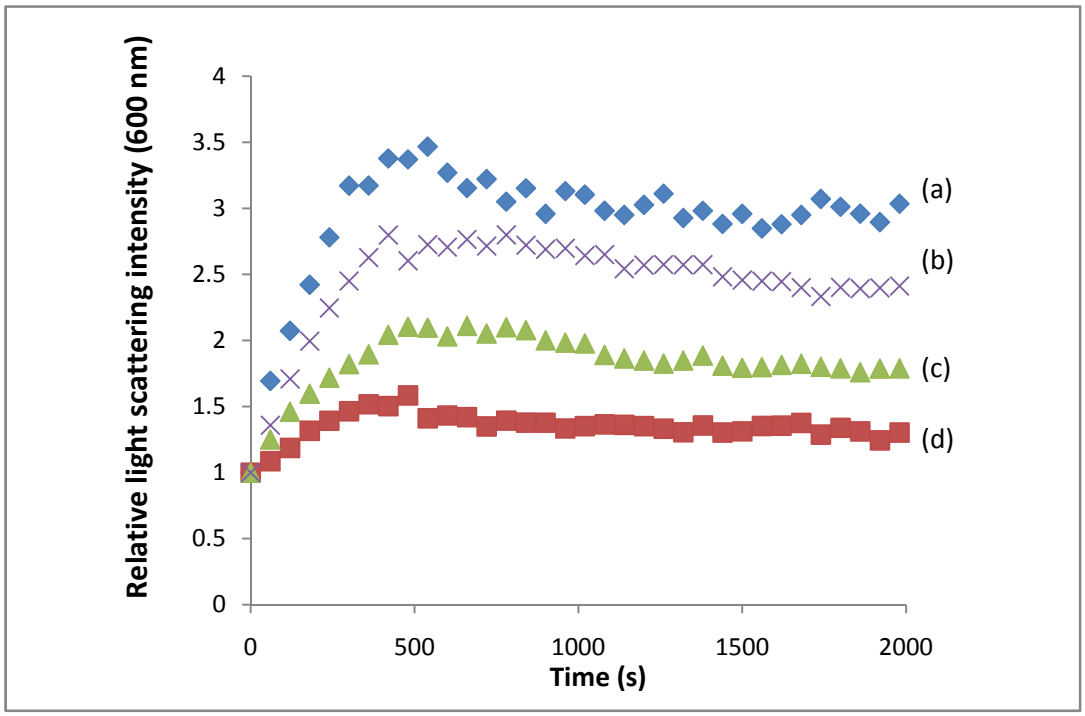

Figure 3.6 Effect of **P1** on FtsZ assembly *in vitro*. *S. auerus* FtsZ (6 μM) was polymerized in 50 mM MOPS, pH 6.5, 50 mM KCl, 10 mM $MgCl_2$ and 1 mM GTP in the absence of **P1** (a), in the presence of 16 μM (b), 35 μM (c) and 70 μM (d) of **P1**. Appropriate blanks were subtracted from all the traces. Each experiment was repeated three times.

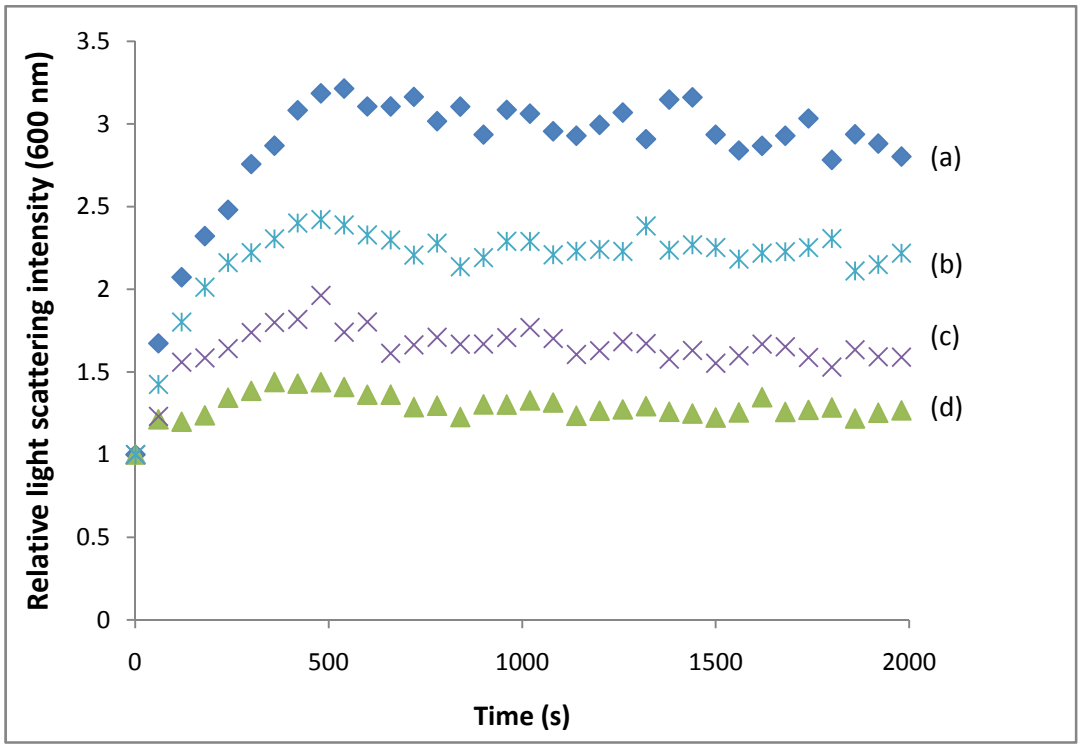

Figure 3.7 Effect of **P2** on FtsZ assembly *in vitro*. *S. auerus* FtsZ (6 μM) was polymerized in 50 mM MOPS, pH 6.5, 50 mM KCl, 10 mM $MgCl_2$ and 1 mM GTP in the absence of **P2** (a), in the presence of 16 μM (b), 35 μM (c) and 70 μM (d) of **P2**. Appropriate blanks were subtracted from all the traces. Each experiment was repeated three times.

3.3.2.1.3 Transmission electron microscopy (TEM) analysis

Electron microscopic analysis of the *S. aureus* FtsZ polymers showed that the thickness of FtsZ bundles was decreased in the presence of compounds **P1** and **P2** in a dose-dependent manner (Figures 3.8 and 3.9). The average thinckness of the bundles was 124 ± 27 nm in the absence of compounds (Figures 3.8 A and 3.9 A). In the presence of 8 μM **P1** and **P2**, the average thickness of bundles was reduced to 54 ± 10 nm and 36 ± 7 nm (Figures 3.8 B and 3.9 B). Only a few short and thin FtsZ filaments can be found when the concentration of **P1** and **P2** reached to 35 μM and 16 μM (Figures 3.8 C and 3.9 C). These results suggested that the phenoxyalkyl group at the C-9 position of palmatine can dramatically enhance the inhibitory activity of palamtine against polymerization of FtsZ.

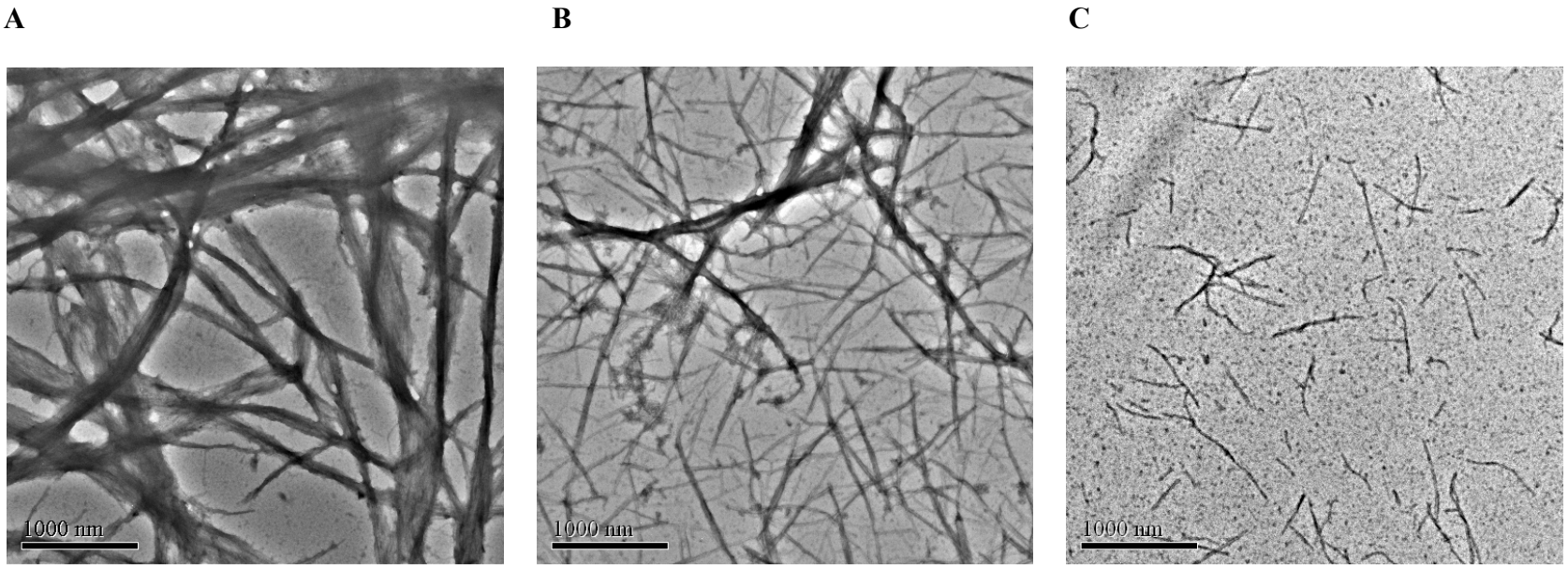

Figure 3.8 Electron micrographs of FtsZ polymers. *S. aureus* FtsZ (12 μM) was polymerized in 50 mM MOPS buffer, pH 6.5, containing 50 mM KCl, 5 mM $MgCl_2$, and 1 mM GTP in the absence and presence of **P1** for 15 min at 37 ^{o}C. The pictures shown are the electron micrographs of FtsZ polymers formed in the absence (A) and presence of 8 μM (B) and 35 μM (C) **P1**. The scale bar = 1000 nm.

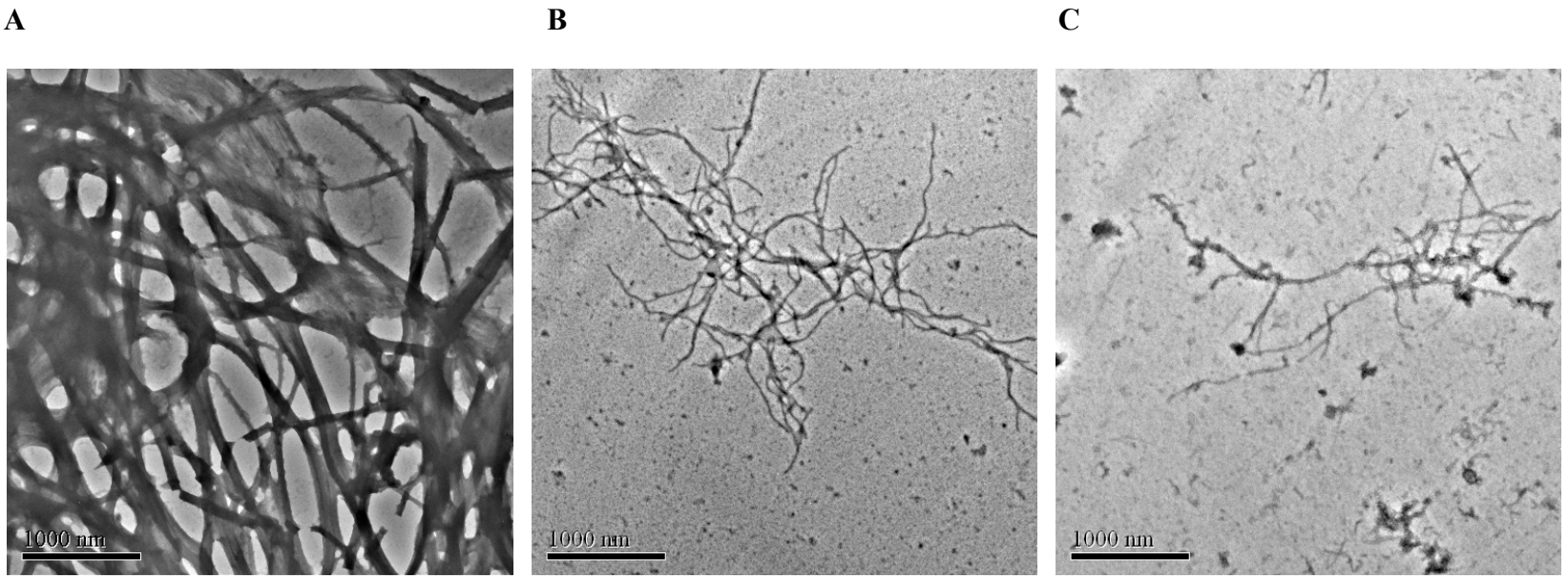

Figure 3.9 Electron micrographs of FtsZ polymers. *S. aureus* FtsZ (12 μM) was polymerized in 50 mM MOPS buffer, pH 6.5, containing 50 mM KCl, 5 mM $MgCl_2$, and 1 mM GTP in the absence and presence of **P2** for 15 min at 37 ^{o}C. The pictures shown are the electron micrographs of FtsZ polymers formed in the absence (A) and presence of 8 μM (B) and 16 μM (C) **P2**. The scale bar = 1000 nm.

3.3.2.2 *In vivo* biological study

3.3.2.2.1 Antimicrobial activity of palmatine and its 9-phenoxyalkyl substituted derivatives

To test the biological activities of palmatine and its derivatives *in vivo*, these compounds were firstly subjected to antimicrobial susceptibility test against a range of Gram-positive and –negative strains, following CLSI standards [93]. The MIC values are shown in Table 3.2. Palmatine possesses antibacterial activity against Gram-positive strains only. It can inhibit the growth of *S. aureus* at a moderate and *B. subtilis* at a high concentration. On the other hand, all the 9-phenoxyalkyl substituted derivatives showed potent antibacterial activity against all Gram-positive strains tested (MICs in the range of 4 to 32 μg/mL), including a methicillin-resistant *S. aureus* (MRSA) strain, an ampicillin-resistant *S. aureus* strain and a vancomycin-resistant *E. faecium* strain. The potency of compounds **P2** and **P6** were more than 60 times that of palmatine against *S. aureus* (Table 3.2 A). Among these derivaties, **P2** and **P6** were also active against Gram-negative pathogenic bacteria.

Table 3.2 A MICs of palmatine and its derivatives against Gram-positve bacteria

Organism	MIC (μg/mL)							
	palmatine	**P1**	**P1-1**	**P2**	**P3**	**P4**	**P5**	**P6**
B. subtilis 168	1024	32	16	8	16	8	16	8
S. aureus ATCC 29213	256	6	6	4	4	4	6	4
S. aureus ATCC 29247	256	6	6	4	4	4	6	4
S. aureus ATCC BAA-41	256	6	6	4	4	4	6	4
E. faecium ATCC 49624	ND	12	12	8	8	8	8	8
E. faecium ATCC 700221	ND	12	12	8	8	8	8	8
E. faecalis ATCC 29212	ND	24	12	8	12	8	12	8
S. epidermidis ATCC 12228	ND	4	6	4	4	4	4	4

ND is not determined.

S. aureus ATCC 29247 is an ampicillin-resistant *S. aureus* strain.

S. aureus ATCC BAA-41 is a methicillin-resistant *S. aureus* (MRSA) strain.

E. faecium ATCC 700221 is a vancomycin-resistant *E. faecium* strain.

Table 3.2 B MICs of palmatine and its derivatives against Gram-negative bacteria

Organism	MIC (μg/mL)							
	palmatine	**P1**	**P1-1**	**P2**	**P3**	**P4**	**P5**	**P6**
E. coli ATCC 25922	>1024	>128	>128	64	128	64	64	64
E.cloacae ATCC BAA-1143	>1024	>128	>128	128	>128	>128	>128	128
K. pneumoniae ATCC BAA-1144	>1024	>128	>128	128	>128	>128	>128	128

3.3.2.2.2 Effects of palmatine, and compound P2 on the morphology of *B. subtilis* cells

In order to verify that palmatine and its 9-phenoxyalkyl substituted derivatives have *in vivo* on-target effect against FtsZ, they were tested against *B. subtilis* 168 cells for their influence on cell morphology. They were found to induce filamentation in *B. subtilis* similar to berberine. As shown in Figure 3.10, the average length of B. subtilis cells in the absence of the compound was found to be 3.8 ± 1.2 μm (Figure 3.10 A). In the presence of 6 660 μM palmatine and 8 μM **P2**, the average length of *B. subtilis* cells were increased to 27 ± 3.4 μm and 69 ± 8.7 μm respectively (Figures 3.10 B and C). No bacterium was found to have a length equal to or more than about 10 μm in the absence of the compounds, whereas more than 50 % and 70 % of the bacteria had a length longer than 10 μm in the presence of palmatine and **P2** (Figure 3.11). Treatment of *B. subtilis* with palmatine and **P2** led to the formation of filamentous cells, suggesting that palmatine and its derivatives may inhibit cell division by disrupting cytokinesis.

A **B** **C**

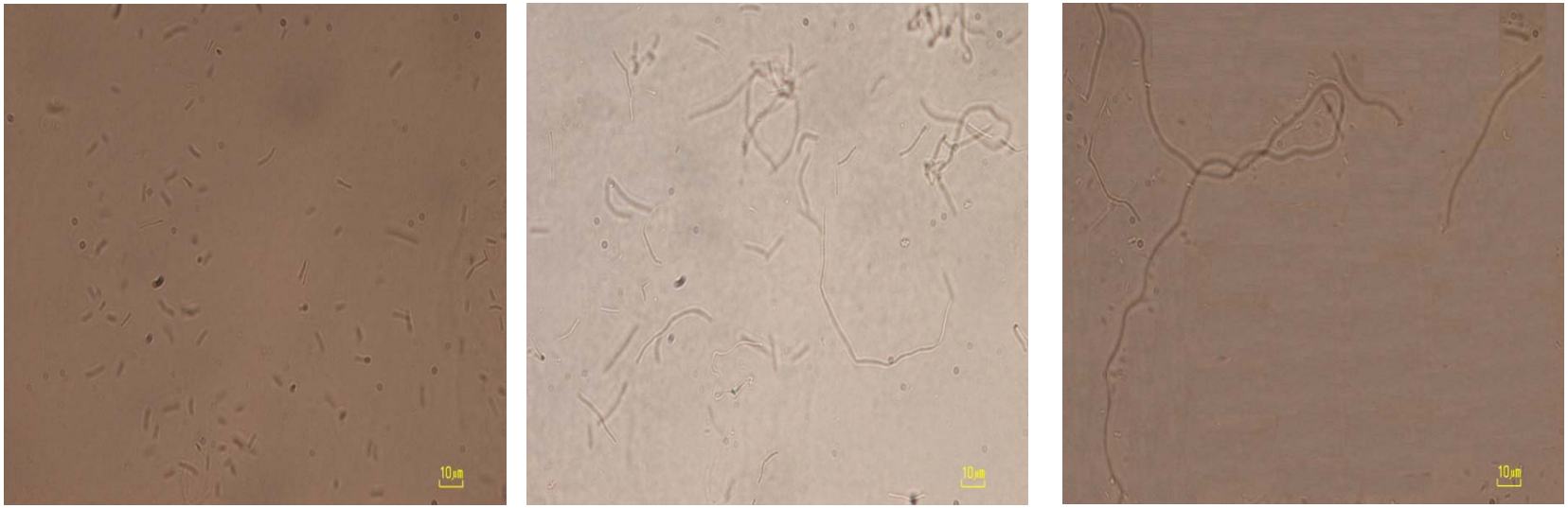

Figure 3.10 Effects of pamatine and **P2** on cell division and cell morphology. *B. subtilis* 168 cells were grown for 4 h in the absence (A) or presence of 660 μM of palmatine (B) or 8 μM of **P2** (C). The cells were observed under a phase contrast microscope. The scale bar is 10 μm. Each experiment was repeated 3 times.

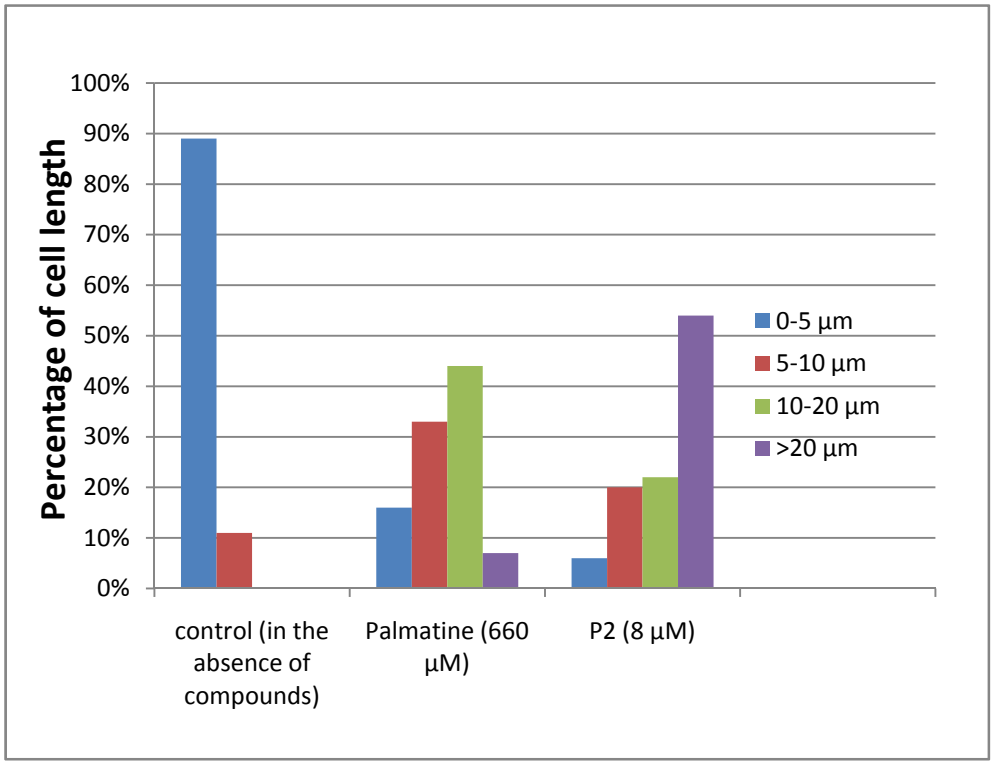

Figure 3.11 Palmatine and **P2** induced cell elongation in *B. subtilis* 168.

3.3.2.2.3 Effects of palmatine and compound P2 on the cell membrane of *B. subtilis* cells

The effects of palmatine and **P2** on the cell membrane of *B. subtilis* 168 were studied with dye FM 4-64. The images showed that palmatine and **P2** did not perturb the membrane of *B. subtilis* (Figure 3.12). The images also showed the formation of septa at the division site in the presence of the compounds (Figures 3.12 B and C), though these septa did not function to complete the cell division.

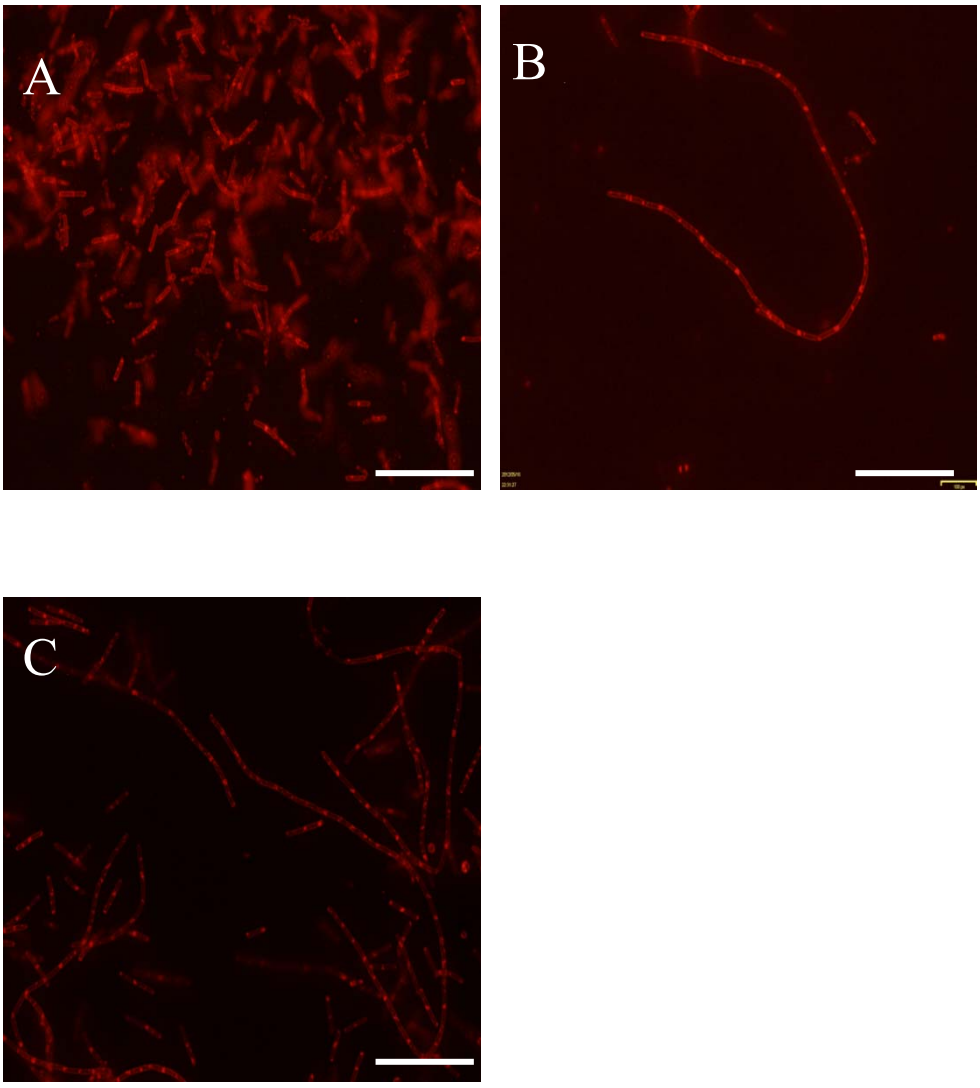

Figure 3.12 Effects of palmatine and **P2** on the cell membrane of *B. subtilis* 168. The bacterial cells were grown in the absence (A) and presence of 660 μM of palmatine (B) or 8 μM of **P2** (C). The *B. subtilis* 168 cells were then observed under a phase-contrast microscope. The scale bar is 10 μm.

3.3.2.2.4 Effects of compound P2 on the formation of cytokinetic Z-ring in *E. coli* cells

Microscopic imaging of live *E. coli* cells with GFP-tagged FtsZ was done at 64 μM of compound **P2**. In the absence of **P2**, the normal pattern of FtsZ localization with fluorescent bands of GFP-tagged FtsZ was observed at the mid-cell (Figure 3.13 A). Treatment with **P2** perturbed the Z-ring morphology and localization (Figure 3.13 B). This phenomenon suggested that **P2** specifically targetd Z-ring spatial arrangement by dissipating the Z-rings.

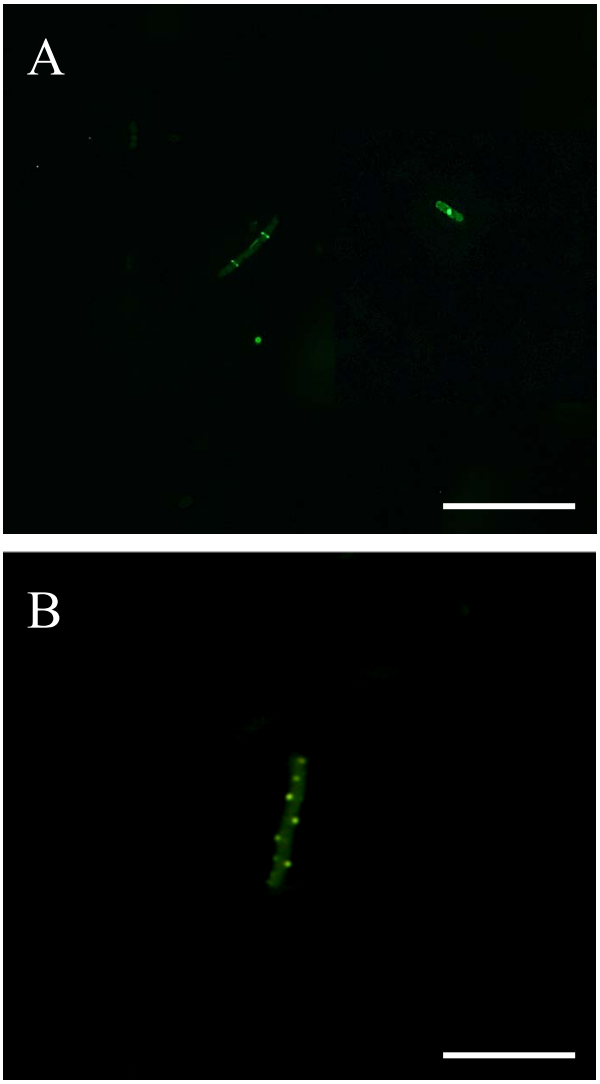

Figure 3.13 Perturbation of cytokinetic Z-ring in *E. coli* (JM109 WM647) as visualized by GFP-tagged FtsZ. The bacterial cells were grown in the absence (A) or presence of 64 μM of **P2** (B). Each scale bar is 10 μm. The experiment was repeated 3 times.

3.4 Concluding remarks

In this chapter, palmatine was verified to inhibit FtsZ assembly like berberine, but at a higher concentration. A few 9-phenoxyalkyl substituted palmatine derivatives were synthesized. Among these derivatives, compounds **P2** and **P6** not only exhibited promising MIC values in the range of 4 – 8 μg/mL (8 – 16 μM) for their antibacterial activity against Gram-positve strains, but also inhibited growth of Gram-negative strains at moderate concentrations. The GTPase activity assay on these derivatives clearly showed the inhibition of GTP hydrolysis activity of FtsZ in a dose dependent manner. Since the physical state of FtsZ polymer is dependent on the rate of GTP hydrolysis, the effect of **P1** and **P2** on the polymerization of FtsZ were examined. The results strongly suggested that these compounds inhibitied FtsZ filament formation and polymerization. The effect on FtsZ polymerization was also examined by TEM, which demonstrated an impressive dose dependent inhibition of FtsZ assembly and a striking suppression of FtsZ protofilament formation at a higher concentration of **P2**. The microscopic images of *B. subtilis* 168 cells treated with these compounds showed that the cell length was elongated more than 10 times.

The images of *E. Coli* JM109, with the assistance of GFP-tagged FtsZ, showed that the Z-rings were dislocated by **P2**. The TEM and microscopic analyses strongly supported an antibacterial mechanism of these compounds through inhibition of FtsZ assembly and Z-ring formation. The binding poses of palmatine and its derivatives as predicted by docking simulations will be discussed in chapter 4.

Chapter 4

Molecular docking simulations of berberine and palmatine derivatives with FtsZ

4.1 Introduction

As previously described in chapters 2 and 3, a series of protoberberine alkaloids with a phenoxy moiety linked by a 3- or 4-carbon chain were synthesized and biochemically studied. All these derivatives showed higher activity than their parent compounds (berberine and palmatine). One possible approach for improving the activity and potency of FtsZ inhibitors is to take advantage of the polymeric nature and multiple binding sites of FtsZ by using bivalent molecular interactions. Bivalent molecular interaction refers to a molecule simultaneously interacting with two domains of the same receptor [102]. Berberine was proposed to bind to the hydrophobic region of GTP binding site of FtsZ protein [35], and some small molecules containing a phenyl ring, such as caffeic acid, cinnamaldehyde, and 2, 6-difluro-3-methoxybenzamide, were proposed to

interact with the T7 loop of FtsZ [103]. However, no attempt has ever been made to investigate the bivalent interaction of small molecules with FtsZ dimer. It thus motivated us to build a homology model for *S. aureus* FtsZ dimer and redock the binding pose of berberine into our FtsZ dimer. Molecular docking simulations were then performed to predict the binding modes of the protoberberine derivatives.

The docking results suggested that protoberberine alkaloid derivatives interact with amino acids of both the putative nucleotide binding site and the helix H8 pocket, which improve the binding to FtsZ. Moreover, docking of a test set containing 7 actives (compounds **B1 to B6**) and 233 decoys also indicated that our built model was capable of discriminating active compounds from decoys, and thus this model will be a valuable tool for *in silico* lead optimization of FtsZ inhibitors.

4.2 Methodology

4.2.1 Homology modeling of the *S.aureus* FtsZ dimer

The sequence of the *S. aureus* FtsZ was retrieved from the National Center for Biotechnology Institute (NCBI) with UniProtKB accession number B5LV58. The crystal structure of the *M. jannaschii* FtsZ dimer (PDB: 1W5B) [104] was retrieved from the Protein Data Bank (PDB) and selected as the template using molecular conversion procedure implemented in the ICM docking software version 3.6-1i [72]. The molecular conversion step removed water molecules, built hydrogens, assigned formal charges and MMFF atom types [105-109], calculated partial charges, optimized protonation states of histidines and flipped glutamine, aspargine and histidine side chains, and performed local minimization of polar hydrogens in the internal coordinate space.

An initial 3D model of the *S. aureus* FtsZ dimer was obtained using ZEGA alignment algorithm implemented in ICM software version 3.6-1i [72, 105, 107-110]. The template was firstly aligned pairwise to the query

sequence with about 47% identical residues with gap opening and extension penalties of 2.4 and 0.15 respectively. Alignment was finally verified and fine-tuned manually. The final alignment is shown in Figure 4.1. The initial 3D model was built by replacing non-identical side chains and inheriting the backbone conformation from the template according to the sequence alignment. During this process, the non-identical residues of the N-terminal GTP binding site and the C-terminal domains of *M. jannaschii* FtsZ were mutated into the corresponding residues of the *S. aureus* FtsZ (Figure 4.1), the model was then refined using the ICM Monte Carlo conformational search that optimize the side chains by removing any steric clashes [72]. After refinement, the structural quality of the *S. aureus* FtsZ model was checked by the Ramachandran plot in ICM software version 3.6-1i [72].

4.2.2 Docking berberine to the model of *S. aureus* FtsZ dimer

4.2.2.1 Ligand preparation

The 2D structure of berberine was built using a ligand editor implemented in the ICM software version 3.6-1i [72]. Protonation state was calculated at pH 7.4 using the automatic pKa model implemented in ICM [5]. Hydrogens were added, MMFF atom types were assigned and berberine was converted into 3D and the energy minimized using ICM software version 3.6-1i [72, 105-109].

4.2.2.2 Docking simulation of berberine

According to literature report, berberine was predicted to bind to the hydrophobic region of the GTP binding site in FtsZ [35]. The GTP hydrophobic pocket was detected by ICM PocketFinder algorithm [111]. In the ICM fast docking procedure, the selected binding pocket was represented by 0.5 Å grid potential maps. The grid potential maps account for hydrogen bonding, hydrophobic, van der Waals and electrostatic interactions between receptor and ligand [111]. Subsequently, flexible ligand (berberine) was docked into the all atom representation of the *S. aureus* FtsZ model with flexible side chains using ICM Biased Probability Monte Carlo (BPMC) global energy minimization procedure [112]. The protein–ligand binding affinity was estimated using an ICM scoring function. The Virtual Library Screening (VLS) scoring function takes into account van der Waals interactions, electrostatic potential, hydrogen bonding, entropy and desolvation energy differences between bound and unbound states of the ligand [113]. The ICM binding score is also used to rank the multiple conformations of the same ligand docked with a receptor. One hundred independent docking runs were performed and the top-scoring

pose of berberine was saved. A full local energy minimization was performed for the top-scoring poses of FtsZ−berberine model with flexible ligand and flexible receptor side chains in the 5 Å proximity of the binding pocket using ICM Biased Probability Monte Carlo (BPMC) algorithm [112]. The resulting ligand-receptor models with acceptable conformational energy were clustered according to the conformations of the binding pocket residues, generating 48 non-redundant conformations. Three parallel dockings of the berberine into the 48 binding pocket conformations were then performed.

4.2.3 Docking protoberberine derivatives to the *S. aureus* FtsZ dimer model

For each compound, a stack of docked complexes with different ligand conformations and orientations was generated. The most realistic complex of each compound was selected on the basis of ICM binding score and similar binding pose with the parent compounds berberine and palmatine.

4.2.4 Benchmarking study

The ability of the *S. aureus* FtsZ dimer model to discriminate the active berberine derivatives from benchmarking decoys was assessed. A test set combining seven berberine derivatives (Table 4.1) with known FtsZ inhibitory activity and 233 decoys was downloaded from DUD version 2 (http://dud.docking.org/) [114]. Benchmarking decoys have similar molecular weight, number of hydrogen bonding groups, logP and number of rotatable bonds compared to the active compounds, but their molecular topologies are different. The 3D geometries were optimized with ICM software version 3.6-1i [72] and the molecules were grouped into an annotated sdf file and docked into the pre-calculated potential grids of *S. aureus* FtsZ dimer model by flexible ligand docking. Twenty independent runs were performed with the maximal number of steps determined by an adaptive algorithm based on the number of rotatable bonds in the ligand multiplied by a thoroughness value set to 3. Finally, compounds from the test set were sorted according to their ICM binding scores.

To assess the performance of virtual ligand screening, a Normalized Square Root AUC (NSQ_AUC) metric which combines overall selectivity of area under the curve (AUC) and enrichment factor measured at 1% dataset cutoff was used [115]. The value of NSQ_AUC was based on a calculation of the area under the receiver operating characteristic (ROC) curve [116]. In a ROC curve the true positive (TP) rate is plotted as a function of the false positive (FP) rate for all positions of the ranked score list. For an ideal model, all true positives are ranked higher than all top-scoring decoys. The resulting ROC plot passes through the upper left corner and AUC is equal to 100. The difference between AUC and NSQ_AUC is that the later is calculated for the ROC curve plotted with X coordinate calculated as the square root of "the percentage of FP", X = Sqrt (FP). Thus, the value of NSQ_AUC is more sensitive to initial enrichment than the commonly used linear AUC [115]. The NSQ_AUC measures and returns the value of 100 for any perfect separation of signal from noise and values close to 0 for a random subset of noise.

4.3 Results and discussion

4.3.1 Homology modeling of FtsZ dimer for *S. aureus*

As mentioned previously, the FtsZ protofilament is formed by the interaction of the N-terminal GTP-binding domain of one subunit with the C-terminal domain of another, forming a longitudinal polymer for bacterial cell division. In order to understand the binding of berberine derivatives that might involve both domains, a molecular docking simulation of berberine against FtsZ dimer was performed.

Until now, only the dimer structure of *M. jannaschii* (PDB: 1W5B) FtsZ has been solved. The dimer crystal structures of other clinically significant bacterial strains such as *S. aureus* and *E. coli* are not available. Therefore, the X-ray crystal structure of *M. jannaschii* FtsZ dimer (PDB: 1W5B) containing two molecules in the asymmetric unit was used as a template to construct a 3D homology model of *S. aureus* FtsZ (UniProtKB accession number: **B5LV58**) and to be used for docking [3]. As shown in Figure 4.1, the overall sequence identity between *M. jannaschii* and *S. aureus* FtsZ is

approximately 47%. Since a high sequence identity exists and both enzymes belong to the same FtsZ family, ICM homology modeling algorithm was employed to build a 3D structure for *S. aureus* FtsZ dimer by only mutating non-identical residues according to the sequence alignment (Figure 4.1). The Ramachandran plot was used to check the stereochemical quality of the resulting *S. aureus* FtsZ dimer model (Figure 4.2). This method is commonly used to analyze the overall structure geometry and residue-by-residue geometry of protein [4]. In the Ramachandran plot, the most favorable combinations of phi-psi value for residues are located at the light blue areas that correspond to the core region of the protein. In this homology model, 92.1 percent of the residues in the core region were found in the Ramachandran plot (Figure 4.2). In addition, the overall conformation of the GTP binding site of the modeled structure is almost the same as the template. The RMSD (Root mean standard derivation) of main chain between the modeled and template structures was 0.9 Å. These results indicated that the modeled structure is ready to be used in molecular docking simulation of berberine.

Figure 4.1 Pairwise sequence alignment between *M. jannaschii* FtsZ and *S. aureus* ATCC 29213. The consensus sequence is given above the alignment ("1-letter codes" = conserved, "#" = hydrophobic, "." = not conserved, "+/–" = conserved charge) and mutations within the nucleotide and helices H7-H8 binding pockets are highlighted with a red frame.

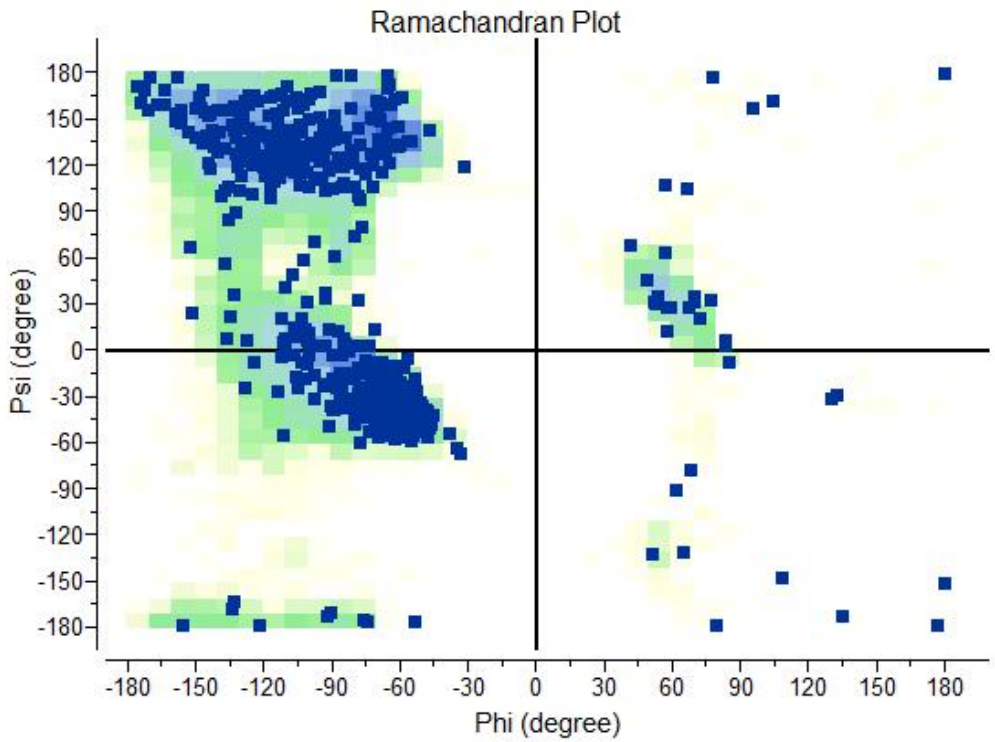

Figure 4.2 Ramachandran plot generated from the homology dimer model for *S. aureus* FtsZ.The light blue, green, and light green regions represent the favored, allowed, and "generously allowed" regions as defined by ICM.

4.3.2 Prediction of binding pose of berberine with *S. aureus* FtsZ dimer

Berberine has been predicted to bind to the GTP hydrophobic pocket in FtsZ based on STD-NMR and molecular docking [35]. In this study, berberine was docked into the hydrophobic region of GTP binding pocket detected by ICM PocketFinder in the *S. aureus* FtsZ dimer model. In order to take into account the FtsZ binding pocket flexibility, multiple conformations of the GTP binding pocket were generated through side chain sampling of the amino acids around berberine. The side chain sampling resulted in 48 energetically favorable pocket conformations. Berberine was then docked to each conformation. The best ICM binding score was –24.94. The top-scored binding pose of berberine is shown in Figure 4.3. In comparison with the literature report on predicted binding pose for berberine in the *E. coli* model [35], the core of berberine was found to be flipped by 180^{o} in the *S.aureus* FtsZ dimer (Figure 4.3), though the same binding regions were observed in both models [35]. In the *S. aureus* FtsZ dimer model, berberine occupied the hydrophobic region in GTP binding site by forming hydrophobic interactions with Gly22, Gly104, Met105, Gly106, Gly107, Arg143 and Phe183. In addition, one hydrogen bond was

formed between the oxygen atom on ring A of berberine and Thr133 (2.73Å). This *S. aureus* FtsZ dimer model was then used to predict the binding modes of the 9-phenoxyalkyl substituted protoberberine derivatives.

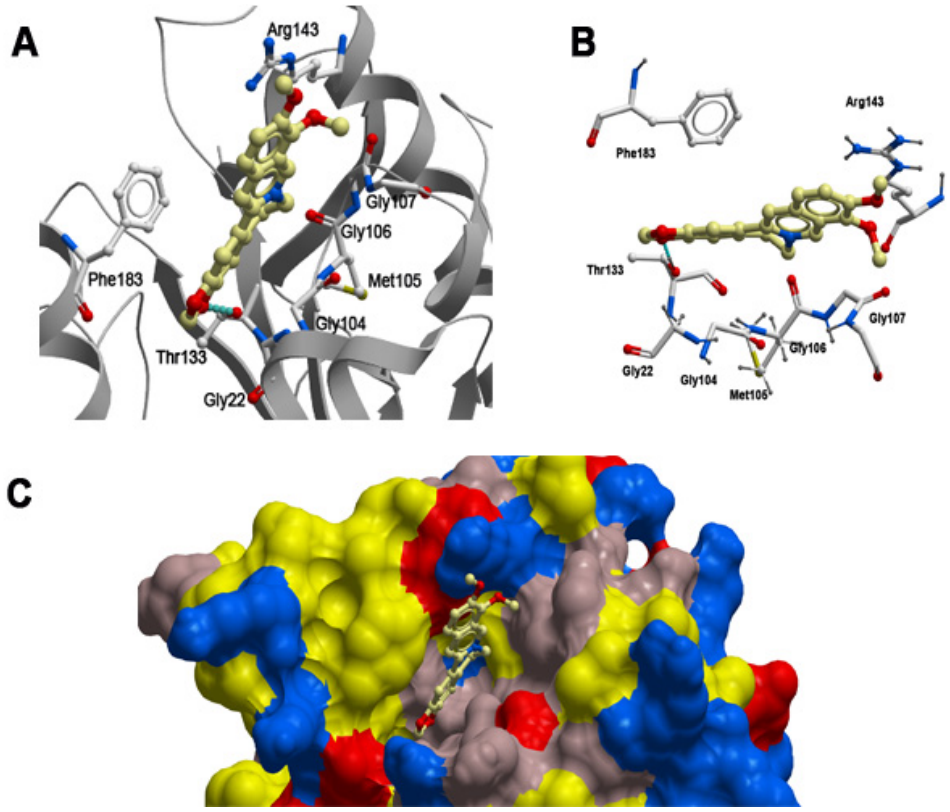

Figure 4.3 Top-scoring binding pose of berberine in the *S. aureus* FtsZ dimer model. (A) The FtsZ model is shown by grey ribbon. Interacting residues are labeled and shown as balls and sticks. Hydrogen bond is represented with cyan sphere. (B) Close-up view of the active site of berberine on FtsZ. (C) Surface map of berberine in the hydrophobic groove of FtsZ. Hydrophobic region is represented in yellow.

4.3.3 Molecular modeling study of protoberberine derivatives with FtsZ dimer

In this study, the ICM-docking algorithm was used to predict interaction mode(s) and assign binding score to rank the derivatives of protoberberine alkaloid according to the quality of their fits to FtsZ, which ideally reflects the affinity of binding [73, 117] .

4.3.3.1 Predicted binding poses of berberine derivatives with FtsZ dimer

In an attempt to better understand the relationship between FtsZ binding and inhibitory activity, the berberine derivatives (**B1** to **B6**) were docked into the *S. aureus* FtsZ dimer model. The ICM binding scores are summarized in Table 4.1. The ICM binding score of all berberine derivatives are better than the ICM standard threshold (−32 kJ/mol), as well as the parent berberine. As shown in Table 4.1, the docking results (ICM binding score) of all derivatives correlated well with the results of *in vitro* GTPase inhibitory activity experiments. Docking with different functional substituents (methyl, bromide, chloride, fluoride, methoxy, nitro) at the phenyl ring of berberine derivatives resulted in similar ICM binding scores. Figure 4.4 illustrates the predicted binding poses of the selected derivatives **B1**−**B3**. Analysis of docking results indicated that the main protein−ligand interactions for these derivatives are hydrophobic. In comparison with the parent compound berberine, the cores of these three derivatives have similar hydrophobic interactions in the GTP binding site such as Gly22, Gly104,

Phe183 and Arg143. Apart from the core interactions with the hydrophobic residues of GTP binding site, the phenyl ring of compounds **B1**–**B3** formed additional hydrophobic interactions with residues at helix H8 and/or T7 loop that also involve in binding the potent FtsZ inhibitor PC197034 (Figure 4.4) [118].

From the predicted binding pose of compound **B1**, additional hydrophobic interactions with Ala73 and Ala186 were observed, as well as hydrophobic interactions of the 3-carbon linked phenoxy moity with residues at C-terminal helix and the stand of adjacent FtsZ monomer including Asp213, Thr216 and Val 217 in helix H8, and Asn291 in stand S9 (Figure 4.4 A). Indeed, Asp213, which is 100% conserved in all known FtsZ sequences, is one of essential residues for GTP hydrolysis [119]. This implies that interaction with conserved residue is potentially useful to avoid the drug resistance problem caused by protein mutation.

Different substituent groups at the ortho- or para-position of the phenyl ring lead to slightly different interactions with the C-terminal domain of the adjacent monomer. As shown in Figures 4.4 B, compound **B2** has hydrophobic interactions with Ala73 and Pro135 in the GTP binding site.

More hydrophobic interactions were found for compound **B3** including Met105, Gly106, Glu146, Pro135 and Lys142 (Figure 4.4 C). But the same hydrophobic interactions with Thr216 and Asn291 in the C-terminal domain of the adjacent monomer were observed for both **B2** and **B3**, revealing that the small substituent at the phenyl group has less effect on the inhibition of FtsZ.

These observations together with the biological test results in chapter 2 suggest that halogen substituted phenoxyalkyl linked berberines, particularly **B2**, are promising in improving the potency and spectrum of activity especially for Gram-negative strains.

The berberine derivatives with 3- or 4-carbon ether linkers (Compounds **B1** and **B1-1**) showed similar docking poses. The docking poses hinted that the 3-C or 4-C linker of berberine derivatives play an important role in driving the phenoxy moiety to bind to the T7 loop of FtsZ.

Table 4.1 Structures, ICM binding scores and *in vitro* inhibition of selected berberine derivatives

Compound	Structure	GTPase inhibitory activity IC_{50} (μM)	ICM score
Berberine	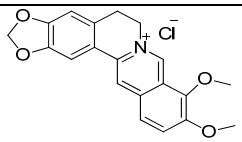	272 ± 46.6	–24.94
B1	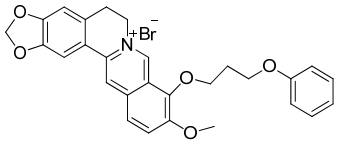	56.8 ± 10.4	–35.06
B1-1	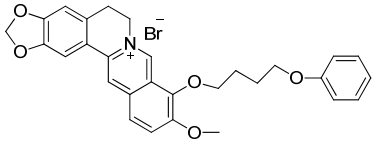	63.5 ± 4.7	–34.51
B2	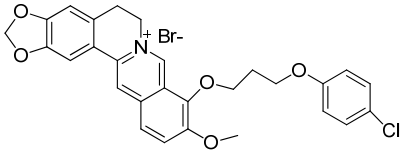	37.8 ± 3.8	–32.33
B3	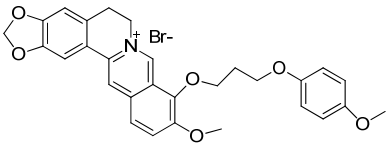	47.3 ± 4.6	–32.41
B4	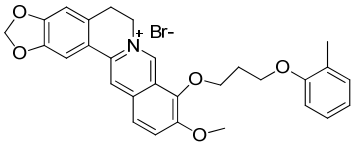	63.7 ± 4.8	–32.13
B5	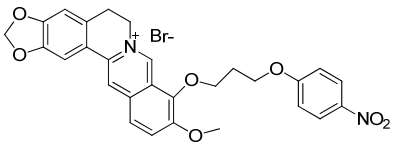	43.4 ± 5.2	–32.05
B6	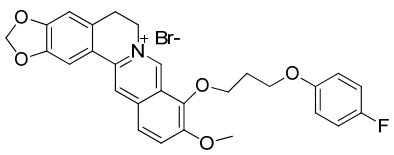	40.1 ± 3.4	–32.71

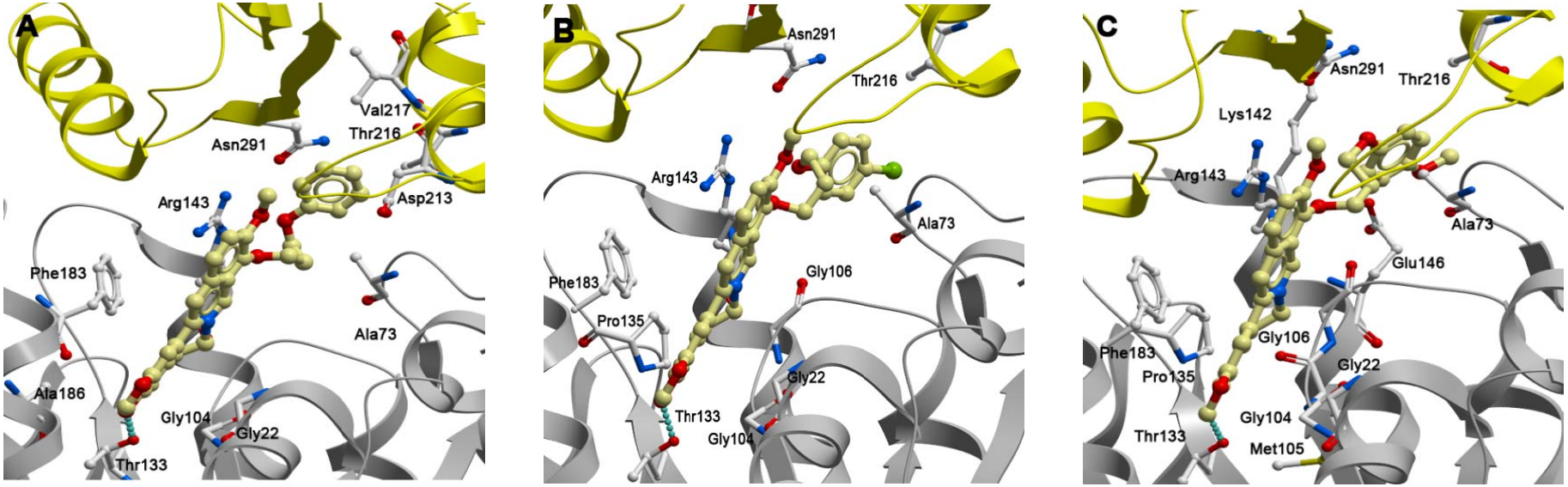

Figure 4.4 Docking poses of berberine derivatives in the *S. aureus* FtsZ dimer model. Interacting residues are labeled and shown in balls and sticks. Compound **B1** (A), compound **B2** (B) and compound **B3** (C).

4.3.3.2 Benckmarking study

To assess the quality of the *S. aureus* FtsZ dimer model and its potential usefulness for drug design applications, a small scale virtual ligand screening was performed using a DUD test set combining seven berberine and its derivatives with 233 decoys [114]. The results are summarized in Figure 4.5. The receiver operating characteristic (ROC) curve suggests that the *S. aureus* FtsZ dimer model demonstrated very good selectivity for berberine derivatives in virtual ligand screening (NSQ_AUC = 70) (Figure 4.5). All active berberine derivatives were ranked in the top 1% of the whole test set. Furthermore, consistent binding poses for all active berberine derivatives were observed. This best performing model can be used for further structure-based drug design and provide an accurate structural template for rational optimization of chemical properties for protoberberine derivatives.

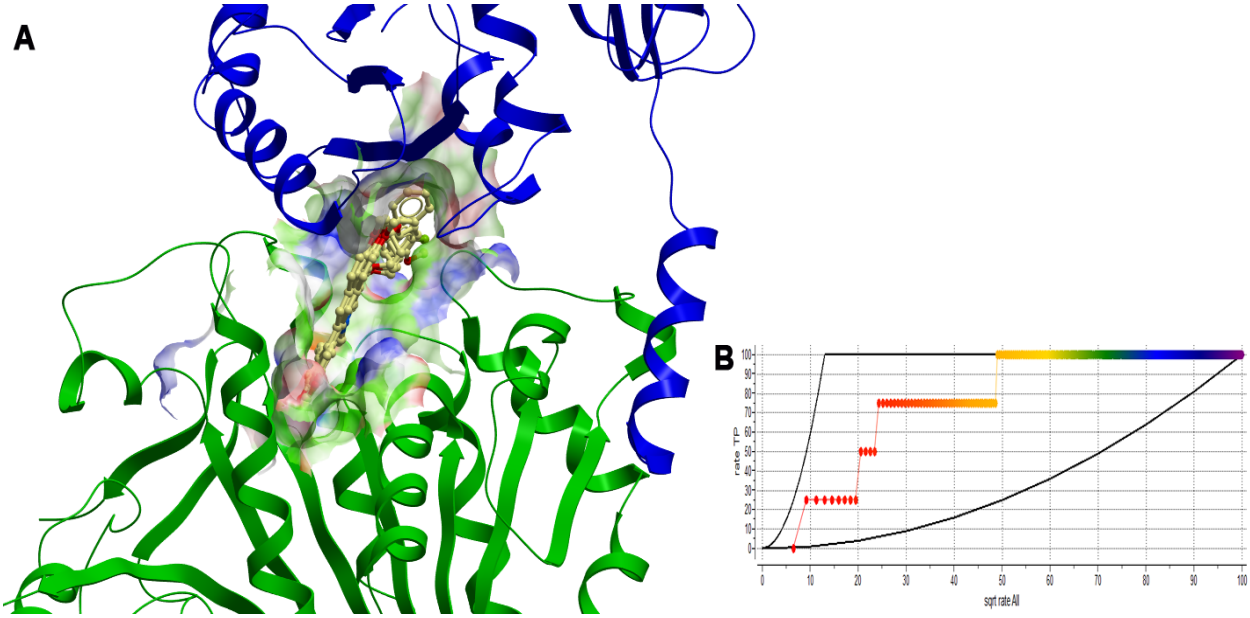

Figure 4.5 Performance of *S. aureus* FtsZ dimer model. (A) Docking poses of 7 berberine derivatives (Compounds **B1-B6** and **B1-1**). The two subunits of the FtsZ dimer model are depicted in ribbon form and are colored green (subunit A) and blue (subunit B). The small molecules are depicted as ball-and-stick models showing carbon (yellow), hydrogen (grey), oxygen (red), nitrogen (blue), and halogen (green) atoms. The binding pocket of the FtsZ dimer is represented as a translucent color surface. (B) Receiver operating characteristic (ROC) curves are shown in semilogarithmic scale.

4.3.3.3 Predicted binding poses of palmatine derivatives with FtsZ dimer

In order to understand the inhibitory activity of the palmatine derivatives, the FtsZ binding modes of all synthesized palmatine derivatives were studied by docking. As shown in Table 4.2, the binding score of all compounds in docking simulations (better than the ICM threshold default value of −32) correlated well with their inhibition activity. In addition, consistent binding poses were observed for all compounds (Figure 4.6). The parent compound palmatine occupied the hydrophobic region of GTP binding site, which is similar to that of berberine (Figure 4.7). Palmatine binds to the FtsZ through hydrophobic interactions with Gly22, Gly104, Gly106, Gly107, Arg134, Pro135 and Phe183. The two methoxyl groups on the C-2 and C-3 positions of palmatine interact hydrophobically with Thr133 and Ala186. In addition, weak hydrogen bonds were formed between Thr133 and the methoxyl groups at the C-2 and C-3 positions (2.5 Å and 2.9 Å).

Consistent with previous observations for berberine derivatives, replacement of an OH group attached to the C-9 position of palmatine with an aromatic ring by a 3-carbon ether linker (compound **P1**) greatly enhanced the activity (Table 4.2). Just like palmatine, the same interactions were observed for the core of compound **P1** in the GTP binding hydrophobic pocket of FtsZ (Figure 4.8). Interestingly, the predicted binding pose for **P1** is totally different from that of berberine derivative **B1**. The two compounds were found to bind to different C-terminal pockets although these two pockets are also partially formed by β sheet S9 (Figure 4.8). As shown in Figure 4.9, a flexible ether linker in compound **P1** was found to bury deeply in the narrow cleft formed by the C-terminal helix H10 and β sheet S9 in chain B through hydrophobic interations with Arg143 in chain A and Gln283 and Met292 in chain B. The oxygen atom of the linker in **P1** formed hydrogen-bonds with Arg143 (2.6 Å and 2.8 Å). These extra interactions might be the reason that compound **P1** is more active than the parent compound palmatine. In the *in vitro* assay, similar inhibitory activities were observed for compounds **P1** with a 3-carbon ether chain and **P1-1** with a 4-carbon ether chain, which correlated well with the docking results of binding scores of −33.19 and −32.05 respectively (Table 4.2). Similar docking poses were observed for both **P1** and **P1-1** (Figure 4.9). On the

basis of experimental and docking results, we postulated that a 3-carbon ether chain is long enough for the phenoxy group to interact with residues at the C-terminal helix H10 and β sheet S9 of the adjacent monomer.

For compounds **P2**–**P6** similar binding scores and predicted binding poses were found (Figure 4.10 and Table 4.2), suggesting that there is no subtle effect of substituents at the phenyl ring on the binding to FtsZ.

Table 4.2 Structures, ICM binding scores and *in vitro* inhibition of selected palmatine derivatives

Compound	Structure	GTPase inhibitory activity IC_{50} (μM)	ICM score
Palmatine	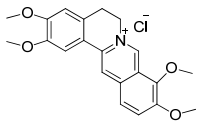	327.71 ± 50.0	–24.17
P1	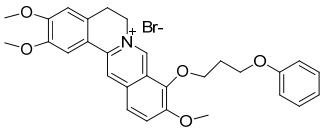	70.1 ± 10.9	–33.19
P1-1	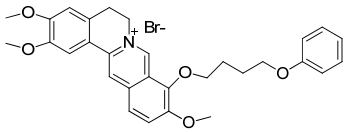	79.2 ± 0.5	–32.05
P2	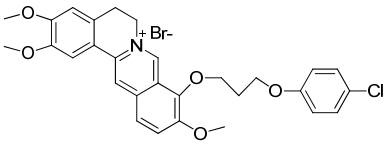	45.1 ± 2.1	–37.24
P3	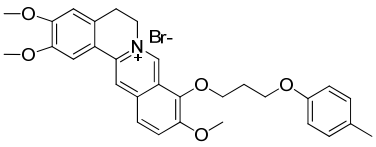	57.4 ± 10.8	–33.64
P4	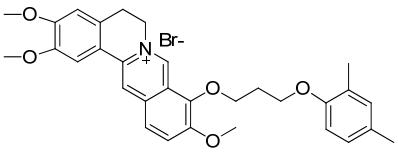	75.3 ± 6.4	–32.49
P5	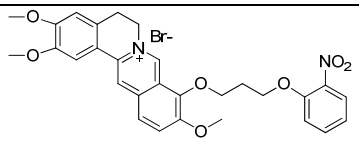	78.6 ± 5.7	–37.14
P6	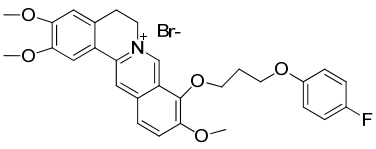	46.8 ± 4.7	–36.89

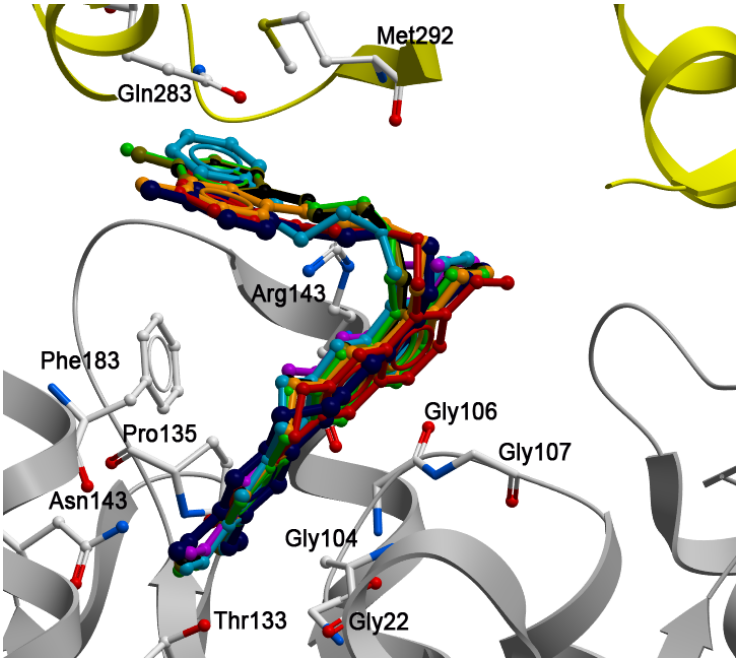

Figure 4.6 Docking poses of palmatine and its derivatives in the *S. aureus* FtsZ dimer model. Interacting residues are labeled and shown in balls and sticks. Palmatine (purple), **P1** (black), **P1-1** (blue), **P2** (green), **P3** (orange), **P4** (dark blue), **P5** (red) and **P6** (brown).

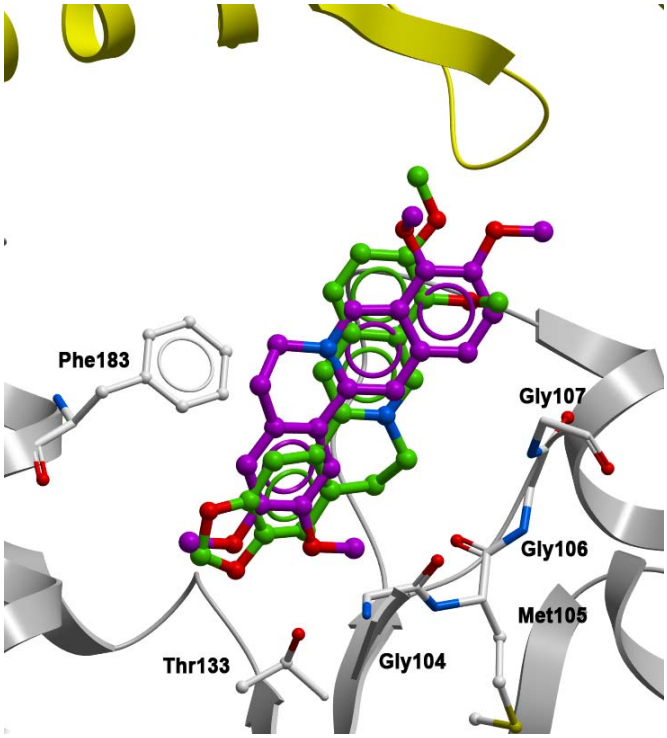

Figure 4.7 A comparison of the docking poses of berberine (carbon – green) and palmatine (carbon - purple) in the GTP binding site of the *S. aureus* FtsZ dimer model. Interacting residues are labeled and shown in balls and sticks.

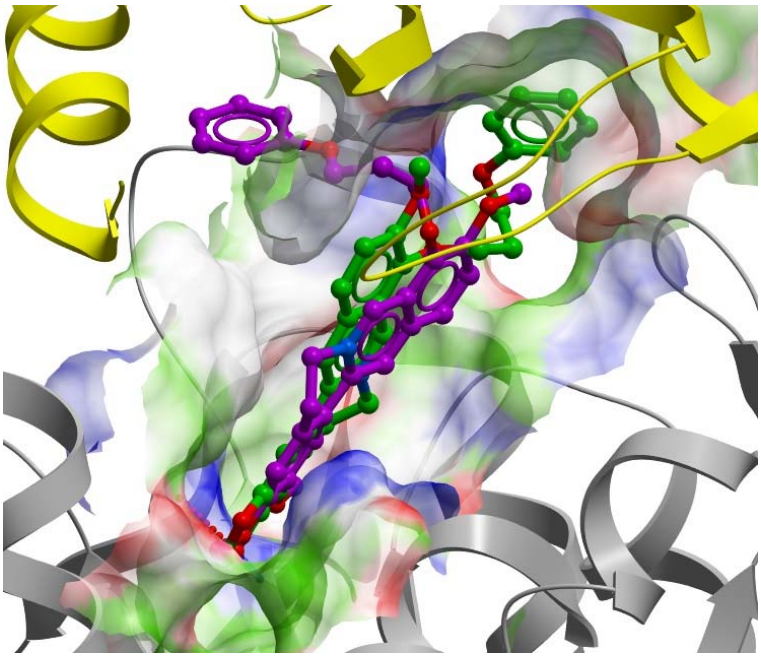

Figure 4.8 Docking poses of compounds **B1** (carbon – green) and **P1** (carbon - purple) in the GTP binding site of the *S. aureus* FtsZ dimer model.

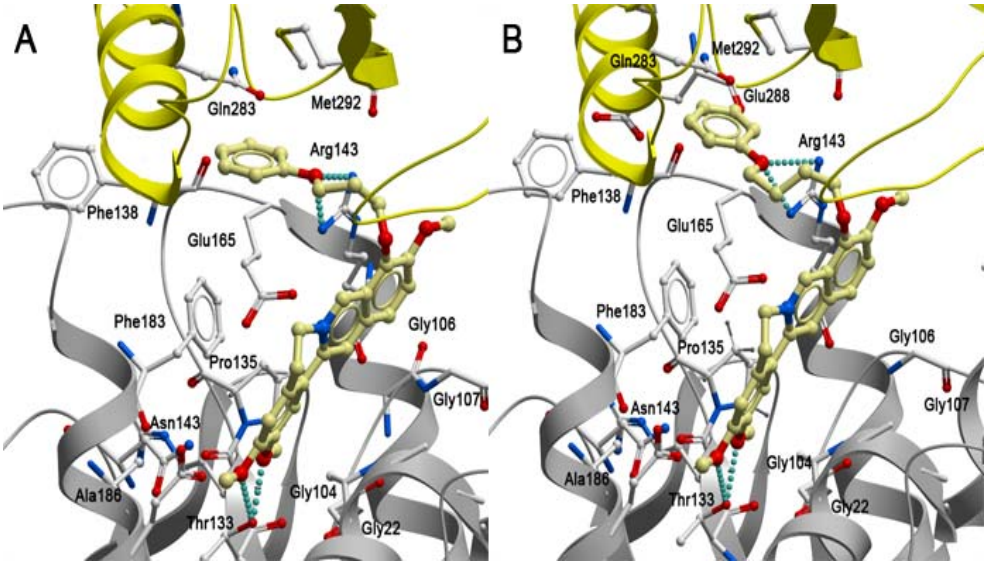

Figure 4.9 Docking poses of palmatine derivatives **P1** (A) and **P1-1** (B) in the *S. aureus* FtsZ dimer model. The structure of FtsZ dimer is represented by ribbon (chain A – grey, chain B – yellow). Interacting residues are labeled and shown in balls and sticks.

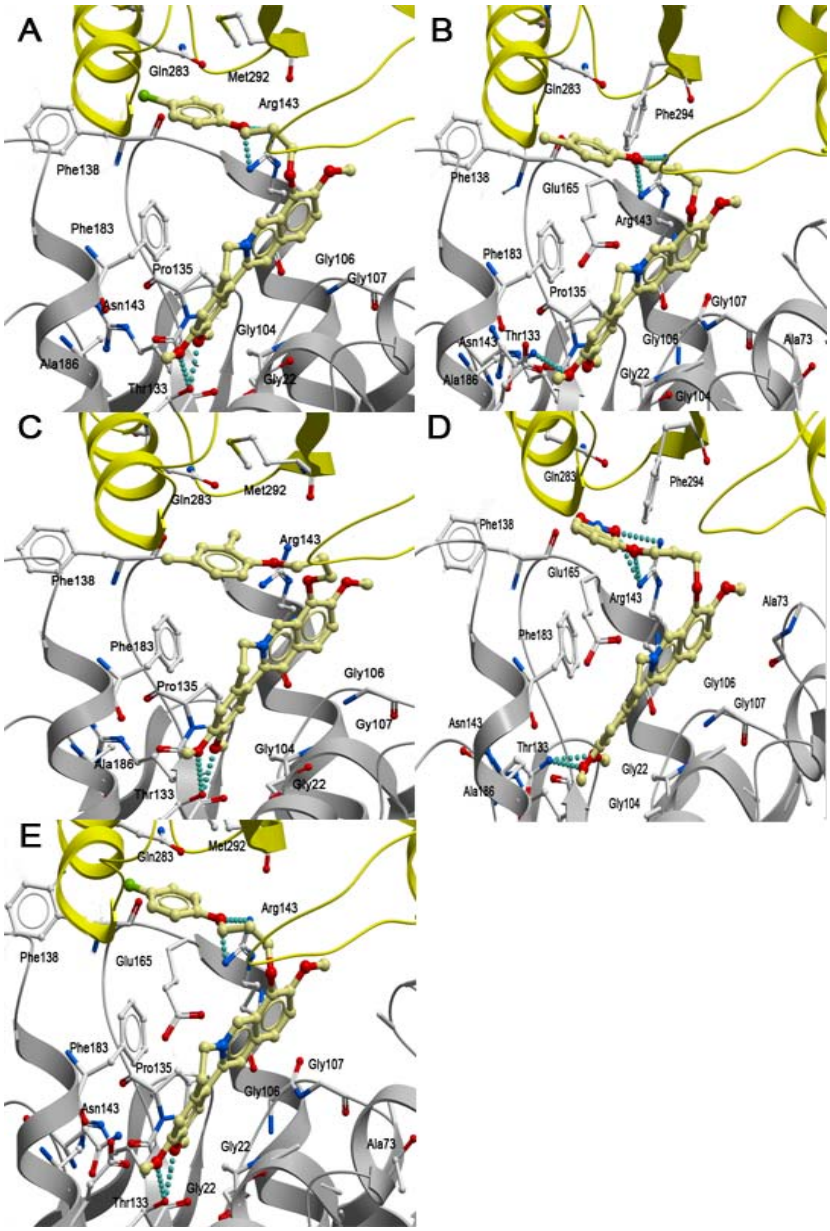

Figure 4.10 Docking poses of palmatine derivatives **P2** (A), **P3** (B), **P4** (C), **P5** (D) and **P6** (E) in the *S. aureus* FtsZ dimer model. The structure of FtsZ dimer is represented by ribbon (chain A – grey, chain B – yellow). Interacting residues are labeled and shown in balls and sticks.

4.4 Concluding remarks

A homology model of *S. aureus* FtsZ dimer was built to predict the binding poses of 9-phenoxyalkyl substituted protoberberine derivatives. The docking results suggested that the 3-carbon ether-linked phenyl group is a key factor for the enhanced activity compared to the parent compounds, since the phenyl ring interacts with the residues at C-terminal domain (helix H8 or T7 loop) of another monomer. The experimental and docking results suggested that the optimal carbon number of the ether linker connecting the aromatic ring to the core berberine or palmatine should be 3. Correlation between inhibitory activity and the linker length was the same in both series of protoberberinium derivatives. Therefore, protoberberine derivatives with aromatic substituents at the 9 position may be used as a template for the future design of bivalent FtsZ inhibitors with potent pharmacokinetic properties.

Chapter 5

Synergistic effect and cytotoxicity tests of berberine and palmatine and their derivatives

5.1 Introduction

Besides identifying new antibiotics with novel mechanisms, another approach to tackle the antibiotic resistance problem is to explore the synergistic effect of two or more antibiotics in the treatment of bacterial infections. In chapters 2 and 3, 9-phenoxyalkyl substituted protoberberines were identified to be FtsZ inhibitors and found to possess strong antimicrobial activities. In order to further improve the antimicrobial efficacies, these compounds were tested in combination with common antibiotics such as ampicillin, oxacillin, ceftazidim and vancomycin against the antibiotic-resistant bacterial strains. The four antibiotics used in this study are commonly used in treating bacterial infections by inhibiting the bacterial cell wall synthesis, but have become less effective due to the emergence of drug-resistant strains.

In addition to synergy tests, *in vitro* cytotoxicity tests were undertaken to evaluate the toxicity effect of compounds **B2** and **P2** on three mammalian cell lines (a mouse fibroblast plus two breast cancer cell lines). Studying the toxicity of lead compounds at an early phase of drug discovery is very important because it alerts and allows the scientists to modify the structure to eliminate or lower the toxicity. Compounds with strong toxicity effect will not be allowed to enter into clinical trials. The selectivity indices of cytotoxicity IC_{50} values versus the MIC values of these compounds were calculated to give an estimation of whether the compounds are good candidates as antibiotics.

5.2 Experimental section

5.2.1 Synergy test

The synergistic effect of protoberberines or their derivatives together with conventional antibiotics was tested using a broth microdilution checkerboard method by comparing the MICs of the two individual agents and in combination [120-122]. The MICs of these compounds were determined using the antimicrobial susceptibility test described in chapter 2. The checkerboard assay is the most common method used to measure antibacterial combination effects [82]. The MIC of each compound was determined individually and in combination at a fixed concentration ratio of 1:1. For instance, a combination of **B2** and ampicillin was tested at a constant volume with concentration ratio of 1:1 against ampicillin-resistant *S. aureus*. The conventional antibiotics used in this assay were purchased from Sigma-Aldrich. The synergistic effect between compounds and antibiotics were evaluated using the fractional inhibitory concentration index (FICI). FICI was calculated as FICI = ($MIC_{a\ combination}/MIC_{a\ alone}$) + ($MIC_{b\ combination}/MIC_{b\ alone}$). The FIC indexes at values of ≤0.5, 0.5 - 1, 1 - 4,

and >4 were defined as synergistic, partial synergistic, additive or indifferent, and antagonistic, respectively [122].

5.2.2 Cytotoxicity test

The cell lines used in this test were stocks in our department. In this assay, 50,000 cells of L929 (a mouse fibroblast acts as a normal cell line) or LCC6 (wild type breast cancer cell line) or LCC6MDR (Pgp-overexpressed breast cancer cell line) were mixed with compounds of various concentrations and made up to a final volume of 100 μL in 96-well plates. The plates were then incubated for 3 days at 37 ^{o}C. The half-maximal inhibition (IC_{50}) of the compounds were determined using the CellTiter 96 AQ_{ueous} Assay (Promega). 2 mg/mL of 3-(4,5-dimethylthiazol-2-yl)-5-(3-carboxy-methoxyphenyl)-2-(4-sulfophenyl)-2H-tetrazolium (MTS, Promega) and 0.92 mg/mL of phenazine methosulfate (PMS, Sigma-Aldrich) were mixed in a ratio of 20:1. A 10 μL aliquot of the freshly prepared MTS/PMS mixture was added into each well, and the plate was incubated at 37 ^{o}C for 2 hours. The optical absorbance at 490 nm was then recorded with a microplate absorbance reader (Bio-Rad). IC_{50} values were calculated from the dose-response curves using the GraphPad (Prism 4.0). All experiments were performed in triplicates and the results were represented as mean ± SEM.

5.3 Results and discussion

5.3.1 Synergistic effect of two antimicrobial agents

The synergistic effects of protoberberins and their derivatives with conventional antibiotics against some drug-ressistant bacterial strains were tested. The individual and combined fractional inhibitory concentration indices (FICIs) for the antibacterial activity of different combinations of compounds are summarized in Tables 5.1 to 5.4. As shown in Tables 5.1 and 5.2, the combination of berberine or palmatine with ampicillin displayed partial synergistic effects against ampicillin-reistant *S. aureus* strain and methicillin-resistant *S. aureus* strain (MRSA), with combined FICIs of 0.83. The antibacterial activity was significantly improved when ampicillin was combined with compound **B2** or **P2**. The FICI values of 0.5 indicated synergism for the compounds with ampicillin against drug-resistant *S. aureus* strains. In addition, partial synergistic or synergistic effects were also observed when protoberberins or their derivatives were combined with oxacillin against MRSA (Table 5.2). The MIC value of **B2** decreased to 0.5 μg/mL (1 μM) when it was used together with ampicillin or

oxacillin against drug-resistant *S. aureus* strains, suggesting **B2** has a potential to be a lead compound of novel antibiotic. When it comes to the vancomycin-resistant *E. faecium* strain, the results are not as good as those with *S. aureus* strains. Only partial synergistic effect was observed when compound **B2** or **P2** was combined with vancomycin against *E. faecium* strain (Table 5.3). In addition, two Gram-negative strains which produce AmpC beta-lactamase were also studied. Partial synergistic effects were observed when **B2** or **P2** was combined with ceftazidim against an *E. cloaca*, which is a high level producer of chromosomal AmpC beta-lactamase (Table 5.4). However, no synergistic effect was observed on the low level AmpC beta-lactamase producing strain *K. pneumonia*.

Table 5.1 Synergy tests of protoberberines and their derivatives plus ampicillin against the ampicillin-resistant *S. aureus* strain (ATCC 29247)

Compound	MIC (μg/mL)	FICI (response)[1]
Berberine	128	
Palmatine	256	
Ampicillin	48	
B2	2	
P2	4	
Berberine + Ampicillin	64 + 16	0.83 (PS)
Palmatine + Ampicillin	128 + 16	0.83 (PS)
B2 + Ampicillin	0.5 + 12	0.5 (S)
P2 + Ampicillin	1 + 12	0.5 (S)

[1] S, synergistic; PS, partial synergistic.

Table 5.2 Synergy tests of protoberberines and their derivatives plus ampicillin or oxacillin against the methicillin-resistant *S. aureus* (MRSA) strain (ATCC BAA-41)

Compound	MIC (μg/mL)	FICI (response)[1]
Berberine	128	
Palmatine	256	
Ampicillin	48	
Oxacillin	256	
B2	2	
P2	4	
Berberine + Ampicillin	64 + 16	0.833 (PS)
Palmatine + Ampicillin	128 + 16	0.833 (PS)
B2 + Ampicillin	0.5 + 12	0.5 (S)
P2 + Ampicillin	1 + 12	0.5 (S)
Berberine + Oxacillin	64 + 64	0.5 (S)
Palmatine + Oxacillin	192 + 64	1.0 (PS)
B2 + Oxacillin	0.5 + 64	0.5 (S)
P2 + Oxacillin	1 + 64	0.5 (S)

[1] S, synergistic; PS, partial synergistic.

Table 5.3 Synergy tests of **B2** and **P2** plus vancomycin against the vancomycin-resistant *E. faecium* strain （ATCC 700221）

Compound	MIC (μg/mL)	FICI (response)[1]
Vancomycin	48	
B2	4	
P2	8	
B2 + Vancomycin	1 + 24	0.75 (PS)
P2 + Vancomycin	4 + 24	1.0 (PS)

[1] PS, partial synergistic.

Table 5.4 Synergy tests of **B2** and **P2** plus ceftazidim against strains producing AmpC beta-lactamase

E. cloacae ATCC BAA-1143 (a high level producer of chromosomal AmpC beta-lactamase commonly used as a control for the AmpC disk test)		
Compound	MIC (μg/mL)	FICI (response)[1]
Ceftazidim	384	
B2	32	
P2	128	
B2 + Ceftazidim	16 + 128	0.83 (PS)
P2 + Ceftazidim	32 + 128	0.58 (PS)

K. pneumonia ATCC BAA-1144 (a low level producer of AmpC beta-lactamase)		
Compound	MIC (μg/mL)	FICI (response)[1]
Ceftazidim	16	
B2	64	
P2	128	
B2 + Ceftazidim	32 + 12	1.25 (A)
P2 + Ceftazidim	64 + 12	1.25(A)

[1] PS, partial synergistic; A, additive.

5.3.2 Cytotoxicity

The toxicity effects of B2 and P2 on three mammalian cell lines were tested. The results are shown in Table 5.5. Compounds **B2** and **P2** were found to exert toxic effects. They inhibit the proliferation of the cancer cells and mouse fibroblast cells (L929 cell lines) in a concentration-dependent manner. For instance, **B2** and **P2** inhibited L929 cells with IC_{50} of 16.4 and 13.3 μM respectively. The toxicity of these compounds may be due to the phenoxyalkyl group, because the parent compound berberine is nontoxic to mammalian cells [87].

The selectivity indices (SI = IC_{50}/MIC) between cytotoxicity IC_{50} and MIC values of these compounds were calculated. For a drug to be considered as a good candidate for antibiotic its SI value should be higher than 10. Table 5.6 shows the selectivity indices of **B2** and **P2**. When **B2** or **P2** was used to treated methicillin-resistant *S. aureus* strain (MRSA) individually, the SI values are 4.1 and 1.67 respectively, revealing that they are strongly toxic effect. However, when **B2** was combinated with ampicillin, the SI value increased to 16.4. This result revealed that these compound can be considered a good candidate against *S. aureus* strain when used together with ampicillin (Table 5.6).

Table 5.5 IC_{50}s of **B2** and **P2** in cytotoxicity assay

Cytotoxicity (IC_{50}, μM)			
Compounds/Cells	LCC6	LCC6MDR	L929
B2	1.8 ± 0.6	20.0 ± 5.1	16.4 ± 4.4
P2	1.1 ± 0.1	32.0 ± 5.3	13.3 ± 1.1

LCC6: wild type breast cancer cell line;

LCC6MDR: Pgp-overexpressed breast cancer cell line;

L929: mouse fibroblast acts as a normal cell line.

Table 5.6 Selectivity indices of compounds **B2** and **P2**

Compound	Cytotoxicity on L929 (IC_{50}, μM)	MIC on MRSA (μM)	SI
B2	16.4	4	4.1
P2	13.3	8	1.67

Compound	Cytotoxicity on L929 (IC_{50}, μM)	MIC (combination with ampicillin) on MRSA (μM)	SI
B2	16.4	1	16.4
P2	13.3	2	6.65

5.4. Concluding remarks

In this chapter, we aimed to identify synergistic interactions between conventional antibiotics with protoberberines or its derivatives. It was found that these compounds exhibited synergistic, partial synergistic and additive effects in combination with clinically used antibiotics. Compounds **B2** and **P2** were found to have a stronger antibacterial activity when combined with ampicillin or oxacillin agaist methicillin-resistant *S.aureus*. On the other hand, the results of cytotoxicity assay and the selectivity indices suggested that although compound **B2** exerted a toxic effect on mammalian cell lines, the toxicity can be reduced when used together with ampicillin against *S.aureus*.

Chapter 6

Conclusions

Natural products and semi-synthetic natural products provide a rich source of bioactive drug like compounds for the development of new drugs. In the past few decades, several antibiotics used in clinical treatment are derived from natural sources, which include penicillin, vancomycin and ampicillin. Developing a new drug from a potent natural product is a good approach for improving the pharmacokinetics and pharmacodynamics. In this study, a modest FtsZ inhibitor, berberine, was used as the lead compound for further structure modification. Besides, after identifying inhibitory activity against FtsZ protein, another protoberberine, palamtine, was modified to improve its biological activities. Some 9-phenoxyalkyl substituted protoberberine derivatives were synthesized and subjected to biological and biochemical studies. All of these derivatives exhibited promising MIC values in the range of 2 to 8 μg/mL for their antibacterial activity against *S. aureus* strains, including ampicillin and methicillin

resistant strains. Moreover, compounds **B2** and **P2** were also found to exhibit activity against some Gram-negative strains. The standard light scattering assay to assess the effect of these compounds on the polymerization of FtsZ clearly showed the inhitbition of FtsZ assembly in a dose dependent manner. On the other hand, these compounds were also found to inhibit the GTPase activity of FtsZ. The results strongly suggest that suppression of GTPase activity destabilizes FtsZ polymer, leading to efficient inhibition of FtsZ polymerization. The effect of protoberberines and their 9-phenoxyalkyl substituted derivatives on FtsZ polymerization was also examined by TEM, which revealed an impressive dose dependent inhibition of *S. aureus* FtsZ assembly. The microscopic images of *B. subtilis* cells treated with these compounds were found to elongate by more than 10 folds. In addition, disturbances of Z-ring formation were also observed when *E. coli* JM109 WM647 was treated with compound **B2** or **P2**. All of these *in vitro* and *in vivo* results strongly suggest that these derivatives have a more potent activity against FtsZ protein and bacterial strains.

Molecular modeling was used to predict the binding poses of protoberberines and their 9-phenoxyalkyl substituted derivatives with a homology *S. aureus* dimer. Interestingly, the docking results showed that

the berberine or palmatine moiety of these derivatives bound to the GTP binding site, while the phenyl ring on the substituent interacted with the residues at the C-terminal domain of FtsZ protein. This is the first report on a small molecule capable of simultaneous interaction with two domains of FtsZ to improve its inhibitory activity.

The synergy study of protoberberines or their derivatives with common antibiotics were also investigated in this study. Synergistic and partial synergistic effects were observed when these compounds were used together with clinically approved antibiotics. Compound **B2** was found to have an impressive antibacterial activity when it was combined with ampicillin or oxacillin against methicillin-resistant *S. aureus* (MRSA). On the contrary, all of these derivatives were found to be toxic on mammalian cell lines. Fortunately, the toxicity of **B2** can be reduced by combining with ampicillin to treat *S. aureus* strains.

Although the findings reported in this thesis are encouraging, the protoberberine derivatives still require further optimization to enhance the binding affinity to FtsZ and reduce the cytotoxicity to mammalian cells. In subsequent lead optimizations, docking simulations could be employed to

screen newly designed derivatives based on the scaffold of compound **B2**. In addition, protein X-ray crystallography can be utilized to confirm the structure of the **B2**-FtsZ dimer complex. This protein-ligand crystal structure can provide important information for further modification of protoberberine derivatives and the design of new bivalent small molecules. On the other hand, the phenyl ring of protoberberine derivatives could be replaced by different heterocyclic rings, such as indole, pyrimidine and quinoline. These functional groups are planar in structure, which is similar to that phenyl ring of compound **B2**. The phenoxy moiety may also be replaced by other fuctionalities such as a benzoyl group. These functional groups may eliminate the tocixity effect led by the metabolic degradation of the phenyl or phenoxy ring. Through an iteration of *in silico* screening, chemical syhthesis and biological tests, one can expect that lead compounds with improved potency and lower cytotoxicity will be identified.

Appendix I: High resolution mass spectra of compounds

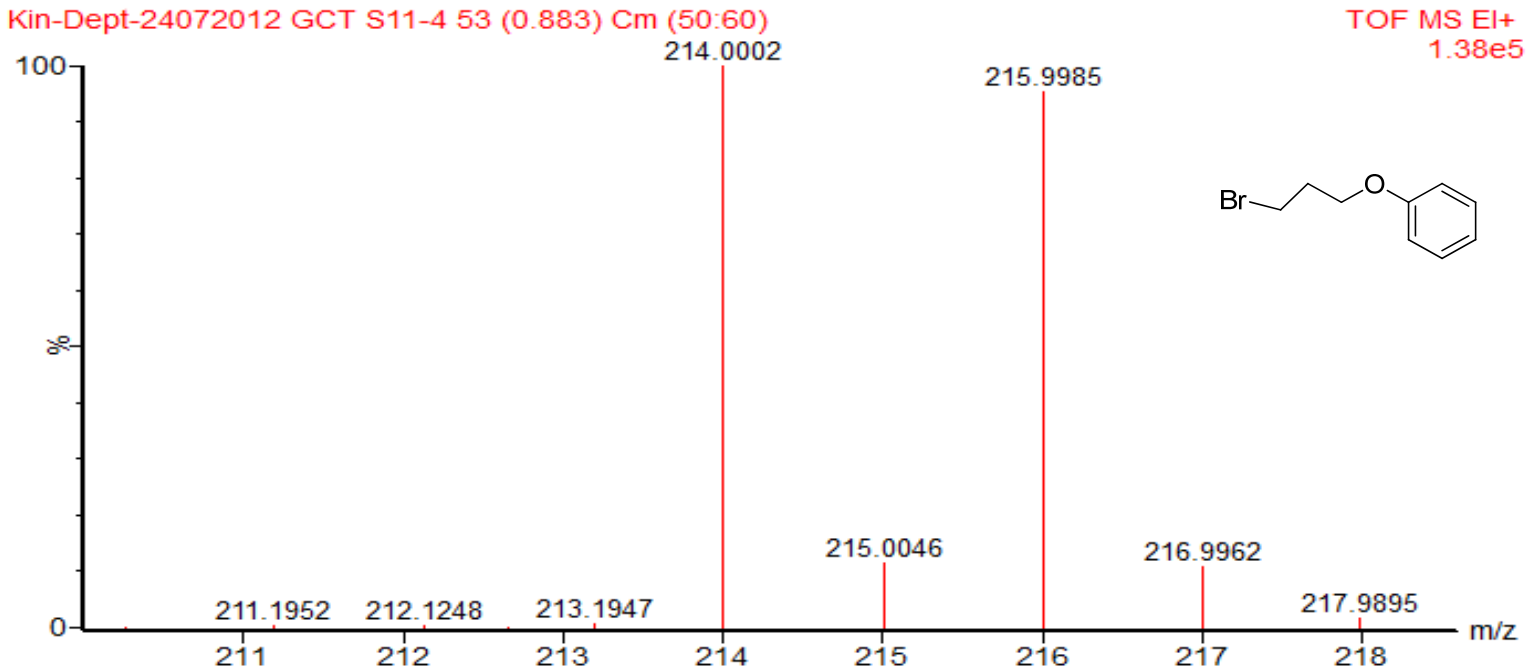

I-1 High resolution mass spectrum of compound **2**

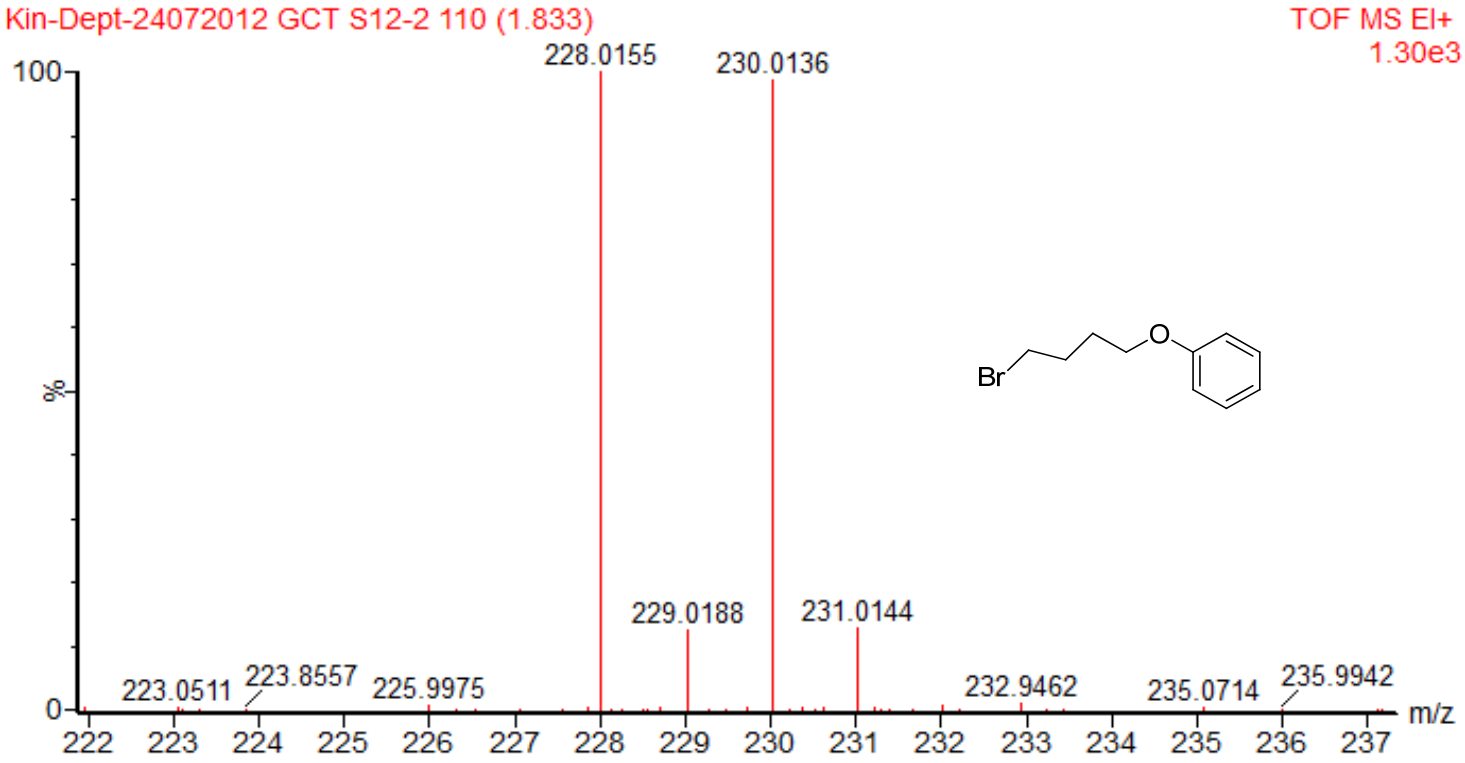

I-2 High resolution mass spectrum of compound **3**

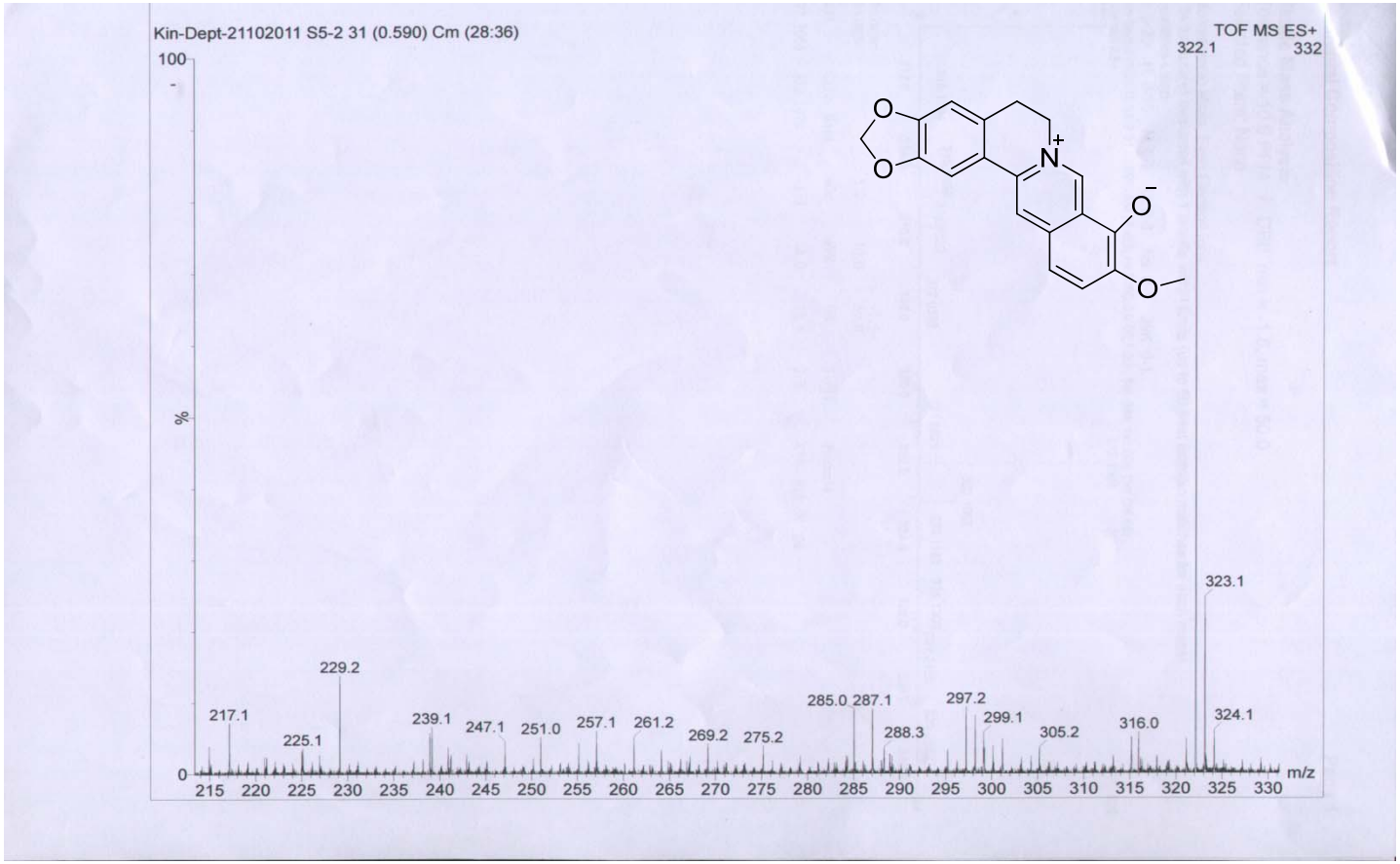

I-3 High resolution mass spectrum of compound **1** (berberrubine)

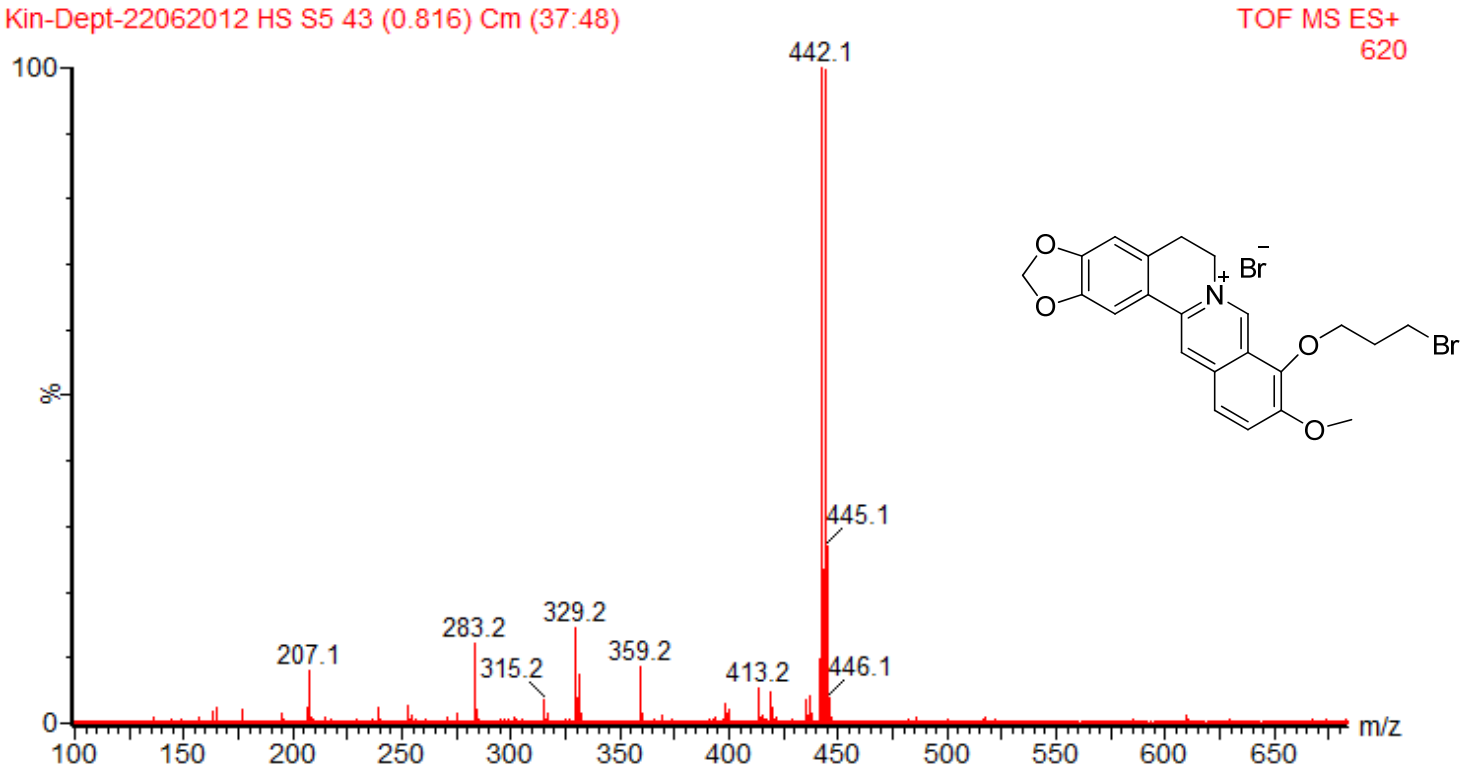

I-4 High resolution mass spectrum of compound **4**

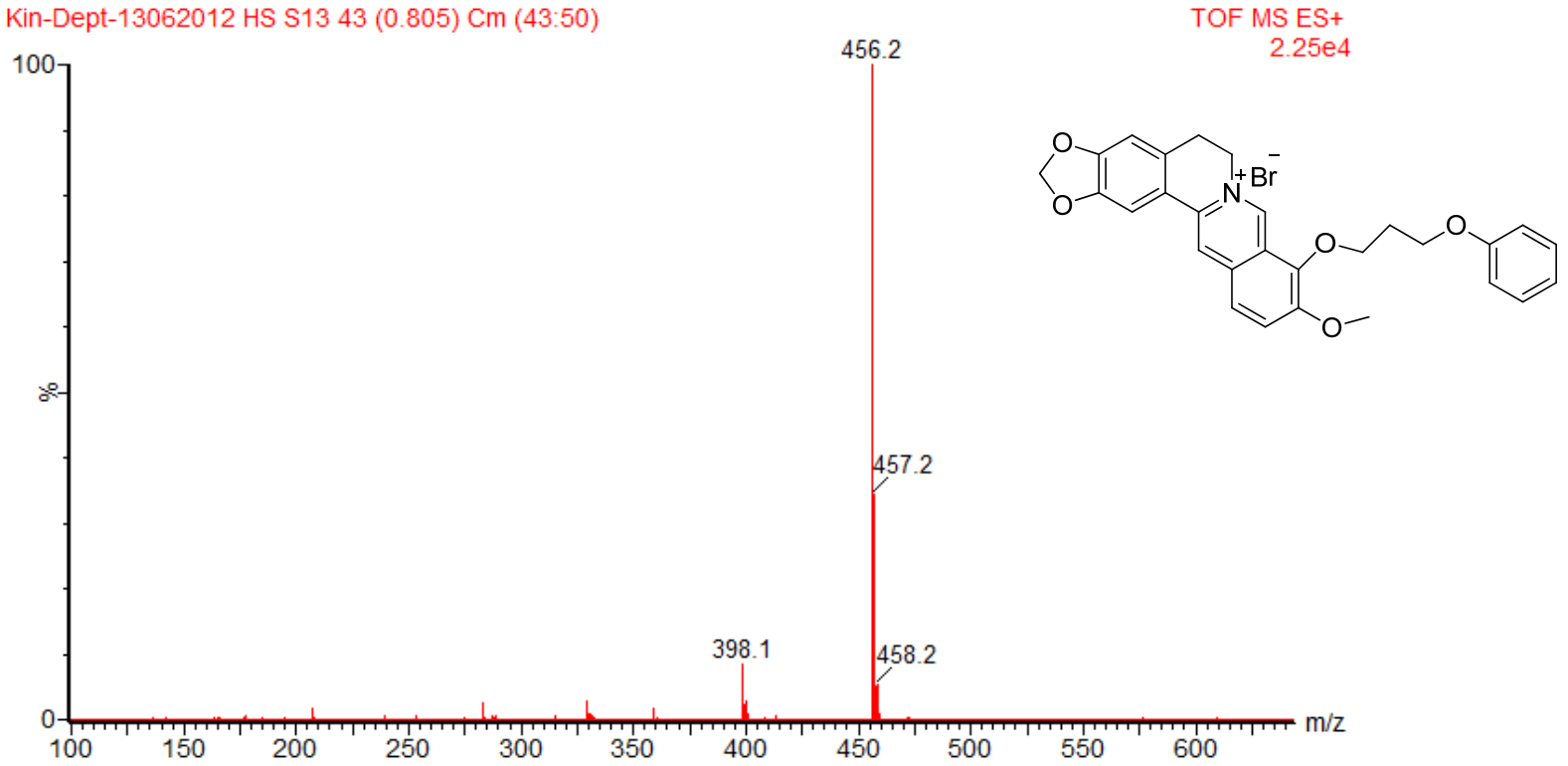

I-5 High resolution mass spectrum of compound **B1**

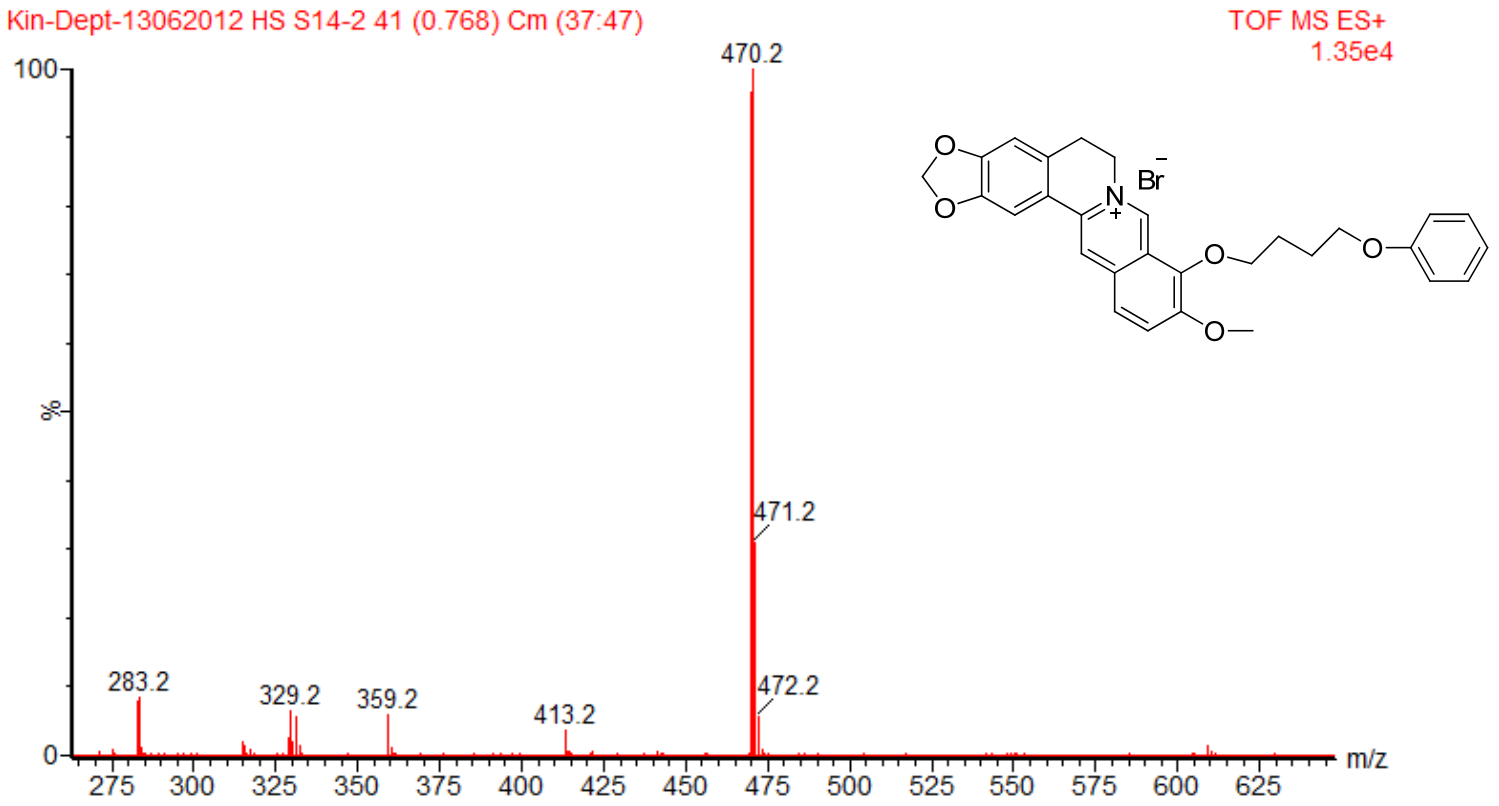

I-6 High resolution mass spectrum of compound **B1-1**

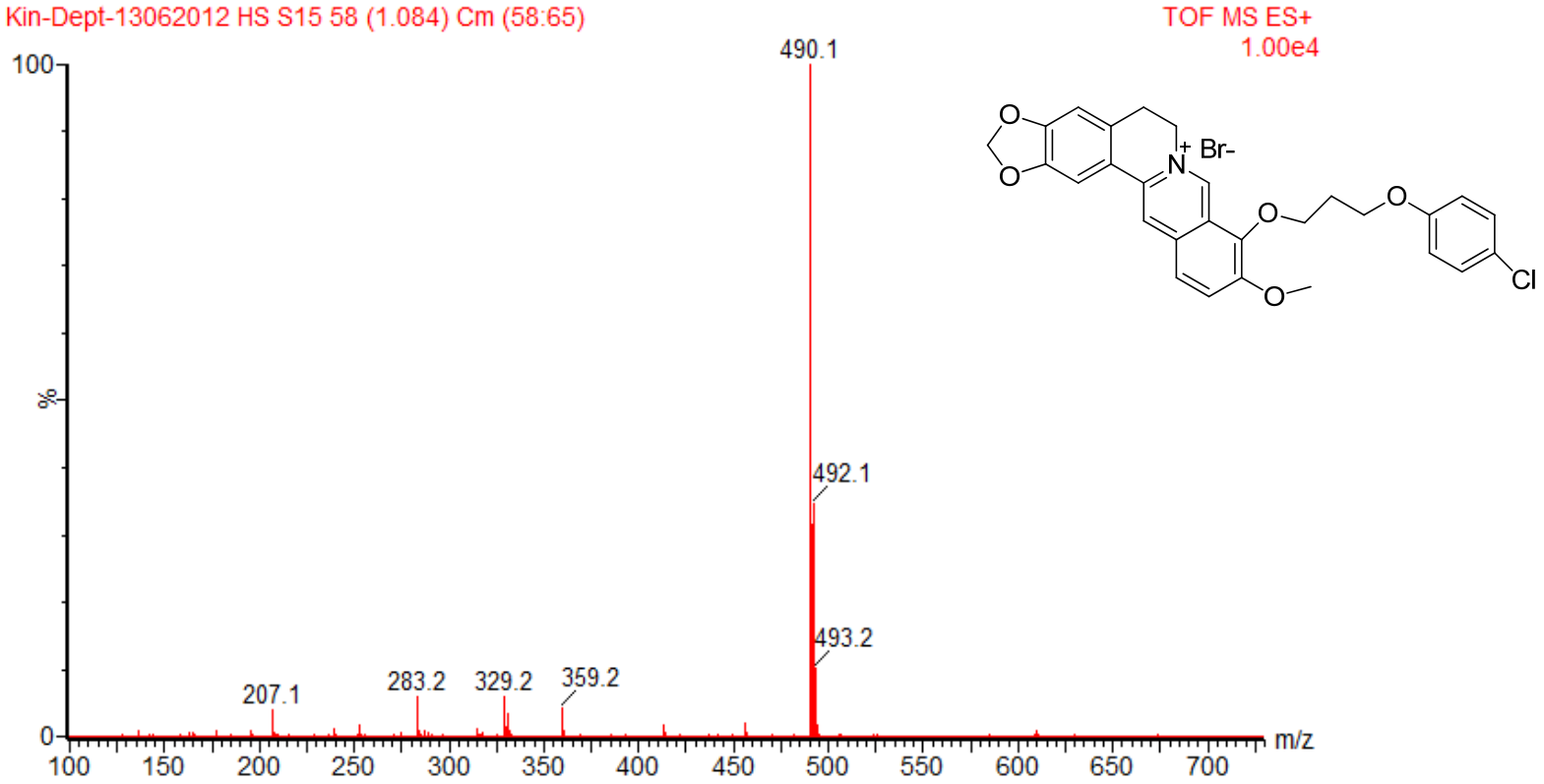

I-7 High resolution mass spectrum of compound **B2**

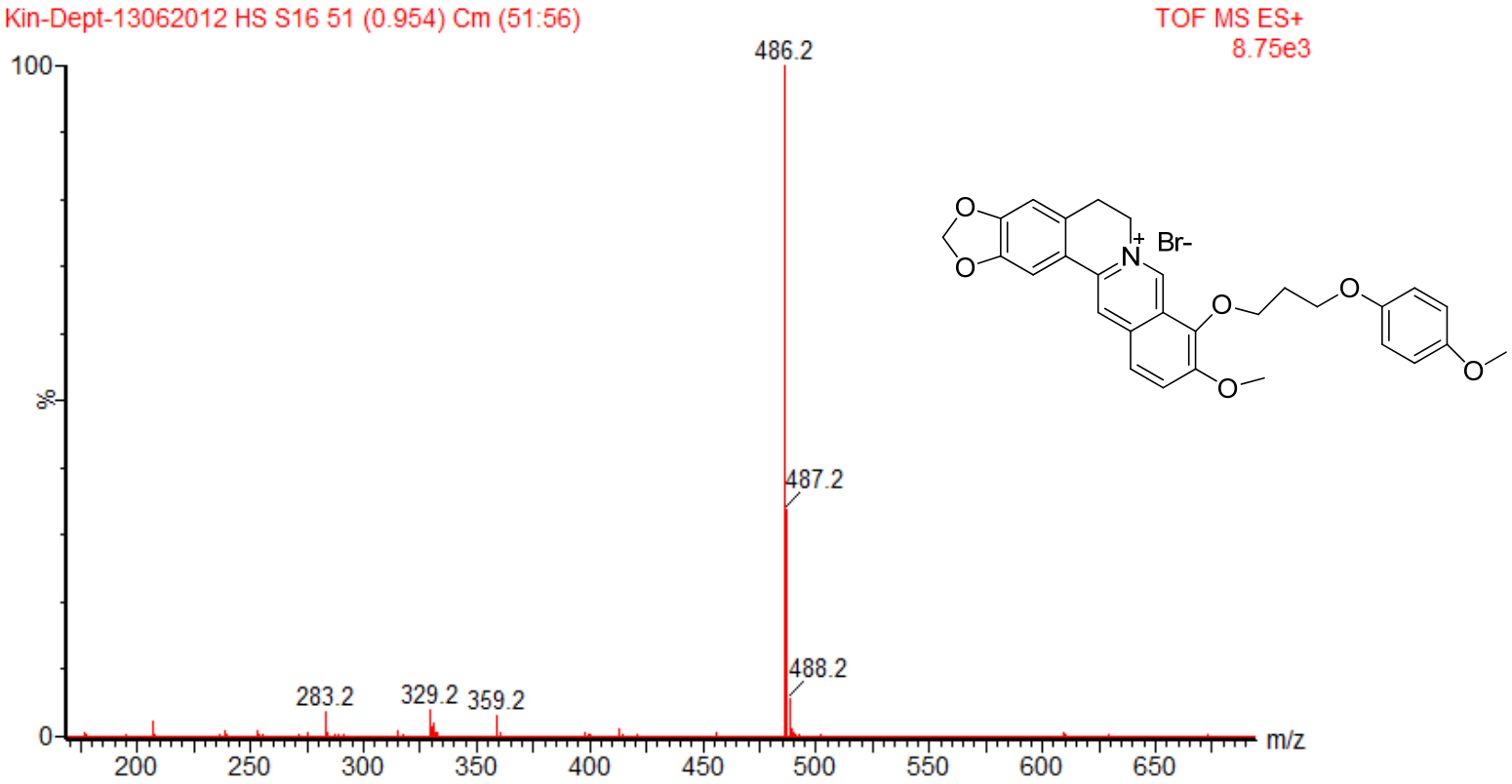

I-8 High resolution mass spectrum of compound **B3**

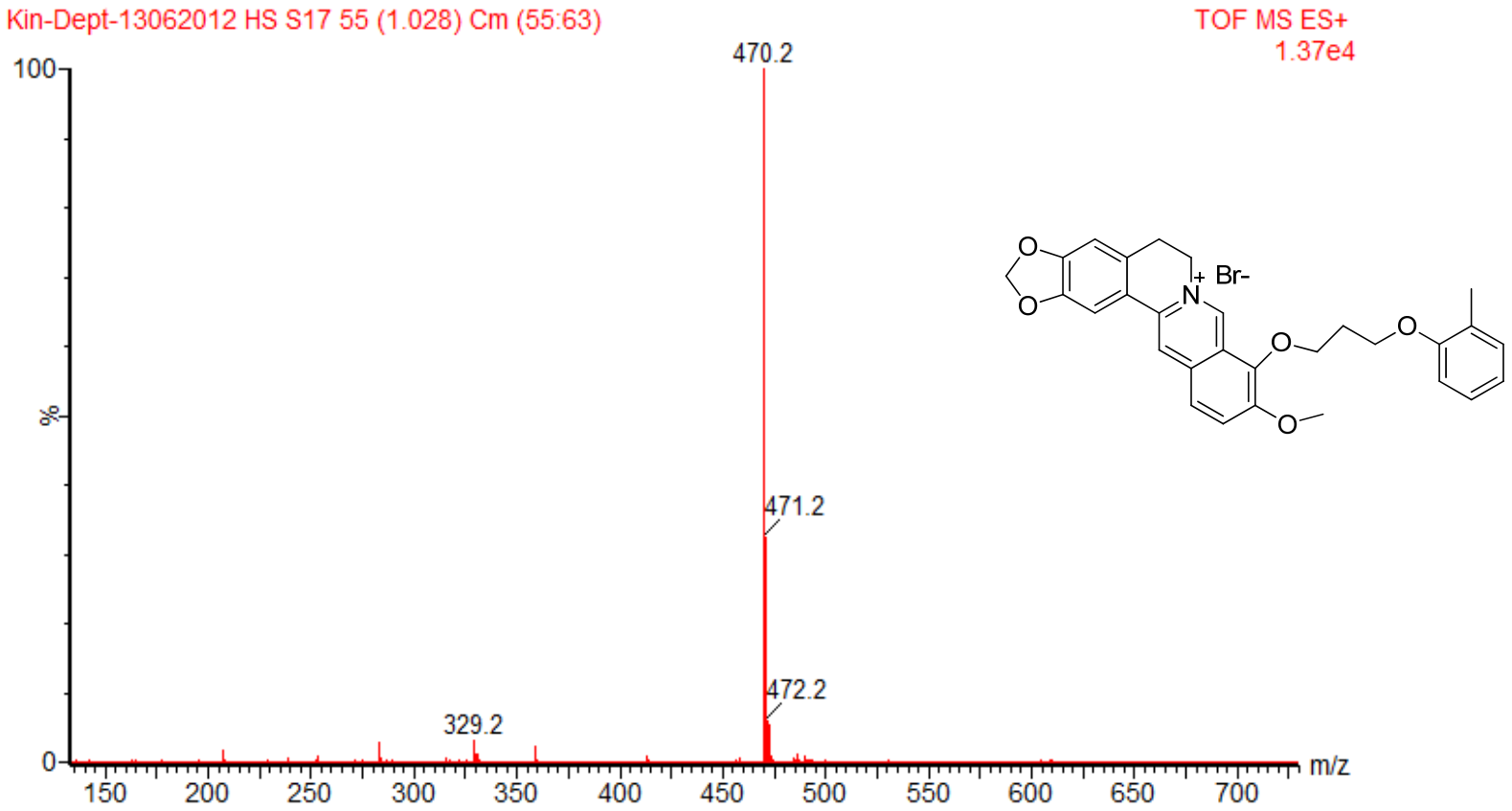

I-9 High resolution mass spectrum of compound **B4**

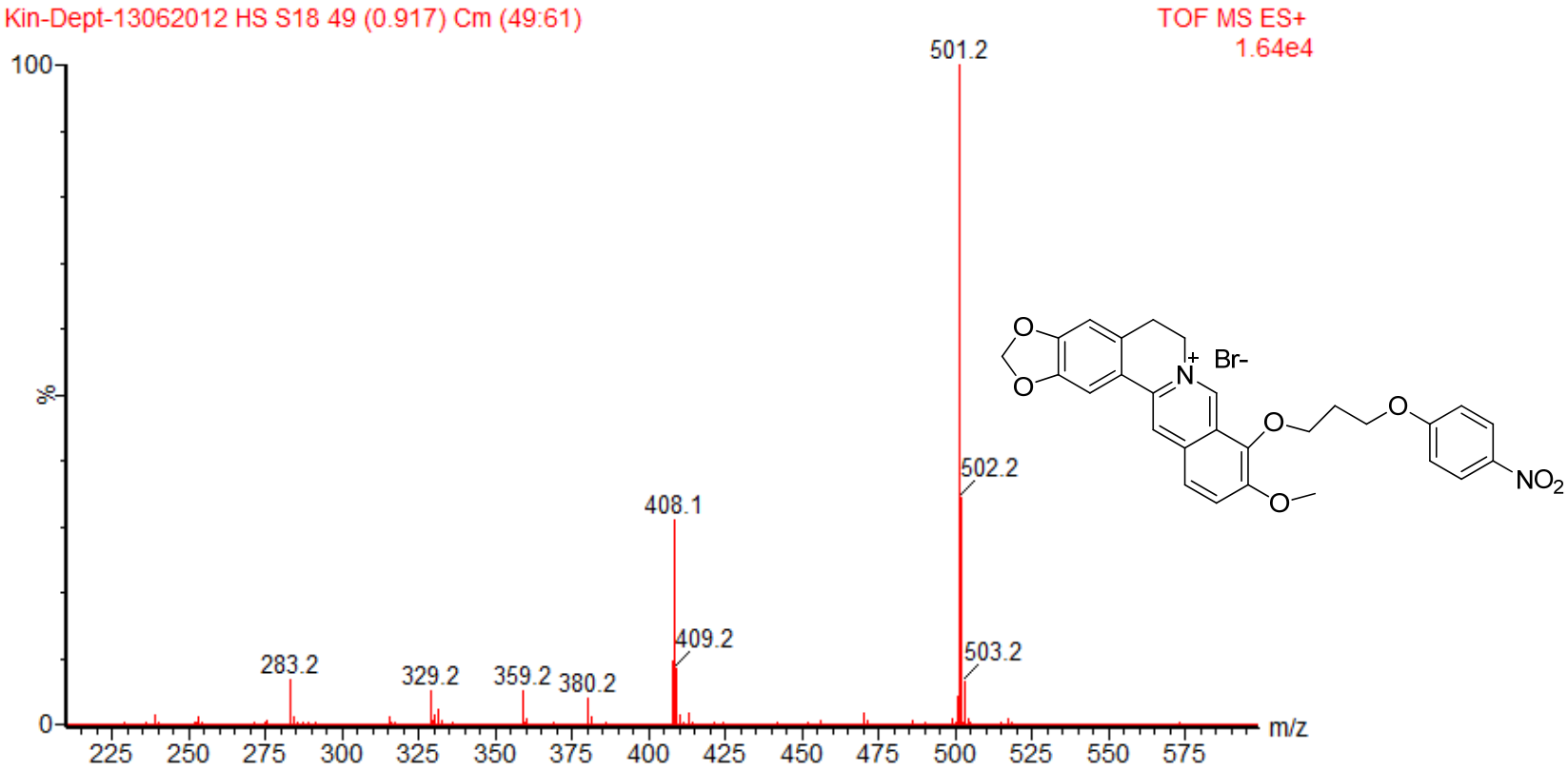

I-10 High resolution mass spectrum of compound **B5**

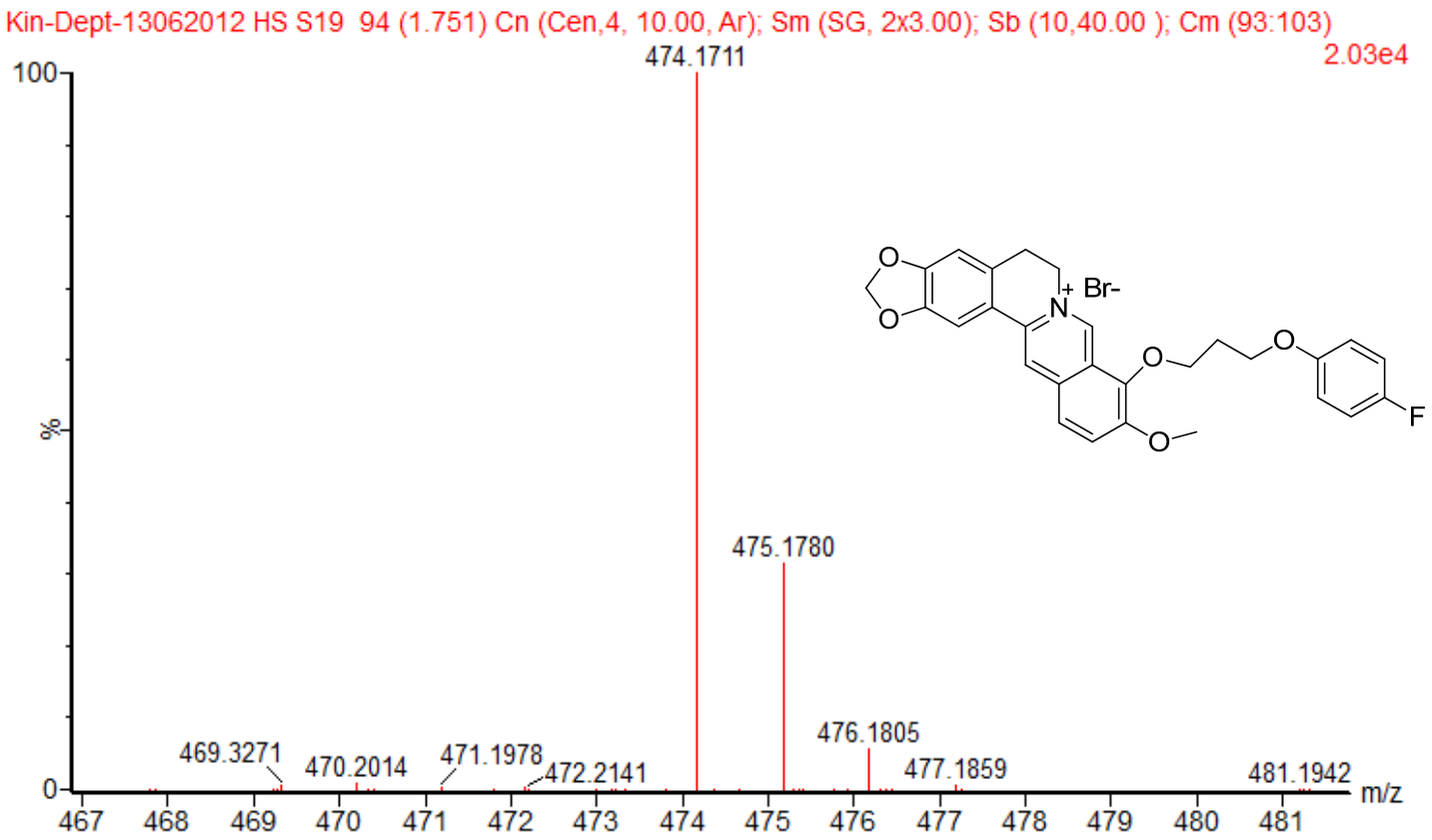

I-11 High resolution mass spectrum of compound **B6**

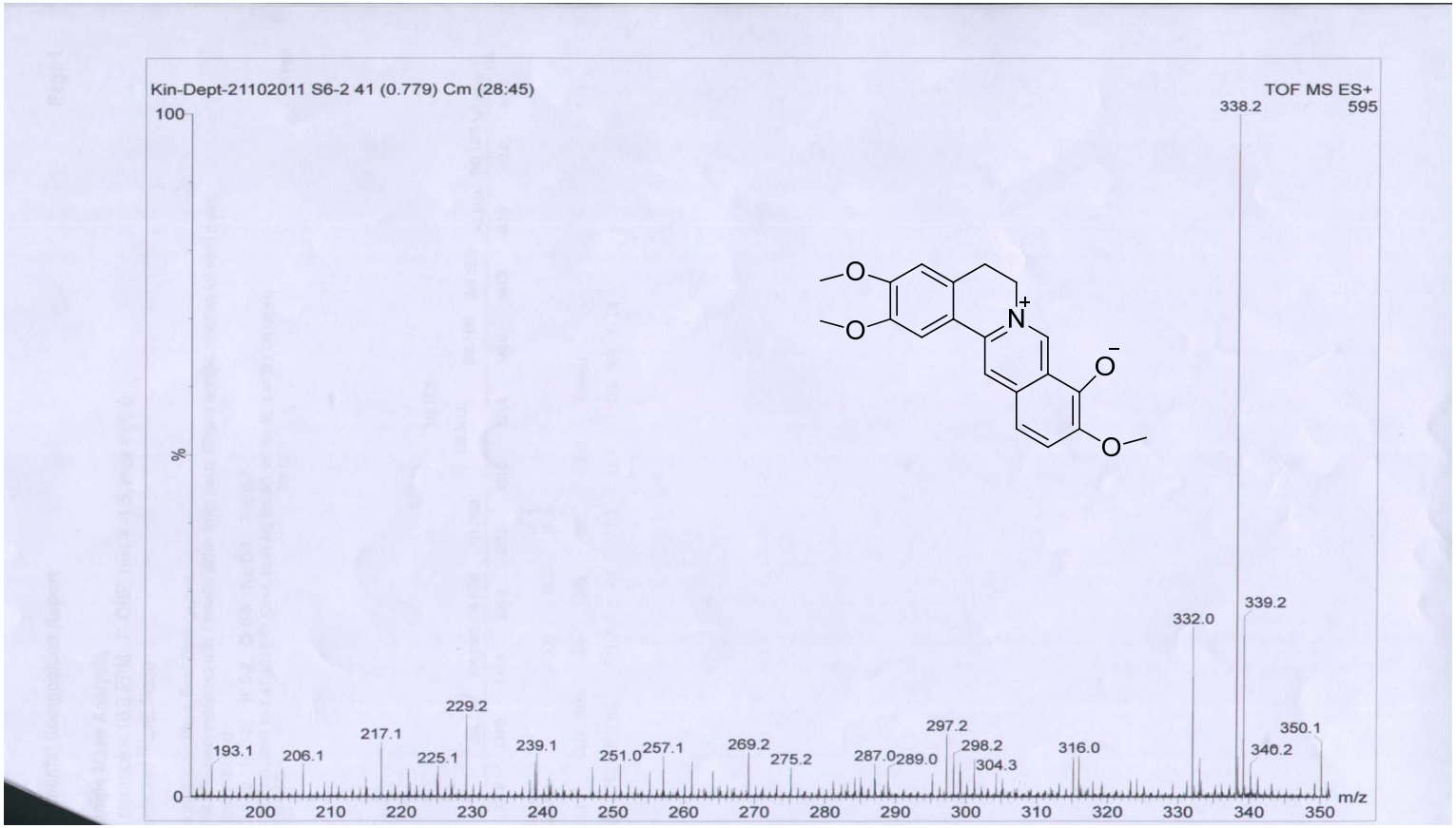

I-12 High resolution mass spectrum of compound demethyl-palmatine

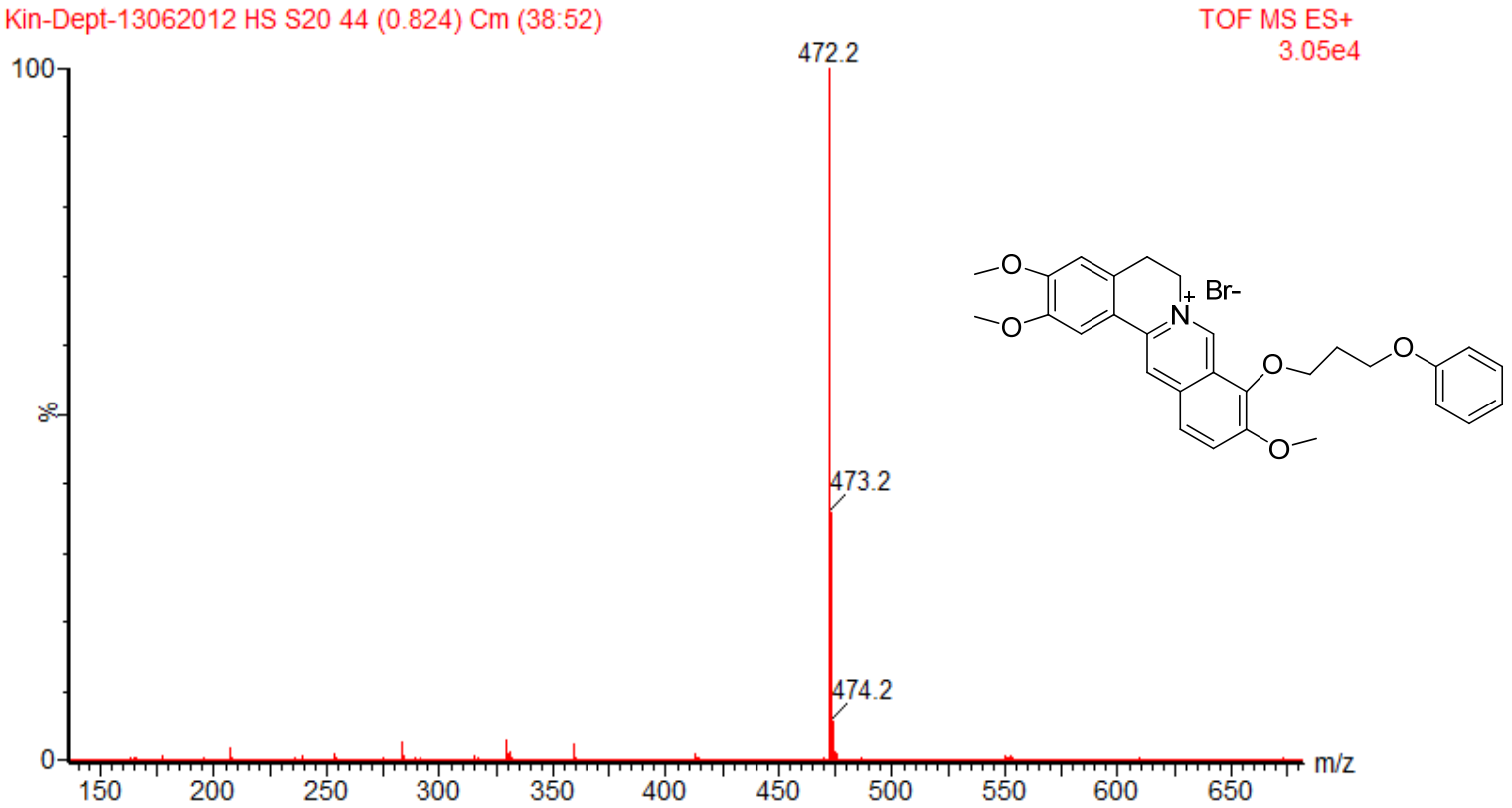

I-13 High resolution mass spectrum of compound **P1**

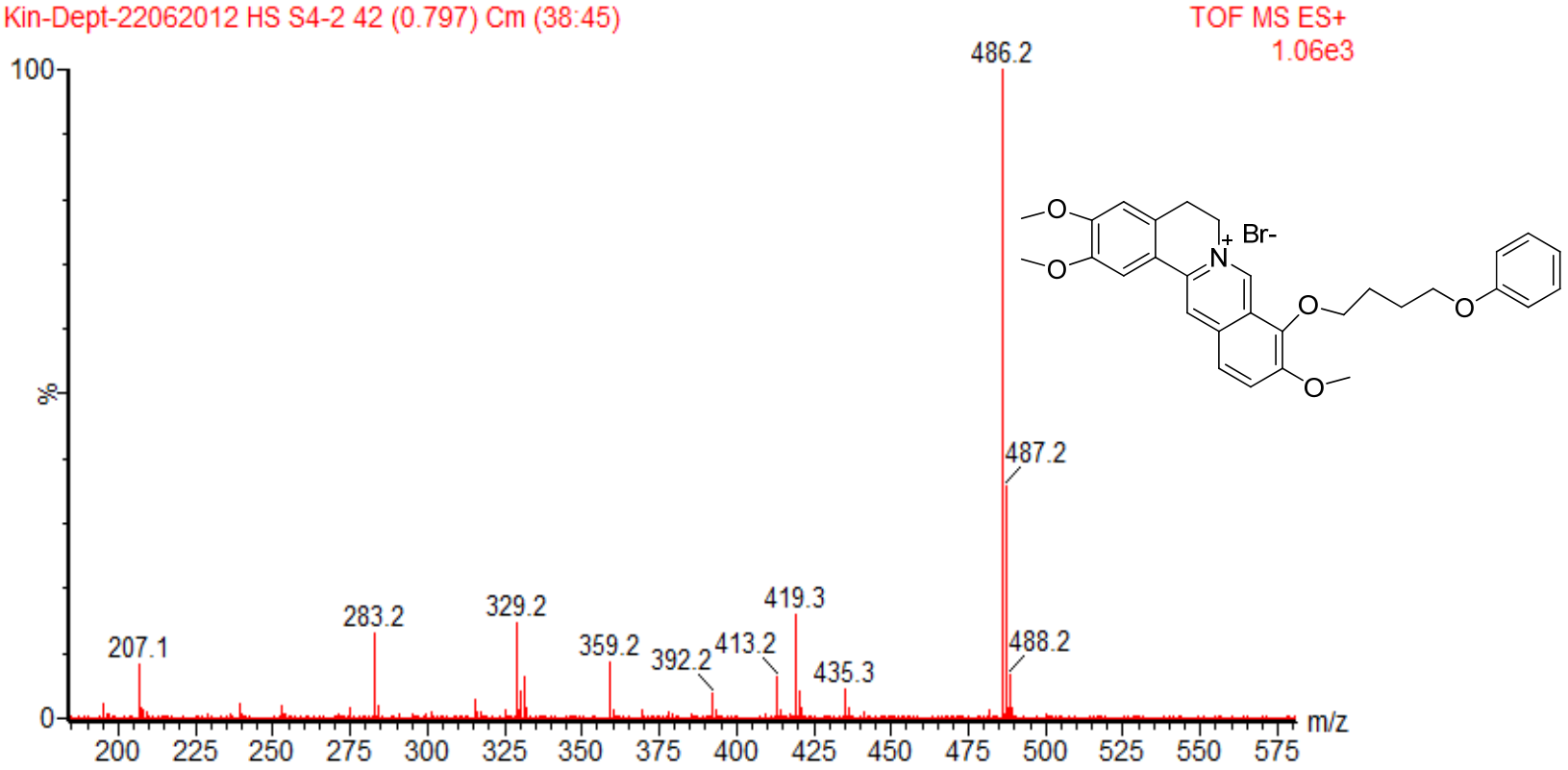

I-14 High resolution mass spectrum of compound **P1-1**

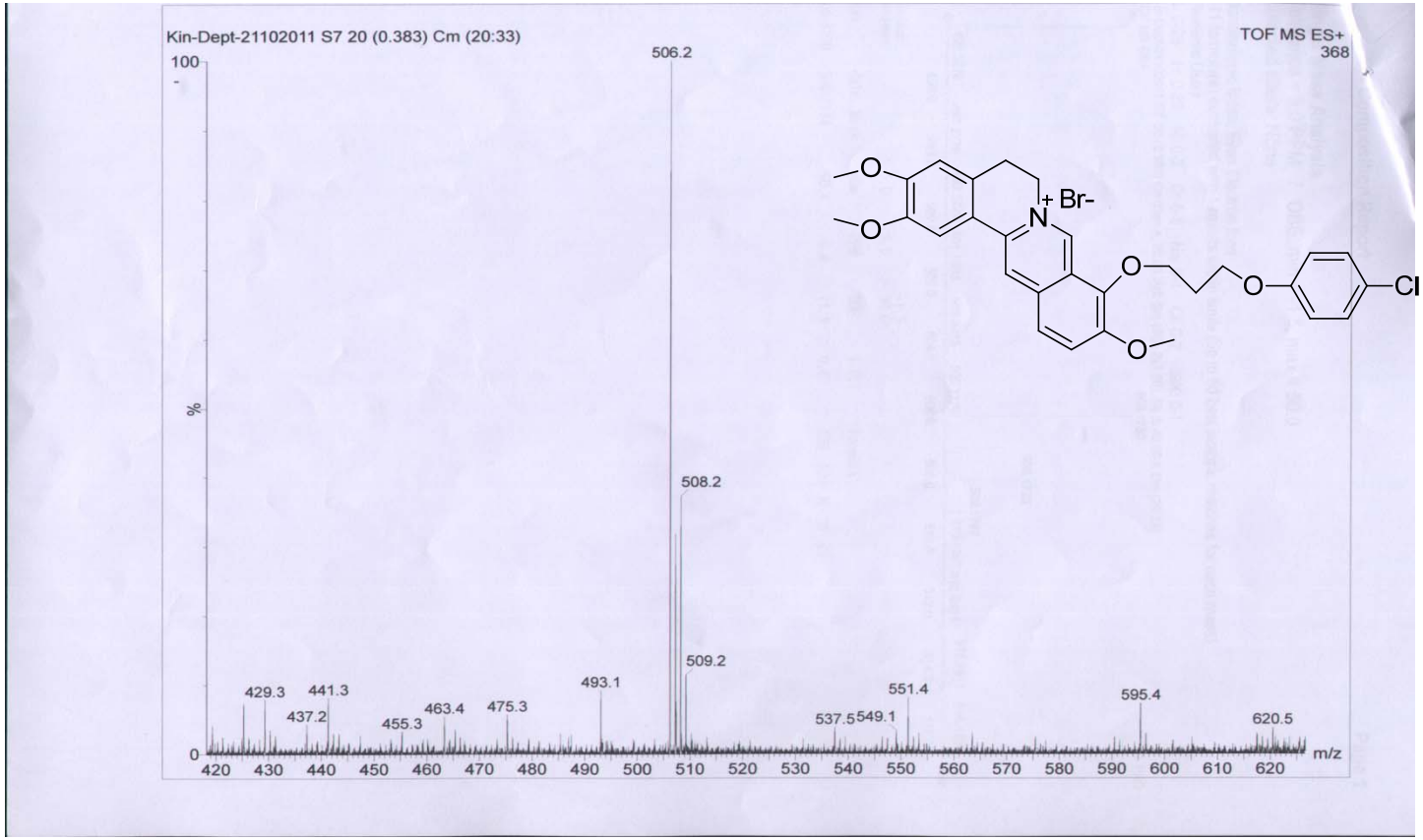

I-15 High resolution mass spectrum of compound **P2**

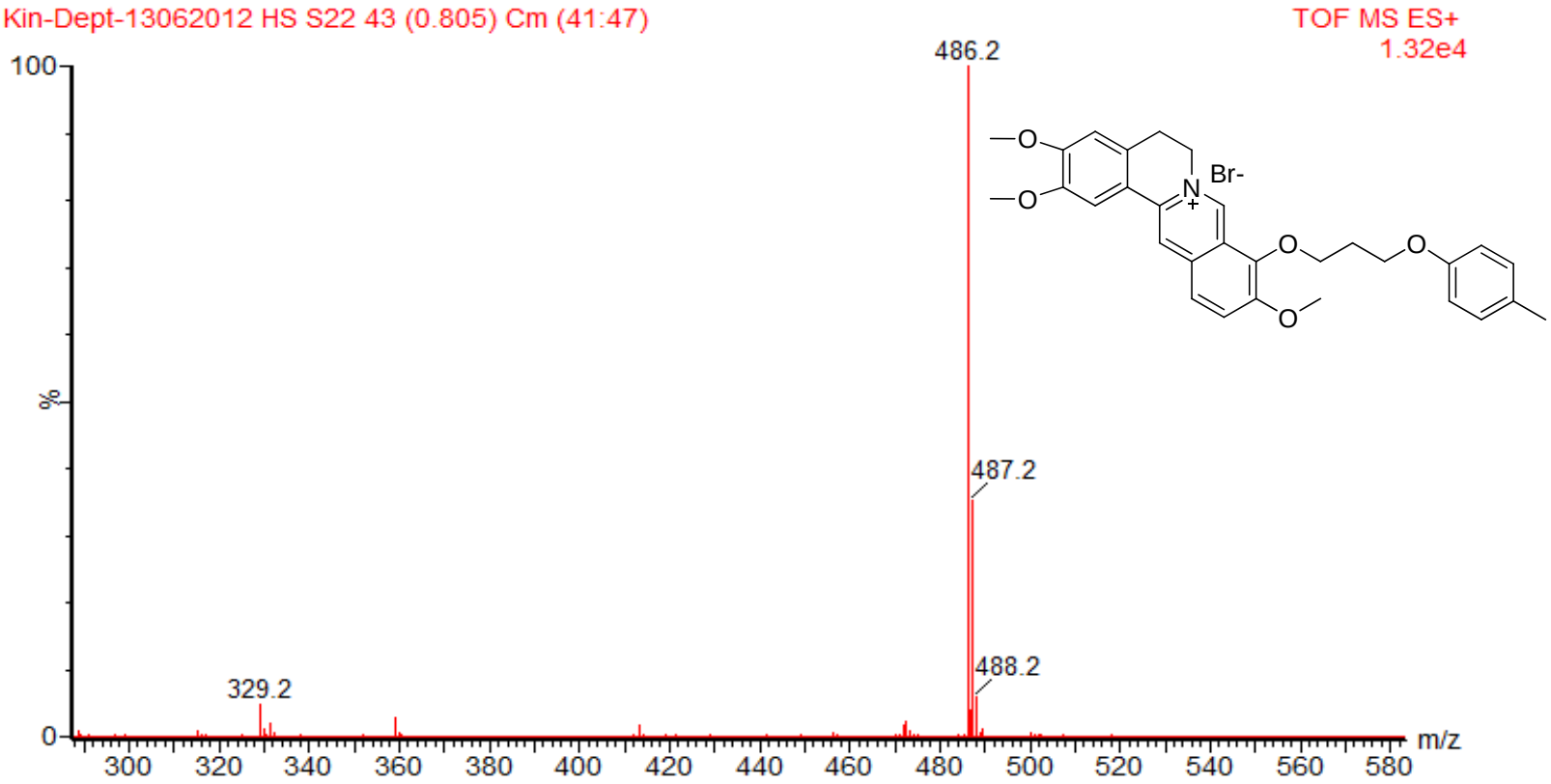

I-16 High resolution mass spectrum of compound **P3**

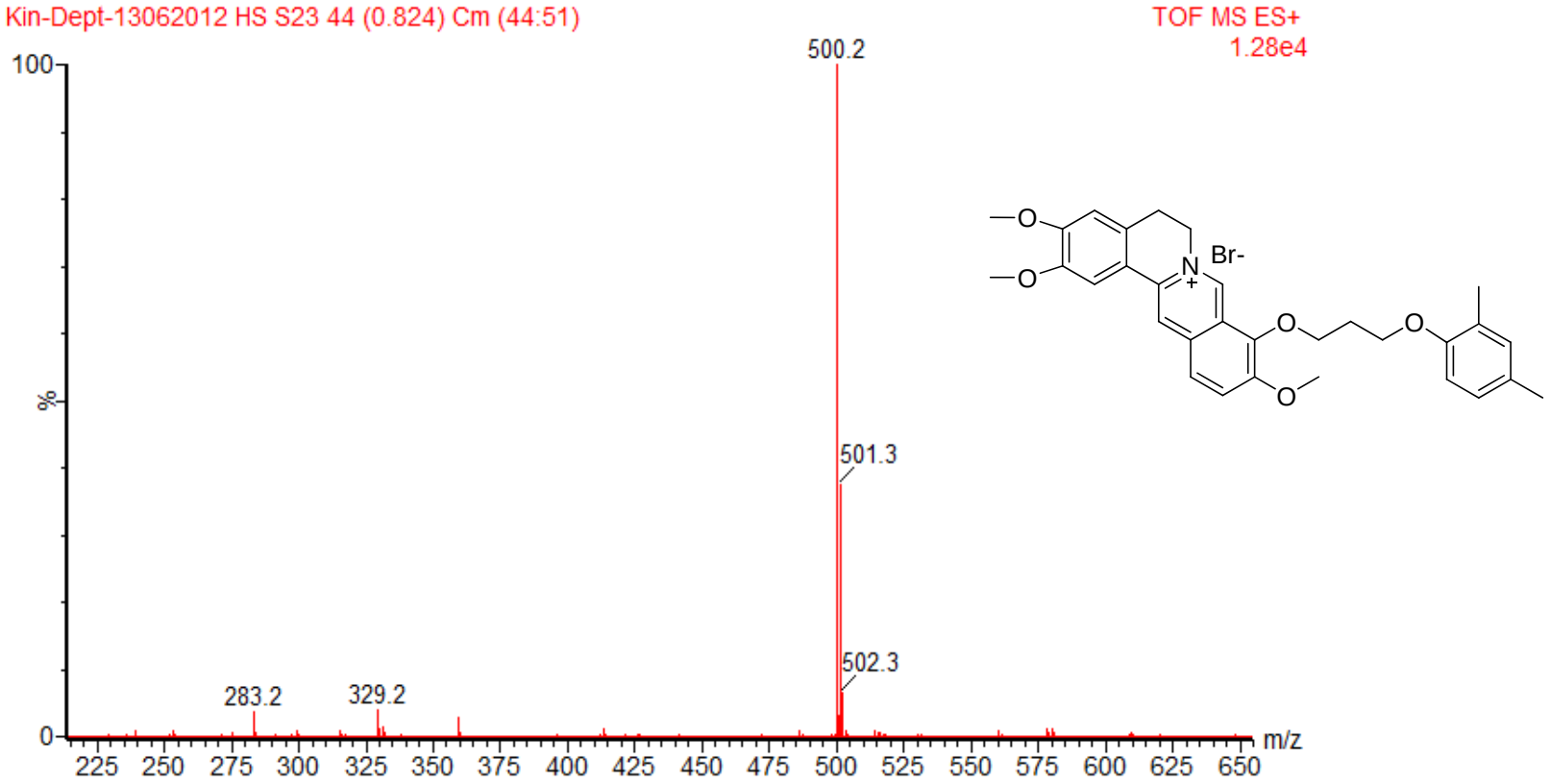

I-17 High resolution mass spectrum of compound **P4**

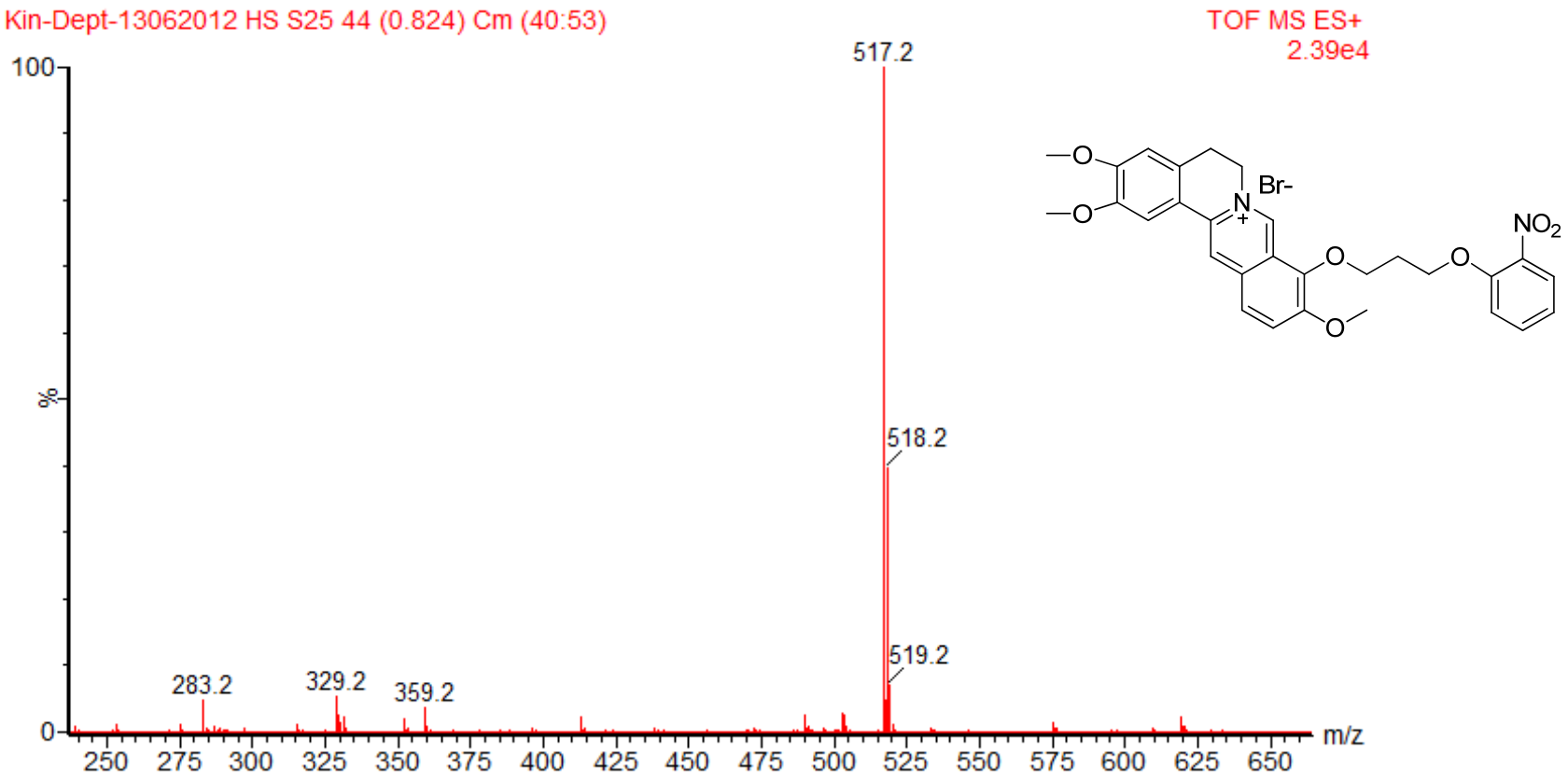

I-18 High resolution mass spectrum of compound **P5**

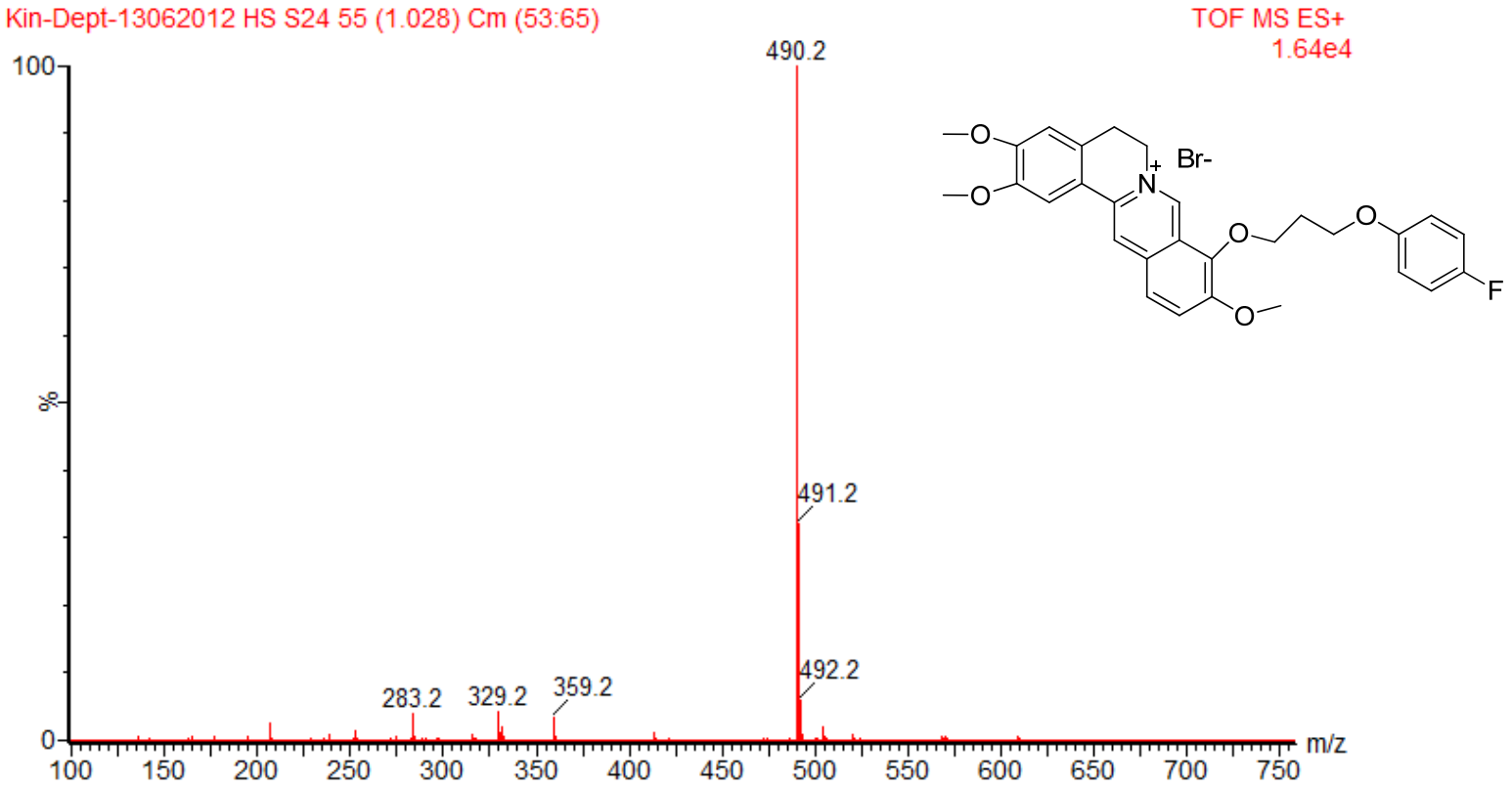

I-19 High resolution mass spectrum of compound **P6**

Appendix II: ^{1}H NMR spectra of compounds

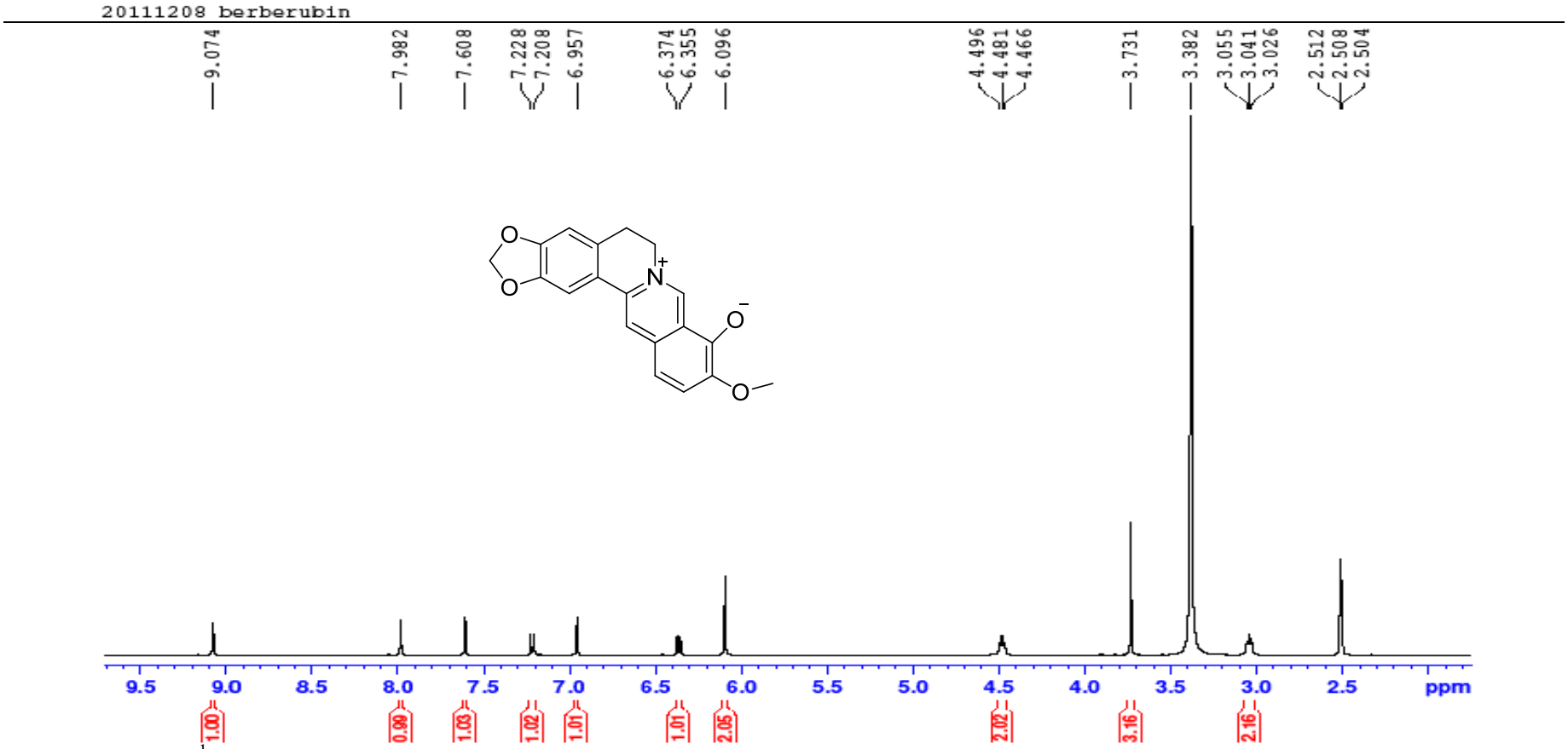

II-1 ^{1}H NMR spectrum of compound **1** (berberrubine)

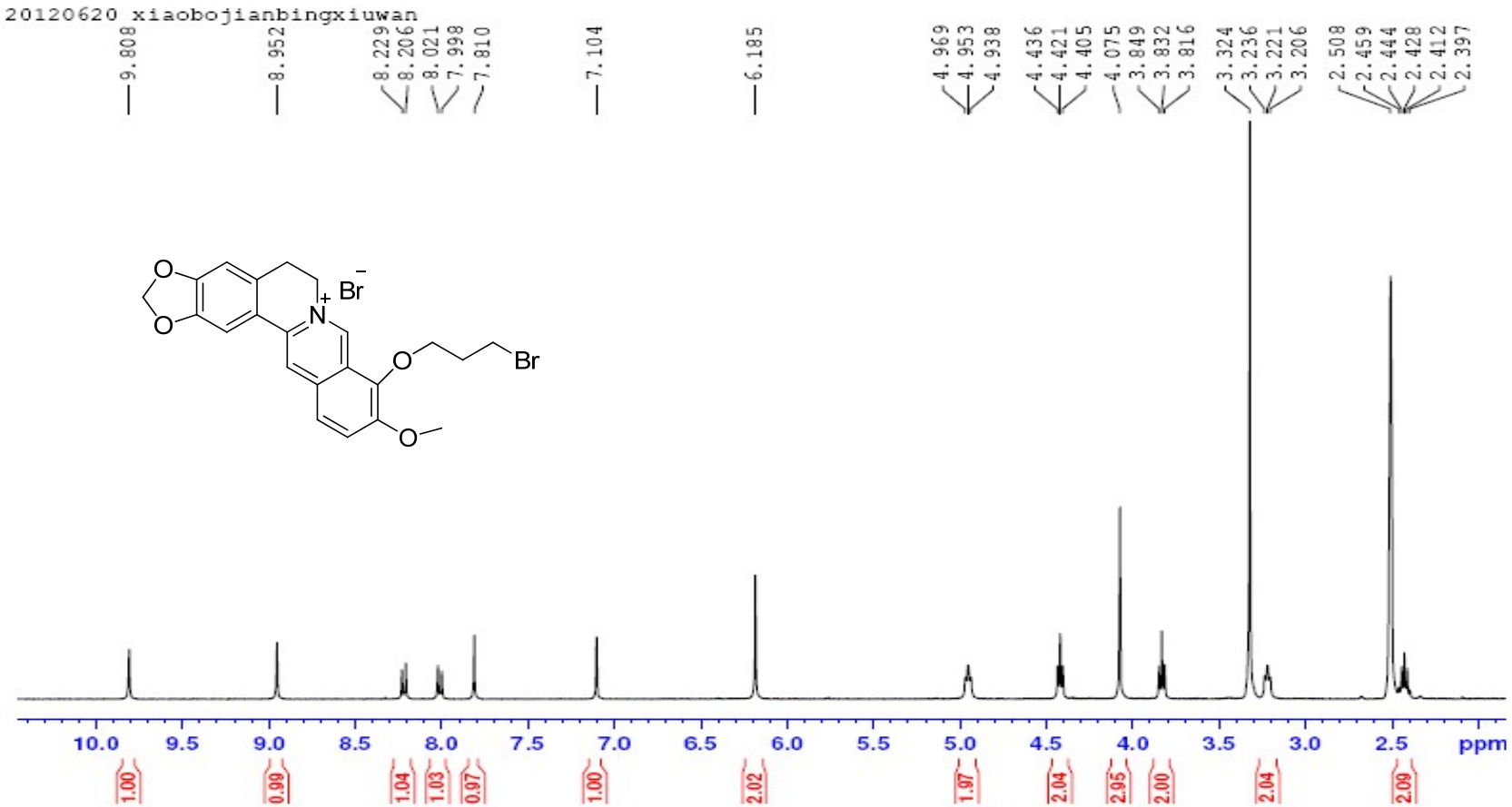

II-2 ^{1}H NMR spectrum of compound **4**

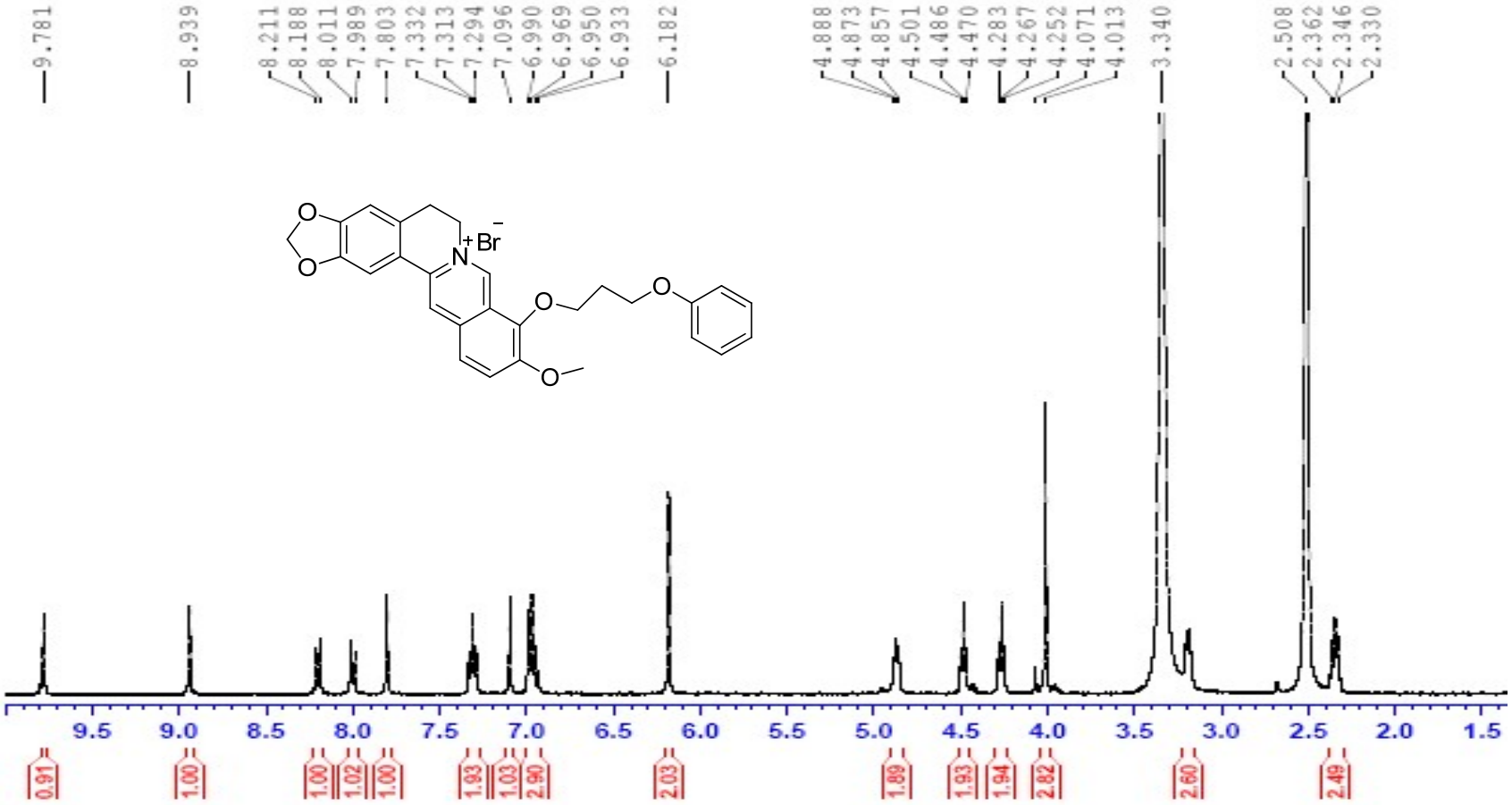

II-3 ^{1}H NMR spectrum of compound **B1**

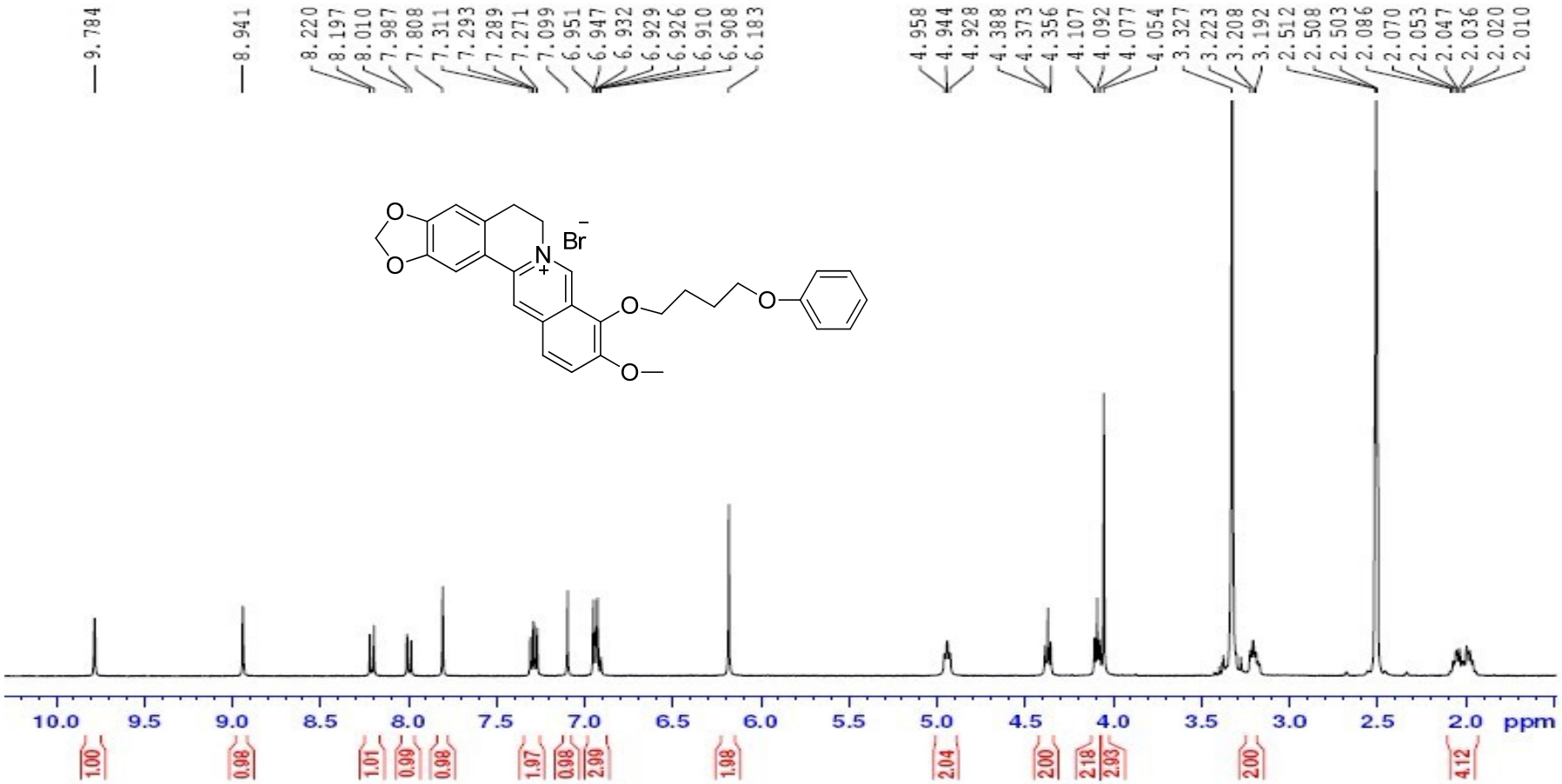

II-4 ^{1}H NMR spectrum of compound **B1-1**

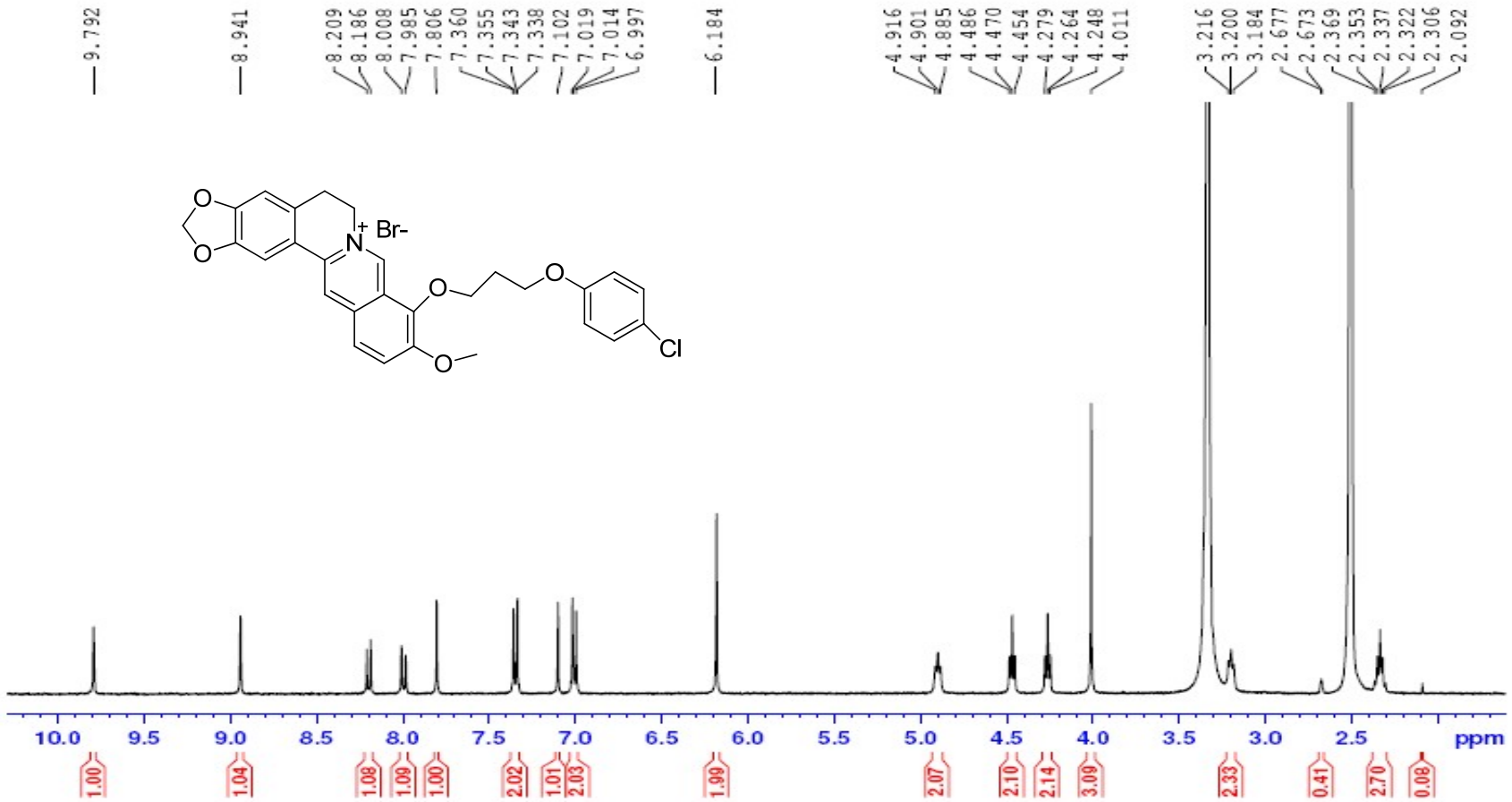

II-5 ^{1}H NMR spectrum of compound **B2**

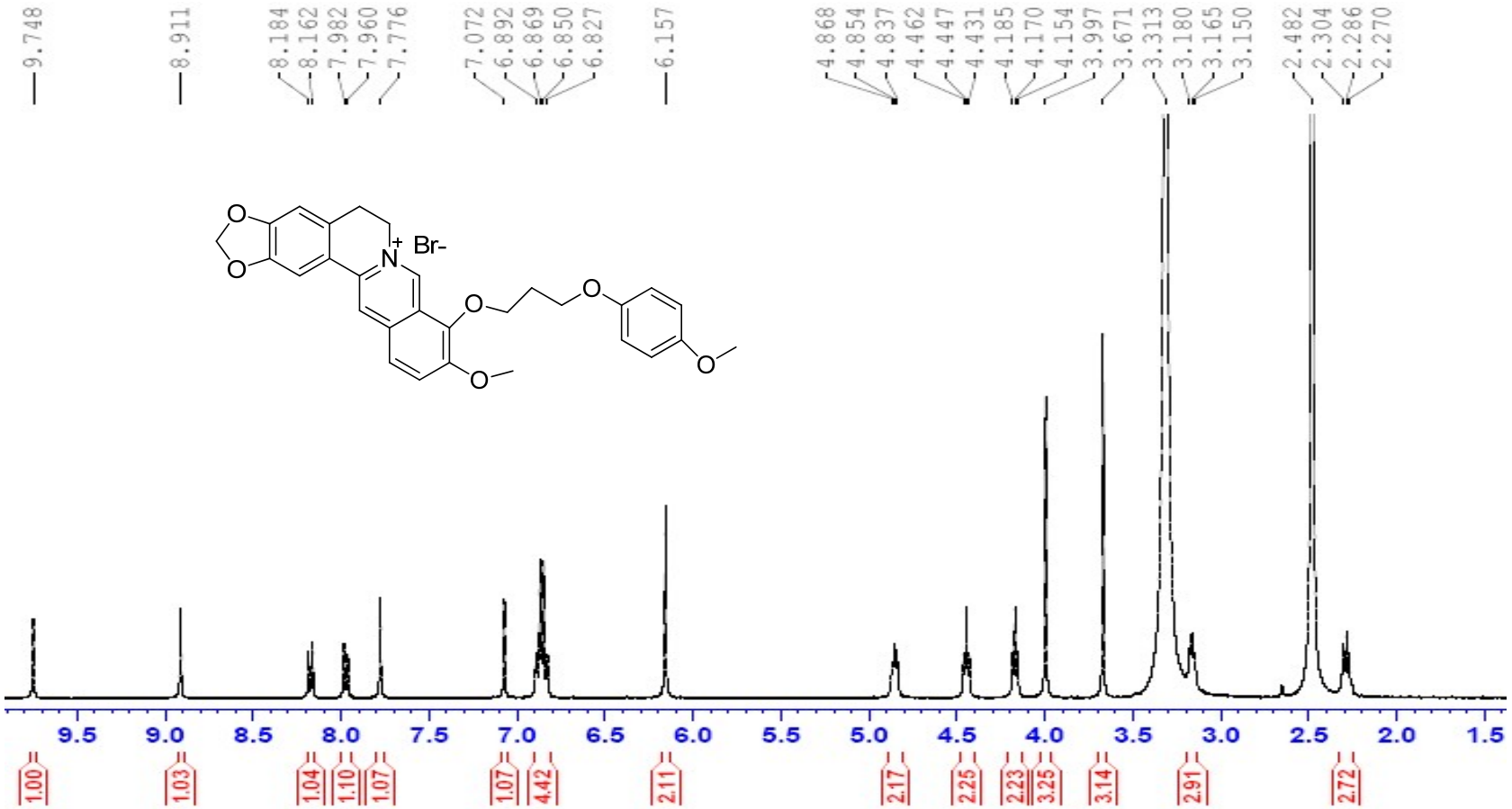

II-6 ^{1}H NMR spectrum of compound **B3**

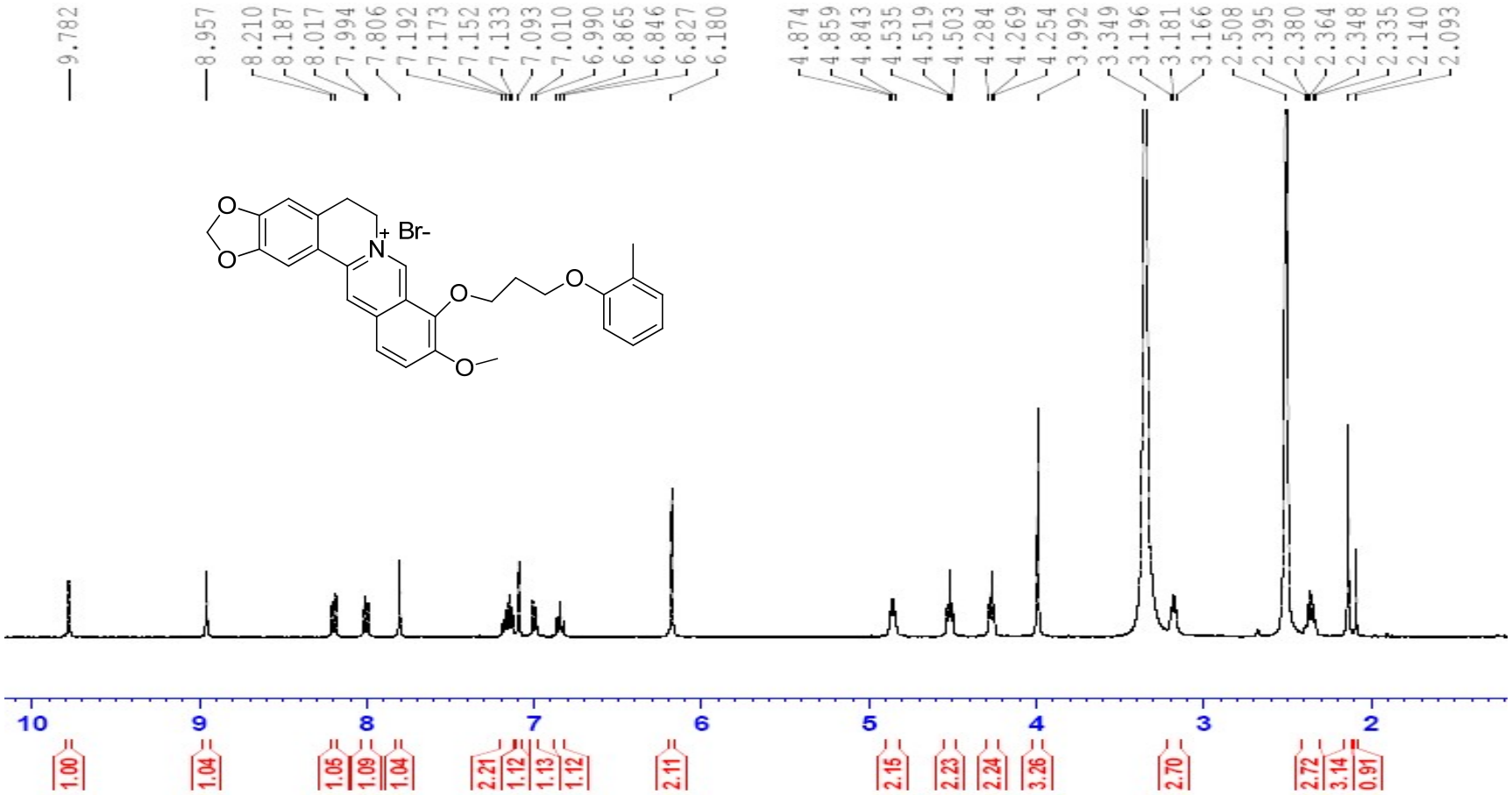

II-7 ^{1}H NMR spectrum of compound **B4**

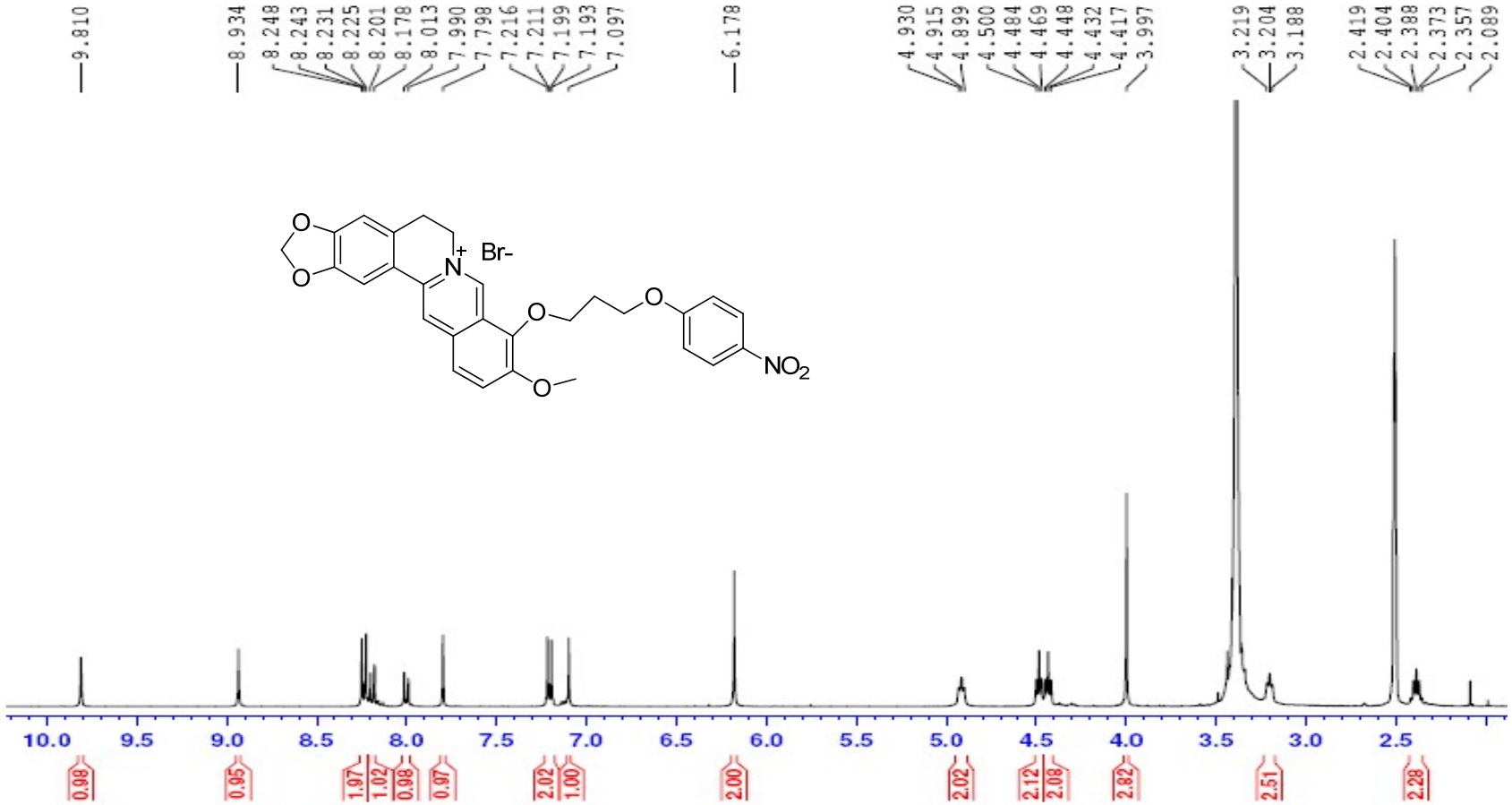

II-8 ^{1}H NMR spectrum of compound **B5**

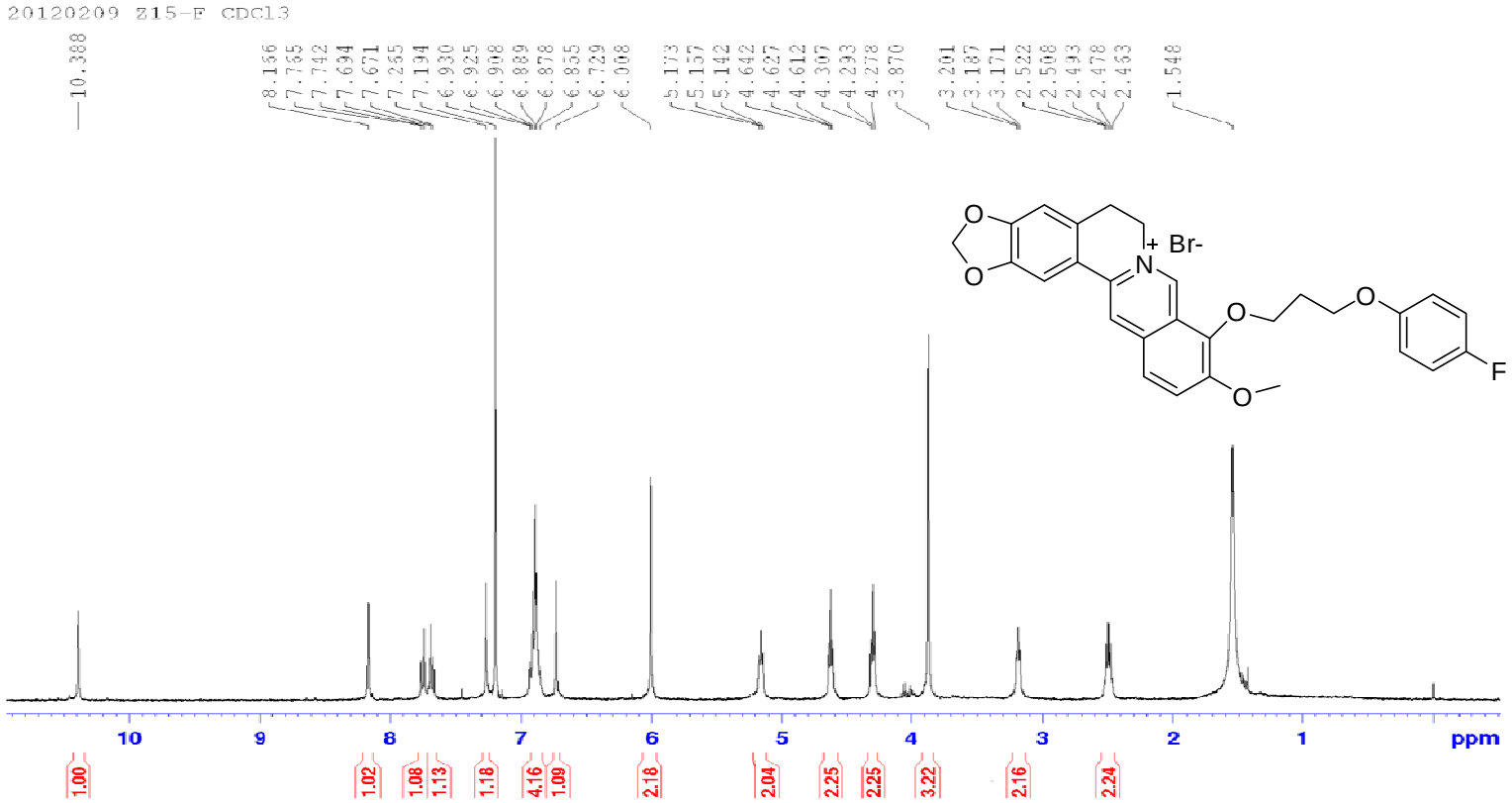

II-9 ^{1}H NMR spectrum of compound **B6**

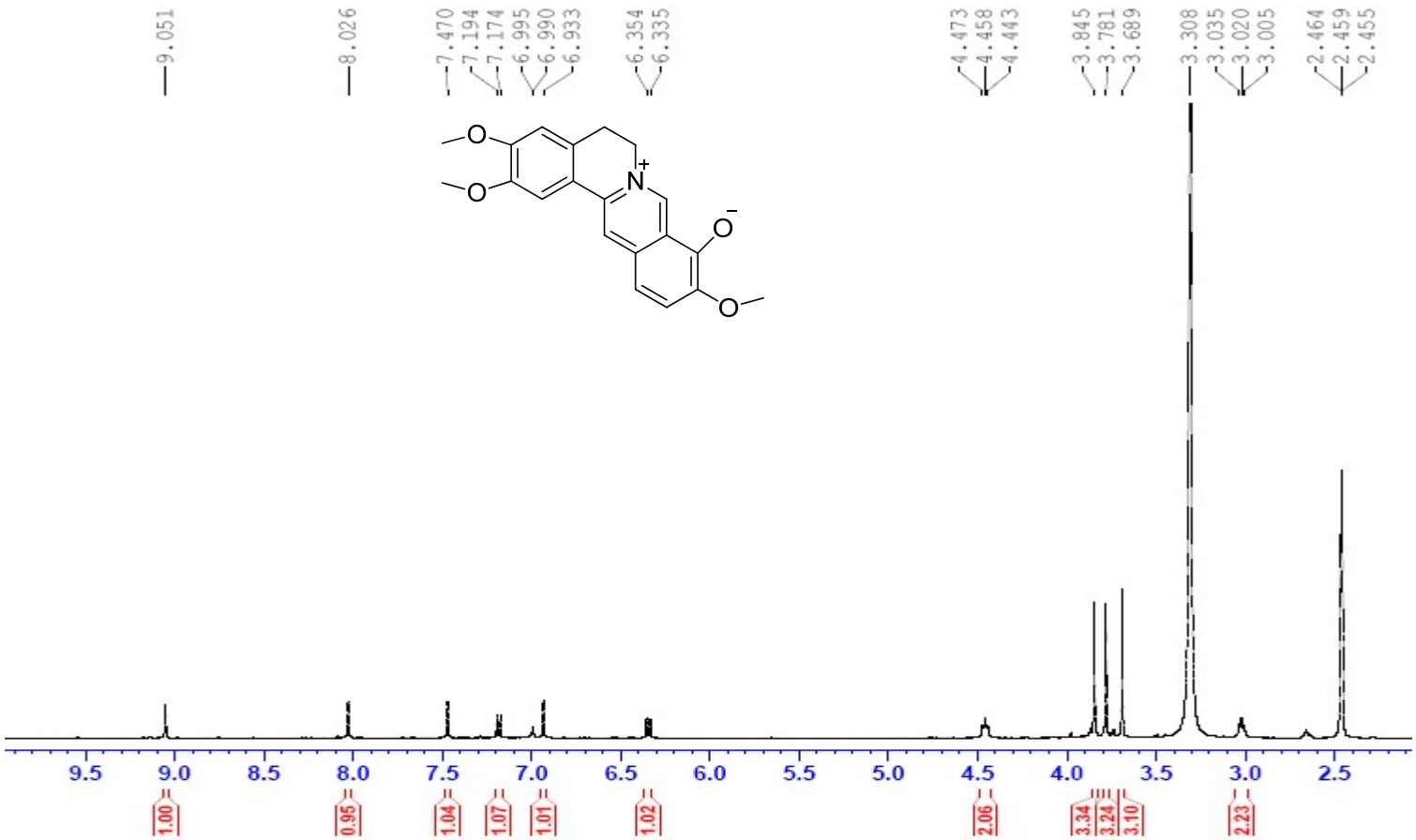

II-10 ^{1}H NMR spectrum of compound demethyl-palmatine

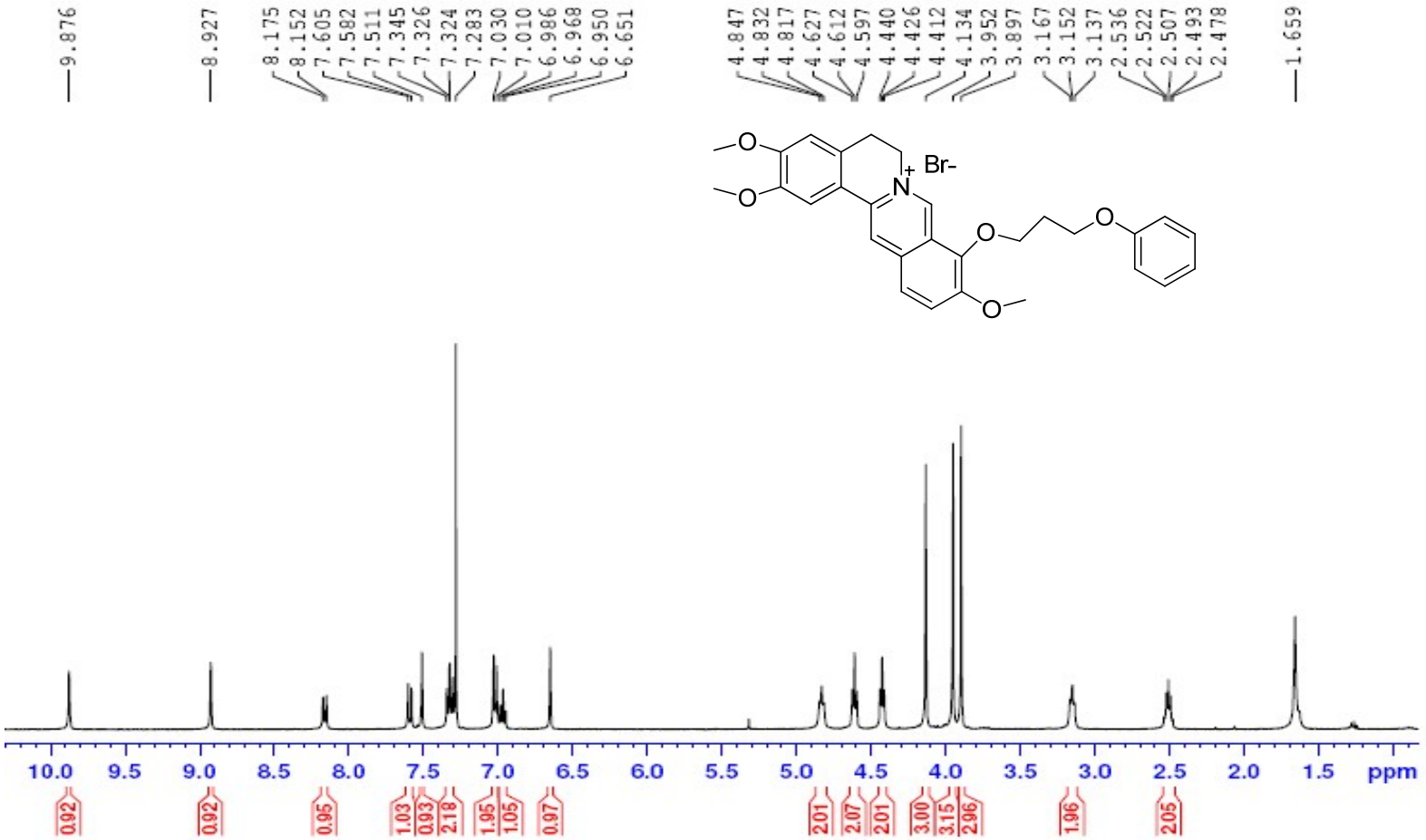

II-11 ^{1}H NMR spectrum of compound **P1**

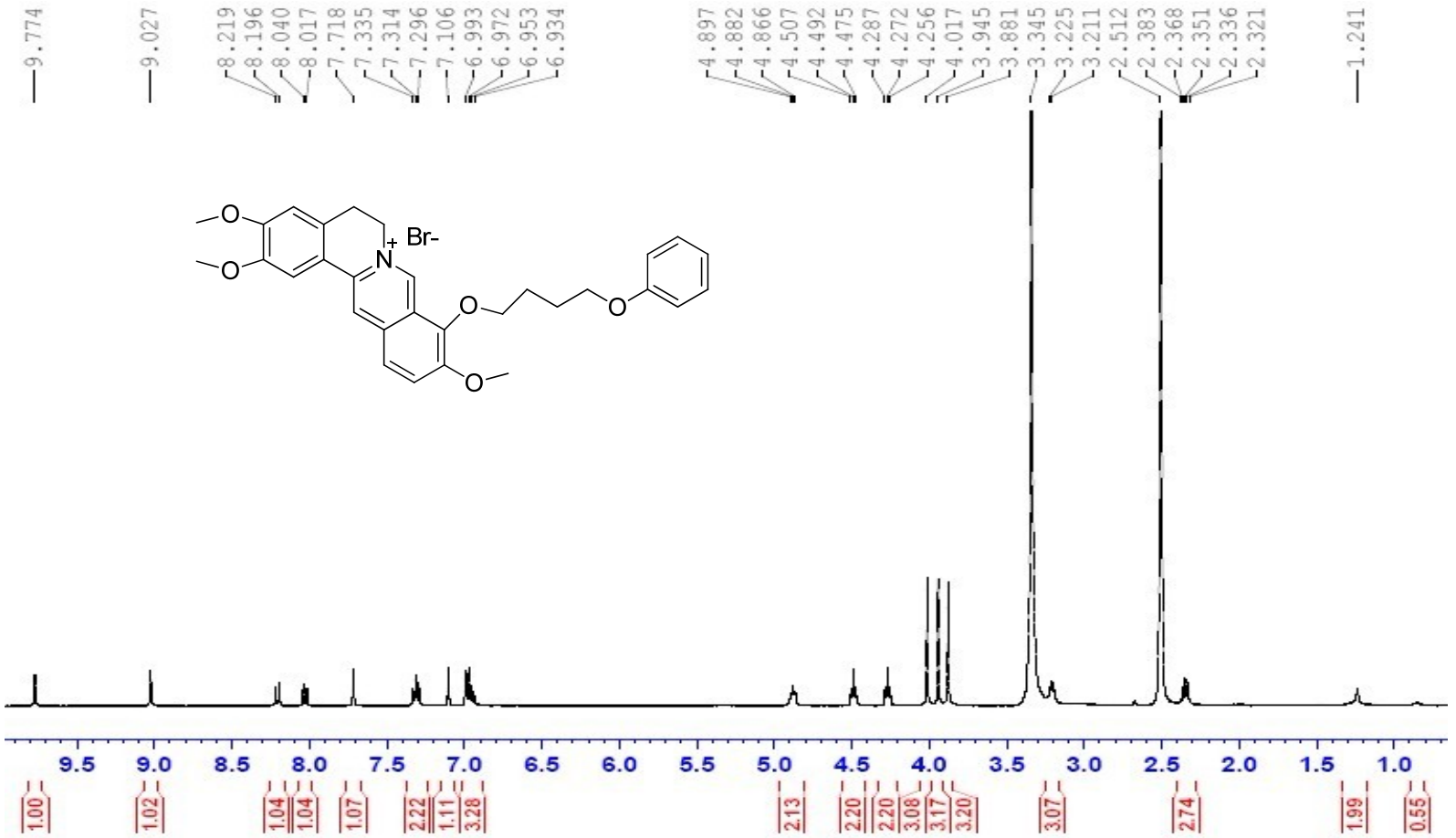

II-12 ^{1}H NMR spectrum of compound **P1-1**

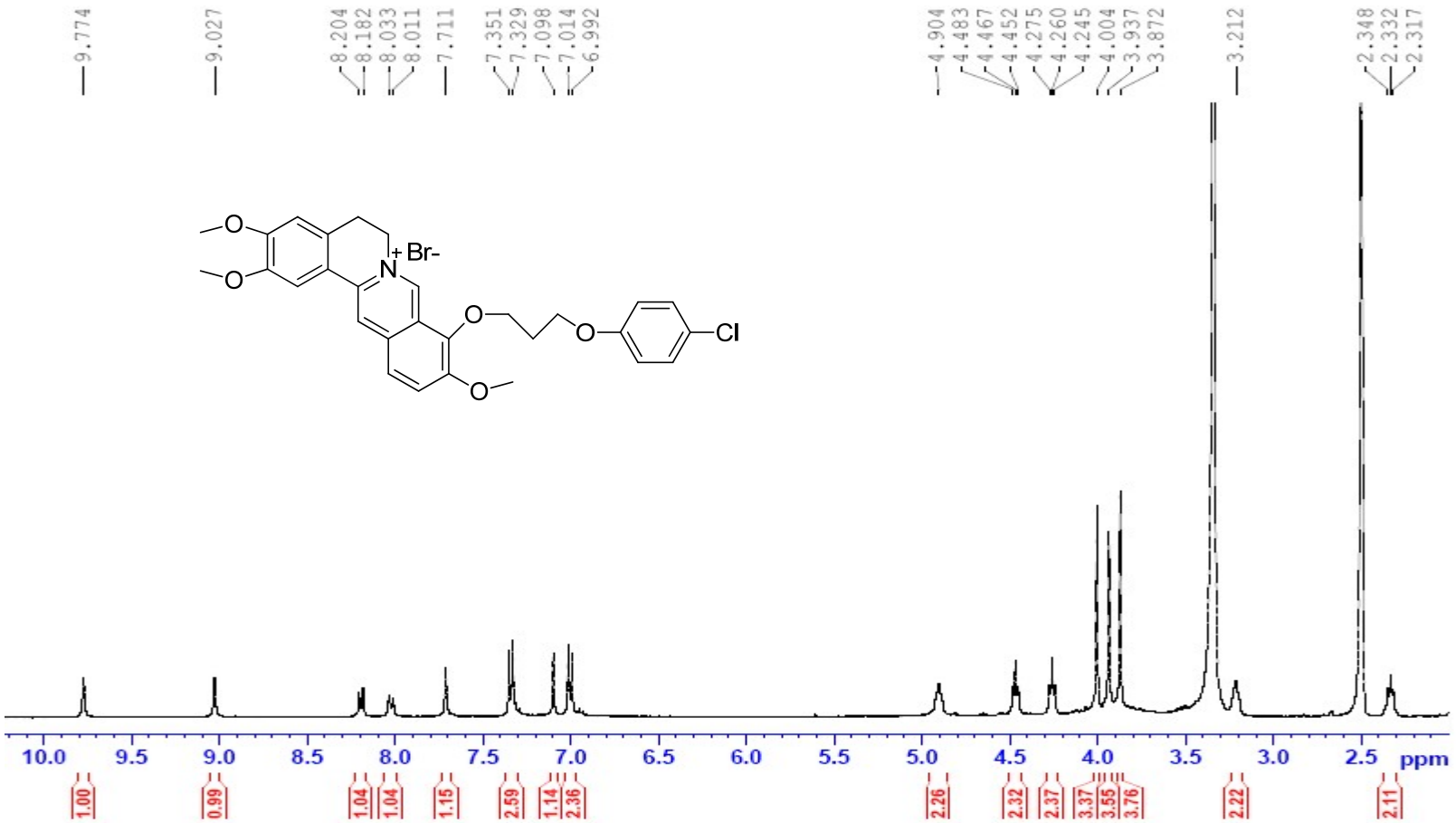

II-13 ^{1}H NMR spectrum of compound **P2**

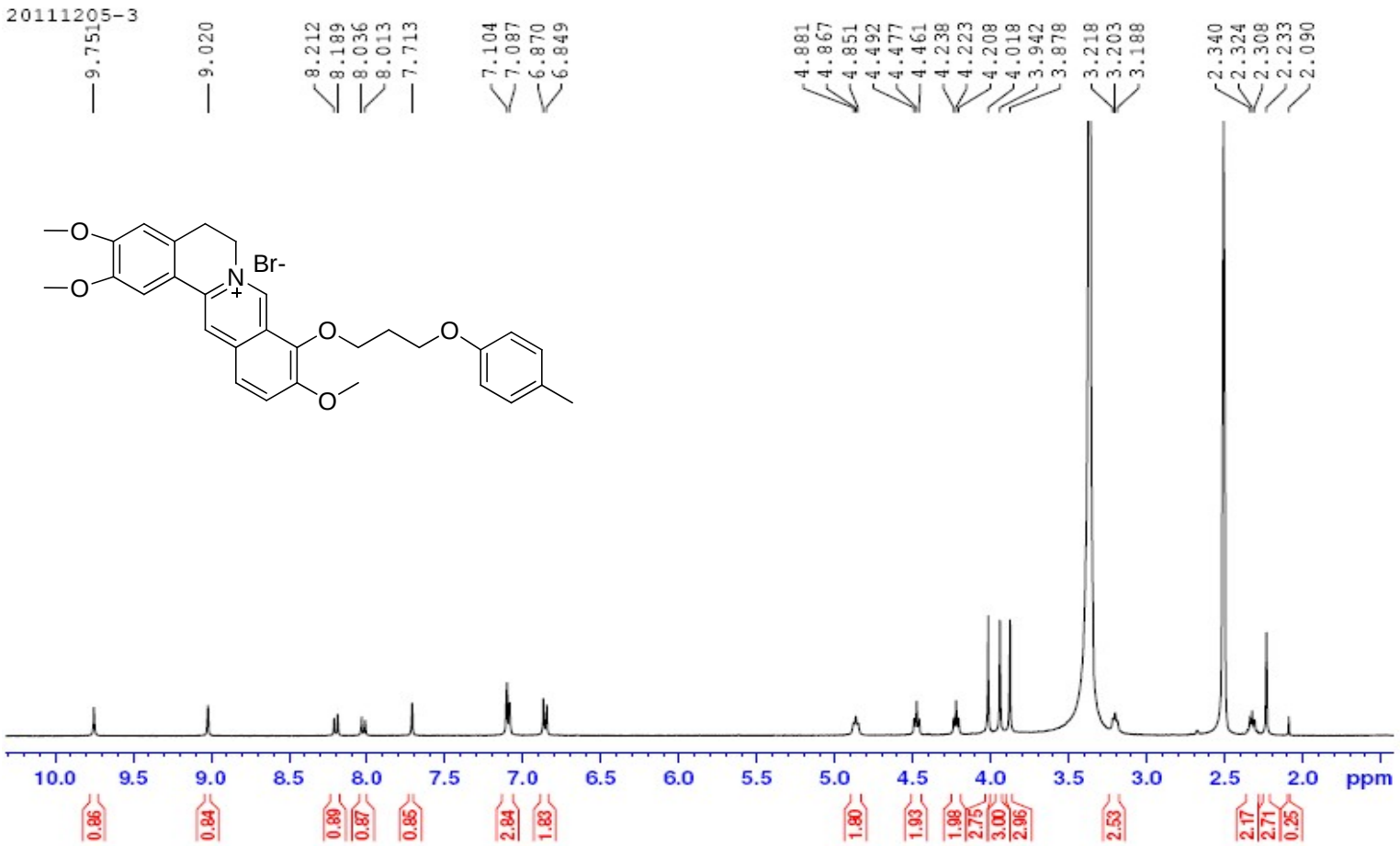

II-14 ^{1}H NMR spectrum of compound **P3**

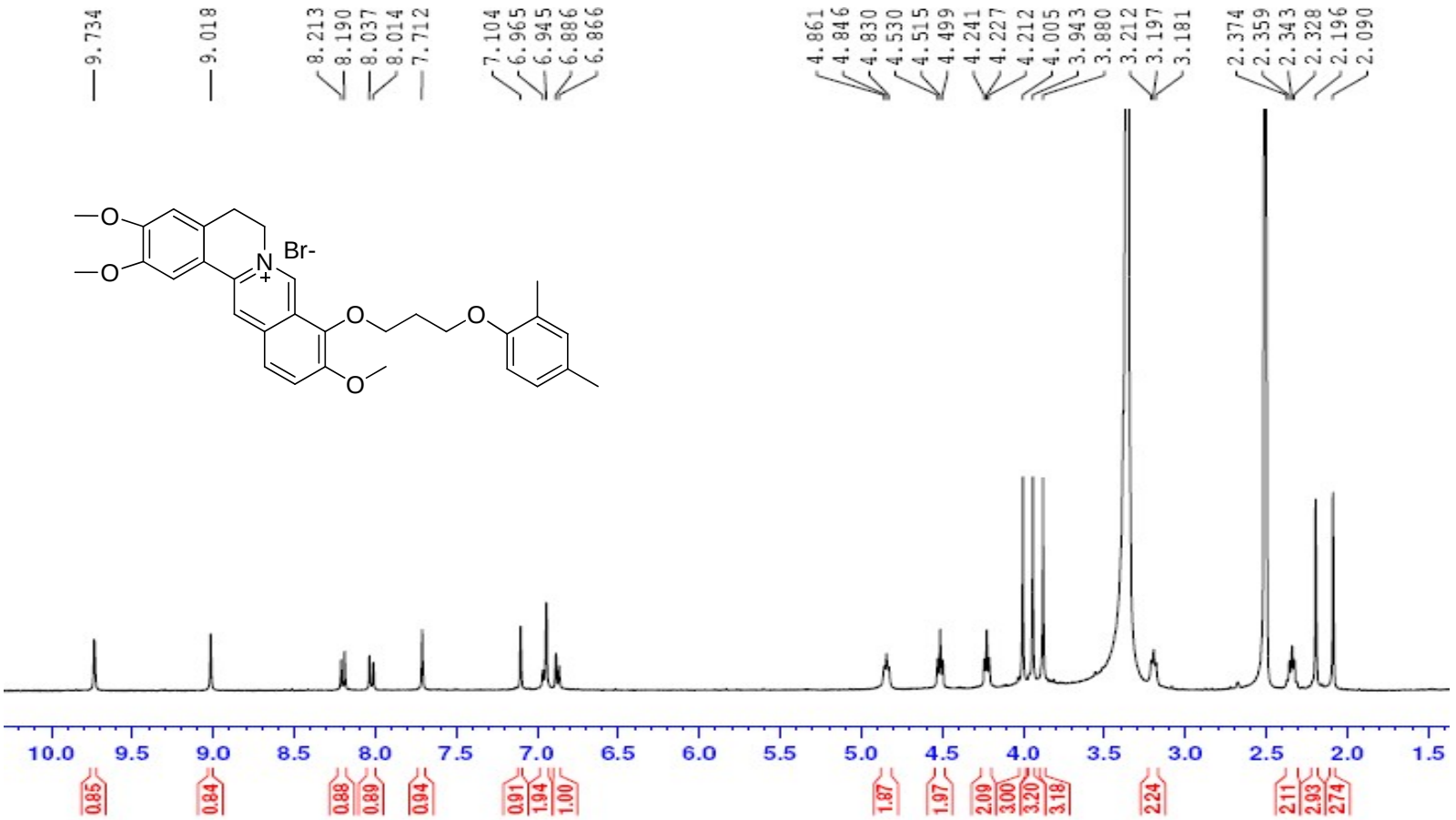

II-15 ^{1}H NMR spectrum of compound **P4**

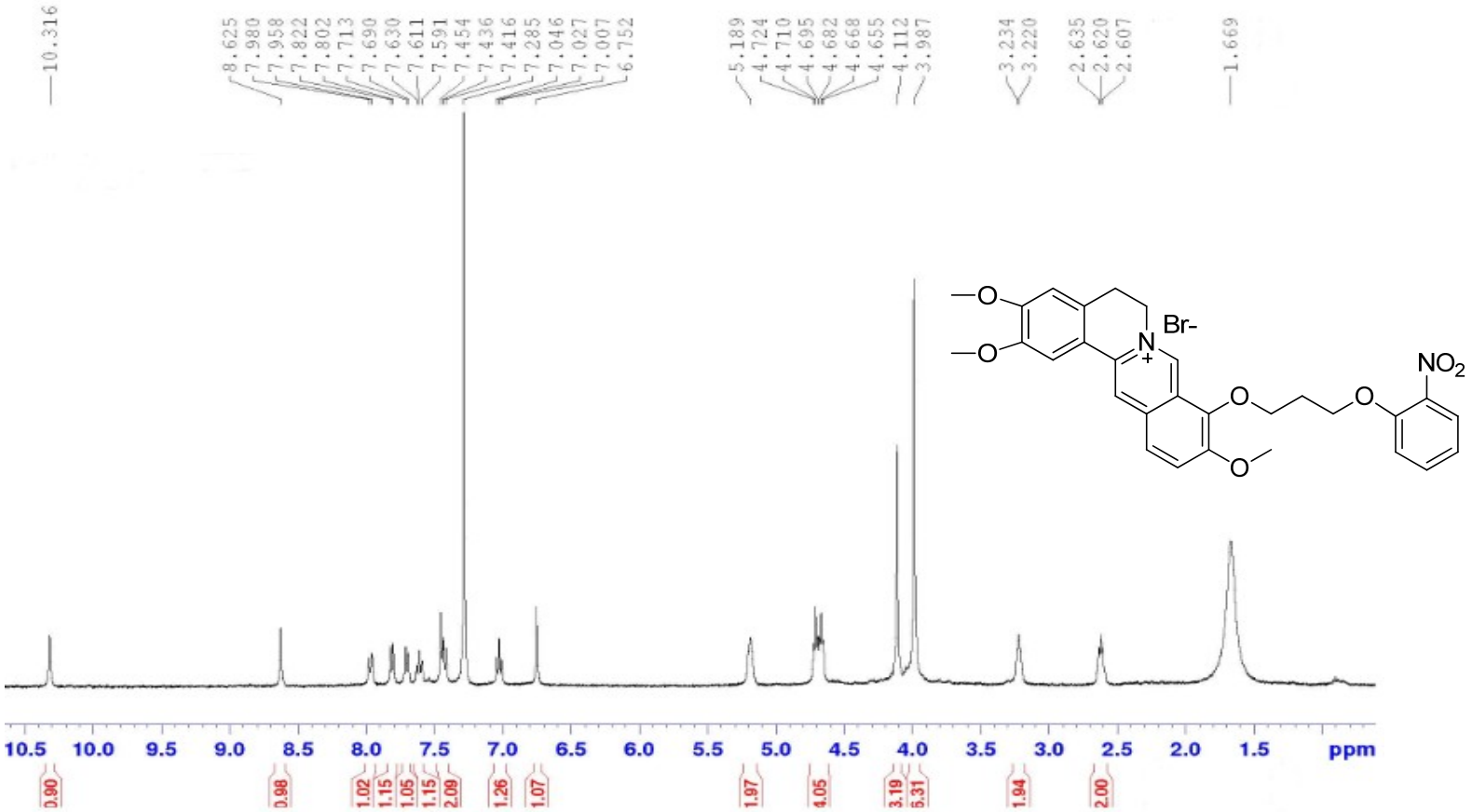

II-16 ^{1}H NMR spectrum of compound **P5**

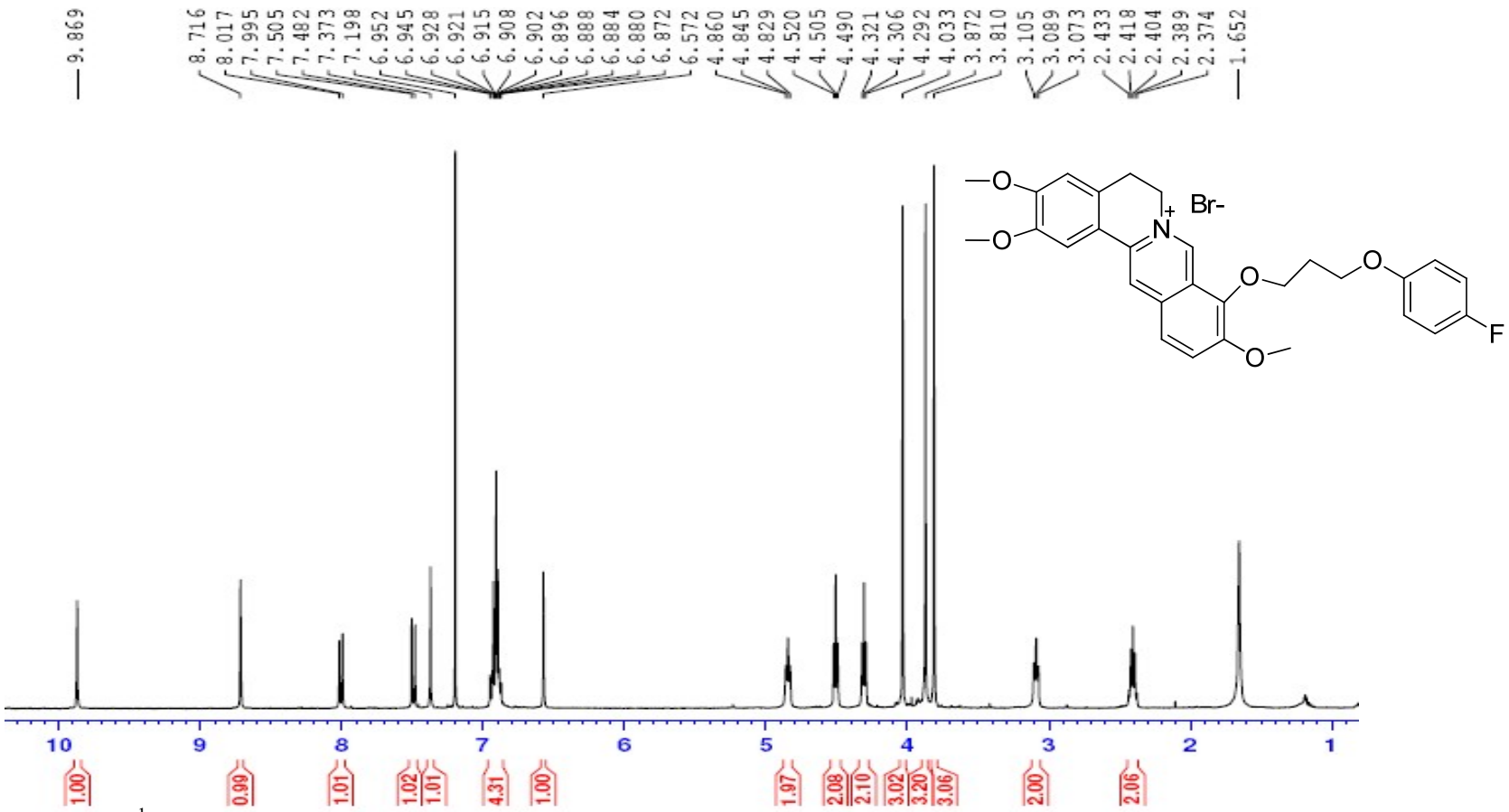

II-17 ^{1}H NMR spectrum of compound **P6**

References

1. Neu, H. C., The crisis in antibiotic resistance. *Science*, 1992. 257(5073): 1064-1073.

2. Levy, S. B., Multidrug resistance--a sign of the times. *The New England Journal of Medicine*, 1998. 338(19): 1376-1378.

3. Plaza, A., Keffer, J. L., Bifulco, G., Lloyd, J. R., & Bewley, C. A., Chrysophaentins A-H, antibacterial bisdiarylbutene macrocycles that inhibit the bacterial cell division protein FtsZ. *Journal of the American Chemical Society*, 2010. 132(26): 9069-9077.

4. Payne, D. J., Microbiology. Desperately seeking new antibiotics. *Science*, 2008. 321(5896): 1644-1645.

5. Kobayashi, S. D. & Deleo, F. R., An update on community-associated MRSA virulence. *Current Opinion in Pharmacology*, 2009. 9(5): 545-551.

6. Kapoor, S. & Panda, D., Targeting FtsZ for antibacterial therapy: a promising avenue. *Expert Opinion on Therapeutic Targets*, 2009. 13(9): 1037-1051.

7. Klein, E., Smith, D. L., & Laxminarayan, R., Hospitalizations and deaths caused by methicillin-resistant Staphylococcus aureus, United States, 1999-2005. *Emerging Infectious Diseases*, 2007. 13(12): 1840-1846.

8. Klevens, R. M., Morrison, M. A., Nadle, J., Petit, S., Gershman, K., Ray, S., Harrison, L. H., Lynfield, R., Dumyati, G., Townes, J. M., Craig, A. S., Zell, E. R., Fosheim, G. E., Mcdougal, L. K., Carey, R. B., & Fridkin, S. K., Invasive methicillin-resistant Staphylococcus aureus infections in the United States. *The Journal of the American Medical Association*, 2007. 298(15): 1763-1771.

9. Cosgrove, S. E., Qi, Y., Kaye, K. S., Harbarth, S., Karchmer, A. W., & Carmeli, Y., The impact of methicillin resistance in Staphylococcus aureus bacteremia on patient outcomes: mortality, length of stay, and hospital charges. *Infection Control and Hospital Epidemiology*, 2005. 26(2): 166-174.

10. Zhang, L. & Wilson, D. P., Trends in notifiable infectious diseases in China: implications for surveillance and population health policy. *PLoS One*, 2012. 7(2): e31076.

11. Ho, P. L., Yung, R. W., Tsang, D. N., Que, T. L., Ho, M., Seto, W. H., Ng, T. K., Yam, W. C., & Ng, W. W., Increasing resistance of

Streptococcus pneumoniae to fluoroquinolones: results of a Hong Kong multicentre study in 2000. *Journal of Antimicrobial Chemotherapy*, 2001. 48(5): 659-665.

12. Mulvey, M. R. & Simor, A. E., Antimicrobial resistance in hospitals: how concerned should we be? *Canadian Medical Association Journal*, 2009. 180(4): 408-415.

13. Webber, M. A. & Piddock, L. J., The importance of efflux pumps in bacterial antibiotic resistance. *Journal of Antimicrobial Chemotherapy*, 2003. 51(1): 9-11.

14. Tenover, F. C., Mechanisms of antimicrobial resistance in bacteria. *American Journal of Infection Control*, 2006. 34(5 Suppl 1): S3-10; discussion S64-73.

15. Bush, K. & Jacoby, G. A., Updated functional classification of beta-lactamases. *Antimicrobial Agents and Chemotherapy*, 2010. 54(3): 969-976.

16. Katayama, Y., Ito, T., & Hiramatsu, K., A new class of genetic element, staphylococcus cassette chromosome mec, encodes methicillin resistance in Staphylococcus aureus. *Antimicrobial Agents and Chemotherapy*, 2000. 44(6): 1549-1555.

17. Vicente, M., Rico, A. I., Martinez-Arteaga, R., & Mingorance, J., Septum enlightenment: assembly of bacterial division proteins. *Journal of Bacteriology*, 2006. 188(1): 19-27.

18. Harry, E., Monahan, L., & Thompson, L., Bacterial cell division: the mechanism and its precison. *International Review of Cytology*, 2006. 253: 27-94.

19. Goehring, N. W. & Beckwith, J., Diverse paths to midcell: assembly of the bacterial cell division machinery. *Current Biology*, 2005. 15(13): R514-526.

20. Errington, J., Daniel, R. A., & Scheffers, D. J., Cytokinesis in bacteria. *Microbiology and Molecular Biology Reviews*, 2003. 67(1): 52-65.

21. Lowe, J. & Amos, L. A., Crystal structure of the bacterial cell-division protein FtsZ. *Nature*, 1998. 391(6663): 203-206.

22. Desai, A. & Mitchison, T. J., Microtubule polymerization dynamics. *Annual Review of Cell and Developmental Biology*, 1997. 13: 83-117.

23. Scheffers, D. J., De Wit, J. G., Den Blaauwen, T., & Driessen, A. J., GTP hydrolysis of cell division protein FtsZ: evidence that the active

site is formed by the association of monomers. *Biochemistry*, 2002. 41(2): 521-529.

24. Scheffers, D. & Driessen, A. J., The polymerization mechanism of the bacterial cell division protein FtsZ. *FEBS Letters*, 2001. 506(1): 6-10.

25. De Boer, P., Crossley, R., & Rothfield, L., The essential bacterial cell-division protein FtsZ is a GTPase. *Nature*, 1992. 359(6392): 254-256.

26. Stricker, J., Maddox, P., Salmon, E. D., & Erickson, H. P., Rapid assembly dynamics of the Escherichia coli FtsZ-ring demonstrated by fluorescence recovery after photobleaching. *Proceedings of the National Academy of Sciences of the United States of America*, 2002. 99(5): 3171-3175.

27. Michie, K. A. & Lowe, J., Dynamic filaments of the bacterial cytoskeleton. *Annual Review of Biochemistry*, 2006. 75: 467-492.

28. Margolin, W., FtsZ and the division of prokaryotic cells and organelles. *Nature Reviews Molecular Cell Biology*, 2005. 6(11): 862-871.

29. Bi, E. F. & Lutkenhaus, J., FtsZ ring structure associated with division in Escherichia coli. *Nature*, 1991. 354(6349): 161-164.

30. Lock, R. L. & Harry, E. J., Cell-division inhibitors: new insights for future antibiotics. *Nature Reviews Drug Discovery*, 2008. 7(4): 324-338.

31. Adams, D. W. & Errington, J., Bacterial cell division: assembly, maintenance and disassembly of the Z ring. *Nature Reviews Microbiology*, 2009. 7(9): 642-653.

32. Haselbeck, R., Wall, D., Jiang, B., Ketela, T., Zyskind, J., Bussey, H., Foulkes, J. G., & Roemer, T., Comprehensive essential gene identification as a platform for novel anti-infective drug discovery. *Current Pharmaceutical Design*, 2002. 8(13): 1155-1172.

33. Wang, J., Galgoci, A., Kodali, S., Herath, K. B., Jayasuriya, H., Dorso, K., Vicente, F., Gonzalez, A., Cully, D., Bramhill, D., & Singh, S., Discovery of a small molecule that inhibits cell division by blocking FtsZ, a novel therapeutic target of antibiotics. *The Journal of Biological Chemistry*, 2003. 278(45): 44424-44428.

34. Beuria, T. K., Singh, P., Surolia, A., & Panda, D., Promoting assembly and bundling of FtsZ as a strategy to inhibit bacterial cell division: a new approach for developing novel antibacterial drugs. *Biochemical Journal*, 2009. 423(1): 61-69.

35. Domadia, P. N., Bhunia, A., Sivaraman, J., Swarup, S., & Dasgupta, D., Berberine targets assembly of Escherichia coli cell division protein FtsZ. *Biochemistry*, 2008. 47(10): 3225-3234.

36. Beuria, T. K., Santra, M. K., & Panda, D., Sanguinarine blocks cytokinesis in bacteria by inhibiting FtsZ assembly and bundling. *Biochemistry*, 2005. 44(50): 16584-16593.

37. Margolin, W., Wang, R., & Kumar, M., Isolation of an ftsZ homolog from the archaebacterium Halobacterium salinarium: implications for the evolution of FtsZ and tubulin. *Journal of Bacteriology*, 1996. 178(5): 1320-1327.

38. Domadia, P., Swarup, S., Bhunia, A., Sivaraman, J., & Dasgupta, D., Inhibition of bacterial cell division protein FtsZ by cinnamaldehyde. *Biochemical Pharmacology*, 2007. 74(6): 831-840.

39. Raychaudhuri, D. & Park, J. T., Escherichia coli cell-division gene ftsZ encodes a novel GTP-binding protein. *Nature*, 1992. 359(6392): 251-254.

40. Mukherjee, A., Dai, K., & Lutkenhaus, J., Escherichia coli cell division protein FtsZ is a guanine nucleotide binding protein. *Proceedings of the National Academy of Sciences of the United States of America*, 1993. 90(3): 1053-1057.

41. Mukherjee, A. & Lutkenhaus, J., Dynamic assembly of FtsZ regulated by GTP hydrolysis. *The EMBO Journal*, 1998. 17(2): 462-469.

42. Lu, C., Reedy, M., & Erickson, H. P., Straight and curved conformations of FtsZ are regulated by GTP hydrolysis. *Journal of Bacteriology*, 2000. 182(1): 164-170.

43. Kolb, P., Ferreira, R. S., Irwin, J. J., & Shoichet, B. K., Docking and chemoinformatic screens for new ligands and targets. *Current Opinion in Biotechnology*, 2009. 20(4): 429-436.

44. Haydon, D. J., Stokes, N. R., Ure, R., Galbraith, G., Bennett, J. M., Brown, D. R., Baker, P. J., Barynin, V. V., Rice, D. W., Sedelnikova, S. E., Heal, J. R., Sheridan, J. M., Aiwale, S. T., Chauhan, P. K., Srivastava, A., Taneja, A., Collins, I., Errington, J., & Czaplewski, L. G., An inhibitor of FtsZ with potent and selective anti-staphylococcal activity. *Science*, 2008. 321(5896): 1673-1675.

45. Matsui, T., Yamane, J., Mogi, N., Yamaguchi, H., Takemoto, H., Yao, M., & Tanaka, I., Structural reorganization of the bacterial cell-division protein FtsZ from Staphylococcus aureus. *Acta Crystallographica Section D: Biological Crystallography*, 2012. 68(Pt 9): 1175-1188.

46. Lappchen, T., Pinas, V. A., Hartog, A. F., Koomen, G. J., Schaffner-Barbero, C., Andreu, J. M., Trambaiolo, D., Lowe, J., Juhem, A., Popov, A. V., & Den Blaauwen, T., Probing FtsZ and tubulin with C8-substituted GTP analogs reveals differences in their nucleotide binding sites. *Chemistry & Biology*, 2008. 15(2): 189-199.

47. Ito, H., Ura, A., Oyamada, Y., Tanitame, A., Yoshida, H., Yamada, S., Wachi, M., & Yamagishi, J., A 4-aminofurazan derivative-A189-inhibits assembly of bacterial cell division protein FtsZ in vitro and in vivo. *Microbiology and Immunology*, 2006. 50(10): 759-764.

48. Stokes, N. R., Sievers, J., Barker, S., Bennett, J. M., Brown, D. R., Collins, I., Errington, V. M., Foulger, D., Hall, M., Halsey, R., Johnson, H., Rose, V., Thomaides, H. B., Haydon, D. J., Czaplewski, L. G., & Errington, J., Novel inhibitors of bacterial cytokinesis identified by a cell-based antibiotic screening assay. *The Journal of Biological Chemistry*, 2005. 280(48): 39709-39715.

49. Margalit, D. N., Romberg, L., Mets, R. B., Hebert, A. M., Mitchison, T. J., Kirschner, M. W., & Raychaudhuri, D., Targeting cell division: small-molecule inhibitors of FtsZ GTPase perturb

cytokinetic ring assembly and induce bacterial lethality. *Proceedings of the National Academy of Sciences of the United States of America*, 2004. 101(32): 11821-11826.

50. Huang, Q., Kirikae, F., Kirikae, T., Pepe, A., Amin, A., Respicio, L., Slayden, R. A., Tonge, P. J., & Ojima, I., Targeting FtsZ for antituberculosis drug discovery: noncytotoxic taxanes as novel antituberculosis agents. *Journal of Medicinal Chemistry*, 2006. 49(2): 463-466.

51. Possoz, C., Newmark, J., Sorto, N., Sherratt, D. J., & Tolmasky, M. E., Sublethal concentrations of the aminoglycoside amikacin interfere with cell division without affecting chromosome dynamics. *Antimicrobial Agents and Chemotherapy*, 2007. 51(1): 252-256.

52. Clardy, J., Fischbach, M. A., & Walsh, C. T., New antibiotics from bacterial natural products. *Nature Biotechnology*, 2006. 24(12): 1541-1550.

53. Hemaiswarya, S., Kruthiventi, A. K., & Doble, M., Synergism between natural products and antibiotics against infectious diseases. *Phytomedicine*, 2008. 15(8): 639-652.

54. Li, Z., Garner, A. L., Gloeckner, C., Janda, K. D., & Carlow, C. K., Targeting the Wolbachia cell division protein FtsZ as a new

approach for antifilarial therapy. *PLOS Neglected Tropical Diseases*, 2011. 5(11): e1411.

55. Rai, D., Singh, J. K., Roy, N., & Panda, D., Curcumin inhibits FtsZ assembly: an attractive mechanism for its antibacterial activity. *Biochemical Journal*, 2008. 410(1): 147-155.

56. Jaiswal, R., Beuria, T. K., Mohan, R., Mahajan, S. K., & Panda, D., Totarol inhibits bacterial cytokinesis by perturbing the assembly dynamics of FtsZ. *Biochemistry*, 2007. 46(14): 4211-4220.

57. Rajamani, R. & Good, A. C., Ranking poses in structure-based lead discovery and optimization: current trends in scoring function development. *Current Opinion in Drug Discovery & Development*, 2007. 10(3): 308-315.

58. De Azevedo, W. F., Jr. & Dias, R., Computational methods for calculation of ligand-binding affinity. *Current Drug Targets*, 2008. 9(12): 1031-1039.

59. Oda, A., Tsuchida, K., Takakura, T., Yamaotsu, N., & Hirono, S., Comparison of consensus scoring strategies for evaluating computational models of protein-ligand complexes. *Journal of Chemical Information and Modeling*, 2006. 46(1): 380-391.

60. Deng, Z., Chuaqui, C., & Singh, J., Structural interaction fingerprint (SIFt): a novel method for analyzing three-dimensional protein-ligand binding interactions. *Journal of Medicinal Chemistry*, 2004. 47(2): 337-344.

61. Amari, S., Aizawa, M., Zhang, J., Fukuzawa, K., Mochizuki, Y., Iwasawa, Y., Nakata, K., Chuman, H., & Nakano, T., VISCANA: visualized cluster analysis of protein-ligand interaction based on the ab initio fragment molecular orbital method for virtual ligand screening. *Journal of Chemical Information and Modeling*, 2006. 46(1): 221-230.

62. Bajorath, J., Integration of virtual and high-throughput screening. *Nature Reviews Drug Discovery*, 2002. 1(11): 882-894.

63. Bleicher, K. H., Bohm, H. J., Muller, K., & Alanine, A. I., Hit and lead generation: beyond high-throughput screening. *Nature Reviews Drug Discovery*, 2003. 2(5): 369-378.

64. Von Itzstein, M., Wu, W. Y., Kok, G. B., Pegg, M. S., Dyason, J. C., Jin, B., Van Phan, T., Smythe, M. L., White, H. F., Oliver, S. W., & Et Al., Rational design of potent sialidase-based inhibitors of influenza virus replication. *Nature*, 1993. 363(6428): 418-423.

65. Greer, J., Erickson, J. W., Baldwin, J. J., & Varney, M. D., Application of the three-dimensional structures of protein target molecules in structure-based drug design. *Journal of Medicinal Chemistry*, 1994. 37(8): 1035-1054.

66. Williams, D. H. & Mitchell, T., Latest developments in crystallography and structure-based design of protein kinase inhibitors as drug candidates. *Current Opinion in Pharmacology*, 2002. 2(5): 567-573.

67. Wlodawer, A. & Vondrasek, J., Inhibitors of HIV-1 protease: a major success of structure-assisted drug design. *Annual Review of Biophysics & Biomolecular Structure*, 1998. 27: 249-284.

68. Lowe, J., Crystal structure determination of FtsZ from Methanococcus jannaschii. *Journal of Structural Biology*, 1998. 124(2-3): 235-243.

69. Leung, A. K., White, E. L., Ross, L. J., & Borhani, D. W., Crystallization of the Mycobacterium tuberculosis cell-division protein FtsZ. *Acta Crystallographica Section D: Biological Crystallography*, 2000. 56(Pt 12): 1634-1637.

70. Cordell, S. C., Robinson, E. J., & Lowe, J., Crystal structure of the SOS cell division inhibitor SulA and in complex with FtsZ.

Proceedings of the National Academy of Sciences of the United States of America, 2003. 100(13): 7889-7894.

71. Oliva, M. A., Trambaiolo, D., & Lowe, J., Structural insights into the conformational variability of FtsZ. *Journal of Molecular Biology*, 2007. 373(5): 1229-1242.

72. Abagyan, R., Totrov, M., & Kuznetsov, D., Icm - a New Method for Protein Modeling and Design - Applications to Docking and Structure Prediction from the Distorted Native Conformation. *Journal of Computational Chemistry*, 1994. 15(5): 488-506.

73. Chan, F. Y., Discovery of novel inhibitors of the bacterial cell division protein FtsZ by computational drug screening coupled with bioassays. PhD Thesis, The Hong Kong Polytechnic University, Hong Kong, 2010.

74. Ulrich-Merzenich, G., Panek, D., Zeitler, H., Vetter, H., & Wagner, H., Drug development from natural products: exploiting synergistic effects. *Indian Journal of Experimental Biology*, 2010. 48(3): 208-219.

75. Berenbaum, M. C., Synergy, additivism and antagonism in immunosuppression. A critical review. *Clinical & Experimental Immunology*, 1977. 28(1): 1-18.

76. Sharom, J. R., Bellows, D. S., & Tyers, M., From large networks to small molecules. *Current Opinion in Chemical Biology*, 2004. 8(1): 81-90.

77. Keith, C. T., Borisy, A. A., & Stockwell, B. R., Multicomponent therapeutics for networked systems. *Nature Reviews Drug Discovery*, 2005. 4(1): 71-78.

78. Chou, T. C., Theoretical basis, experimental design, and computerized simulation of synergism and antagonism in drug combination studies. *Pharmacological Reviews*, 2006. 58(3): 621-681.

79. Desbois, A. P., Lang, S., Gemmell, C. G., & Coote, P. J., Surface disinfection properties of the combination of an antimicrobial peptide, ranalexin, with an endopeptidase, lysostaphin, against methicillin-resistant Staphylococcus aureus (MRSA). *Journal of Applied Microbiology*, 2010. 108(2): 723-730.

80. Wagner, H. & Ulrich-Merzenich, G., Synergy research: approaching a new generation of phytopharmaceuticals. *Phytomedicine*, 2009. 16(2-3): 97-110.

81. Acar, J. F., Antibiotic synergy and antagonism. *Medical Clinics of North America*, 2000. 84(6): 1391-1406.

82. Hall, M. J., Middleton, R. F., & Westmacott, D., The fractional inhibitory concentration (FIC) index as a measure of synergy. *Journal of Antimicrobial Chemotherapy*, 1983. 11(5): 427-433.

83. Zhang, Q., Cai, L., Zhong, G., & Luo, W., Simultaneous determination of jatrorrhizine, palmatine, berberine, and obacunone in Phellodendri Amurensis Cortex by RP-HPLC. *Zhongguo Zhong Yao Za Zhi*, 2010. 35(16): 2061-2064.

84. Zhang, W. J., Ou, T. M., Lu, Y. J., Huang, Y. Y., Wu, W. B., Huang, Z. S., Zhou, J. L., Wong, K. Y., & Gu, L. Q., 9-Substituted berberine derivatives as G-quadruplex stabilizing ligands in telomeric DNA. *Bioorganic & Medicinal Chemistry*, 2007. 15(16): 5493-5501.

85. Huang, Z. J., Zeng, Y., Lan, P., Sun, P. H., & Chen, W. M., Advances in structural modifications and biological activities of berberine: an active compound in traditional Chinese medicine. *Mini-Reviews in Medicinal Chemistry*, 2011. 11(13): 1122-1129.

86. Iwasa, K., Kamigauchi, M., Ueki, M., & Taniguchi, M., Antibacterial activity and structure-activity relationships of berberine analogs. *European Journal of Medicinal Chemistry*, 1996. 31(6): 469-478.

87. Serafim, T. L., Oliveira, P. J., Sardao, V. A., Perkins, E., Parke, D., & Holy, J., Different concentrations of berberine result in distinct cellular localization patterns and cell cycle effects in a melanoma cell line. *Cancer Chemotherapy and Pharmacology*, 2008. 61(6): 1007-1018.

88. Iwasa, K., Nanba, H., Lee, D. U., & Kang, S. I., Structure-activity relationships of protoberberines having antimicrobial activity. *Planta Medica*, 1998. 64(8): 748-751.

89. Iwasa, K., Lee, D. U., Kang, S. I., & Wiegrebe, W., Antimicrobial activity of 8-alkyl- and 8-phenyl-substituted berberines and their 12-bromo derivatives. *Journal of Natural Products*, 1998. 61(9): 1150-1153.

90. Sheng, C., Wang, W., Che, X., Dong, G., Wang, S., Ji, H., Miao, Z., Yao, J., & Zhang, W., Improved model of lanosterol 14alpha-demethylase by ligand-supported homology modeling: validation by virtual screening and azole optimization. *ChemMedChem*, 2010. 5(3): 390-397.

91. Huang, L., Luo, Z., He, F., Lu, J., & Li, X., Synthesis and biological evaluation of a new series of berberine derivatives as dual

inhibitors of acetylcholinesterase and butyrylcholinesterase. *Bioorganic & Medicinal Chemistry*, 2010. 18(12): 4475-4484.

92. Mayer, M. & Meyer, B., Group epitope mapping by saturation transfer difference NMR to identify segments of a ligand in direct contact with a protein receptor. *Journal of the American Chemical Society*, 2001. 123(25): 6108-6117.

93. Wayne, P., Methods for dilution antimicrobial susceptibility tests for bacteria that grow aerobically. *CLSI document M07-A7*, 2006.

94. Mukherjee, A. & Lutkenhaus, J., Analysis of FtsZ assembly by light scattering and determination of the role of divalent metal cations. *Journal of Bacteriology*, 1999. 181(3): 823-832.

95. Mayer, M. & James, T. L., Detecting ligand binding to a small RNA target via saturation transfer difference NMR experiments in D(2)O and H(2)O. *Journal of the American Chemical Society*, 2002. 124(45): 13376-13377.

96. Meyer, B. & Peters, T., NMR spectroscopy techniques for screening and identifying ligand binding to protein receptors. *Angewandte Chemie International Edition*, 2003. 42(8): 864-890.

97. Czaplewski, L. G., Collins, I., Boyd, E. A., Brown, D., East, S. P., Gardiner, M., Fletcher, R., Haydon, D. J., Henstock, V., Ingram, P.,

Jones, C., Noula, C., Kennison, L., Rockley, C., Rose, V., Thomaides-Brears, H. B., Ure, R., Whittaker, M., & Stokes, N. R., Antibacterial alkoxybenzamide inhibitors of the essential bacterial cell division protein FtsZ. *Bioorganic & Medicinal Chemistry Letters*, 2009. 19(2): 524-527.

98. Wang, Y. M., Zhao, L. B., Lin, S. L., Dong, S. S., & An, D. K., Determination of berberine and palmatine in cortex phellodendron and Chinese patent medicines by HPLC. *Yao Xue Xue Bao*, 1989. 24(4): 275-279.

99. Bhadra, K. & Kumar, G. S., Therapeutic potential of nucleic acid-binding isoquinoline alkaloids: binding aspects and implications for drug design. *Medicinal Research Reviews*, 2011. 31(6): 821-862.

100. Jia, F., Zou, G., Fan, J., & Yuan, Z., Identification of palmatine as an inhibitor of West Nile virus. *Archives of Virology*, 2010. 155(8): 1325-1329.

101. Qin, Y., Chen, W. H., Pang, J. Y., Zhao, Z. Z., Liu, L., & Jiang, Z. H., DNA-binding affinities and sequence specificities of protoberberine alkaloids and their demethylated derivatives: a comparative study. *Chemistry & Biodiversity*, 2007. 4(2): 145-153.

102. Chan, K. F., Zhao, Y., Burkett, B. A., Wong, I. L., Chow, L. M., & Chan, T. H., Flavonoid dimers as bivalent modulators for P-glycoprotein-based multidrug resistance: synthetic apigenin homodimers linked with defined-length poly(ethylene glycol) spacers increase drug retention and enhance chemosensitivity in resistant cancer cells. *Journal of Medicinal Chemistry*, 2006. 49(23): 6742-6759.

103. Schaffner-Barbero, C., Martin-Fontecha, M., Chacon, P., & Andreu, J. M., Targeting the assembly of bacterial cell division protein FtsZ with small molecules. *ACS Chemical Biology*, 2012. 7(2): 269-277.

104. Oliva, M. A., Cordell, S. C., & Lowe, J., Structural insights into FtsZ protofilament formation. *Nature Structural & Molecular Biology*, 2004. 11(12): 1243-1250.

105. Halgren, T. A. & Nachbar, R. B., Merck molecular force field .4. Conformational energies and geometries for MMFF94. *Journal of Computational Chemistry*, 1996. 17(5-6): 587-615.

106. Halgren, T. A., Merck molecular force field .5. Extension of MMFF94 using experimental data, additional computational data,

and empirical rules. *Journal of Computational Chemistry*, 1996. 17(5-6): 616-641.

107. Halgren, T. A., Merck molecular force field .3. Molecular geometries and vibrational frequencies for MMFF94. *Journal of Computational Chemistry*, 1996. 17(5-6): 553-586.

108. Halgren, T. A., Merck molecular force field .2. MMFF94 van der Waals and electrostatic parameters for intermolecular interactions. *Journal of Computational Chemistry*, 1996. 17(5-6): 520-552.

109. Halgren, T. A., Merck molecular force field .1. Basis, form, scope, parameterization, and performance of MMFF94. *Journal of Computational Chemistry*, 1996. 17(5-6): 490-519.

110. Abagyan, R. A. & Batalov, S., Do aligned sequences share the same fold? *Journal of Molecular Biology*, 1997. 273(1): 355-368.

111. An, J. H., Totrov, M., & Abagyan, R., Pocketome via comprehensive identification and classification of ligand binding envelopes. *Molecular & Cellular Proteomics*, 2005. 4(6): 752-761.

112. Abagyan, R. & Totrov, M., Biased Probability Monte-Carlo Conformational Searches and Electrostatic Calculations for Peptides and Proteins. *Journal of Molecular Biology*, 1994. 235(3): 983-1002.

113. Schapira, M., Abagyan, R., & Totrov, M., Nuclear hormone receptor targeted virtual screening. *Journal of Medicinal Chemistry*, 2003. 46(14): 3045-3059.

114. Huang, N., Shoichet, B. K., & Irwin, J. J., Benchmarking sets for molecular docking. *Journal of Medicinal Chemistry*, 2006. 49(23): 6789-6801.

115. Katritch, V., Rueda, M., Lam, P. C. H., Yeager, M., & Abagyan, R., GPCR 3D homology models for ligand screening: Lessons learned from blind predictions of adenosine A2a receptor complex. *Proteins-Structure Function and Bioinformatics*, 2010. 78(1): 197-211.

116. Triballeau, N., Acher, F., Brabet, I., Pin, J. P., & Bertrand, H. O., Virtual screening workflow development guided by the "receiver operating characteristic" curve approach. Application to high-throughput docking on metabotropic glutamate receptor subtype 4. *Journal of Medicinal Chemistry*, 2005. 48(7): 2534-2547.

117. Abagyan, R. & Totrov, M., High-throughput docking for lead generation. *Current Opinion in Chemical Biology*, 2001. 5(4): 375-382.

118. Tan, C. M., Therien, A. G., Lu, J., Lee, S. H., Caron, A., Gill, C. J., Lebeau-Jacob, C., Benton-Perdomo, L., Monteiro, J. M., Pereira, P. M., Elsen, N. L., Wu, J., Deschamps, K., Petcu, M., Wong, S., Daigneault, E., Kramer, S., Liang, L., Maxwell, E., Claveau, D., Vaillancourt, J., Skorey, K., Tam, J., Wang, H., Meredith, T. C., Sillaots, S., Wang-Jarantow, L., Ramtohul, Y., Langlois, E., Landry, F., Reid, J. C., Parthasarathy, G., Sharma, S., Baryshnikova, A., Lumb, K. J., Pinho, M. G., Soisson, S. M., & Roemer, T., Restoring methicillin-resistant Staphylococcus aureus susceptibility to beta-lactam antibiotics. *Science Translational Medicine*, 2012. 4(126): 126ra135.

119. Nogales, E., Downing, K. H., Amos, L. A., & Lowe, J., Tubulin and FtsZ form a distinct family of GTPases. *Nature Structural & Molecular Biology*, 1998. 5(6): 451-458.

120. Chung, J. G., Wu, L. T., Chu, C. B., Jan, J. Y., Ho, C. C., Tsou, M. F., Lu, H. F., Chen, G. W., Lin, J. G., & Wang, T. F., Effects of berberine on arylamine N-acetyltransferase activity in human bladder tumour cells. *Food and Chemical Toxicology*, 1999. 37(4): 319-326.

121. Lehar, J., Krueger, A. S., Avery, W., Heilbut, A. M., Johansen, L. M., Price, E. R., Rickles, R. J., Short, G. F., 3rd, Staunton, J. E., Jin, X., Lee, M. S., Zimmermann, G. R., & Borisy, A. A., Synergistic drug combinations tend to improve therapeutically relevant selectivity. *Nature Biotechnology*, 2009. 27(7): 659-666.

122. Sung, W. S. & Lee, D. G., Mechanism of decreased susceptibility for Gram-negative bacteria and synergistic effect with ampicillin of indole-3-carbinol. *Biological & pharmaceutical bulletin*, 2008. 31(9): 1798-1801.